No172

ELECTRON SCATTERING BY MOLECULES II. EXPERIMENTAL METHODS AND DATA

S. TRAJMAR, D.F. REGISTER and A. CHUTJIAN

California Institute of Technology, Jet Propulsion Laboratory, Pasadena, California 91109, U.S.A.

NORTH-HOLLAND PUBLISHING COMPANY – AMSTERDAM

PHYSICS REPORTS (Review Section of Physics Letters) 97, No. 5 (1983) 219–356. North-Holland Publishing Company

ELECTRON SCATTERING BY MOLECULES II. EXPERIMENTAL METHODS AND DATA

S. TRAJMAR, D.F. REGISTER* and A. CHUTJIAN

California Institute of Technology, Jet Propulsion Laboratory, Pasadena, California 91109, U.S.A.

Received February 1983

Contents:

1. Introduction 221
2. Definition of cross sections 222
3. Experimental methods 223
   3.1. Electron impact spectroscopy 223
   3.2. Total scattering cross section measurements 224
   3.3. Integral cross section measurements 226
   3.4. Momentum transfer cross sections 227
   3.5. Differential cross sections 227
   3.6. Normalization procedures 229
   3.7. Experimental uncertainties, error estimation 231
   3.8. Study of superexcited states (innershell and multi-electron excitations) 232
   3.9. Coincidence measurements 233
   3.10. Electron scattering in laser fields 233
   3.11. Electron collision measurements at high energies: Generation of optical data 234
4. Summary of experimental data 235
   4.1. H_2 235
   4.2. N_2 260
   4.3. O_2 279
   4.4. CO 292
   4.5. NO 304
   4.6. HX (X = F, Cl, Br, I) 305
   4.7. Alkali dimers 309
   4.8. Alkali halide molecules 311
   4.9. Other diatomic molecules 313
   4.10. H_2O 313
   4.11. H_2S 316
   4.12. HCN 318
   4.13. OCS 318
   4.14. CO_2 318
   4.15. N_2O 326
   4.16. SO_2 326
   4.17. NH_3 327
   4.18. As_4 330
   4.19. CH_4 331
   4.20. Hydrocarbons 335
   4.21. Halocarbons 343
   4.22. SF_6 343
   4.23. UF_6 348
   4.24. Other polyatomic molecules 349
References 349

Abstract:

Experimental techniques for measuring electron–molecule collision cross sections are briefly summarized. A survey of the available experimental cross section data is presented. The emphasis here is on elastic scattering, rotational, vibrational and electronic excitations, total electron scattering, and momentum transfer in the few eV to few hundred eV impact energy range. Reference is made to works concerned with high energy electron scattering, innershell and multi-electron excitations, coincidence methods and electron scattering in laser fields.

* Present address: Phillips Petroleum Co., Bartlesville, OK 74003, U.S.A.

Single orders for this issue

PHYSICS REPORTS (Review Section of Physics Letters) 97, No. 5 (1983) 219–356.

Copies of this issue may be obtained at the price given below. All orders should be sent directly to the Publisher. Orders must be accompanied by check.

Single issue price Dfl. 76.00, postage included.

1. Introduction

The decade of the '70's has witnessed a dramatic increase in activity in the general area of electron molecule collision physics. Total electron scattering cross sections, ionization cross sections and optical excitation function measurements have been complemented in many cases by more detailed studies of vibrational-rotational excitation, resonance phenomena and dissociative processes to name just a few. However, many of these data are of a qualitative nature. With the possible exception of N_2, electron impact cross sections for molecular collisions have not been systematically quantified.

Massey et al. [1] reviewed the status of electron molecule scattering up to the late '60's and Kieffer [2–4] summarized the available data up to 1970. More recently Kieffer [5] and Schulz [6] reviewed vibrational excitation at low electron impact energies and compiled electron collision cross sections for modeling gas discharge lasers. Golden et al. [7] treated the problem of rotational excitation of molecules by electron impact. A set of integral elastic, momentum transfer, viscosity and total electron collision cross sections was recommended for H_2, N_2, O_2, CO and CO_2 on the basis of a critical evaluation of all available data in the 10^{-3} to 10^4 eV range by Hayashi [8]. Although a large number of electron collision studies have been carried out, we still do not have a comprehensive body of cross section data for any molecule and the accuracy of the available data is only moderate (about ±20 to 50%). Systematic improvements in experimental techniques and the increased understanding of the nature of electron atom (molecule) collisions gained in the last decade should, however, remedy this situation in the coming years. In particular, the development of reliable normalization procedures [9] and the availability of accurate He [10] cross sections (which can serve as standard) should greatly improve the reliability of absolute cross section measurements for electron molecule scattering.

The present review is intended to update the experimental aspects of cross section measurements and to summarize the data which have become available since about 1970. The emphasis is placed on elastic scattering, rotational, vibrational and electronic excitation processes and total scattering cross sections in the near threshold to few hundred eV impact energy range. It is in this range where a large majority of cross sections have their maxima, and where theoretical calculations of cross sections are very difficult. Elastic cross sections quoted in this review include unresolved pure rotational excitations unless specifically stated otherwise. Electron impact dissociation (which may be considered as excitation to a continuum electronic state) will be briefly treated for H_2 only. An excellent review on this topic including dissociation to both neutral and charged fragments has been published by Compton and Bardsley [11]. Electron scattering at high impact energies [12, 13], innershell and multi-electron excitations (super excited states) [14–17], electron–photon coincidence measurements [18–21], and electron collisions in laser fields [22, 23] will be only briefly mentioned. Threshold phenomena, resonances, dissociative attachment and ionization (including electron–electron and electron–ion coincidence measurements) will not be covered. These topics have been reviewed recently [3, 24–29]. However, we include in our survey absolute cross section data available in the resonance energy regions.

In treating electronic excitation processes for molecules, complications arise because of the large variety of electronic-vibrational-rotational excitations to discrete electronic states, and excitations to continuum states which lead to dissociation and generation of ground, excited and ionized fragments. Cross sections for all of these processes as a function of impact energy and electron scattering angle, cross sections differential with respect to energy, and angular distributions of the dissociation fragments could in principle be measured. This would result in an overwhelming amount of information. Some of these processes are best studied by other than electron scattering techniques, for example detection of ionic products or emitted light from excited molecules or fragments. Studies of this nature have been

$\sigma_n^{\mathrm{M}}(E_0)$ cross sections,

$$\sigma_n(E_0) = 2\pi \int_0^{\pi} [\mathrm{DCS}_n(\theta)]_{E_0} \sin\theta \, \mathrm{d}\theta \tag{3}$$

$$\sigma_n^{\mathrm{M}}(E_0) = 2\pi \int_0^{\pi} [\mathrm{DCS}_n(\theta)]_{E_0} \left[1 - \frac{k_{\mathrm{f}}}{k_{\mathrm{i}}} \cos\theta\right] \sin\theta \, \mathrm{d}\theta \tag{4}$$

where k_{i} and k_{f} are the magnitude of the initial and final momenta of the electron, respectively. The total (or as sometimes called "grand total") scattering cross section is the sum of all integral cross sections:

$$\sigma_{\mathrm{T}}(E_0) = \sum_n \sigma_n(E_0) . \tag{5}$$

For experiments where the scattered electron is detected in coincidence with other secondary particles (electrons, photons, ions, neutral fragments), one has to define in addition cross sections differential in the energy and angle of these secondary species.

All of these cross sections may be defined in terms of scattering amplitudes, or S, T or R matrix elements. As these quantities are the usual results of theoretical work and are only rarely amenable to direct experimental measurements, discussion of them will be left to the theoretical survey.

3. Experimental methods

The experimental methods for cross section measurements are only briefly discussed here. More detailed descriptions can be found in ref. [9] and other references quoted therein.

3.1. Electron impact spectroscopy

Although the aim of the present paper is to survey quantitative cross section measurement techniques and data, it is deemed useful to discuss briefly the qualitative (or spectroscopic) aspects of electron scattering. This will serve to introduce the question of selection rules and the general behavior of cross sections with respect to impact energy, scattering angle, and the nature of the scattering states involved.

A large number of electron scattering studies has been concerned with the study of relative excitation probabilities (relative energy and angular distributions of scattered electrons) and with transitions made allowed by the relaxation of dipole selection rules in electron scattering [31, 32]. These studies are especially useful for identifying spin and symmetry forbidden excitation processes, and through them new low-lying metastable states of molecules. The relative scattering intensities (or relative cross sections) obtained in these experiments are also useful for generating cross section data once the cross section for any one process becomes available.

carried out primarily by photon detection. The information generated is mainly qualitative and very frequently given in the form of graphs. We deem it appropriate to refer to these works but do not review them in detail. A parallel review by Buckley [30] deals with theoretical methods and results.

2. Definition of cross sections

The quantity which characterizes a scattering process and which is needed in the analysis of practical systems and devices where electron collisions play a role is the cross section. It represents the time-independent probability for the occurrence of a particular process. The interaction between an electron and a molecule is a function of the electron velocity, the type of process, and the scattering angle. Consequently, the cross sections are functions of these same parameters. In experiments where only scattered electrons are detected for a particular process (n) as a function of scattering polar angles (θ, ϕ), impact energy (E_0), and energy-loss (E) we must, in general, define the doubly differential cross section $\partial^2\sigma_n(E_0, E, \Omega)/\partial E\, \partial\Omega$.

In most measurements several conditions apply which reduce the complexity associated with the defined cross section. When the incident energy is far from threshold and resonance regions, the cross section does not change appreciably over the energy distribution of the primary electron beam and it may be well represented as an average doubly differential cross section associated with the mean incident energy. (That is, averaging over the primary electron energy distribution can be neglected.) For discrete excitation processes this cross section may be integrated over the energy-loss profile to obtain the differential (in angle) cross section $\mathrm{d}\sigma_n(E_0, \Omega)/\mathrm{d}\Omega$. Finally, since target molecules are usually randomly oriented, the measurement can only yield a cross section averaged over molecular orientations, independent of the azimuthal angle ϕ. The measuring apparatus averages over a finite energy and angular range and the quantity which is determined in beam–beam experiments is:

$$[\mathrm{DCS}_n(\theta)]_{E_0} = \overline{[\mathrm{d}\sigma_n(\Omega)/\mathrm{d}\Omega]}_{E_0}\,. \tag{1}$$

$\mathrm{DCS}_n(\theta)_{E_0}$ is in units of area per unit solid angle.

In practice it is seldom possible to measure the cross section for a well defined individual process. In most cases one measures the average cross section for a number of experimentally indistinguishable processes. Hyperfine and magnetic sublevel structures are distinguished only in special scattering experiments utilizing laser excitations or electron–photon coincidence techniques. Similarly cross sections associated with various target and electron spin orientations are usually averaged in a measurement. With the limitations imposed by presently available energy resolutions, one cannot resolve individual rotational transition except in H_2, and only incompletely resolve vibrational structure in complex molecules. For a comparison of experiment with theory a procedure which averages over unresolved initial states (i) and sums over unresolved final states (f) has to be carried out:

$$[\mathrm{DCS}_n(\theta)]_{E_0} = \sum_{\mathrm{i}} \sum_{\mathrm{f}} N_{\mathrm{i}}[\mathrm{DCS}_n^{\mathrm{if}}(\theta)]_{E_0} \tag{2}$$

where N_{i} is the fractional population in the initial state, i.

Integration of the DCS over all scattering angles yields the integral $\sigma_n(E_0)$ and momentum transfer

Studies of scattering intensities as a function of impact energy and scattering angle have revealed some general characteristics of cross sections with respect to these parameters. Excitation processes requiring spin exchange have integral cross sections which reach their peak value near threshold and decrease rapidly at high energies. The angular distribution (differential cross section) for spin exchange processes are nearly isotropic. These effects can be understood by considering the short range nature of spin exchange interaction. Optically allowed (dipole) excitation processes usually reach their maximum probability at an impact energy which is of the order of ten times the excitation energy and exhibit forward peaking angular characteristics. Scattering processes dominated by long-range (dipole or Coulomb) interactions show extremely forward peaking distributions. For example rotational excitation ($\Delta J = \pm 1$) of alkali halide molecules have cross sections of the order of 10^{-13} cm^2/sr in the forward direction and 90% of the integral cross section comes from scattering in the 0° to 10° angular range. No generally valid trend can be recognized for transitions which are optically forbidden by symmetry except in some special cases, such as for $+ \leftrightarrow -$ excitation processes which have zero cross sections at 0° and at 180° scattering angles. Elastic cross sections generally peak at around a few eV impact energy, and show forward peaking angular behavior at high energy and isotropic or backward peaking behavior at low energy.

There are few generally valid selection rules for electron impact excitation processes. Most of the selection rules can be derived only for special conditions (e.g. for particular scattering angles or for particular target orientations) and, therefore, can be easily overcome by proper choice of experimental conditions. For a summary of electron impact selection rules the reader is referred to refs. [33 and 34].

3.2. *Total scattering cross section measurements*

There are three methods commonly used for total scattering cross section measurements: the transmission method, the recoil method, and the transmission method with time-of-flight discrimination.

In the transmission method the attenuation of an electron beam passing through a gas is measured and is related to the total scattering cross section. One encounters some problems in dealing with questions of: (1) forward scattering into the view cone of the detector, (2) treating electrons which undergo multiple collisions and are scattered back into the view cone of the detector, (3) defining the proper path length. In addition pressure and current-dependent problems (multiple scattering, space charge effects) have to be checked and minimized. Since a large fraction of the forward scattering arises from inelastic processes, this problem may be greatly reduced by use of a retarding potential analyzer. These questions should be carefully addressed in each measurement since they determine the error limits for the cross section data. The transmission technique has been applied to a large number of molecules.

The recoil technique is basically also a transmission technique wherein the attenuation of the molecular beam, rather than the electron beam is measured. This method has been applied extensively to atomic species but applies equally well (in principle) to molecules. The major difficulty is the need for high angular resolution and accurate quantitative detection of neutral molecules. These difficulties very likely account for the absence of application of the recoil technique to molecules so far.

In the time-of-flight method the time distribution of the electron beam signal is converted to an energy distribution with an empty gas cell. When gas is present in the cell, the attenuation of the electron beam as a function of energy (time distribution) can be determined and related to the total scattering cross section as in other transmission experiments. The time-of-flight approach avoids some of the problems common to conventional transmission methods. It is limited at low impact energies (below few tenths of an eV) by flux and at high impact energies (above 50 eV) by time resolution

capabilities. Since inelastic forward scattering cannot be energetically discriminated against in the time-of-flight measurements, caution must be used on molecular systems, especially those with large polarizabilities or permanent dipole moments. The method has been applied to about a dozen molecular species.

The total scattering cross sections measured by these techniques are in general accurate to within a few percent and the data obtained by various investigators agree with each other within this error limit. Table 1 summarizes total cross section measurements for molecules. (Total cross sections obtained from swarm or from low-energy differential elastic scattering measurements are not included.) The total cross section measurement techniques have been only very briefly treated here since a detailed discussion of them is given in ref. [9].

Recently Sokolov and Sokolova [35a] developed a new method for total collision cross section measurements which works well at low impact energies and low vapor pressure and does not require a monoenergetic beam of electrons. They applied this technique to H_2O, H_2S and SO_2. This method makes use of electron cyclotron resonance. It is, however, an indirect method. Schulters et al. [356] deduced total scattering cross sections by studying the line shape of electron cyclotron reasonance signal as a function of gas pressure at 295 K (corresponding to 0.038 eV mean electron energy). They found good agreement with cross sections obtained by drift tube measurements in the case of H_2, N_2, O_2, CO, CO_2, H_2O, N_2O, CH_3NH_2 and CH_3CN.

Table 1
Summary of recent total electron scattering cross section measurements for molecules

H_2 Reference	Energy range (eV)	Method	Error limits
Ferch et al. 1980, 1981, ref. [78]	0.02–2.0	Transmission with time of flight	±2.5%
Dalba et al. 1980, ref. [79]	0.02–100	Transmission	1.7 to ±5%
van Wingerden et al. 1980, ref. [80]	25–750	Transmission	3.1 to ±5.4%
van Wingerden et al. 1980, ref. [80]	20–2000	Semi-empirical	±5%
Jones and Bonham 1981, ref. [81]	0.6–50	Transmission with time of flight	±3%
Hoffman et al. 1982, ref. [82]	2–500	Transmission	±2%

Other molecules Reference	Molecule	Energy range (eV)	Method
Miller and Kasdan 1973, ref. [233]	Na_2, K_2	0.5 to 50	Recoil
Slater et al. 1974, ref. [238]	CsF	0 to 15	Recoil
Becker et al. 1974, ref. [239]	CsCl	0 to 15	Recoil
Slater et al. 1974, ref. [240]	KI	0 to 15	Recoil
Baldwin 1974, ref. [142]	N_2	0 to 2	Time of flight
Mathur and Hasted 1977, ref. [141]	N_2	1 to 4	Transmission

Table 1 (*Cont.*)

Reference	Molecule	Energy range (eV)	Method
Szmytkowski and Zubek 1978, ref. [202]	CO, CO_2, OCS	1 to 8	Transmission
Gus'kov et al. 1978, ref. [204]	CO	0.05 to 6.0	Time of flight
Hasted et al. 1979, ref. [142]	CO, N_2, CO_2, CH_4, C_2H_4	0.3 to 5	Transmission
Kennerly et al. 1979, ref. [288]	SF_6	0.5 to 100	Time of flight
Barbarito et al. 1979, ref. [275]	CH_4	0 to 16	Transmission
Blaauw et al. 1980, ref. [138]	N_2	15 to 750	Transmission
Kennerly 1980, ref. [137]	N_2	0.5 to 50	Time of flight
Dalba et al. 1980, ref. [139]	N_2, O_2, NO	100 to 1600	Transmission
Bonham 1980, ref. [287]	CO_2, CH_4, CCl_4, CCl_3F, CCl_2F_2, $CClF_3$, CF_4	0.5 to 100	Time of flight
Zubek et al. 1981, ref. [256]	H_2S, CO_2, N_2O, SO_2	0.5 to 10	Transmission
Sokolov and Sokolova 1981, ref. [246]	H_2O, H_2S, SO_2	0 to 10	Indirect
Ferch et al. 1981, ref. [259]	CO_2	0.07 to 2	Time of flight
Ferch et al. 1982, refs. [289, 290]	SF_6	0.036 to 1.0	Time of flight
Hoffman et al. 1982, ref. [140]	N_2, CO_2	2 to 700	Transmission
Miller et al. 1982, ref. [234]	Li_2	0.5 to 10	Recoil

3.3. Integral cross section measurements

Integral electron impact excitation cross sections for molecules have been primarily obtained in the past by measuring optical excitation functions (or line excitation cross sections); that is, apparent (direct + cascade) electron impact excitation cross sections for emission at a particular wavelength as a function of impact energy. Photoemission from a particular state excited by electron impact is monitored in these experiments. The optical excitation function can be corrected to various degrees of approximation to yield electron impact excitation cross sections. The experimental determination of the electron impact excitation cross section requires knowledge of the absolute measurement of photon emission rate, branching ratios for decay paths of the excited states, and the scattering geometry. Further complications arise because of cascade contributions to the population of the excited state under study, polarization effects, radiation trapping for high target densities and superelastic scattering. A large number of molecular transitions have been studied in the visible and measurements are now being extended into the vacuum UV region at several laboratories.

At low impact energies the trapped electron method developed by Schulz [36] can be used to get electron impact excitation functions. A number of relative measurements were carried out but

normalization of the data to the absolute scale encounters problems and no cross section data have been reported by this method.

The generation of integral cross sections from differential measurements will be discussed below.

3.4. Momentum transfer cross sections

Elastic momentum transfer cross sections at low energies (below a few eV) are commonly and most accurately determined by the electron swarm technique. Beam/beam experiments which yield both elastic and inelastic momentum transfer cross sections are mandatory at higher energies.

In the swarm method a stream of electrons enters the diffusion chamber and travels through the gas under the influence of a uniform electric field. The swarm proceeds to the anode, undergoing multiple collisions with the gas and spreading by diffusion. Elastic and inelastic collisions with the gas manifest themselves by affecting the Boltzmann collision integral, thus the macroscopic transport properties. The cross sections are parameters in the Boltzmann equations. If cross sections are known their validity and consistency can be checked by comparing experimentally measured and calculated transport properties and electron distribution functions. At low electron energies where only a few collision channels are open this procedure can yield reliable and accurate cross sections. At higher energies where many channels are open, ambiguities develop in fitting the observed transport properties to the theoretical expressions, and therefore in determination of cross sections. Recent efforts to improve the reliability and extend the range of applicability of the swarm technique are concerned with more accurate solutions of the Boltzmann equation. For a thorough discussion of this technique see ref. [37].

Compilation and summary of momentum transfer data have been published by Itikawa [38], Spencer and Phelps [39] and M. Hayashi [8].

The swarm and the beam/beam measurements cover complementary energy ranges and it is important to compare the cross section data obtained by these two methods in the overlapping energy range.

3.5. Differential cross sections

3.5.1. Instrumentation

The major components of a typical electron impact spectrometer are the electron gun, target gas source, and electron detector, all enclosed in a vacuum chamber. To make background scattering negligible the pressure in the vacuum chamber should be of about 10^{-6} Torr or lower while the density in the target beam is about 10^{13} molecules/cm^3 (corresponding to an equivalent pressure of a few times 10^{-4} Torr). The magnetic field in the chamber has to be reduced to below a few milligauss and the entire electron path has to be shielded from electric and magnetic fields.

The target molecular beam is generated by effusing the gas through an orifice, tube or capillary array. In some cases, secondary beam defining apertures may be used to improve beam collimation. Special beam sources for generating beams of materials with very low vapor pressures at room temperature, and of metastable and free radical species have also been used. The ideal target beam is small in size with a uniformly high density. With this type of beam the scattering geometry is independent of scattering angle and measured scattering intensities are directly proportional to cross sections. The major problem here lies in the determination of molecular density in the target. Static gas targets were widely used in earlier electron impact cross section measurements. The large target size assures good signal levels. The target density is uniform and can be accurately measured through pressure and temperature deter-

minations. One encounters problems, however, in differential cross section measurements because of the change of scattering geometry with angle.

The electron beam is generated by thermionic emission and proper collimation. Electrostatic energy selectors are most commonly used to produce a nearly monoenergetic beam. The electrons are transported from the source to the scattering region by electrostatic lens systems. Similar lens systems and energy selectors are applied in the detector [40]. The scattered electron signal is detected by an electron multiplier which generates ideally a voltage pulse for each electron for counting purposes. To improve signal to noise conditions multi-channel scaling techniques are usually applied.

3.5.2. Relationship between cross section and scattering signal intensity in beam–beam experiments

The first step in obtaining differential cross sections is to record the energy loss spectra at various scattering angles and incident energies. A typical energy loss spectrum for N_2 is shown in fig. 1. The location of spectral features characterizes the energy level scheme of the target, and the scattering intensities are related to corresponding cross sections.

A typical geometry for an electron-beam molecular-beam experiment is shown in fig. 2. The molecular beam is crossed by the electron beam at 90°. The intersection of these two beams within the

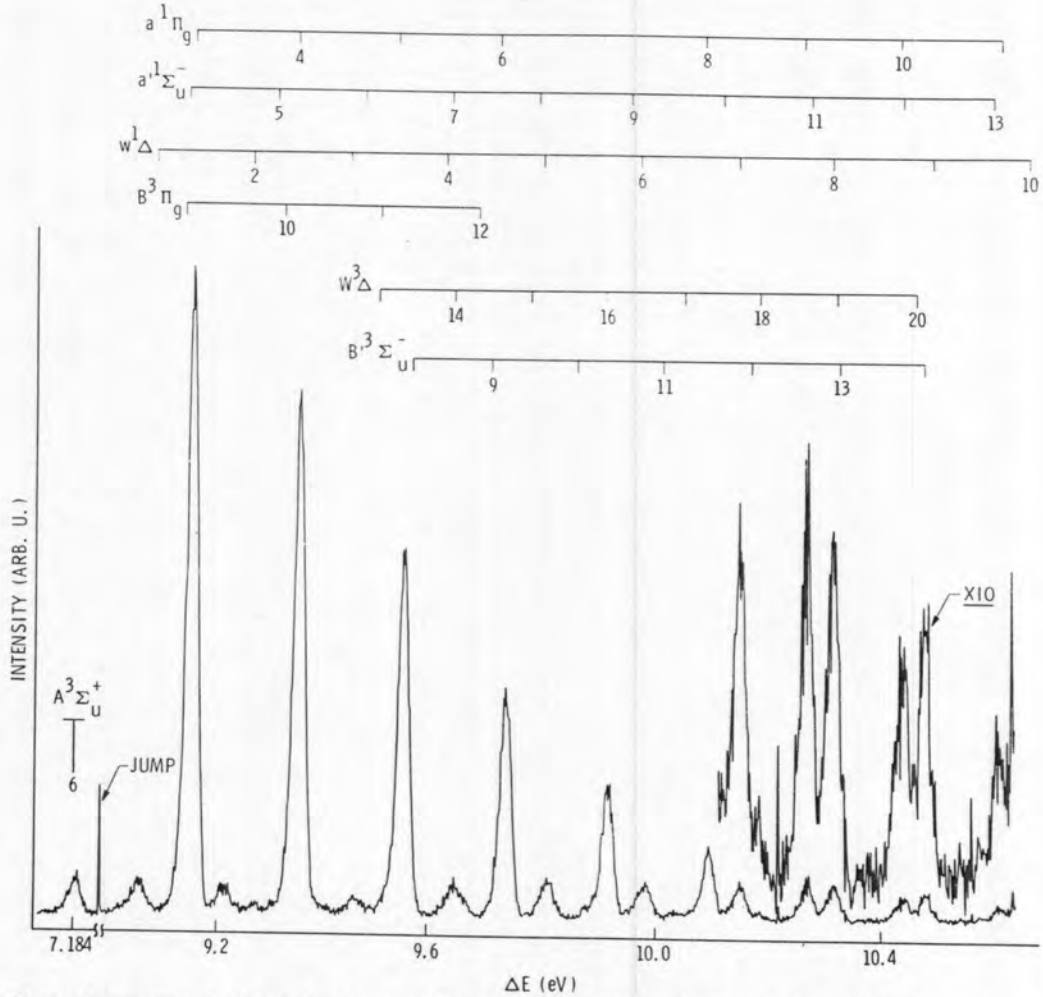

Fig. 1. Energy-loss spectrum for N_2 at 15.5 eV impact energy and 20° scattering angle. (D.F. Register and S. Trajmar, unpublished.)

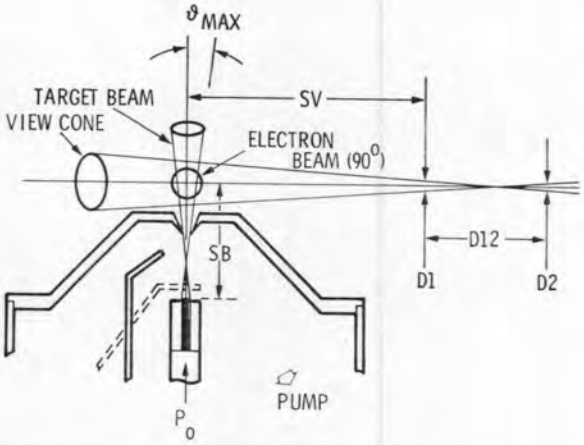

Fig. 2. Scattering geometry for differential cross section measurement. The maximum divergence angle (ϑ_{max}) of the geometrically collimated gas beam. the geometrical parameters (SV, SB, D12) are indicated. D1 and D2 refer to the diameter of the detector apertures.

view cone of the detector represents the scattering volume from which the scattered electron signal is collected. The general relationship between the scattered signal (I) and the corresponding cross section involves integration over the scattering volume and solid angle of detection. It involves also the target and electron beam densities, distribution functions, and the instrument function. The extraction of the desired cross section from this expression is complicated. The situation becomes more manageable if a differential cross section, which is averaged over the energy and angular resolution of the apparatus, is lifted out of the integral. Then the relationship for scattering process n becomes:

$$I_n(E_0, \theta) = \mathrm{DCS}_n(E_0, \theta)\, V_{\mathrm{eff}}(\theta)\,. \tag{6}$$

Here all the flux, geometrical and instrumental functions are included in $V_{\mathrm{eff}}(\theta)$, which is obtained by the appropriate integrations. The values of the effective scattering volume (or "path length") can be calculated at each impact energy as a function of scattering angle. Therefore, absolute values of the differential cross section can, in principle, be obtained. It is, however, an easier and more reliable procedure to calculate relative path length corrections and normalize the relative cross sections by other methods. (For detailed discussion see ref. [41].)

3.6. Normalization procedures

In principle, one can obtain absolute cross sections for a given process by measuring the appropriate signal, and all parameters relating that signal to the desired cross section as discussed above. This procedure is generally followed for measuring total scattering and ionization cross sections, optical excitation functions and sometimes for differential cross sections especially at high impact energies. This procedure becomes difficult, time consuming and inaccurate for determining differential cross sections at low and intermediate impact energies. For this reason and because a large effort has been directed in recent years toward measuring differential cross sections at low and intermediate energies, we discuss the normalization procedures for this case in more detail.

The phase-shift analysis method which is commonly applied to elastic scattering by atoms at low impact energies (see e.g. ref. [10]) is not applicable to molecules. Inelastic channels (rotational-vibrational excitation) open at very low energies, the non-spherical character of the target

complicates the analysis, a large number of partial waves are needed because of the polarizability, etc.

A more reliable approach to normalization utilizes total electron scattering, excitation and ionization cross sections. Total cross sections can be measured with about 1–3% accuracy and are becoming available for a large number of molecules. The integral elastic cross section σ_{ELAS} is obtained from the expression

$$\sigma_{ELAS} = \sigma_T - \sigma_{ION} - \sigma_{EXC} \tag{7}$$

and is utilized to normalize relative experimental elastic data, which in turn can be used to normalize inelastic data. The ionization cross section σ_{ION} is usually available with an accuracy of about 5%. The total excitation cross section (σ_{EXC}) is usually not available at low energies, but can be estimated with acceptable accuracy. At higher impact energies, σ_{EXC} is comparable to the other quantities in eq. (7) and the estimation accuracy will greatly influence the calibration.

Optical excitation functions have been measured for several molecules. These apparent excitation cross sections can be corrected for cascade effects to some level of accuracy, and used as direct integral-excitation cross sections for approximate normalization of relative DCS data. In each case a careful assessment of possible errors has to be made. The apparent excitation cross sections themselves, without cascade corrections, are useful in modeling atmospheric and planetary emission phenomena such as dayglow and auroras.

High-energy, low-angle electron impact measurements have been used to generate optical f-values by extrapolation of the generalized oscillator strength $F^G(K)$ to zero momentum transfer. One can, however, reverse the procedure and utilize available optical f-values to normalize relative generalized oscillator strengths which were obtained from and are equivalent to the experimentally measured DCS. The main difficulty with this procedure is the requirement of extrapolating the generalized oscillator strength (obtained from the relative DCS) to zero momentum transfer. This is usually performed by plotting the relative $F^G(K)$ against K^2 and observing the small K^2 tendency in the curve. For an inelastic process the limit of zero momentum transfer is unphysical since even zero degree scattering corresponds to a non-zero K value. The other problem is that the most important points in this extrapolation are the low angle DCS points which are experimentally the most uncertain. This uncertainty in the low angle data arises mainly from the difficulties of accurate effective path length corrections at low scattering angles and the rapid change of DCS with angle.

In principle theoretical calculations could also serve as a basis for normalizing relative cross section data. In general, however, the theoretical calculations have not been accurate enough for this purpose. Lately for simple species (H, He) highly accurate theoretical results have been obtained which certainly satisfy the criteria for a standard. Similar developments for the lighter molecular species can be expected in the future. One should consider, however, the limitations of the theoretical model. A model may well describe a process at a particular energy or angular range but not in other ranges, and may be reliable for certain types of transitions but not for others. At the present time, theoretical calculations are most useful in cases where it is difficult to obtain quantitative experimental data (for corrosive materials, free radical or excited species, etc.) but have to be checked against experiment in at least a few cases.

A more practical and reliable way of obtaining absolute elastic cross sections is by normalizing the relative data (available usually only at a fixed impact energy in the same arbitrary units) to a secondary standard [9, 42]. The natural choice for this standard is the He elastic cross section. It is known accurately over a wide energy and angular range and He is experimentally easy to handle. In this

approach, an unknown molecular elastic differential cross section may be determined by comparing the electron scattering intensities for He and for the molecule in question. In such measurements the absolute electron and molecular beam densities or distributions need not be known. The desired elastic cross section may be determined by knowing relative target densities for the two gases provided that the electron beam flux and its spatial and energy distribution, the detector efficiency, and the target beam flux distribution *remain the same for both gases* during the measurement. Under these conditions, effective path length corrections for the two gases will cancel to a very good approximation and the scattering intensity ratios may be related to the DCS ratios as:

$$\frac{I(E_0, \theta)_X}{I(E_0, \theta)_{He}} = \frac{\mathrm{DCS}(E_0, \theta)_X \, \rho_{He}}{\mathrm{DCS}(E_0, \theta)_{He} \, \rho_X} \tag{8}$$

where ρ represents the target density of He or the gas X under study. This expression then yields the DCS for the gas under study for known $\mathrm{DCS}(E_0, \theta)_{He}$. A detailed discussion of this question is found in ref. [9].

3.7. Experimental uncertainties, error estimation

Perhaps as significant as the reported cross section is the accuracy which may be associated with that cross section. It is imperative, therefore, that error estimates associated with experimental results be as realistic as possible. In this subsection we will attempt to point out some of the experimental uncertainties associated with cross section measurements.

In any measurement it must be assumed that there is an underlying absolute parameter (in this case the cross section) which is obscured by the apparatus and personnel attempting to measure this parameter. In this sense, those experiments are usually most accurate which require the minimum number of operations and personnel to deduce the desired value. This does not imply that the best experiments are technically unsophisticated. On the contrary, experiments which are the simplest to interpret are often the most elegant. For instance, crossed-beam differential cross section measurements are usually performed under conditions where significant path length and background corrections need to be applied. Measurements performed with chopped collimated beams will certainly provide more precise angular distributions, yet the technology and cost are considerably greater.

Experimental uncertainties may arise from either systematic or random sources. Systematic errors arise due to known or unknown corrections which, if not applied, give an overall bias to the results. Random errors arise from the statistical nature of any measurement and may be reduced by repeating the experiment a large number of times. To cite the example mentioned previously, an effective path length correction may be considered a systematic error. If this geometry correction is not included in the analysis, the 'correct' angular distribution will *never* be obtained from such measurements. The count rate in such an experiment represents a random error whose statistical uncertainty is $1/\sqrt{N}$ where N is the accumulated number of counts. This error may be reduced by either increasing count rate or accumulation time. The background count rate, on the other hand, represents a systematic error with an associated statistical uncertainty.

In many experiments, most systematic errors may be either avoided or corrected. Temperature dependence of pressure readings, temporal drift in electron optics, timing calibrations in coincidence measurements, geometry and background corrections in crossed beam experiments and path length corrections in time-of-flight measurements are all examples of correctable systematic errors. As these

corrections are also subject to statistical uncertainties, it is clearly desirable to reduce the magnitude of the systematic effects within the constraint of retaining sufficient count rates. Once systematic corrections have been applied, one is still left with a lingering doubt of unknown systematic errors. This doubt can only be quieted by comparing the results against independent measurements which claim comparable accuracy.

Once measurement errors have been reduced to statistical uncertainties, standard techniques for data analysis as described in most elementary statistics texts [43, 44] may be employed. A conventional analysis defines the mean value of a measurement and its standard deviation. Alternatively, errors in a measurement may be calculated as the root mean square (RMS) value of all contributing errors. For instance, if a single measurement is made in an electron–molecule scattering experiment, the observed count rate may be a function of the incident electron current, pressure in the scattering chamber, flow rate of the molecular gas, detection efficiency, noise level in the external circuitry and several other parameters. Each of these parameters has an associated error, y_i (usually expressed as a percent) which, in the absence of systematic effects, contributes to the total measurement error as

$$\bar{y} = \sqrt{\sum_i y_i^2}\,. \tag{9}$$

If data must be normalized to some external reference which is independent of the experiment under study, errors associated with this normalization must also be considered. In a relative flow measurement, for instance, the error associated with the data must be combined with estimated errors in the calibration standard to arrive at a total probable error.

In certain special cases, a set of data points X_j with associated errors for each point δ_j may represent a process whose behavior as a function of the experimental variables is presumed to be well known. Under these conditions it is further possible to define the χ^2 value for this distribution as:

$$\chi^2 = \frac{1}{M-P}\sum_{j=1}^{M}\left(\frac{f_j - \bar{X}_j^2}{\delta_j}\right) \tag{10}$$

where M is the number of data points, f_j is the function which is presumed to represent the jth data point ($\bar{X}_j$) and P is the number of independent variables available in f_j. Such a situation arises, for instance, in the elastic angular distribution for low energy electron–atom scattering which may be represented by a phase shift expression for f_j. The phase shifts are independent variables and may be determined by either a variational analysis [9] or a grid search technique [43]. In either case, the criterion is the minimization of χ^2. If errors in the data are purely statistical and if the functional form of f_j truly represents $\bar{X}_j$, then $\chi^2_{\min}$ is expected to be unity. A careful analysis of the dependence of χ^2 on the variables can then lead to an estimate of the reliability of the data set [45–47].

3.8. Study of superexcited states (innershell and multi-electron excitations)

When the excitation energy of a molecular state is greater than the lowest ionization potential, we are dealing with a superexcited state. Such states are produced in electron impact processes by exciting innershell electrons or more than one (valence and/or innershell) electron at the same time to higher molecular orbitals. The decay of the superexcited state can proceed by photon emission, electron ejection (autoionization), or molecular dissociation.

There has been a great deal of interest recently in innershell excitation processes [15, 48–51]. From the point of view of resolution the electron impact technique becomes competitive with optical techniques at high energy losses corresponding to innershell excitations [15, 51]. In addition, it is a much more convenient and inexpensive approach than the use of UV and X-ray sources or synchrotrons. Energy loss spectroscopy has demonstrated that a considerable fraction of the oscillator strength is associated with such transitions. Investigations so far have been mainly concerned with spectroscopic information and no absolute cross section data exist for innershell processes.

3.9. Coincidence measurements

Coincidence techniques in electron impact studies have recently seen increased application to cross section measurements. The general scope of these experiments may be roughly divided into two areas: electron–electron (or ion) and electron–photon coincidence measurements. We are concerned here only with the latter case, where photons arising from the decay of a particular electron-impact excited molecular level are detected in delayed coincidence with the inelastic electron.

Electron–photon coincidence measurements have seen extensive applications in atomic collision phenomena [18, 52, 53]. These experiments attempt to study fundamental relationships among the magnetic sublevel populations in electron-impact excitation of a particular atomic energy level and can generate scattering amplitudes and cross sections for individual magnetic sublevel excitations by electron impact. The basic theory of angular correlations [54, 55] has recently been extended to molecules [56]. For the molecular case, however, the experimental situation is complicated by the rotational and vibrational structures. Preliminary work on H_2 electron–photon coincidence measurements has been reported by Malcolm and McConkey [52, 57] and has recently been reviewed by McConkey [52]. No cross section data are available as yet.

One little-used capability of the electron–photon coincidence technique lies in separating cross sections for two very close-lying, or even degenerate, energy levels in an atom or molecule. While the electron energy channel contains unresolved inelastic scattering, one may rely on coincident photon emissions to measure cross sections. Applications of this method have been made to He [58, 59] and to the hydrogen atom [60].

3.10. Electron scattering in laser fields

The availability of high intensity, narrow frequency-band lasers has opened up new possibilities for electron scattering studies. These studies can yield information on the interaction of molecules, electrons and photons which could not be obtained previously and which is of practical importance in the field of laser plasma interactions. The general treatment of the problem of electron scattering in electromagnetic fields and the interpretation of experimental observations is quite complex. To the usual problem of treating the interaction of an electron with an N-electron molecule additional difficulties arise when the laser field is introduced: (1) the energy states of the molecule may be modified (dressed states); (2) multi-photon excitation and ionization of the molecule may take place; (3) multi-photon free–free electron transitions (bremsstrahlung, inverse bremsstrahlung) can occur; and (4) the close dynamics of the scattering process may be affected by n-photon transitions in the temporary $(N+1)$-electron molecular ion. Both theoretical and experimental efforts in this area have been limited mainly to atoms, and to special situations where one particular interaction dominates and others can be neglected or treated as perturbations. The experimental investigations carried out so far fall into two

categories: (1) electron scattering by laser excited species, and (2) free–free radiative transitions.

In the first category low-power tunable dye lasers are used to excite the target species to specific states and the electron scattering by these excited species is studied. In this case for the photon interaction the resonant excitation of the target is the dominant process. The interaction of the free electron with the field and the distortion of the energy level scheme of the target can be neglected. Total cross section measurements on laser excited Na have been reported by Bhaskar et al. [61] and Jaduszliver et al. [62] and differential cross sections for laser excited Ba by Register et al. [63]. The technique has not been applied to molecular species mainly due to the difficulty of producing tunable lasers in the UV or IR regions.

When the laser is operated in the single frequency mode, individual isotopes and hyperfine levels can be pumped. With the selection of proper polarization of the laser light, the population of the magnetic sublevels can also be controlled. Thus a polarized target (aligned and/or oriented) can be prepared for electron scattering measurements. Not only cross sections for individual magnetic sublevel excitations but also scattering amplitudes can be obtained from measuring superelastic scattering intensities. The excitation with polarized light and subsequent measurement of superelastic electron scattering intensities is equivalent to the time inverse electron–photon coincidence measurement and has been discussed for atomic species in general by Hertel and Stoll [64]. Application of this technique to molecules has not yet been reported.

The second category of experiments is concerned with free–free radiative transitions in strong electromagnetic fields. Here the photon energy is chosen to be far away from resonance (even for multi-photon processes) and the dominant interaction of the photon field is with the free electron. The present situation in this particular area has been summarized by Gavrila and Van der Wiel [65]. Elastic scattering by Ar and H_2 in a high-power pulsed CO_2 laser field has been studied by Weingartshofer et al. [66]. In addition to the regular elastic scattering feature, features appear on both sides of the elastic peak. These additional features are separated by an energy corresponding to a laser photon and represent induced and inverse bremsstrahlung. The overall integrated intensity of these features is equal to the elastic scattering intensity without the laser field (assuming identical scattering conditions) and therefore cross sections for the individual free–free electron transitions can be obtained through the calibration of the field free elastic scattering [67]. In these experiments, based on present day theories, the nature of the target plays no role and scattering by atoms or molecules should make no difference. Experimental verification of this prediction remains to be seen.

An interesting way of studying resonances in the free–free transition channels has been pointed out by Jung and Kruger [68] and Jung and Taylor [69]. In this scheme the non-resonant background scattering is eliminated by the proper choice of scattering geometry and laser light polarization and the signal originates only from resonance scattering. Thus instead of the resonance interference (Beutler–Fano) profile, one observes regular peaks at resonances.

3.11. Electron collision measurements at high energies: Generation of optical data

Experimental techniques for cross section measurements at high impact energies ($E_0 > 100$ eV) are similar to those described here for lower impact energies. The control and focusing of the electron beam is, however, more easily achieved at higher energies because influences of space charge, electric and magnetic fields, and surface effects are greatly diminished. The scattering geometry and experimental parameters can be accurately determined and absolute cross sections can be obtained directly from scattered signal intensities. One may face some problems associated with secondary electrons generated by high-energy electron–surface collisions and this has to be kept in mind.

Geiger and coworkers (see for example ref. [70]) generated energy-loss spectra of molecules with about 10 meV energy resolution using electrons of around 25 keV energy and Wien filters [12, 71] as energy selectors and analyzers. Their spectra represent relative optical excitation cross sections. No attempt was made to extract absolute cross section data from their measurements. Bromberg made accurate elastic differential cross section measurements at a few hundred eV kinetic energies and low scattering angles utilizing a static gas target, unselected electron beam and an electrostatic analyzer [72]. He experimentally determined all parameters relating the measured signal to the cross section and produced absolute cross sections with a few percent accuracy. A large number of quantitative fast electron impact experiments have been carried out with the aim of obtaining optical oscillator strengths. The pioneering work in developing the technique and instrumentation was carried out by Lassettre and coworkers [73] and Bromberg [72]. Very recently Brion and coworkers and Van der Wiel and coworkers have applied elegant coincidence techniques to obtain quantitative photoionization, photofragmentation and photofluorescence cross sections by high-energy electron impact methods. Normalization of the experimental data to the absolute scale was achieved in some of these experiments by application of the Thomas–Kuhn–Reiche sum rule. A comprehensive review of these techniques and results are given by Brion and Hamnett [13].

In generating optical data from high energy electron impact measurements, the fact is utilized that these electrons behave like pseudo-photons and that the generalized oscillator strength obtained from electron impact cross section data converges to the dipole oscillator strength (or photoabsorption cross section) in the zero momentum transfer limit. For detailed discussion of the underlying principles the reader is referred to refs. [74 and 75]. Here we only briefly state the basic philosophy.

Bethe [76] defined the generalized oscillator strength for electron impact processes as:

$$f_n^{\mathrm{G}}(K) = \frac{E}{2}\frac{k_{\mathrm{i}}}{k_{\mathrm{f}}} K^2 \, \mathrm{DCS}_n^{\mathrm{B}}(K) \tag{15}$$

where $\mathrm{DCS}_n^{\mathrm{B}}(K)$ is the differential cross section for process n in the Born approximation as a function of momentum transfer, K. E is the energy loss and k_{i} and k_{f} are the magnitude of the electron momentum before and after scattering respectively. It is easily shown that in the zero momentum transfer limit $f_n^{\mathrm{G}}(K)$ becomes equal to the optical f-value, f_n^0. Lassettre et al. [77] extended the use of eq. (15) to cases where the Born approximation does not hold and defined the apparent generalized oscillator strength, $f_n^{\mathrm{AG}}(K)$ by the same relationship. They were able to show that $f_n^{\mathrm{AG}}(K)$ also converges to the optical f-value in the zero momentum transfer limit.

In practice one either makes several measurements at various angles and energies, plots the $f_n^{\mathrm{AG}}(K)$ values as a function of K^2, and extrapolates the resulting curve to zero momentum transfer, or carries out the experiment at a sufficiently high impact energy and low (preferably zero) scattering angle such that the results correspond to the optical limit.

In recent years, high energy electrons have also been used to investigate innershell excitation processes as pointed out above.

4. Summary of experimental data

4.1. H_2

Electron H_2 scattering processes have been extensively studied and these studies served as testing ground for theoretical models and approximations. From a practical point of view these processes are of

importance in thyratron switches, planetary ionospheres, and interstellar media. In general cross section measurements have been carried out for a large variety of electron impact processes but very limited amount of information is available on the electron impact excitation of the electronic states of H_2. This is due to the fact that the vibrational manifolds of the electronic states heavily overlap and the interpretation and unfolding of the energy-loss spectra are difficult.

Total scattering cross sections

Total electron scattering cross sections for H_2 have been measured recently by Ferch et al. [78], Dalba et al. [79], van Wingerden et al. [80], Jones and Bonham [81] and Hoffman et al. [82]. In table 1 the energy ranges covered and methods used by these investigators are given and cross section data are summarized in table 2. (For a compilation of the earlier data see refs. [1 and 5].) Among the cross sections which can be measured the total cross section is the most reliable. As shown in table 2, various measurements for H_2 agree to within a few percent in the entire energy range from a few hundredths of an eV to a few thousand eV.

In fig. 3 the total cross sections [78–83] are shown together with elastic scattering [42, 84, 85], rotational [84, 86, 87], vibrational [86, 88] and electronic excitation [80], total ionization [80, 89] and momentum transfer [42, 86, 87] cross sections. This figure serves as a guide to the general magnitude and behavior of cross sections associated with various electron impact processes. The picture is, however, incomplete. Cross sections in certain energy ranges are not available, only fragmentary information exists for electronic excitation, dissociation and ionization processes, and discrepancies exist among measurements related to the same process. This discrepancy usually *increases* as the measurements aim for finer details of the collision process. Since even fragmentary data on various electronic excitation processes would overcrowd the figure, only the $B^1\Sigma_u^+$ electronic state excitation cross section below 100 eV impact energy and the overall electronic excitation curve above 100 eV are shown.

Elastic scattering cross sections

Differential elastic cross section measurements have been carried out by Linder and Schmidt [84], Lloyd et al. [90], Srivastava et al. [42], Weingartshofer et al. [91], Fink et al. [92], van Wingerden et al. [84], and Shyn and Sharp [93]. In table 3 the energy and angular ranges, method of normalization, and estimated errors are indicated. The contribution from rotational excitation was separated from elastic scattering only in the case of Linder and Schmidt.

The DCS data below 100 eV impact energy are collected in table 4. Since it is difficult to measure cross sections at low impact energies, these data should in general be considered less reliable than those at intermediate and high energies. In all three cases in table 4 relative scattering intensities as a function of the angle were measured at fixed impact energies. The intensities were transformed to relative cross sections and normalized. Linder and Schmidt extrapolated their distributions to 0° and 180° for elastic and all open inelastic channels and integrated to get relative integral cross sections. The sum of the relative integral cross sections was then normalized to the total scattering cross section values of Golden et al. [83]. Srivastava et al. [42] normalized their data against the He elastic cross section data of McConkey and Preston [94]. More accurate He elastic cross sections have recently become available (Register et al. [10]). These were used to renormalize the data of Srivastava et al. [42] and results are given in table 4. The average correction factor which had to be applied to the original data of Srivastava et al. was about 1.23 which agrees with the factor suggested by van Wingerden et al. [80]. Shyn and Sharp [93] normalized their relative H_2 DCS data at 10 eV against He which in turn they normalized to the theoretical calculation of LaBahn and Callaway [96]. In their measurements the scattered signal

Table 2a
Total electron scattering cross sections for H_2, 10^{-16} cm^2 units. (From Ferch et al., 1980, ref. [78]; Dalba et al., 1980, ref. [79]; van Wingerden et al., 1980, ref. [80]; and Jones and Bonham, 1981, ref. [81].)

	Reference				Reference			Reference		
E_0(eV)	78[a]	79	81	E_0(eV)	79	81	E_0(eV)	80 meas.	80 semi-emp.	81
0.020	7.41	–	–	3.0	–	16.2	13.0	–	–	8.62
0.030	7.77	–	–	3.2	–	16.2	13.5	–	–	8.39
0.040	8.05	–	–	3.4	–	16.1	14.0	–	–	8.15
0.060	8.52	–	–	3.5	16.55	–	14.5	–	–	7.84
0.080	8.79	–	–	3.6	–	16.2	15.0	–	–	7.75
0.100	9.19	–	–	3.8	–	16.0	16.0	–	–	7.39
0.150	9.75	–	–	4.0	–	15.7	17.0	–	–	6.94
0.200	10.05	–	–	4.2	–	15.8	18.0	–	–	6.71
0.250	10.45	–	–	4.4	–	15.6	19.0	–	–	6.44
0.300	10.71	9.27	–	4.5	15.79	–	20.0	–	6.21	6.23
0.350	10.95	–	–	4.6	–	15.3	21.0	–	–	5.96
0.400	11.21	–	15.1	4.8	–	15.1	22.0	–	–	5.74
0.450	11.36	–	–	5.0	–	14.9	23.0	–	–	5.69
0.500	11.62	–	–	5.5	–	14.4	24.0	–	–	5.49
0.6	(11.9)	11.56	11.9	6.0	14.22	13.9	25.0	5.75	–	5.29
0.8	(12.4)	–	12.4	6.5	–	13.4	26.0	–	–	5.18
1.0	(12.8)	14.00	13.1	7.0	–	13.0	28.0	–	–	4.89
1.2	(13.2)	–	13.6	7.5	–	12.4	30.0	4.89	4.58	4.68
1.4	(13.5)	–	14.0	8.0	12.35	12.0	32.0	–	–	4.43
1.5	(13.7)	15.37	–	8.5	–	11.4	34.0	–	–	4.26
1.6	–	–	14.7	9.0	–	11.1	35.0	4.44	–	–
1.8	–	–	15.0	9.5	–	10.8	36.0	–	–	4.17
2.0	–	16.16	15.4	10.0	10.78	10.3	38.0	–	–	4.16
2.2	–	–	15.7	10.5	–	10.1	40.0	4.00	4.05	3.76
2.4	–	–	15.8	11.0	–	9.68	45.0	3.86	–	3.59
2.5	–	16.16	–	11.5	–	9.40	50.0	3.62	–	3.29
2.6	–	–	15.9	12.0	–	9.11	60.0	–	3.43	–
2.8	–	–	16.1	12.5	–	8.86	70.0	–	–	–
							75.0	–	2.92	–

[a]Numbers in parentheses were obtained from fig. 9 of ref. [78].

Table 2b
Total electron scattering cross sections for H_2, 10^{-16} cm^2 units. (From Hoffman et al., 1982, ref. [82].)

E(eV)		E(eV)	
2.0	17.0 ± 0.1	35	4.66 ± 0.03
2.9	17.3 ± 0.2	40	4.30 ± 0.01
3.9	17.6 ± 0.13	45	3.98 ± 0.01
4.9	15.6 ± 0.07	50	3.66 ± 0.09
6.8	14.3 ± 0.07	75	2.92 ± 0.02
8.8	12.2 ± 0.09	100	2.56 ± 0.04
10.8	10.56 ± 0.04	150	1.98 ± 0.01
12.9	9.48 ± 0.03	200	1.69 ± 0.03
14.9	8.48 ± 0.02	300	1.27 ± 0.03
20	6.72 ± 0.04	400	1.04 ± 0.03
25	5.79 ± 0.04	500	0.87 ± 0.02
30	4.92 ± 0.05		

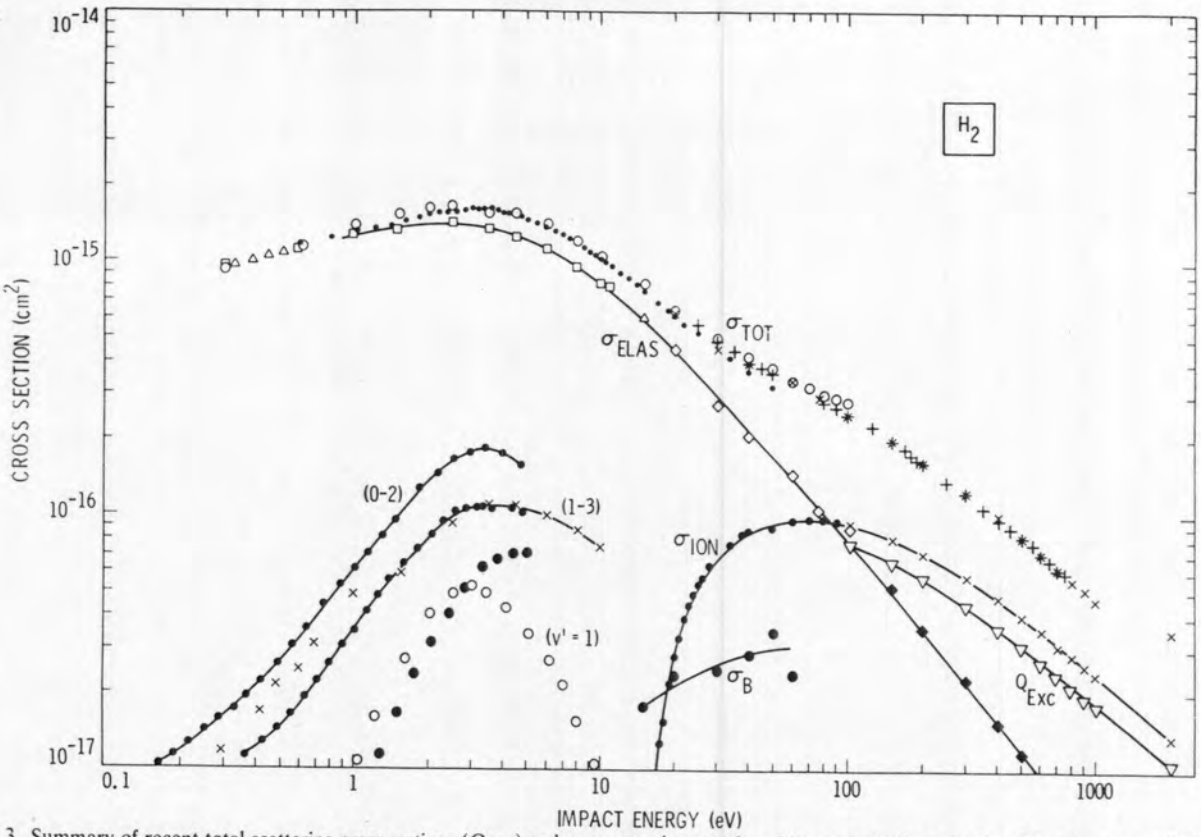

Fig. 3. Summary of recent total scattering cross sections (Q_{TOT}) and representative samples of integral elastic scattering (Q_{ELAS}), rotational [$(0\rightarrow 2)$, $(1\rightarrow 3)$], vibrational ($v' = 1$), overall electronic excitation (Q_{EXC}), and total ionization cross sections (Q_{ION}). The symbols are as follows. Total scattering cross section: △, Golden et al. [83]; □, Ferch et al. [78]; ○, Dalba et al. [79]; +, van Wingerden et al. [80]; ×, van Wingerden et al. (semi-empirical) [80]; ●, Jones and Bonham [81]. Elastic scattering: □, Linder and Schmidt [84]; ◆, van Wingerden (semi-empirical) [80]; ◇, Srivastava et al. [42] (multiplied by 1.23, see text). Rotational excitation $(0\rightarrow 2)$: ●, Gibson [86]; Crompton et al. [87]. Rotational excitation $(1\rightarrow 3)$: ●, Gibson [86]; ×, Linder and Schmidt [84]. Vibrational excitation ($v' = 1$): ●, Gibson [86]; ○, Ehrhardt et al. [88]; □, Linder and Schmidt [84]. Overall electronic excitation: ▽, van Wingerden et al. [80]. Total ionization: ●, Rapp and Englander-Golden [89]; ×, van Wingerden et al. [80]. The symbols ● and the curve indicated as σ_B represent the excitation cross section for the $B^1\Sigma_u^+$ state from Srivastava and Jensen [109].

Table 3
Summary of elastic cross section measurements for H_2

Reference	Energy range (eV) Angular range (deg)	Method of normalization	Error limits
Linder and Schmidt 1971, ref. [84]	0.6–10.8 20–120°	to total scattering cross section of ref. [83]	(9%)
Lloyd et al. 1974, ref. [90]	100 and 200 20–130°	to Born theory at 60°	–
Lloyd et al. 1974, ref. [90]	30 and 50 20–130°	to Born theory at 60°	–
Srivastava et al. 1975, ref. [42]	3–75 20–135°	against He elastic of ref. [94]	15%
Fink et al. 1975, ref. [92]	100–1000 3–130°	to theory at 90°	–
van Wingerden et al. 1977, ref. [85]	100–2000 5–50°	against N_2 elastic of ref. [95]	7%
Shyn and Sharp 1981, ref. [93]	2–200 6–156°	against He elastic of ref. [96]	13%
Weingartshofer et al. 1970, ref. [91]	11–13 20°, 50° and 110°	to total scattering cross section of ref. [83]	20%

Table 4
Differential elastic scattering cross sections for H_2 below 100 eV impact energies[a]

A. Linder and Schmidt 1971, ref. [84] (10^{-16} cm^2/sr units)

Scattering angle (Deg)	Collision energy [eV]									
	0.6	1.0	1.5	2.5	3.5	4.5	6.0	8.0	10.0	10.8
20	0.39	0.46	0.61	1.35	1.86	2.24	2.49	2.60	2.61	2.64
30	0.42	0.46	0.57	1.15	1.57	1.83	2.02	2.10	1.99	2.05
40	0.47	0.49	0.57	0.97	1.29	1.49	1.61	1.61	1.44	1.52
50	0.53	0.55	0.60	0.84	1.09	1.22	1.28	1.25	1.11	1.12
60	0.61	0.63	0.66	0.79	0.92	0.97	1.00	0.96	0.80	0.83
70	0.72	0.75	0.75	0.78	0.82	0.81	0.80	0.73	0.61	0.59
80	0.82	0.87	0.89	0.82	0.78	0.73	0.66	0.57	0.45	0.44
90	0.93	0.99	1.03	0.92	0.79	0.70	0.57	0.46	0.35	0.34
100	1.01	1.09	1.17	1.02	0.84	0.70	0.52	0.40	0.28	0.27
120	1.14	1.28	1.44	1.33	1.03	0.84	0.57	0.35	0.23	0.20

[a]Rotational excitation is not included in these data.

B. Srivastava et al. 1975, ref. [42] (10^{-16} cm^2/sr units)

Scattering angle (Deg)	E_0(eV)									
	3	5	7	10	15	20	30	40	60	75
[0]	1.67	2.68	2.85	2.62	2.91	2.50	1.90	1.88	1.19	1.23
[10]	1.57	2.43	2.60	2.36	2.50	2.09	1.51	1.40	0.92	0.84
20	1.48	2.15	2.18	2.06	2.07	1.67	1.13	0.987	0.648	0.502
	(6.43)	(8.21)	(7.09)	(5.34)	(4.41)	(3.22)	(2.17)	(2.03)	(1.66)	(1.53)
30	1.34	1.86	1.80	1.65	1.55	1.16	0.723	0.528	0.322	0.204
	(5.28)	(6.95)	(6.14)	(4.82)	(3.94)	(2.79)	(1.86)	(1.57)	(1.32)	(1.06)
40	1.20	1.56	1.45	1.29	0.08	0.791	0.444	0.304	0.171	0.098
	(4.27)	(5.58)	(5.04)	(4.13)	(3.21)	(2.37)	(1.54)	(1.29)	(1.08)	(0.83)
50	1.09	1.37	1.32	1.09	0.806	0.569	0.287	0.179	0.095	0.051
	(3.47)	(4.61)	(4.55)	(3.70)	(2.76)	(2.08)	(1.32)	(1.06)	(0.89)	(0.65)
70	0.911	0.979	0.815	0.682	0.403	0.276	0.11	0.069	0.033	0.018
	(2.33)	(2.75)	(2.54)	(2.36)	(1.63)	(1.35)	(0.84)	(0.71)	(0.56)	(0.45)
90	0.929	0.788	0.629	0.427	0.23	0.13	0.061	0.033	0.016	0.010
	(1.94)	(1.82)	(1.66)	(1.34)	(0.98)	(0.74)	(0.55)	(0.47)	(0.42)	(0.38)
115	1.17	0.828	0.534	0.29	0.12	0.072	0.031	0.018	0.010	0.007
	(1.99)	(1.53)	(1.13)	(0.76)	(0.05)	(0.38)	(0.31)	(0.30)	(0.34)	(0.38)
135	1.45	0.973	0.590	0.27	0.11	0.059	0.024	0.016	0.009	0.006
	(2.18)	(1.57)	(1.08)	(0.63)	(0.39)	(0.29)	(0.23)	(0.27)	(0.34)	(0.37)
[140]	1.58	1.01	0.609	0.28	0.12	0.060	0.023	0.017	0.009	0.006
[150]	1.69	1.11	0.650	0.29	0.12	0.059	0.021	0.017	0.008	0.006
[160]	1.83	1.18	0.685	0.30	0.12	0.060	0.019	0.017	0.008	0.006
[170]	1.95	1.25	0.708	0.32	0.13	0.062	0.018	0.018	0.008	0.006
[180]	2.01	1.31	0.729	0.34	0.14	0.064	0.019	0.019	0.007	0.005

The cross sections in this table were obtained by renormalizing the original data of Srivastava et al. on the basis of the more recent He data [10]. The angles in brackets refer to extrapolated values and the numbers in parentheses are the measured DCS ratios of H_2 versus He.

Table 4 (*Cont.*)

C. Shyn and Sharp 1981, ref. [93] (10^{-18} cm^2/sr units)

Scattering angle (deg)	Collision energy (eV)									
	2	3	5	7	10	15	20	30	40	60
6	–	–	–	–	–	–	–	365.0	342.1	245.5
12	107.6	182.3	336.2	340.3	375.0	384.2	337.6	289.0	232.2	164.1
18	–	–	–	–	–	–	–	199.7	160.1	98.3
24	97.9	155.2	264.4	288.3	290.3	253.0	210.0	137.3	102.5	57.7
30	–	–	–	–	–	–	–	–	–	–
36	92.5	125.1	201.5	210.2	200.5	163.4	126.0	68.6	48.2	25.2
48	78.5	102.7	154.3	157.9	141.5	101.8	75.3	36.7	25.3	11.6
60	67.8	89.7	120.6	117.9	109.0	65.2	44.7	21.5	13.5	5.8
72	64.5	79.0	97.6	88.8	79.4	43.1	27.9	13.0	8.4	3.2
84	73.2	74.7	85.1	70.3	59.7	28.8	18.0	8.4	5.4	1.95
96	88.2	78.5	73.9	62.5	47.0	21.2	12.6	5.9	3.8	1.41
108	109.7	100.4	90.2	61.3	41.8	17.0	9.9	4.6	3.0	1.12
120	140.8	132.8	100.7	66.0	40.9	15.3	8.7	3.9	2.1	1.08
132	170.0	156.3	120.6	74.3	42.4	15.1	8.7	3.9	1.9	1.00
144	205.4	190.6	140.9	89.6	46.0	16.0	8.9	3.9	1.8	1.04
156	237.1	233.6	156.7	97.8	46.9	16.4	9.0	4.0	1.9	1.08
168	269.0	276.7	(164.1)	(102.9)	(47.8)	(17.0)	(9.3)	(4.1)	(2.2)	(1.12)

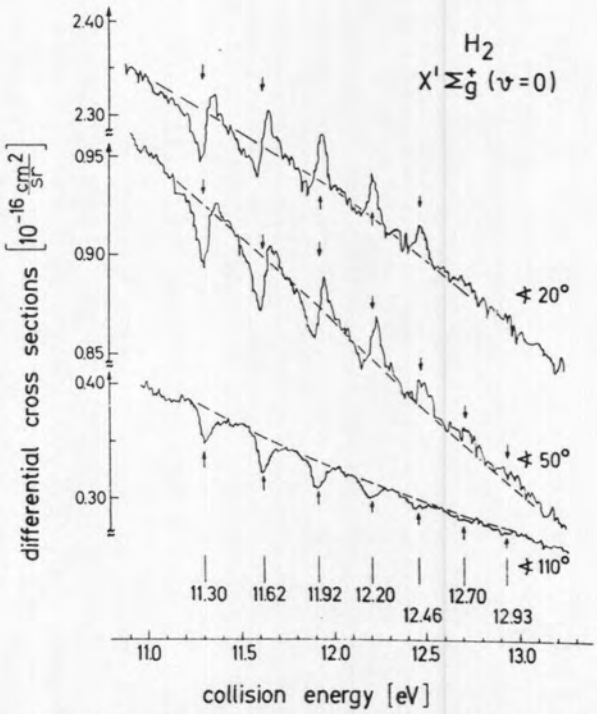

Fig. 4. Energy dependence of the elastic differential cross section for H_2 at three different scattering angles. Note the different absolute scales to the left. Dotted lines were constructed by extrapolation of the low- and high-energy sides of the direct elastic scattering and were included to emphasize the rapid variation of the shapes of the resonance peaks with collision energy and scattering angle. Energy positions of the resonance peaks are shown at the bottom and are indicated with vertical arrows for each curve. (From ref. [91].)

intensity was measured without the use of a lens system in the detector and it was assumed that no change in detector efficiency occurred with impact energy. Weingartshofer et al. [91] measured the energy dependence of the elastic DCS at 20°, 50° and 110° scattering angles in the 11 to 13 eV impact energy range where the cross sections are influenced by sharp resonances. Their results are shown in fig. 4.

Differential elastic cross sections at and above 100 eV impact energies are summarized in table 5. The calibration method for these data is indicated in table 3. In general the elastic cross sections are in agreement to within about 30%.

Linder and Schmidt [84], Srivastava et al. [42], van Wingerden [85], and Shyn and Sharp [93] have extrapolated and integrated their differential cross sections. A summary of their results is given in table 6. The extrapolation introduced errors in addition to those associated with the DCS data but there is a reasonably good agreement among the experimental results.

Table 5
Differential elastic scattering cross sections for H_2 at and above 100 eV impact energies
A. Fink et al. 1975, ref. [92] (10^{-19} cm^2/sr units)

	E_0(eV)				
θ (deg)	100	200	400	600	1000
(0)	(8010)	(3375)	(1590)	(1180)	(1162)
3	5100	2100	1010	730	619
4	4400	1850	890	620	547
5	3780	1540	760	520	438
6	3280	1280	650	450	370
7	2850	1150	570	376	308
8	2450	960	500	320	252
9	2100	810	430	270	203
10	1820	720	380	231	171
12	1404	570	290	164	96
14	1170	440	220	119	60.8
16	950	350	160	79	37.0
18	790	275	116	53	25.0
20	652	221	85	37.6	17.5
24	440	143	47.7	20.6	11.7
28	320	91	28.5	12.6	6.5
32	230	60	18.2	8.5	4.4
36	161	41	12.7	6.1	3.0
40	117	26	9.5	4.7	1.9
45	78	19.5	7.1	3.2	1.15
50	56	14.1	5.1	2.3	0.76
55	41	10.7	3.8	1.53	0.54
60	30.8	8.4	2.8	1.12	0.395
65	24	6.8	2.1	0.82	0.31
70	18.8	5.85	1.57	0.62	0.25
80	13.2	4.07	0.99	0.42	0.16
90	10.2	2.93	0.68	0.30	0.104
100	8.5	2.11	0.50	0.212	0.079
110	7.0	1.61	0.39	0.176	0.063
120	6.1	1.30	0.32	0.141	0.049
130	5.4	1.07	0.27	0.117	0.0395

Table 5 (*Cont.*)

B. van Wingerden et al. 1977, ref. [85] (a_0^2/sr units)

	E_0(eV)								
θ (deg)	100	150	200	300	400	500	700	1000	2000 ($\times 10^2$)
5	9.46	6.52	5.02	3.82	2.59	2.26	1.58	1.44	104
6	8.68	5.61	4.30	3.39	2.26	1.93	1.36	1.21	81.3
7	7.86	4.91	3.75	2.86	1.99	1.66	1.18	0.984	61.4
8	6.98	4.33	3.28	2.42	1.75	1.44	1.00	0.800	44.9
9	6.16	3.84	2.87	2.00	1.55	1.24	0.850	0.642	31.9
10	5.45	3.42	2.51	1.76	1.33	1.08	0.714	0.510	21.7
12	4.39	2.68	1.95	1.34	0.997	0.795	0.492	0.315	10.9
14	3.55	2.11	1.55	1.03	0.743	0.572	0.332	0.195	6.37
15	3.15	1.90	1.39	0.895	0.643	0.480	0.273	0.157	5.23
16	2.79	1.74	1.23	0.791	0.556	0.406	0.225	0.128	4.35
18	2.30	1.44	0.976	0.617	0.403	0.289	0.153	0.0884	3.21
20	1.92	1.17	0.800	0.478	0.303	0.211	0.108	0.0625	2.31
25	1.24	0.716	0.458	0.249	0.149	0.100	0.0537	0.0315	1.12
30	0.820	0.443	0.276	0.136	0.0797	0.0556	0.0316	0.0183	0.523
35	0.552	0.278	0.161	0.0805	0.0483	0.0348	0.0207	0.0113	0.279
40	0.372	0.175	0.101	0.0530	0.0328	0.0244	0.0137	0.0062	0.169
45	0.254	0.117	0.0692	0.0375	0.0242	0.0180	0.0088	0.0037	0.115
50	0.158	0.083	0.0474	0.0278	0.0171		0.0064	0.0025	0.069

C. Shyn and Sharp 1981, ref. [93] (10^{-18} cm^2/sr units)

	E_0(eV)		
θ (deg)	100	150	200
6	207.1	175.8	124.1
12	105.0	73.5	60.5
18	57.8	37.4	31.9
24	33.1	21.6	14.7
30	20.9	13.9	8.4
36	12.4	7.9	5.6
48	5.0	2.65	1.97
60	2.5	1.39	1.08
72	1.5	0.85	0.75
84	1.03	0.59	0.44
96	0.71	0.46	0.28
108	0.66	0.36	0.22
120	0.57	0.31	0.19
132	0.53	0.23	0.15
144	0.50	0.17	0.12
156	0.46	0.15	0.11
168	(0.41)	(0.13)	(0.10)

Table 6
Integral elastic scattering cross sections for H_2 (10^{-16} cm^2 units)

E_0(eV)	Linder– Schmidt [84][a]	Srivastava et al. [42][b]	Shyn–Sharp [93]	van Wingerden et al. [85]	van Wingerden et al. (semi-emp.) [80]
0.29	9.60				
0.58	11.15				
0.98	12.34				
1.48	13.23				
2.00	–		14.4		
2.50	14.11		–		
3.00	–	14.8	15.8		
3.49	13.61	–	–		
4.49	12.81	–	–		
5.0	–	13.7	15.9		
5.97	11.26	–	–		
7.0	–	11.1	13.58		
8.01	9.68	–	–		
9.98	8.32	–	–		
10.0	–	8.27	11.29		
10.08	8.04	–	–		
15		5.89	7.55		
20		4.15	5.61		
30		2.30	3.36		
40		1.70	2.50		
60		1.00	1.27		
75		0.70	–		
100			0.77	0.89	
150			0.50	0.52	
200			0.39	0.36	
300				0.23	
400				0.15	
500				0.12	
600				–	0.095
700				0.073	–
750				–	0.069
800				–	0.066
900				–	0.059
1000				0.052	
2000				0.027	

[a]Numerical values were taken from ref. [5]. Rotational excitation is not included.
[b]These values were obtained from the renormalized DCS data of Srivastava et al. as given in table 4.

Elastic momentum transfer cross sections have been obtained from the swarm measurements by Crompton et al. [87] and Gibson [86] and from beam measurements of Srivastava et al. [42] and Shyn and Sharp [93] (see table 7). The low energy swarm data and the intermediate energy beam data fit well together and support each other. Very recently Freeman and Wada [97] reported ultra low energy momentum transfer measurements. They found a Ramsauer–Townsend minimum at 9 meV for H_2 with a momentum transfer cross section of 6×10^{-16} cm^2.

Rotational excitation

At room temperature H_2 is a mixture of para (nuclear spin, $I = 0$) and ortho ($I = 1$) species and the population in the $J = 0, 1, 2, 3$ rotational levels are about 11.5%, 62.8%, 12.8% and 11.9% (1% in other

Table 7
Momentum transfer cross sections for H_2

A. Crompton et al. 1969, ref. [87] (10^{-16} cm^2 units)

E_0 (eV)	σ^M	E_0 (eV)	σ^M
0	6.4	0.15	11.4
0.01	7.3	0.2	12.0
0.02	8.0	0.3	13.0
0.03	8.5	0.4	13.9
0.04	8.96	0.5	14.7
0.05	9.28	0.6	15.6
0.06	9.56	0.7	16.3
0.07	9.85	0.9	17.1
0.08	10.1	1.1	17.7
0.09	10.3	1.4	18.2
0.10	10.5	1.6	18.3
0.11	10.7	1.8	18.2
0.13	11.0	2.0	18.0

B. Gibson 1970, ref. [86] (data are taken from ref. [5])

E_0 (eV)	σ^M (cm^2)	E_0 (eV)	σ^M (cm^2)	E_0 (eV)	σ^M (cm^2)
1.001 – 002	7.254 – 016	1.148 – 001	1.085 – 015	9.338 – 001	1.755 – 015
1.313 – 002	7.443 – 016	1.432 – 001	1.131 – 015	1.175 – 000	1.815 – 015
1.691 – 002	7.761 – 016	1.745 – 001	1.163 – 015	1.398 – 000	1.802 – 015
2.178 – 002	6.028 – 016	2.213 – 001	1.219 – 015	1.718 – 000	1.790 – 015
2.328 – 002	5.440 – 016	2.718 – 001	1.281 – 015	2.094 – 000	1.763 – 015
3.615 – 002	8.801 – 016	3.392 – 001	1.335 – 015	2.492 – 000	1.722 – 015
4.619 – 002	9.252 – 016	5.157 – 001	1.415 – 015	3.698 – 000	1.681 – 015
5.857 – 002	9.647 – 016	5.119 – 001	1.500 – 015	3.212 – 000	1.530 – 015
7.485 – 002	9.978 – 016	6.337 – 001	1.602 – 015	3.734 – 000	1.491 – 015
9.416 – 002	1.040 – 015	7.784 – 001	1.684 – 015	4.306 – 000	1.387 – 015
				4.774 – 000	1.301 – 015

C. Srivastava et al. 1975, ref. [42] (10^{-16} cm^2 units)[a]

E_0 (eV)	3	5	7	10	15	20	30	40	60	75
σ^M	15.7	12.0	8.35	5.14	2.80	1.73	0.801	0.515	0.268	0.167

[a]These values were obtained from the renormalized DCS values of Srivastava et al. as given in table 4.

D. Shyn and Sharp 1981, ref. [93] (10^{-16} cm^2 units)

E_0 (eV)	2	3	5	7	10	15	20	30	40	60	100	150	200
σ^M	17.1	17.0	14.0	10.14	7.07	3.29	2.11	1.02	0.64	0.29	0.15	0.083	0.060

rotational states). The $J = \pm 2$ selection rule for rotational excitation of homonuclear molecules holds quite well for electron impact excitation [84]. H_2 is the only molecule for which the rotational excitation structure can be resolved with present-day electron scattering technology. Differential cross sections for the $(1 \rightarrow 3)$ rotational excitation have been measured by Linder and Schmidt [84], Wong and Schulz [98], and Srivastava et al. [99]. The energy and angular ranges covered in these investigations are indicated in table 8. In all cases inelastic to elastic scattering intensity ratios were measured and calibration was achieved by utilizing elastic cross sections obtained by the same authors. The results are summarized in table 9.

Linder and Schmidt [84] extrapolated and integrated their DCS and obtained integral rotational excitation cross sections. From the measurements of Wong and Schulz [98] at 4.5 eV and of Srivastava et al. [99] at 40 eV, we obtain approximate integral cross sections of 10.7 and $1.3 \times 10^{-17}\,\mathrm{cm}^2$, respectively for the $(1 \rightarrow 3)$ transition. Integral cross sections can also be obtained from swarm

Table 8
Summary of rotational excitation cross section measurements for H_2

Reference	Energy range Angular range	Transition $(J'' \rightarrow J')$	Method Type of cross section	Estimated error
Linder–Schmidt 1971, ref. [84]	1.5–10.0 eV 20–120°	$1 \rightarrow 3$	beam/beam DCS, σ	±10%
Wong–Schulz 1974, ref. [98]	4.5 eV 20–100°	$1 \rightarrow 3$	beam/beam DCS	±10%
Srivastava et al. 1975, ref. [99]	40 eV; 10–135° 3–40 eV; 20° 15–100 eV; 115°	$1 \rightarrow 3$	beam/beam DCS	±20%
Gibson 1970, ref. [86]	0.077–4.77 eV 0.045–4.81 eV	$1 \rightarrow 3$ $0 \rightarrow 2$	Swarm σ	–
Crompton et al. 1969, ref. [87]	0.044–0.50 eV	$0 \rightarrow 2$	Swarm σ	±5% (below 0.4 eV)

Table 9
Differential excitation cross sections for the $(1 \rightarrow 3)$ rotational excitation of H_2 ($10^{-17}\,\mathrm{cm}^2/\mathrm{sr}$ units)

A. Linder and Schmidt 1971, ref. [84]

Scattering angle (deg)	Collision energy [eV]						
	1.5	2.5	3.5	4.5	6.0	8.0	10.0
20	0.60	0.97	1.06	1.17	1.11	0.91	0.73
30	0.57	0.93	1.10	1.13	1.08	0.93	0.75
40	0.56	0.86	1.02	1.09	0.99	0.82	0.70
50	0.53	0.83	0.97	1.02	0.88	0.79	0.70
60	0.54	0.80	0.94	0.97	0.85	0.74	0.64
70	0.52	0.77	0.87	0.85	0.77	0.72	0.65
80	0.58	0.71	0.84	0.87	0.75	0.72	0.61
90	0.59	0.73	0.81	0.84	0.79	0.66	0.56
100	0.53	0.70	0.80	0.78	0.73	0.65	0.51
110	0.53	0.67	0.80	0.74	0.71	0.65	0.54
120	0.52	0.66	0.79	0.80	0.73	0.58	0.55

Table 9 (*Cont.*)

B. Wong and Schulz 1974, ref. [98][a]

Scattering angle (deg)	Impact energy 4.5 eV
20	1.05
30	0.95
40	1.00
50	0.85
60	0.80
70	0.85
80	0.85
90	0.80
100	0.80

[a]Values were obtained from fig. 3 of ref. [98].

C. Srivastava et al. 1975, ref. [99]

Scattering angle (deg)	Impact energy 40 eV	Impact energy (eV)	Scattering angle (deg) 20	115
10	0.23	3	1.00	–
20	0.15	5	1.04	–
35	0.084	7	0.80	–
50	0.066	10	0.48	–
70	0.11	15	–	0.35
90	0.11	20	–	0.25
105	0.11	30	–	0.16
115	0.11	40	0.15	0.11
135	0.11	60	–	0.067
		75	–	0.046
		80	–	0.062
		100	–	0.043

The values of ref. [99] have been renormalized on the basis of the H_2 elastic cross sections (table 4B).

measurements at low energies. Crompton et al. [87] deduced rotational excitation cross sections for parahydrogen ($0 \rightarrow 2$). Gibson [86] has carried out swarm measurements and obtained rotational excitation cross sections both for para ($0 \rightarrow 2$) and ortho ($1 \rightarrow 3$) hydrogen and for deuterium. The swarm method yields more accurate data than the beam–beam method at low energies but becomes unreliable above about 0.5 eV. The data are summarized in table 10. The cross sections for parahydrogen ($0 \rightarrow 2$) are considerably larger than for orthohydrogen ($1 \rightarrow 3$). Their peak values of 1.8 and 1.1×10^{-16} cm^2 respectively is reached at about 3.5 eV but surprisingly even at 40 eV the ($1 \rightarrow 3$) cross section was found to be about 1.3×10^{-17} cm^2. The large cross sections at low energies are due to resonance excitation mechanisms.

More detailed discussions of rotational excitation are given by Takayanagi and Itikawa [100] and Golden et al. [101].

Table 10

Integral rotational excitation cross sections for H_2

$J = 0 \rightarrow 2$ excitation

A. Crompton et al. 1969, ref. [87] (10^{-16} cm^2 units)

Energy (eV)	σ	Energy (eV)	σ
0.047	0.0185	0.20	0.120
0.050	0.027	0.25	0.137
0.055	0.035	0.30	0.160
0.060	0.042	0.35	0.185
0.065	0.048	0.40	0.210
0.07	0.053	0.45	0.236
0.08	0.060	0.50	0.263
0.09	0.068		
0.10	0.074		
0.11	0.079		
0.13	0.089		
0.15	0.099		

B. Gibson 1970, ref. [86]. Tabulated data are taken from ref. [5].

Energy (eV)	σ (cm^2)	Energy (eV)	σ (cm^2)	Energy (eV)	σ (cm^2)
4.500 − 002	1.008 − 018	1.166 − 001	8.098 − 0.18	8.797 − 001	5.217 − 017
4.532 − 002	1.316 − 018	1.282 − 001	8.714 − 018	1.006 + 000	6.138 − 017
4.674 − 002	1.733 − 018	1.454 − 001	9.531 − 018	1.141 + 000	7.105 − 017
4.859 − 002	2.245 − 018	1.650 − 001	1.051 − 017	1.295 + 000	8.223 − 017
5.093 − 002	2.750 − 018	1.902 − 001	1.159 − 017	1.437 + 000	9.518 − 017
5.380 − 002	3.234 − 018	2.176 − 001	1.268 − 017	1.880 + 000	1.102 − 016
5.685 − 002	3.681 − 018	2.508 − 001	1.409 − 017	1.921 + 000	1.286 − 016
5.960 − 002	4.058 − 018	2.869 − 001	1.554 − 017	2.197 + 000	1.453 − 016
6.397 − 002	4.583 − 018	3.229 − 001	1.714 − 017	2.513 + 000	1.628 − 016
6.922 − 002	5.052 − 018	3.635 − 001	1.905 − 017	2.943 + 000	1.767 − 016
7.432 − 002	5.524 − 018	4.157 − 001	2.209 − 017	3.393 + 000	1.826 − 016
8.106 − 002	6.041 − 018	4.830 − 001	2.594 − 017	3.702 + 000	1.793 − 016
8.702 − 002	6.500 − 018	5.523 − 001	3.027 − 017	4.008 + 000	1.741 − 016
9.343 − 002	6.881 − 018	6.416 − 001	3.590 − 017	4.478 + 000	1.620 − 016
1.077 − 001	7.344 − 018	7.572 − 001	4.363 − 017	4.810 + 000	1.556 − 016

$(1 \rightarrow 3)$ excitation

A. Linder and Schmidt 1971, ref. [84]. Tabulated data are taken from ref. [5].

Energy (eV)	σ (cm^2)	Energy (eV)	σ (cm^2)
2.922 − 001	1.187 − 017	2.504 + 000	9.275 − 017
4.174 − 001	1.686 − 017	3.527 + 000	1.096 − 016
4.800 − 001	2.123 − 017	4.529 + 000	1.103 − 016
5.843 − 001	2.467 − 017	6.010 + 000	1.007 − 016
6.887 − 001	3.060 − 017	6.014 + 000	9.773 − 017
9.809 − 001	4.714 − 017	1.002 + 001	7.568 − 017
1.523 + 000	5.805 − 017		

Table 10 (*Cont.*)
B. Gibson 1970, ref. [86]. Tabulated data are taken from ref. [5].

Energy (eV)	σ (cm^2)	Energy (eV)	σ (cm^2)	Energy (eV)	σ (cm^2)
7.771 − 002	9.972 − 019	2.085 − 001	6.229 − 018	1.234 + 000	4.830 − 017
7.789 − 002	1.163 − 018	2.311 − 001	6.571 − 018	1.378 + 000	5.593 − 017
8.015 − 002	1.663 − 018	2.643 − 001	7.767 − 018	1.577 + 000	6.479 − 017
8.337 − 002	1.894 − 018	2.999 − 001	8.851 − 018	1.789 + 000	7.383 − 017
8.604 − 002	2.157 − 018	3.404 − 001	0.843 − 018	2.014 + 000	8.345 − 017
9.021 − 002	2.397 − 018	3.632 − 001	1.113 − 017	2.286 + 000	9.432 − 017
9.533 − 002	2.665 − 018	4.247 − 001	1.257 − 017	2.554 + 000	1.015 − 016
1.002 − 001	2.963 − 018	4.819 − 001	1.456 − 017	2.853 + 000	1.058 − 016
1.087 − 001	3.267 − 018	5.426 − 001	1.660 − 017	3.112 + 000	1.085 − 016
1.180 − 001	3.603 − 018	6.206 − 001	1.935 − 017	3.316 + 000	1.094 − 016
1.297 − 001	3.976 − 018	6.987 − 001	2.244 − 017	3.617 + 000	1.077 − 016
1.438 − 001	4.438 − 018	7.866 − 001	2.599 − 017	3.947 + 000	1.063 − 016
1.556 − 001	4.718 − 018	8.856 − 001	3.060 − 017	4.375 + 000	1.044 − 016
1.697 − 001	5.120 − 018	9.892 − 001	3.543 − 017	4.773 + 000	1.011 − 016
1.681 − 001	5.647 − 018	1.114 + 000	4.171 − 017		

Vibrational excitation

A summary of measurements concerning vibrational excitation is given in table 11.

Differential cross sections for the rotationally unresolved ($v = 0 \rightarrow v = 1, 2, 3$) vibrational excitation was measured by Ehrhardt et al. [88]. They found cross sections independent of angle in the energy

Table 11
Summary of measurements on vibrational excitation of H_2

Reference	Energy and Angular range	Excitation	Method Type of cross section	Estimated error
Ehrhardt et al.	5–110°		beam–beam	
1968, ref. [88]	0.027–10.23 eV	$v = 1$	DCS, Q_v	
	1.03–8.01 eV	$v = 2$		±15%
	1.86–7.21 eV	$v = 3$		
Linder–Schmidt	20–120°	$v = 1, \Delta J = 0$	beam–beam	±10%
1971, ref. [84]	1.5–10.8 eV	$v = 1, (1 \rightarrow 3)$	DCS, Q_v	
Wong–Schulz	4.5 eV; 20–100°	$v = 1, \Delta J = 0$	beam–beam	
1974, ref. [98]	4.5 eV; 20–100°	$v = 1, (1 \rightarrow 3)$	DCS	
	4.5 eV; 20–100°	$v = 2, \Delta J = 0$		±10%
	4.5 eV; 20–100°	$v = 2, (1 \rightarrow 3)$		
	4.5 eV; 20–80°	$v = 3, (\Delta J = 0)$		
	4.5 eV; 20–80°	$v = 3, (1 \rightarrow 3)$		
Crompton et al.	0.7–1.2 eV	$v = 1$	swarm	±5%
1970, ref. [102]			Q_v	
Gibson	0.588–4.92 eV	$v = 1$	swarm	±5%
1970, ref. [86]			Q_v	
Weingartshofer et al.	11.0–13.0 eV		beam–beam	
1970, ref. [91]	10°, 40°, 90°	$v = 1$	Diff. excit.	±20%
	10°, 90°	$v = 2$	functions	
	10°, 70°, 100°, 120°	$v = 3$		
	100°	$v = 4$		

Table 12

Differential vibrational excitation cross sections for H_2

A. Linder and Schmidt 1971, ref. [84] (10^{-18} cm^2/sr units)

Scatt. angle (deg)	Collision energy [eV]						
	1.5	2.5	3.5	4.5	6.0	8.0	10.8
20	3.80	6.50	6.60	5.38	4.35	2.33	–
30	2.96	5.40	5.73	4.45	3.35	1.91	0.86
40	2.22	3.93	4.40	3.58	2.66	1.45	0.60
50	1.60	2.90	3.32	2.92	1.83	1.09	0.43
60	1.03	2.10	2.50	2.28	1.33	0.85	0.31
70	1.08	1.37	1.67	1.34	0.88	0.63	0.19
80	0.68	0.91	1.10	0.98	0.75	0.42	0.16
90	0.67	0.73	0.78	0.65	0.52	0.36	0.19
100	0.68	0.70	0.72	0.56	0.61	0.39	0.24
110	1.02	0.73	0.89	0.75	0.65	0.46	0.39
120	1.34	1.24	1.17	1.01	0.91	0.65	(113°)

$v = 1; J = 1 \rightarrow 3$

Scatt. angle (deg)	Collision energy [eV]						
	1.5	2.5	3.5	4.5	6.0	8.0	10.8
20	0.66	1.24	1.25	1.11	0.93	0.69	–
30	0.59	1.20	1.24	1.02	0.89	0.65	0.25
40	0.61	1.08	1.13	1.01	0.84	0.67	0.23
50	0.66	1.04	1.14	0.97	0.78	0.62	0.25
60	0.60	1.08	1.05	1.04	0.78	0.59	0.23
70	0.79	0.99	1.00	0.90	0.71	0.60	0.22
80	0.81	0.94	1.02	1.00	0.82	0.57	0.23
90	0.70	0.89	1.03	0.91	0.76	0.52	0.23
100	0.86	0.92	1.00	0.89	0.80	0.53	0.23
110	0.66	0.80	0.95	0.94	0.77	0.50	0.22
120	0.86	0.81	1.00	0.94	0.75	0.52	

Table 12 (*Cont.*)

B. Wong and Schulz 1974, ref. [98][a]

$v = 1; \Delta J = 0$		$v = 1; J = 1 \rightarrow 3$	
Scattering angle (deg)	DCS (10^{-18} cm^2/sr)	Scattering angle (deg)	DCS (10^{-18} cm^2/sr)
20	5.5	20	1.2
30	4.0	30	1.1
40	3.1	40	1.0
50	2.3	50	0.95
60	1.9	60	1.00
70	1.2	70	0.95
80	0.90	80	0.93
90	0.67	90	0.90
100	0.61	100	0.90

$v = 2; \Delta J = 0$		$v = 2; J = 1 \rightarrow 3$	
Scattering angle (deg)	DCS (10^{-19} cm^2/sr)	Scattering angle (deg)	DCS (10^{-19} cm^2/sr)
20	4.0	20	1.1
30	3.1	30	1.0
40	2.7	40	0.95
50	1.8	50	0.90
60	1.2	60	0.85
70	0.85	70	0.85
80	0.65	80	0.85
90	0.60	90	0.83
100	0.61	100	0.82

$v = 3; \Delta J = 0$		$v = 3; J = 1 \rightarrow 3$	
Scattering angle (deg)	DCS (10^{-20} cm^2/sr)	Scattering angle (deg)	DCS (10^{-20} cm^2/sr)
20	4.0	20	1.3
40	2.2	40	1.1
60	1.3	60	1.1
80	0.8	80	1.1

[a]Values were obtained from fig. 3 of ref. [98].

range of their studies (0.03 to 10 eV). By integration and normalization to elastic scattering they also obtained integral cross sections (see table 13).

Linder and Schmidt [84] and Wong and Schulz [98] also applied beam–beam techniques, but with sufficient energy resolution to resolve rotational structure associated with vibrational excitation, hence to generate differential cross sections for individual vibrational–rotational excitations (table 12). Linder and Schmidt extrapolated and integrated their cross sections to obtain integral cross sections. In the case of the Wong and Schulz's data we carried out an extrapolation and integration which yielded approximate integral cross section. (See table 13.) Simultaneous transitions involving $v = 0 \rightarrow 1$ vibrational and $J = 1 \rightarrow 3$ rotational excitation account for about 25% of all $v = 1$ vibrational excitation in normal hydrogen. The two sets of measurements are in good agreement.

Crompton et al. [102] and Gibson [86] obtained $v = 0 \rightarrow 1$ integral vibrational excitation cross sections from swarm measurements both for parahydrogen and for normal hydrogen. Attempts to separate the vibrational excitation cross section into pure vibrational and vibration–rotation excitations led to

Table 13
Integral vibrational excitation cross sections for H_2

A. $v = 0 \rightarrow 1$

Ehrhardt et al. 1968, ref. [88]. Data taken from ref. [5].

Energy (eV)	σ (cm^2)	Energy (eV)	σ (cm^2)	Energy (eV)	σ (cm^2)
2.700 − 002	6.900 − 020	2.020 + 000	4.031 − 017	4.710 + 000	3.717 − 017
1.900 − 001	1.400 − 019	2.070 + 000	4.187 − 017	4.500 + 000	3.629 − 017
3.300 − 001	2.800 − 019	2.140 + 000	4.350 − 017	4.910 + 000	3.541 − 017
4.300 − 001	2.200 − 019	2.210 + 000	4.475 − 017	5.050 + 000	3.427 − 017
4.900 − 001	5.600 − 019	2.290 + 000	4.625 − 017	5.190 + 000	3.333 − 017
5.500 − 001	9.700 − 019	2.370 + 000	4.730 − 017	5.310 + 000	3.245 − 017
6.000 − 001	1.720 − 018	2.460 + 000	4.832 − 017	5.430 + 000	3.144 − 017
6.600 − 001	2.670 − 018	2.540 + 000	4.913 − 017	5.600 + 000	3.023 − 017
7.400 − 001	3.690 − 018	2.670 + 000	4.981 − 017	5.760 + 000	2.922 − 017
8.000 − 001	4.710 − 018	2.700 + 000	5.029 − 017	5.910 + 000	2.807 − 017
8.500 − 001	5.860 − 018	2.500 + 000	5.063 − 017	6.090 + 000	2.700 − 017
9.100 − 001	6.660 − 018	2.890 + 000	5.091 − 017	6.270 + 000	2.585 − 017
9.700 − 001	7.960 − 018	2.960 + 000	5.105 − 017	6.430 + 000	2.478 − 017
1.000 + 000	9.450 − 018	3.020 + 000	5.115 − 017	6.630 + 000	2.363 − 017
1.070 + 000	1.095 − 017	3.100 + 000	5.105 − 017	6.600 + 000	2.249 − 017
1.120 + 000	1.305 − 017	3.200 + 000	5.085 − 017	6.980 + 000	2.128 − 017
1.180 + 000	1.454 − 017	3.290 + 000	5.033 − 017	7.220 + 000	1.086 − 017
1.220 + 000	1.596 − 017	3.400 + 000	4.975 − 017	7.420 + 000	1.865 − 017
1.260 + 000	1.725 − 017	3.500 + 000	4.897 − 017	7.600 + 000	1.737 − 017
1.320 + 000	1.881 − 017	3.590 + 000	4.802 − 017	7.790 + 000	1.623 − 017
1.370 + 000	2.051 − 017	3.690 + 000	4.705 − 017	8.000 + 000	1.516 − 017
1.430 + 000	2.207 − 017	3.800 + 000	4.607 − 017	8.220 + 000	1.422 − 017
1.480 + 000	2.397 − 017	3.680 + 000	4.499 − 017	8.520 + 000	1.321 − 017
1.540 + 000	2.546 − 017	3.980 + 000	4.411 − 017	8.820 + 000	1.228 − 017
1.600 + 000	2.736 − 017	4.060 + 000	4.310 − 017	9.110 + 000	1.134 − 017
1.650 + 000	2.893 − 017	4.160 + 000	4.236 − 017	9.380 + 000	1.047 − 017
1.700 + 000	3.081 − 017	4.220 + 000	4.155 − 017	9.600 + 000	9.670 − 018
1.770 + 000	3.305 − 017	4.320 + 000	4.060 − 017	9.860 + 000	9.200 − 018
1.540 + 000	3.495 − 017	4.390 + 000	3.993 − 017	1.007 + 001	5.740 − 018
1.910 + 000	3.671 − 017	4.490 + 000	3.912 − 017	1.023 + 001	8.540 − 018
1.960 + 000	3.854 − 017	4.600 + 000	3.804 − 017		

Table 13 (*Cont.*)

Gibson 1970, ref. [86]. Data taken from ref. [5].

Energy (eV)	σ (cm^2)	Energy (eV)	σ (cm^2)	Energy (eV)	σ (cm^2)
5.681 − 001	9.942 − 019	1.057 + 000	7.246 − 018	2.431 + 000	4.081 − 017
6.168 − 001	1.236 − 018	1.118 + 000	8.325 − 018	2.610 + 000	4.575 − 017
6.417 − 001	1.457 − 018	1.181 + 000	9.640 − 018	2.848 + 000	5.085 − 017
6.730 − 001	1.786 − 018	1.269 + 000	1.125 − 017	3.208 + 000	5.942 − 017
7.227 − 001	2.315 − 018	1.363 + 000	1.380 − 017	3.391 + 000	6.292 − 017
7.640 − 001	2.864 − 018	1.475 + 000	1.637 − 017	3.564 + 000	6.609 − 017
8.012 − 001	3.371 − 018	1.609 + 000	2.007 − 017	3.819 + 000	6.830 − 017
8.469 − 001	4.032 − 018	1.728 + 000	2.382 − 017	4.069 + 000	7.001 − 017
8.952 − 001	4.669 − 018	1.886 + 000	2.758 − 017	4.370 + 000	7.062 − 017
9.388 − 001	5.494 − 018	2.042 + 000	3.169 − 017	4.921 + 000	7.010 − 017
1.000 + 000	6.362 − 018	2.210 + 000	3.611 − 017		

Crompton et al. 1970, ref. [102]. Data taken from ref. [5].

Energy (eV)	σ (cm^2)
7.000 − 001	1.900 − 018
1.000 + 000	6.000 − 018
1.200 + 000	9.500 − 018

Linder and Schmidt 1971, ref. [84]. Data taken from ref. [5].

Energy (eV)	σ (cm^2)
1.470 + 000	1.975 − 017
2.480 + 000	2.720 − 017
3.456 + 000	2.854 − 017
4.475 + 000	2.370 − 017
5.963 + 000	1.870 − 017
7.999 + 000	1.155 − 017
9.975 + 000	7.601 − 018
1.080 + 001	6.110 − 018

B. $\underline{v = 0 \rightarrow 2}$

Ehrhardt et al. 1968, ref. [88]. Data taken from [5].

Energy (eV)	Cross section (cm^2)	Energy (eV)	Cross section (cm^2)	Energy (eV)	Cross section (cm^2)
1.030 + 000	3.400 − 020	2.390 + 000	2.760 − 018	4.420 + 000	3.680 − 018
1.180 + 000	6.400 − 020	2.490 + 000	2.950 − 018	4.590 + 000	3.580 − 018
1.310 + 000	9.400 − 020	2.590 + 000	3.140 − 018	4.770 + 000	3.490 − 018
1.390 + 000	1.700 − 019	2.690 + 000	3.290 − 018	4.980 + 000	3.370 − 018
1.470 + 000	2.900 − 019	2.810 + 000	3.440 − 018	5.180 + 000	3.320 − 018
1.560 + 000	4.200 − 019	2.910 + 000	3.520 − 018	5.400 + 000	3.260 − 018
1.630 + 000	5.600 − 019	3.010 + 000	3.650 − 018	5.590 + 000	3.180 − 018
1.710 + 000	5.900 − 019	3.130 + 000	3.720 − 018	5.800 + 000	3.110 − 018
1.780 + 000	8.700 − 019	3.240 + 000	3.780 − 018	6.010 + 000	3.010 − 018
1.860 + 000	1.020 − 018	3.380 + 000	3.840 − 018	6.190 + 000	2.920 − 018
1.950 + 000	1.250 − 018	3.510 + 000	3.900 − 018	6.430 + 000	2.850 − 018
2.020 + 000	1.490 − 018	3.620 + 000	3.950 − 018	6.680 + 000	2.760 − 018
2.070 + 000	1.670 − 018	3.740 + 000	3.950 − 018	6.930 + 000	2.670 − 018
2.130 + 000	1.880 − 018	3.870 + 000	3.920 − 018	7.170 + 000	2.600 − 018
2.180 + 000	2.090 − 018	4.010 + 000	3.880 − 018	7.390 + 000	2.570 − 018
2.240 + 000	2.300 − 018	4.130 + 000	3.820 − 018	7.680 + 000	2.520 − 018
2.310 + 000	2.520 − 018	4.290 + 000	3.743 − 018	7.870 + 000	2.510 − 018
				8.010 + 000	2.510 − 018

Table 13 (*Cont.*)

C. $v = 0 \rightarrow 3$

Ehrhardt et al. 1968, ref. [88]. Data taken from ref. [5].

Energy (eV)	Cross section (cm^2)	Energy (eV)	Cross section (cm^2)	Energy (eV)	Cross section (cm^2)
1.864 + 000	1.000 − 019	3.143 + 000	3.990 − 019	4.822 + 000	3.290 − 019
2.026 + 000	1.550 − 019	3.297 + 000	3.990 − 019	5.068 + 000	3.200 − 019
2.131 + 000	1.900 − 019	3.466 + 000	4.040 − 019	5.321 + 000	3.060 − 019
2.279 + 000	2.390 − 019	3.621 + 000	4.100 − 019	5.567 + 000	2.910 − 019
2.419 + 000	2.940 − 019	3.775 + 000	3.950 − 019	5.841 + 000	2.820 − 019
2.567 + 000	3.230 − 019	3.958 + 000	3.860 − 019	6.164 + 000	2.730 − 019
2.721 + 000	3.530 − 019	4.169 + 000	3.770 − 019	6.389 + 000	2.540 − 019
2.876 + 000	3.780 − 019	4.344 + 000	3.570 − 019	6.656 + 000	2.400 − 019
3.037 + 000	3.890 − 019	4.625 + 000	3.430 − 019	6.937 + 000	2.210 − 019
				7.211 + 000	2.020 − 019

D. Rotationally resolved vibrational excitation

Linder and Schmidt 1971, ref. [84]. Data taken from ref. [5].

$v = 0 \rightarrow 1$, $\Delta J = 0$. $v = 0 \rightarrow 1$, $J = 1 \rightarrow 3$.

Energy (eV)	σ (cm^2)	Energy (eV)	σ (cm^2)
1.470 + 000	1.975 − 017	1.532 + 000	8.978 − 018
2.480 + 000	2.720 − 017	2.468 + 000	1.198 − 017
3.456 + 000	2.854 − 017	3.498 + 000	1.363 − 017
4.475 + 000	2.370 − 017	4.512 + 000	1.216 − 017
5.963 + 000	1.870 − 017	5.996 + 000	1.009 − 017
7.999 + 000	1.155 − 017	8.006 + 000	6.985 − 018
9.975 + 000	7.601 − 018	9.997 + 000	3.881 − 018
1.080 + 001	6.110 − 018	1.080 + 001	2.845 − 018

Wong and Schulz 1974, ref. [98]

$E_0 = 4.5$ eV

Process		
v	J	Cross section[a] (10^{-18} cm^2)
1	$\Delta J = 0$	17.8
1	$J = 1 \rightarrow 3$	11.0
2	$\Delta J = 0$	1.44
2	$J = 1 \rightarrow 3$	1.09
3	$\Delta J = 0$	0.14
3	$J = 1 \rightarrow 3$	0.14

[a]Numerical values were read from fig. 3 of ref. [98] and extrapolated and integrated by us.

ambiguities. There is some disagreement between the beam results of Ehrhardt et al. [88] and the swarm results of Crompton et al. [102] and Gibson [86] near threshold (see table 13).

The above studies were carried out at impact energies of 10 eV and below. Trajmar et al. [103] studied rotationally unresolved vibrational excitation at intermediate energies (7 to 81.6 eV) in a beam–beam arrangement in the 10° to 80° angular range. The DCS values were normalized to the total scattering cross sections of Golden et al. [83]. This procedure, however, involved an extensive angular extrapolation (and integration) as well as estimation of missing inelastic contributions. Consequently, these data are not as reliable in absolute magnitude as the low energy data (where no electronic channels are open). No tabulation for these DCS is given but only graphical presentations in ref. [103]. At 10 eV there is a good agreement between the results of Trajmar et al. [103] and Ehrhardt et al. [88].

The energy dependence of the $v = 1, 2$ and 3 vibrational excitation cross sections were measured by Weingartshofer et al. [91] at several scattering angles in the 11–13 eV impact energy range where resonances strongly influence the cross section behavior. Their results are shown in figs. 5–7. Depending on the natural width of the resonances, the peak cross sections will be dependent to some extent upon the instrumental resolution.

Chang and Wong [104] studied the isotope effect in the differential cross section for pure rotational and vibrational-rotational excitation in H_2 and D_2 at 4 eV impact energy. The results are shown in table 14 and can be understood using frame transformation theory [105].

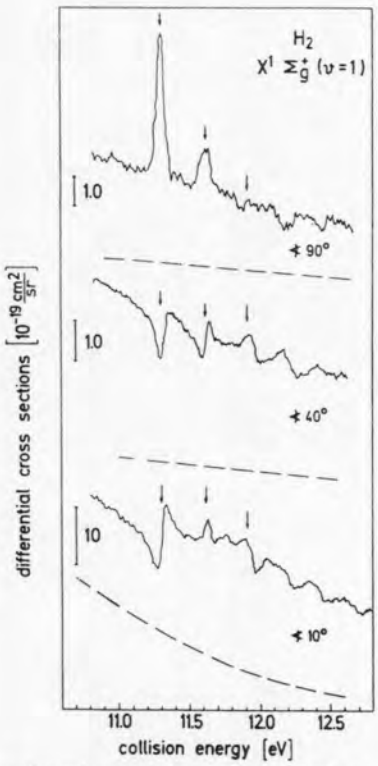

Fig. 5. Energy dependence of the absolute differential cross section for the $v = 1$ vibrational excitation of H_2 for three different scattering angles. The zero lines are dashed. The length of bars to the left represent scaling factors in units of 10.0×10^{-19} cm²/sr for the 10° curve and 1.0×10^{-19} cm²/sr for the 40° and 90° curves. (From ref. [91].)

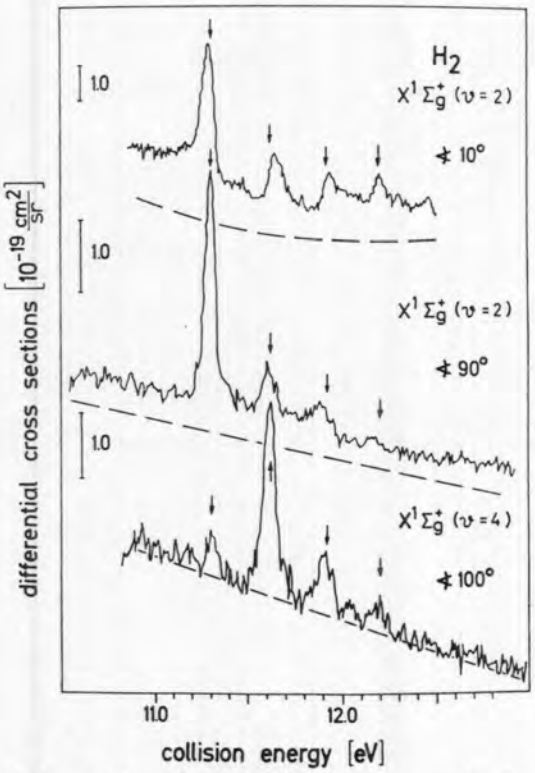

Fig. 6. Energy dependence of the differential cross section for $v = 2$ and 4 vibrational excitation at different scattering angles. The zero lines are dashed. The length of the bars to the left represent the scaling factors in units of 1.0×10^{-19} cm²/sr. (From ref. [91].)

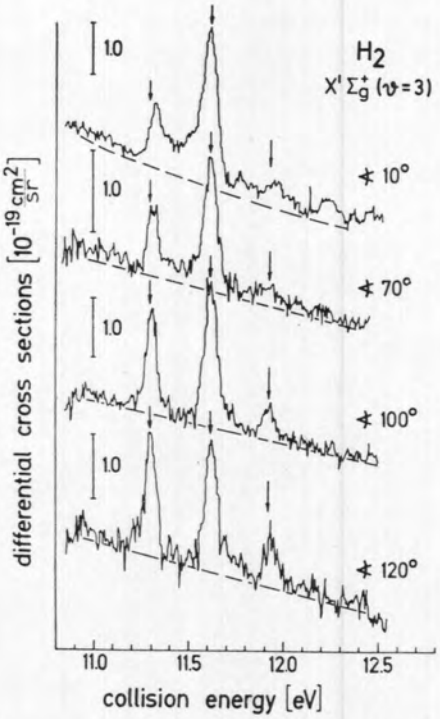

Fig. 7. Energy dependence of the differential cross section for the $v = 3$ vibrational excitation of H_2 at four different scattering angles. The zero lines are dashed. The length of the bars to the left of each curve represents absolute scaling factors in units of 1.0×10^{19} cm²/sr. (From ref. [91].)

Table 14
Ratio of D_2 to H_2 vibrational-rotational excitation cross sections at 4 eV impact energy and 90° scattering angle (Chang and Wong 1977, ref. [104])

Cross sections	Theory[a]	Experiment[b]				
		$\Delta j = 0$	$j = 0$	$j = 1$	$j = 2$	$j = 3$
Rotational ($v = 0 \to 0$, $j \to j+2$)	1.00		0.96	1.10	0.80	1.15
Vibration-rotational ($v = 0 \to 1$, $j \to j+2$)	0.71		0.72	0.79	0.72	0.78
Elastic ($v = 0 \to 0$, $\Delta j = 0$)	1.00	1.05				
Pure vibrational ($v = 0 \to 1$, $\Delta j = 0$)	0.56	0.55				

[a]Estimated accuracy is 1%.

[b]Except for the elastic result, all others are measured as ratios to the elastic cross sections. The estimated errors are 5% for the elastic, and about 10% for the other measurements.

Electronic excitation

Electron impact excitation cross sections for the electronic states of H_2 measured by electron scattering techniques are extremely limited. This is primarily due to the difficulty of resolving the heavily overlapping band structure of electronic transitions in the electron energy-loss spectra. The situation is further complicated by the large variety of other (non-discrete) excitation processes which lead to dissociation with ground, excited, and ionized fragments. Most of the available data were derived from studying the optical radiation caused by electron impact.

Here we will discuss work which leads to absolute excitation cross sections from the measurement of scattered electron energy and angular distributions. Cross sections derived by other methods are only summarized in tabular form. These cross sections are frequently in relative units and usually include contributions from processes other than direct electron impact excitation (such as cascade).

Weingartshofer et al. [91] studied the excitation of the $b^3\Sigma_u^+$ and $B^1\Sigma_u^+$ states at impact energies ranging from 10 to 16 eV and scattering angles from 10° to 120°. In this region the excitation of the $B^1\Sigma_u^+$ state occurs mainly through a series of resonances beginning at 11.30 eV, while the cross section for the $b^3\Sigma_u^+$ state is composed of both resonant and non-resonant contributions. Relative branching ratios for the decay of resonance series I in terms of absolute cross sections are given in table 15. Measured scattering intensities were converted to absolute cross sections by utilizing the total scattering cross sections of Ramsauer and Kollath [106] and Golden et al. [83]. The estimated error in the resulting data is 20%. Fig. 8 shows the 40° DCS for the $v = 0, 1$ and 2 vibrational levels of the $B^1\Sigma_u^+$ state as a function of impact energy. Table 16 gives absolute differential cross sections for excitation of the $B^1\Sigma_u^+$ ($v = 0, 1, 2$) states at impact energies corresponding to the peaks $v' = 0, 1, 2, 3, 4$ of series I, and $v'' = 0, 1$ of series II resonances. The series I resonance was found to decay into all energetically accessible channels, while series II decays with large probability only into $v = 1$ and 2 of the $B^1\Sigma_u^+$ electronic state.

The differential excitation function for the dissociative $b^3\Sigma_u^+$ channel at 10.47 eV energy loss and 70° scattering angle is shown in fig. 9. The broad feature represents the non-resonant contribution to the $b^3\Sigma_u^+$ excitation and the sharp structures are due to resonance contributions. Trajmar et al. [107] investigated the direct excitation of the $b^3\Sigma_u^+$ state at higher impact energies. Their results are shown in fig. 10. Direct excitation of this antibonding state is the dominant process leading to dissociation of H_2 into ground state H atoms. However, as the impact energy increases cascade contributions from higher electronic states to the $b^3\Sigma_u^+$ state, and consequently to the generation of atomic hydrogen, also become significant.

Excitation of the $c^3\Pi_u$, $e^3\Sigma_u^+$, $g^3\Sigma_g^+$, $d^3\Pi_u$, $k^3\Pi_u$ and $n^3\Pi_u$ states was also studied by Weingartshofer et

Table 15
Relative branching ratios for H_2 for the decay of resonance series I in terms of absolute cross sections (10^{-17} cm^2). (Weingartshofer et al. 1970, ref. [91])[a]

	Exit channel	$v' = 0$	$v' = 1$	$v' = 2$	$v' = 3$	$v' = 4$	$v' = 5$
$B^1\Sigma_u^+$	$v = 2$	...	0.27	0.39	0.09	0.14	0.14
	$v = 1$	...	0.41	0.29	0.39	0.18	0.10
	$v = 0$	0.67	1.4	0.76	0.21	...	...
$b^3\Sigma_u^+$ [b]	11.02 eV	...	0.11	0.10	0.042	0.020	0.008
	10.76 eV	0.031	0.087	0.063	0.039	0.015	...
	10.47 eV	0.042	0.063	0.048	0.024	0.007	...
	10.17 eV	0.033	0.045	0.022	0.011	0.004	...
$b^3\Sigma_u^+$	Integrated values	2.0	2.5	2.5	1.4	1.0	
$X^1\Sigma_g^+$	$v = 5$	...	0.09	...	...	...	...
	$v = 4$	0.04	0.2	0.06	0.02	...	...
	$v = 3$	0.14	0.23	0.02	...	...	...

[a]The estimated error for the cross sections is about 20%.
[b]Within an energy band of $\Delta E \approx 60$ meV.

Table 16
Differential cross sections for the excitation of the $B^1\Sigma_u^+$ state of H_2

A. Weingartshofer et al., 1970, ref. [91]
Excitation cross sections for the $v = 0$, 1 and 2 states via resonance series rsI(v') and rsII(v'), (10^{-19} cm^2/sr units).

Scattering angle (deg)	rs I(v')								rs II(v')	
	$v'=0$ $v=0$	$v'=1$ $v=0$	$v'=2$ $v=0$	$v'=1$ $v=1$	$v'=2$ $v=1$	$v'=3$ $v=1$	$v'=2$ $v=2$	$v'=4$ $v=2$	$v''=0$ $v=1$	$v''=1$ $v=2$
10	9.9	27.4	16.0	8.5	6.4	6.5	5.2	2.1	6.0	4.8
20	7.4	22.5	13.4	6.2	4.9	5.8	4.2	1.8	4.4	3.5
30	6.4	21.8	11.7	6.3	4.7	5.5	4.1	1.4	4.0	3.1
40	5.4	20.0	9.5	6.0	3.6	5.0	4.0	1.1	3.0	3.3
50	5.1	17.0	7.6	5.4	3.0	4.5	3.8	1.0	2.7	3.3
60	4.9	13.5	5.7	4.8	2.3	3.8	4.3	1.0	2.4	3.2
70	4.4	10.5	3.7	3.8	2.1	3.0	3.7	1.1	2.5	2.9
80	4.2	7.9	2.9	2.8	1.5	2.2	3.2	1.0	2.0	2.7
90	4.1	6.0	2.3	2.3	1.6	1.9	2.8	0.9	1.7	2.5
100	4.2	6.0	2.3	2.1	1.4	1.9	2.3	0.9	1.8	2.4
110	4.4	7.1	2.9	2.0	1.8	2.3	2.0	0.9	1.7	2.2
120	5.0	7.9	3.1	2.5	2.1	2.5	2.1	0.7	2.0	1.8

B. Srivastava et al., 1977, ref. [109]
Excitation of the $v = 2$ state (10^{-20} cm^2/sr units).

Scattering angle (deg)	E_0(eV)								
	10	20	30	40	50	70	90	115	135
15	(17)	10.0 ± 5.2	6.4 ± 2.0	5.2 ± 1.4	4.9 ± 1.2	3.7 ± 1.0	3.3 ± 1.0	3.0 ± 1.1	3.1 ± 1.1
20	(52)	29.5 ± 7.0	13.9 ± 7.0	7.2 ± 19	5.4 ± 1.6	4.0 ± 1.4	3.5 ± 1.0	3.2 ± 1.2	4.6 ± 2.6
30	(90)	43.9 ± 11.0	17.8 ± 4.3	7.9 ± 2.0	4.7 ± 1.2	3.0 ± 0.8	2.1 ± 0.6	1.1 ± 0.4	0.60 ± 0.27
40	(170)	53.3 ± 12.7	13.5 ± 3.5	4.1 ± 1.2	2.8 ± 0.9	1.7 ± 0.5	1.3 ± 0.5	0.75 ± 0.34	0.62 ± 0.34
50	(150)	(46.0)	(10.0)	(2.7)	(2.0)	(1.3)	(1.0)	(0.49)	(0.3)
60	(120)	33.0 ± 8.6	7.25 ± 2.2	1.9 ± 0.6	1.6 ± 0.7	1.2 ± 0.6	0.92 ± 0.5	6.32 ± 0.18	0.17 ± 0.09

Numbers in parentheses have been obtained by extra- or interpolations. The original data of ref. [109] were renormalized as explained in connection with the elastic cross sections (table 4B).

Table 17
Differential cross sections for the $c^3\Pi_u$ ($v = 1$) state (Weingartshofer 1975, ref. [108])

Scattering angle (deg)	Absolute cross section × 10^{19} (cm^2 sr^{-1})[a]
5	180
8	150
10	60
20	20
40	15
90	15
125	20
132	30

[a]Estimated error limits: ±30%.

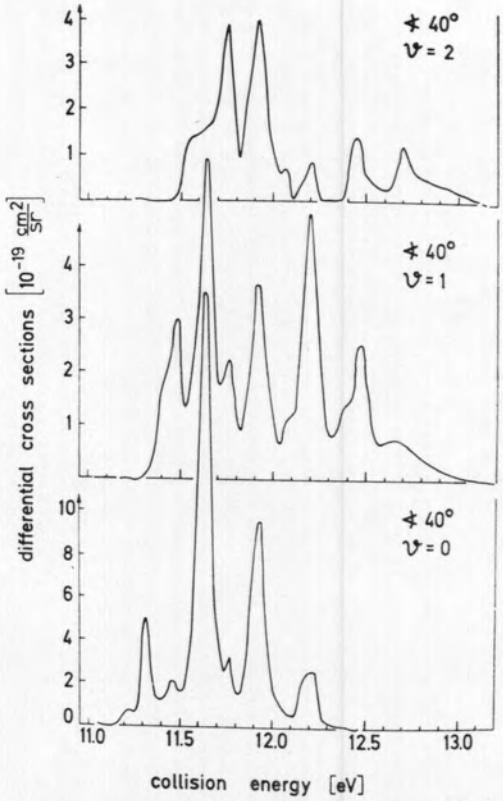

Fig. 8. Energy dependence of the differential cross section for excitation of the $v = 0$, 1 and 2 vibrational levels of the $B^1\Sigma_u^+$ state of H_2. The scattering angle is 40° and the curves were smoothed to bring out the significant structure that appears in all tracings. Note the different absolute scales. Resonance series II appears weak in the channel $v = 0$, but rather strong in the channels $v = 1$ and 2. (From ref. [91].)

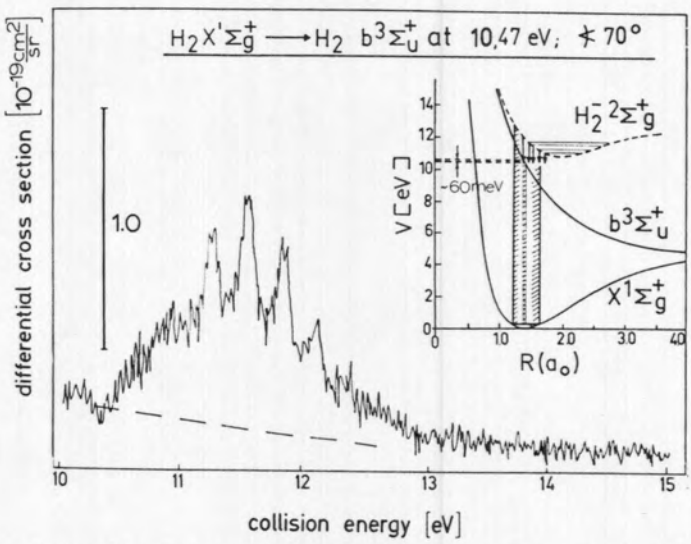

Fig. 9. Energy dependence of the absolute differential cross section for excitation into a narrow band (~60 meV) at 14.47 of the dissociative continuum $b^3\Sigma_u^+$ channel by electron collision with H_2. The zero line is dashed. The length of the bar to the left of the curve represents the absolute scaling factor in units of 1.0×10^{-19} cm²/sr. The insert illustrates the autoionization of the H_2^- ion into the energy band. The Franck–Condon region is subdivided such that direct excitation can only occur in the center part, while transitions into the resonance take place over the whole width. (From ref. [91].)

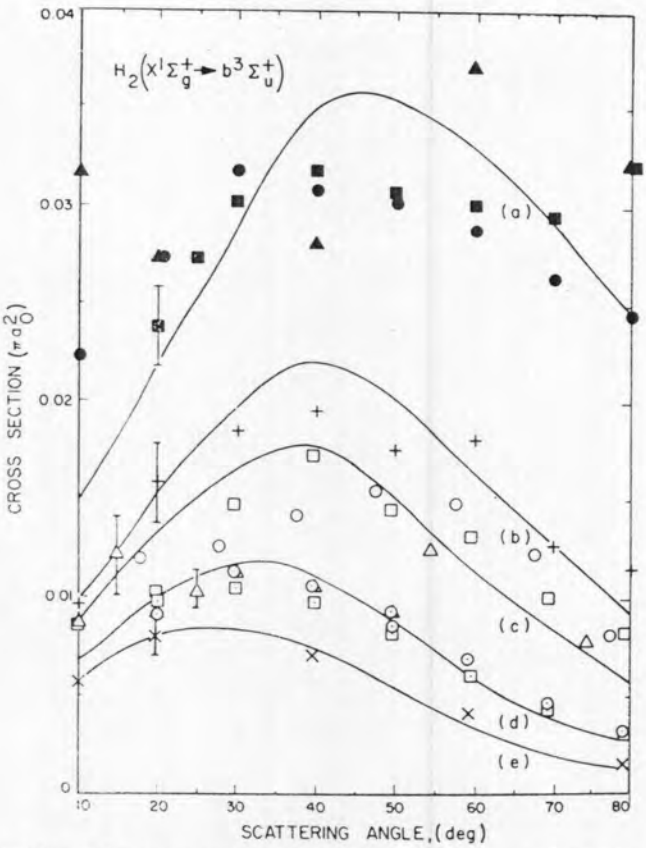

Fig. 10. Differential cross section of the $X^1\Sigma_g^+ \rightarrow b^3\Sigma_u^+$ transition in H_2 as a function of scattering angle. Solid curves are theoretical and points are experimental. Different symbols indicate different experiments. Incident energies are (a) 25 eV: ●, ■, ▲; (b) 35 eV: +; (c) 40 eV: ○, □, △; (d) 50 eV: ⊙, ⊡, ◬; (e) 60 eV: ×. (From ref. [107].)

al. [108] in the resonance region. They determined absolute differential cross sections for the $c^3\Pi_u$ ($v = 1$) state at 10° in the 12.0 to 13.5 eV impact energy range (fig. 11), and for the threshold peak of this same state in the 5° to 132° angular range (table 17). Their differential excitation functions for the unresolved $d^3\Pi_u$ ($v = 1$) + $g^3\Sigma_u^+$ ($v = 1$) states at 7° scattering angle in the 14.0 to 16.5 eV impact energy range are shown in fig. 12. Normalization was achieved by comparison to the $B^1\Sigma_u^+$ ($v = 0$) channel for which cross sections were determined previously [91]. The authors also present in ref. [108] the differential excitation function for the $B^1\Sigma_u^+$ ($v = 0$) state at 8.5° from 11 to 14 eV (fig. 13).

Srivastava and Jensen [109] studied excitation of the $B^1\Sigma_u^+$ ($v = 2$) state in the 15–60 eV impact energy and 10–135° angular ranges. Their differential cross sections are included in table 16 and their integral excitation cross sections for this band and for the overall $B^1\Sigma_u^+$ state are given in table 18. The DCS were normalized against H_2 elastic scattering, which in turn was normalized to He. We have renormalized their original cross section values in tables 16 and 18 on the basis of the more recent He elastic cross section data of Register et al. [10].

Optical excitation function measurements are summarized in table 19. (See e.g., ref. [120] for identification of symbols.) Studies of dissociation by electron impact leading to excited atomic hydrogen are listed in table 20.

Gerhart [132] generated semi-empirical cross sections for electronic excitation by using all the available data on cross sections and their energy dependence. The data were then normalized to the generalized oscillator strength distribution at high impact energies. These data were somewhat revised

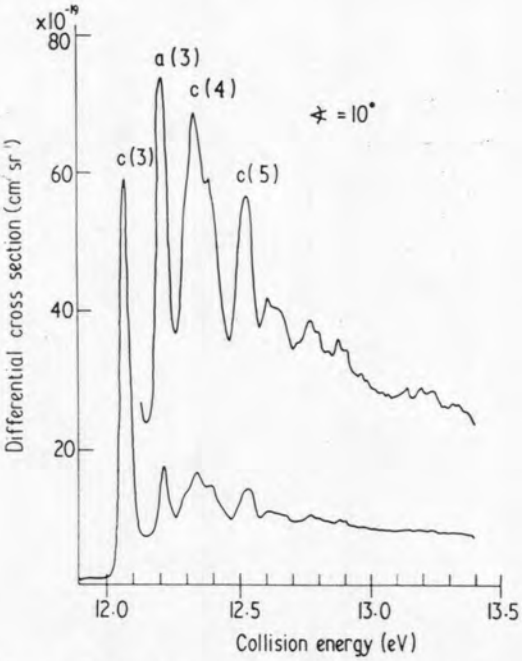

Fig. 11. Energy dependence of the differential cross section of the $v = 1$ level of the $c^3\Pi_u$ state of H_2. The scale of cross sections does not apply to the amplified portion of the curve. The bracketed numbers correspond to the vibrational levels of resonance bands 'c' and 'a' (From ref. [108].)

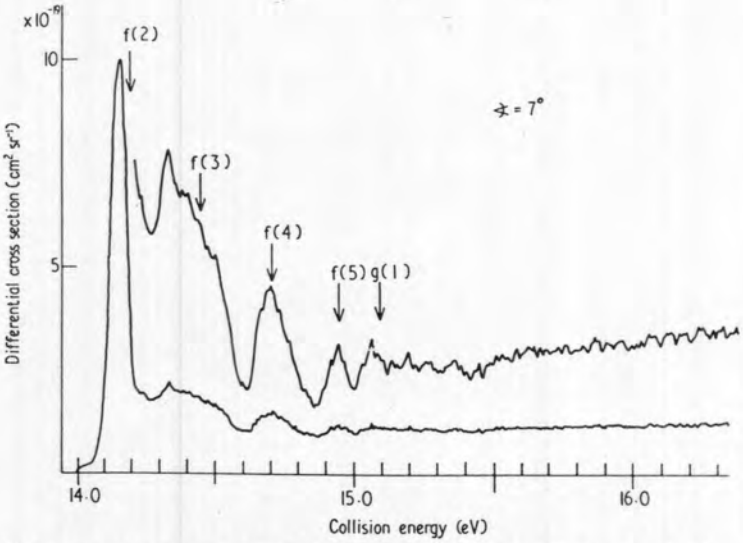

Fig. 12. The energy dependence of the differential cross section of the level $v = 1$ of the $d^3\Pi_u$ and $g^3\Sigma_u^+$ states of H_2 which cannot be resolved. The scale of cross sections does not apply to the amplified portion of the curve. The arrows and bracketed numbers correspond to the energy positions of the levels of resonance bands 'f' and 'g'. (From ref. [108].)

by Douthat [133]. Miles et al. [134] gave representations of the cross sections in terms of parameterized analytical functions. van Wingerden et al. [80] utilized total electron scattering data to check the consistency of the sum of the empirical cross section data. These cross sections have been frequently used by modelers because of a lack of measured cross sections. Very recently de Heer [135] has summarized the situation on electronic excitation, dissociation and ionization of H_2, D_2 and T_2.

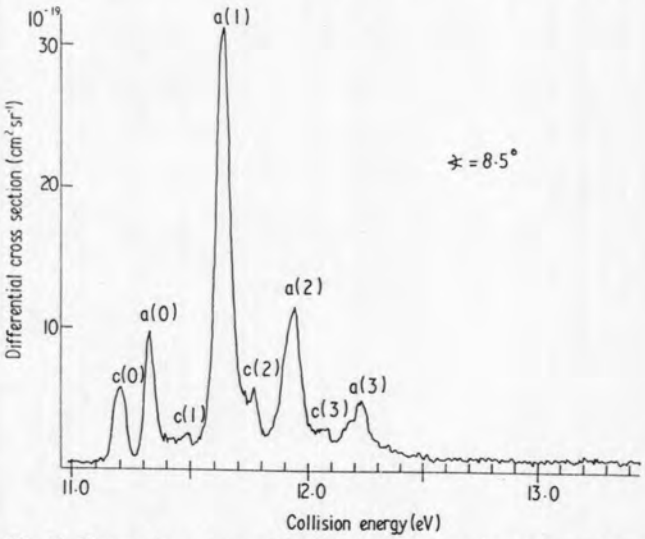

Fig. 13. Energy dependence of the differential cross section of the $v = 0$ level of the $B^1\Sigma_u^+$ state of H_2. The bracketed numbers correspond to levels of resonance bands 'c' and 'a'. (From ref. [108].)

Table 18
Integral cross sections for the excitation of the $B^1\Sigma_u^+$ state of H_2 (Srivastava et al., 1977, ref. [109], corrected on the basis of the elastic cross sections of table 4B)

E_0 (eV)	$\sigma_v = 2$ 10^{-20} cm²	$\Sigma_v \sigma_v$ 10^{-18} cm²
15	55 ± 16	17 ± 5
20	79 ± 23	25 ± 7
30	76 ± 23	24 ± 7
40	87 ± 26	28 ± 8
50	(75)	(24)
60	56 ± 17	18 ± 5

Values in parentheses were obtained by interpolation.

Table 19
Summary of optical excitation function measurements in H_2

State	Impact energy (eV)[a]	Reference
$C^1\Pi_u$	50 – 6000	de Heer–Carriere, 1971, ref. [110]
$C^1\Pi_u$	T – 300	Stone–Zipf, 1972, ref. [111]
$d^3\Pi_u$	T – 100	Baltayan–Nedelec, 1976, ref. [112]
$d^3\Pi_u$	T – 100	Mohlmann–de Heer, 1976, ref. [113]
$G^1\Sigma_g^+$	T – 500	Anderson–Watson, 1977, ref. [114]
$E^1\Sigma_g^+$, $F^1\Sigma_g^+$, $H^1\Sigma_g^+$	T – 300	Watson–Anderson, 1977, ref. [115]
$G^1\Sigma_g^+$, $I^1\Pi_g$, $K^1\Sigma_g^+$, $M^1\Sigma_g^+$, $N^1\Sigma_g^+$	50	Day et al., 1979, ref. [116]
$B^1\Sigma_u^+$, $C^1\Pi_u$	T – 300	Malcolm et al., 1979, ref. [117]
$d^3\Pi_u$	T – 100	Bogdanova et al., 1981, ref. [118]
$B^1\Sigma_u^+$, $C^1\Pi_u$	T – 400	Ajello–Srivastava, 1981, ref. [119]

[a]T means threshold.

Table 20
Summary of studies of the electron-impact dissociation of H_2, HD and D_2 leading to excited atoms

Reference	Molecule	Energy range (eV)	Radiation[a]
Mumma and Zipf, 1971, ref. [121]	H_2	0–400	L_α
de Heer and Carrier, 1971, ref. [110]	H_2	50–6000	L_α
McConkey and Donaldson, 1972, ref. [122]	H_2	20–2000	L_α
Walker and St. John, 1974, ref. [123]		200	H_α, H_β, H_γ, H_δ, H_ε
Khayrallah, 1976, ref. [124]	H_2, D_2	10–540	H_α, H_β, H_γ
Freund et al., 1976, ref. [125]	H_2	0–400	L_α, H_α, H_β, H_γ, H_δ
Möhlmann et al., 1977, ref. [126]	H_2, D_2	0–2000	H_α, H_β, H_γ
Karolis and Harting, 1978, ref. [127]	H_2, D_2	0–100	H_α, H_β
Möhlmann et al., 1978, ref. [128]	H_2, HD, D_2	0–2000	L_α
		0–2000	H_β
Möhlmann and de Heer, 1979, ref. [129]	H_2	100	H_n (n = 3 to 11)
Bose and Linder, 1979, ref. [130]	H_2	11–16	L_α
Higo and Ogawa, 1981, ref. [131]	D_2	17–100	H_β

[a]L_n and H_n refer to the Lyman and Balmer series radiation, respectively.

4.2. N_2

Electron scattering cross sections in molecular nitrogen are particularly important since N_2 is often used as a buffer gas in many types of swarm and discharge plasmas such as gaseous mixtures for both high-voltage standoff, and for various configurations of high-power switches. Solutions to Boltzmann's equation [136] require a complete and consistent set of elastic and inelastic cross sections for modeling purposes. Nitrogen, as the major component of the atmosphere, also plays a critical role in phenomena such as auroras, and generation of characteristic missile, satellite, and space-shuttle re-entry emissions.

Total scattering cross sections

Recent measurements of Kennerly [137], Blaauw et al. [138], Dalba et al. [139], Hoffmann [140], Mathur and Hasted [141a], and Hasted et al. [142b] have yielded total scattering cross sections in the energy range 0.5–1600 eV with a stated experimental accuracy of 5% or less. These measurements are summarized in table 21 and figs. 14 and 15. Baldwin [142] reported total scattering cross sections in the 0 to 2 eV impact energy range. (See table 21.) As in the case of H_2, the measurements agree with one another to 7% or better over the energy range where overlap in the data exists.

Momentum-transfer cross sections have been measured by Freeman and Wada [97] in a low-density swarm experiment over the approximate energy range 6.6–50 meV. A cross section of 1.7×10^{-16} cm^2 at 13 meV (Ramsauer–Townsend minimum) is reported.

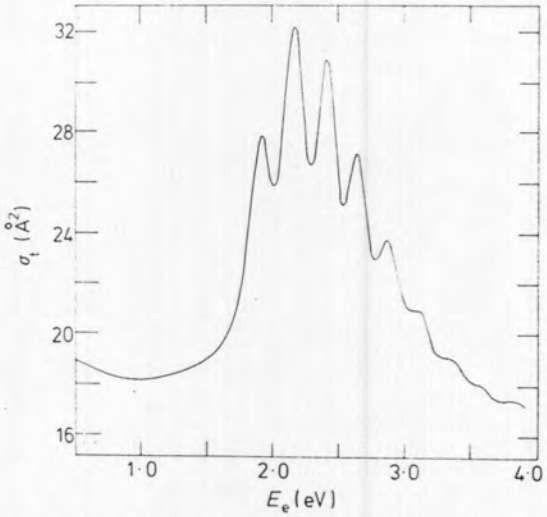

Fig. 14. Total electron scattering cross sections in N_2 in the energy range 0.5–3.9 eV as measured in transmission. (From ref. [141].)

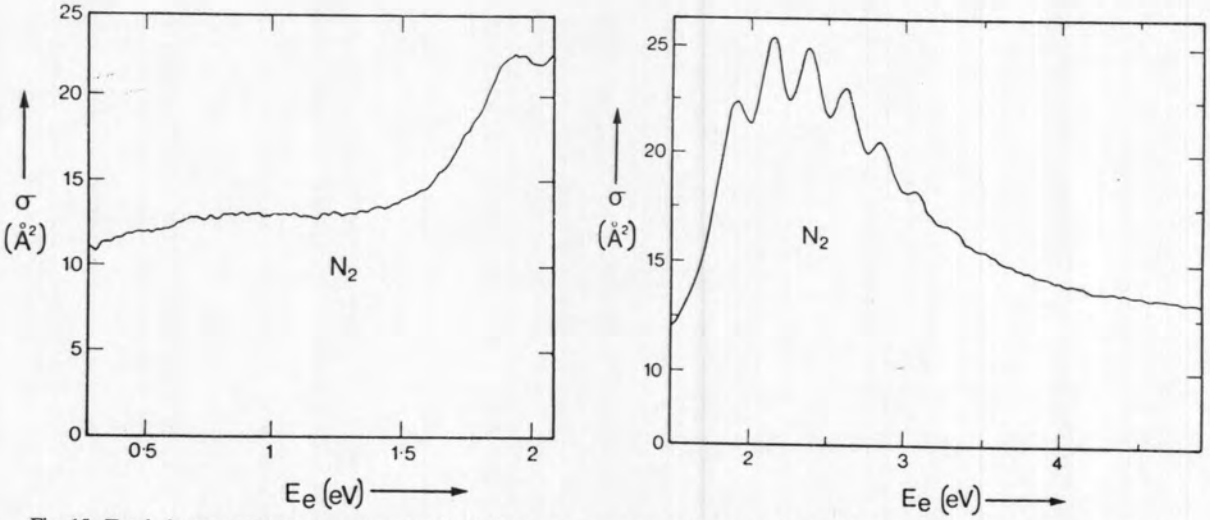

Fig. 15. Total electron scattering cross section in N_2 in the energy ranges 0.3–2.1 eV (left) and 1.5–4.7 eV (right). (From ref. [141b].)

Table 21
Total electron scattering cross sections for N_2 (10^{-16} cm^2 units)

A. Kennerly 1980, ref. [137]

E_0 (eV)	σ_T	E_0 (eV)	σ_T	E_0 (eV)	σ_T	E_0 (eV)	σ_T	E_0 (eV)	σ_T	E_0 (eV)	σ_T
0.519	8.79	1.317	10.44	2.236	32.62	3.523	15.05	6.251	11.15	14.01	12.54
0.535	8.74	1.333	10.36	2.254	31.11	3.557	15.05	6.331	11.09	14.28	12.56
0.552	8.91	1.349	10.61	2.272	29.75	3.591	14.55	6.414	11.15	14.56	12.50
0.570	8.94	1.365	10.66	2.290	28.32	3.626	14.51	6.497	11.12	14.85	12.58
0.588	9.14	1.381	10.55	2.308	27.14	3.662	14.16	6.583	11.10	15.14	12.69
0.607	8.90	1.398	10.75	2.326	26.19	3.698	14.14	6.670	11.12	15.45	12.63
0.628	9.43	1.415	10.76	2.345	26.36	3.734	13.86	6.759	11.11	15.76	12.58
0.649	9.07	1.432	10.80	2.364	27.64	3.772	13.71	6.849	11.23	16.09	12.65
0.672	9.30	1.450	10.96	2.383	28.82	3.809	13.63	6.942	11.02	16.42	12.78
0.695	9.38	1.468	10.97	2.403	30.79	3.848	13.34	7.036	11.06	16.77	12.80
0.720	9.21	1.487	10.98	2.422	32.06	3.886	13.50	7.133	11.08	17.13	12.88
0.747	9.14	1.505	11.24	2.442	33.03	3.926	13.31	7.231	11.05	17.49	12.84
0.774	9.53	1.524	11.29	2.463	31.80	3.966	13.09	7.331	11.05	17.87	13.07
0.804	9.38	1.544	11.40	2.483	30.85	4.007	13.21	7.434	10.99	18.26	12.92
0.835	9.55	1.563	11.58	2.504	29.19	4.048	12.92	7.538	11.08	18.67	13.02
0.868	9.73	1.584	11.79	2.525	27.25	4.090	12.89	7.645	10.97	19.09	13.13
0.898	9.89	1.604	11.86	2.546	25.83	4.132	12.88	7.754	11.11	19.52	13.24
0.907	9.91	1.625	12.04	2.567	25.18	4.176	12.48	7.866	11.00	19.97	13.25
0.916	9.81	1.647	12.30	2.589	25.19	4.220	12.44	7.980	11.01	20.43	13.23
0.925	9.97	1.668	12.66	2.611	25.63	4.264	12.54	8.096	11.18	20.91	13.35
0.934	9.75	1.691	13.00	2.633	27.03	4.310	12.34	8.215	10.88	21.41	13.39
0.943	9.85	1.713	13.51	2.656	27.90	4.356	12.31	8.337	11.18	21.92	13.36
0.953	9.84	1.736	13.79	2.679	27.78	4.402	12.25	8.461	11.30	22.46	13.40
0.962	9.93	1.760	14.44	2.702	26.74	4.450	12.19	8.588	11.25	23.01	13.21
0.972	9.96	1.784	15.28	2.725	25.90	4.498	12.15	8.718	11.26	23.59	13.20
0.982	9.87	1.809	16.36	2.749	24.33	4.547	11.95	8.851	11.31	24.18	13.04
0.992	9.97	1.834	17.46	2.773	22.95	4.597	12.00	8.987	11.41	24.80	12.96
1.002	9.91	1.853	18.61	2.798	22.19	4.648	11.99	9.126	11.44	25.44	12.86
1.012	9.88	1.866	19.12	2.822	22.32	4.700	11.89	9.269	11.40	26.11	12.83
1.023	9.86	1.879	20.23	2.848	22.49	4.752	11.90	9.415	11.47	26.80	12.76
1.033	9.96	1.892	21.19	2.873	22.84	4.806	11.79	9.564	11.71	27.53	12.60
1.044	10.05	1.906	22.26	2.899	23.28	4.860	11.74	9.717	11.69	28.28	12.63
1.055	10.04	1.922	23.23	2.925	22.39	4.915	11.64	9.874	11.78	29.06	12.41
1.066	10.01	1.936	24.26	2.951	21.64	4.971	11.63	10.03	11.79	29.88	12.33
1.078	10.21	1.951	25.40	2.978	20.51	5.028	11.56	10.20	11.83	30.73	12.19
1.089	10.10	1.965	25.95	3.005	19.73	5.086	11.71	10.37	11.79	31.62	12.24
1.101	10.17	1.980	25.88	3.033	19.29	5.146	11.49	10.54	11.82	32.55	11.91
1.113	10.07	1.994	25.84	3.061	19.30	5.206	11.60	10.72	11.86	33.52	11.73
1.125	10.06	2.009	25.61	3.089	19.17	5.267	11.44	10.90	11.86	34.53	11.67
1.137	9.95	2.024	25.37	3.118	19.24	5.329	11.49	11.08	11.93	35.59	11.65
1.150	10.03	2.039	24.52	3.147	18.69	5.393	11.25	11.27	11.81	36.70	11.48
1.162	10.22	2.055	23.81	3.176	18.22	5.457	11.39	11.47	11.89	37.86	11.41
1.175	10.31	2.070	23.69	3.206	17.46	5.523	11.36	11.67	11.91	39.07	11.35
1.188	10.15	2.086	23.83	3.236	16.95	5.590	11.29	11.88	11.95	40.35	11.32
1.202	10.14	2.102	24.13	3.267	16.75	5.658	11.47	12.09	11.93	41.69	10.93
1.215	10.34	2.118	25.26	3.298	16.69	5.727	11.19	12.31	11.97	43.10	10.90
1.229	10.27	2.134	27.18	3.328	16.60	5.798	11.35	12.53	11.86	44.58	11.02
1.243	10.33	2.151	29.13	3.360	16.51	5.870	11.36	12.76	12.13	46.14	10.60
1.258	10.32	2.167	30.77	3.391	16.02	5.943	11.25	13.00	12.07	47.78	10.27
1.272	10.43	2.184	32.78	3.423	15.90	6.018	11.27	13.24	12.24	49.51	10.45
1.287	10.42	2.201	33.22	3.456	15.37	6.094	11.11	13.49	12.43	51.33	10.27
1.302	10.31	2.219	33.58	3.489	15.16	6.172	11.15	13.74	12.43		

Table 21 (*cont.*)

B. Blaauw et al. 1980, ref. [138]; Dalba et al. 1980, ref. [139]; and Hoffman et al. 1982, ref. [140].

E_0 (eV)	Ref. [138]	Ref. [140]	E_0 (eV)	Ref. [138]	Ref. [139]	Ref. [140]
2.2		30.9	100.0	8.98		8.64
2.8		24.7	121.0	–	8.98	–
3.8		14.5	125.0	8.16	–	–
4.6		12.2	144	–	8.22	–
5.7		12.1	150	7.49	–	7.26
6.6		11.7	175	6.91	–	–
7.7		11.6	196	–	6.97	–
8.8		12.0	200.0	6.42	–	6.22
9.7		12.3	225.0	5.99	–	–
10.0		12.3	250.0	5.66	–	–
11.7		12.1	256	–	5.86	–
12.2		12.1	275.0	5.35	–	–
14.7		13.2	300.0	5.08	–	4.86
17.5	13.37	–	324	–	5.10	–
20.0	13.62	13.8	325.0	4.84	–	–
22.5	13.64	–	350.0	4.63	–	–
25.0	13.50	–	375.0	4.44	–	–
27.5	13.18	–	400.0	4.27	4.42	4.07
30.0	12.85	12.8	450.0	3.96	–	–
32.5	12.54	–	484	–	3.82	–
35.0	12.28	–	500.0	3.69	–	3.46
40.0	–	12.0	550.0	3.43	–	–
45.0	11.64	–	576	–	3.39	–
50.0	11.48	11.3	600.0	3.19	–	3.10
55.0	11.07	–	650.0	2.97	–	–
60.0	10.77	–	676	–	2.99	–
70.0	10.21	–	700.0	2.77	–	2.83
75.0	–	9.9	750.0	2.62	–	
80	9.80		784		2.62	
90	9.37		900		2.33	
			1024		2.12	
			1156		1.91	
			1296		1.72	
			1444		1.56	
			1600		1.42	

C. Baldwin 1974, ref. [142].

E_0 (eV)	σ_T	E_0 (eV)	σ_T
1.56	11.67	0.53	9.01
1.34	10.83	0.48	9.00
1.16	10.38	0.44	7.85
1.02	9.98	0.41	6.71
0.90	9.83	0.38	5.80
0.80	9.61	0.35	6.73
0.71	9.45	0.32	4.67
0.64	9.37	0.30	7.65
0.58	9.13		

Elastic scattering cross sections

Elastic differential scattering cross sections have been recently measured by DuBois and Rudd [143], Shyn and Carignan [144] and Srivastava et al. [145a]. Calibrations to the absolute cross section scale were made in each case either by an absolute measurement (with referencing of the effective path length to total scattering cross section) [143], by comparison of scattered count rates to a calculated He cross section [144], or a measured He cross section [145a]. A value of 9.77×10^{-16} cm^2 for the elastic scattering cross section at 20 eV is reported by Truhlar et al. [145b] obtained by normalization to the difference of the total and ionization cross sections. Absolute elastic differential cross sections have been reported by Bromberg [146] at energies of 300, 400 and 500 eV, and by Jansen et al. [147] at ten electron energies between 100 and 3000 eV. These data are presented here in tables 22 and 23. Kambara and Kuchitsu [148a] report relative elastic differential cross sections at 50, 100, 300 and 500 eV. Their data at 300 and 500 eV may be normalized to the absolute measurements [146, 147] for comparing the shape of their differential cross section (see, for example, table 10 of ref. [147]). Finn

Table 22
Elastic differential cross sections in N_2. Units are 10^{-16} cm^2/sr. (From Bromberg 1970, ref. [146].)

	E_0 (eV)		
θ (deg)	300	400	500
2	21.0	21.4	19.5
2.5	19.2	18.4	17.7
3	18.0	17.2	16.2
3.5	16.7	15.4	14.9
4	15.5	14.4	13.7
5	13.2	12.2	11.4
6	11.3	10.3	9.62
7	9.63	8.64	7.94
8	8.26	7.30	6.55
9	6.99	6.10	5.33
10	5.89	5.05	4.34
12	4.18	3.43	2.83
14	2.93	2.28	1.83
16	2.06	1.54	1.22
18	1.44	1.06	0.848
20	1.02	0.764	0.624
25	0.496	0.426	0.395
30	0.326	0.301	0.285
35	0.242	0.224	0.199
40	0.190	0.162	0.126
45	0.148	0.115	0.0846
50	0.113	0.0804	0.0591
55	0.0846	0.0588	0.0473
60	0.0633	0.0476	0.0409
65	0.0524	0.0412	0.0350
70	0.0451	0.0378	0.0291
80	0.0392	0.0288	0.0193
90	0.0342	0.0213	0.0148
100	0.0288	0.0168	0.0132
110	0.0244	0.0154	0.0106

Table 23
Elastic differential cross sections in N_2. Units are 10^{-16} cm^2/sr. (From Jansen et al. 1976, ref. [147].)

	E_0 (eV)									
θ (deg)	100	150	200	300	400	500	750	1000	2000	3000
5	17.1	16.5	15.3	13.2	12.0	11.1	9.41	8.37	5.82	3.47
10	10.0	8.65	7.59	6.05	5.07	4.34	3.02	2.24	1.01	0.692
15	5.68	4.40	3.56	2.52	1.90	1.51	0.946	0.739	0.456	0.234
20	3.05	2.11	1.61	1.07	0.826	0.675	0.484	0.420	0.186	0.0809
25	1.60	1.05	0.790	0.526	0.451	0.403	0.322	0.248	0.0778	0.0358
30	0.871	0.557	0.440	0.333	0.305	0.286	0.203	0.133	0.0451	0.0203
35	0.512	0.342	0.291	0.257	0.230	0.207	0.115	0.0731	0.0278	0.0122
40	0.330	0.237	0.218	0.211	0.174	0.139	0.0678	0.0493	0.0165	0.00748
45	0.233	0.185	0.176	0.160	0.122	0.0868	0.0473	0.0378	0.0120	0.00512
50	0.178	0.153	0.144	0.114	0.0829	0.0585	0.0384	0.0260	0.00854	0.00350
>50[a]	0.151	0.136	0.129	0.101	0.0630	0.0526	0.0325	0.0204	0.00627	0.00286
[a]At θ =	54.0	54.1	54.1	53.4	54.0	53.3	53.9	53.9	53.9	53.8

Table 24
Differential cross sections for elastic scattering of electrons from N_2 in the 20–800 eV energy range. Numbers in parentheses at the head of each column multiply the entries in that column. Units are 10^{-16} cm^2/sr. (From DuBois and Rudd, 1976, ref. [143].)

	E_0 (eV)						
θ (deg)	20 (1)	50 (1)	100 (1)	200 (1)	400 (10)	500 (10)	800 (10)
2					185	162	116
3				20.4	164	141	107
4			17.1	17.6	144	119	91.8
5		14.4	15.7	15.4	122	99.7	77.3
6		13.1	14.3	13.4	104	82.9	60.8
8		10.9	11.7	10.2	72.8	57.4	37.0
10		9.30	8.99	7.42	46.5	37.2	21.7
12	4.51	7.56	7.06	5.38	31.9	24.9	13.8
14	3.86	6.55	5.57	3.95	21.5	16.2	8.65
15	–	5.99	4.82	3.44	17.9	13.3	7.34
16	3.72	5.57	4.28	2.97	14.6	11.0	6.33
20	2.97	3.92	2.66	1.63	7.64	6.05	4.23
25	2.35	2.50	1.48	0.762	4.56	3.89	2.78
30	1.94	1.59	0.784	0.426	3.16	2.78	1.60
40	1.22	0.692	0.305	0.217	1.72	1.29	0.552
50	0.778	0.319	0.167	0.147	0.815	0.574	0.333
60	0.484	0.177	0.109	0.104	0.504	0.400	0.178
70	0.330	0.114	0.0801	0.0734	0.395	0.286	0.118
80	0.218	0.0809	0.0745	0.0538	0.297	0.189	0.0876
85	0.194	0.0700	–	–	–	–	–
90	0.192	0.0661	0.0770	0.0479	0.218	0.147	0.0616
95	0.221	0.0683	–	–	–	–	–
100	0.275	0.0795	0.0801	0.0554	0.179	0.129	0.0498
110	0.398	0.130	0.0882	0.0518	0.167	0.115	0.0423
120	0.521	0.209	0.104	0.0532	0.160	0.0941	0.0350
130	0.627	0.314	0.131	0.0526	0.148	0.0854	0.0308
140	0.725	0.420	0.158	0.0524	0.137	0.0812	0.0279
150	0.787	0.532	0.192	0.0524	0.132	0.0818	0.0270

and Doering [148b] reported relative differential and normalized integral elastic cross sections. Their integral cross section results are given in table 27B.

The combined energy range in the differential measurements was 1.5–1000 eV, over an angular range 2°–168°. Results of these differential cross section measurements are given in tables 24–27, where data of table 26 have been renormalized to the recent He elastic measurements [10]. In general, there is good

Table 25
Differential cross sections for elastic scattering of electrons from N_2 in the energy range 1.5–400 eV. Entries in parentheses refer to extrapolated data. Units are 10^{-18} cm^2/sr. (From Shyn and Carignan, 1980, ref. [144].)

	E_0 (eV)									
θ (deg)	1.5	1.9	2.1	2.4	3.0	4.0	5.0	7.0	10.0	15.0
6										
12	98.8	275.4	329.3	340.4	298.8	184.2	158.7	210.9	255.2	463.0
18										
24	73.2	213.3	253.3	271.9	262.0	162.9	161.7	202.8	240.1	314.7
30										
36	49.4	151.2	177.3	209.9	212.2	159.4	159.9	191.3	199.1	196.8
48	54.5	106.7	125.4	139.2	155.9	125.7	134.8	169.7	153.5	126.2
60	64.7	94.5	100.1	99.0	108.3	95.1	103.0	129.9	103.2	75.3
72	78.3	101.3	92.5	82.7	77.9	71.4	77.9	88.1	62.7	44.7
84	86.8	104.0	92.5	74.0	66.0	56.1	62.9	67.5	46.9	24.5
96	86.6	99.9	87.4	69.6	61.7	50.2	57.5	55.9	36.1	26.2
108	81.7	94.5	82.3	69.6	68.2	52.5	56.9	59.9	45.0	38.6
120	71.5	90.5	88.7	87.0	79.0	59.6	61.1	71.5	60.3	50.0
132	64.7	121.5	127.9	128.3	115.8	73.8	70.7	82.6	76.4	72.6
144	68.1	190.4	216.6	211.0	174.3	92.1	87.5	101.7	93.7	92.2
156	102.1	278.1	325.5	332.8	237.1	116.9	100.6	110.8	108.0	108.7
168	(140.0)	(363.2)	(402.8)	(463.3)	(300.0)	(141.7)	(113.8)	(120.3)	(121.9)	(125.1)

	E_0 (eV)									
θ (deg)	20	30	40	50	70	100	150	200	300	400
6					1655.4	1592.6	1429.7	1348.9	1129.1	1063.7
12	674.8	875.8	991.0	1047.5	1102.4	934.3	740.8	629.4	414.8	380.4
18					552.2	429.5	323.8	256.0	152.1	117.3
24	421.1	408.5	403.1	360.1	297.9	212.7	138.3	96.8	57.1	51.6
30					139.2	90.3	64.0	45.6	32.0	31.2
36	216.2	182.6	144.0	105.4	77.8	48.4	33.0	26.9	21.7	20.9
48	117.7	75.6	53.0	38.0	26.7	19.5	16.4	14.6	11.0	9.0
60	63.3	35.1	23.7	17.7	13.3	10.9	10.5	9.6	5.8	4.7
72	33.3	19.1	13.5	10.2	7.4	7.5	7.4	6.0	3.8	3.6
84	19.6	13.3	8.5	6.6	6.3	7.3	5.9	4.5	3.4	2.6
96	22.1	12.4	7.9	6.6	7.5	7.4	5.7	4.1	3.0	2.0
108	34.8	18.4	12.3	11.0	10.8	8.2	6.3	4.3	2.4	1.7
120	52.5	30.8	24.2	21.4	17.6	10.5	7.3	4.8	2.3	1.6
132	70.0	50.6	42.8	35.8	24.5	13.6	8.6	5.2	2.4	1.6
144	93.5	77.6	65.1	51.6	31.7	18.0	9.5	5.2	2.5	1.6
156	121.2	104.2	90.4	67.7	39.2	22.6	10.7	5.1	2.5	1.6
168	(148.8)	(130.9)	(115.8)	(83.7)	(46.6)	(28.1)	(11.8)	(5.1)	(2.5)	(1.6)

Table 26
Elastic N_2 differential cross sections (10^{-16} cm^2/sr). In parentheses are the ratios σ_{N^2}/σ_{He}. The angles in brackets refer to extrapolated values. (From Srivastava et al., 1976, ref. [145a].)[a]

	E_0 (eV)									
θ (deg)	5.0	7.0	10.0	15.0	20.0	30.0	40.0	50.0	60.0	75.0
[0]	1.85	2.15	3.28	5.91	7.35	9.75	11.0	11.4	11.9	7.10
[10]	1.83	2.14	3.05	4.83	6.09	7.21	8.00	8.60	7.45	4.80
20	1.70	2.07	2.76	3.68	4.54	4.83	4.54	4.14	3.56	2.81
	(6.49)	(6.73)	(7.15)	(7.85)	(8.78)	(9.23)	(9.33)	(9.49)	(9.13)	(8.57)
30	1.73	1.92	2.32	2.56	2.77	2.39	2.07	1.60	1.26	0.939
	(6.49)	(6.54)	(6.75)	(6.50)	(6.69)	(6.15)	(6.17)	(5.61)	(5.15)	(4.88)
40	1.67	1.86	1.93	1.67	1.61	1.14	0.843	0.632	0.459	0.333
	(6.00)	(6.49)	(6.18)	(4.98)	(4.81)	(3.97)	(3.58)	(3.30)	(2.91)	(2.81)
50	1.44	1.61	1.54	1.26	0.974	0.593	0.398	0.295	0.216	0.155
	(4.84)	(5.55)	(5.21)	(4.33)	(3.56)	(2.73)	(2.35)	(2.19)	(2.01)	(1.98)
60	1.20	1.31	1.24	0.902	0.623	0.332	0.230	0.177	0.122	0.0952
	(3.69)	(4.34)	(4.31)	(3.43)	(2.69)	(1.93)	(1.83)	(1.79)	(1.57)	(1.71)
70	0.918	1.01	0.867	0.563	0.382	0.180	0.143	0.113	0.0742	0.0619
	(2.58)	(3.14)	(3.00)	(2.28)	(1.87)	(1.28)	(1.45)	(1.48)	(1.26)	(1.48)
80	0.743	0.770	0.602	0.352	0.248	0.132	0.0944	0.0807	0.0576	0.0569
	(1.89)	(2.22)	(2.00)	(1.46)	(1.31)	(1.08)	(1.16)	(1.30)	(1.23)	(1.74)
90	0.628	0.603	0.434	0.276	0.191	0.112	0.0758	0.0597	0.0563	0.0742
	(1.45)	(1.59)	(1.36)	(1.13)	(1.04)	(1.00)	(1.06)	(1.13)	(1.45)	(2.81)
100	0.585	0.556	0.475	0.396	0.265	0.130	0.0791	0.0772	0.0697	0.0685
	(1.23)	(1.34)	(1.39)	(1.57)	(1.44)	(1.23)	(1.20)	(1.64)	(2.08)	(3.10)
115	0.584	0.648	0.607	0.512	0.444	0.213	0.154	0.173	0.149	0.117
	(1.08)	(1.37)	(1.58)	(1.87)	(2.32)	(2.09)	(2.47)	(4.07)	(5.11)	(6.40)
135	0.657	0.830	0.865	0.799	0.672	0.457	0.412	0.363	0.244	0.219
	(1.06)	(1.52)	(1.97)	(2.61)	(3.29)	(4.37)	(6.60)	(8.79)	(9.07)	(13.46)
[140]	0.69	0.89	0.93	0.87	0.75	0.56	0.50	0.43	0.29	0.26
[150]	0.75	1.05	1.12	1.04	0.90	0.71	0.75	0.60	0.35	0.32
[160]	0.83	1.28	1.35	1.21	1.05	0.91	1.08	0.78	0.42	0.41
[170]	0.93	1.46	1.60	1.36	1.18	1.09	1.42	0.95	0.46	0.49
[180]	1.06	1.80	1.90	1.47	1.27	1.23	1.79	1.09	0.49	0.53

[a]The cross section values in this table were obtained from the published N_2 to He elastic scattering intensity ratios of Srivastava et al. [145] and the recent He cross sections of Register et al. [10].

agreement among the different sets of data. Measurements of DuBois and Rudd tend to be smaller at small angles at 20 eV, but agreement improves at higher angles, and at 50 eV.

All sets of data have been extrapolated to 0° and 180°, and integral elastic cross sections (which in all cases include pure rotational excitations) have been reported. These integrated data are presented in table 27. One sees the general satisfactory agreement between refs. [144] and [145a] while the lower forward scattering differential cross sections at 20 eV in ref. [143] have led to a smaller cross section at that energy.

Relative elastic differential cross sections have also been reported by Hermann et al. [149] at energies of 90–1000 eV. They were normalized to absolute cross sections by theoretical calculations in an independent-atom model. These results (of table I, ref. [149]) are generally about factors 1.4–1.6 larger than the experimentally-normalized data in tables 24–27.

Table 27

A. Integral (σ) and momentum transfer (σ^M) elastic scattering cross sections in N_2. Units are 10^{-16} cm^2.

E_0 (eV)	DuBois–Rudd 1976, ref. [143]	Shyn–Carignan 1980, ref. [144]		Srivastava et al. 1976, ref. [145][a]	
	σ	σ	σ^M	σ	σ^M
1.5		9.6	10.0		
1.9		16.7	17.1		
2.1		17.5	18.1		
2.4		17.4	16.8		
3.0		14.8	12.6		
4.0		11.1	9.6		
5.0		11.2	9.2	11.7	9.25
7.0		12.5	10.8	13.3	10.9
10.0		11.7	9.3	13.3	10.5
15.0		11.3	8.2	12.1	8.85
20.0	9.13	12.1	8.3	11.2	7.33
30.0	–	10.3	6.0	8.89	5.01
40.0	–	9.4	4.7	8.12	4.66
50.0	7.22	8.5	4.1	7.03	3.82
60.0	–	–	–	5.45	2.55
70.0	–	7.3	2.8	–	–
75.0	–	–	–	4.31	2.29
100.0	4.96	5.6	1.76		
150.0	–	4.5	1.17		
200.0	3.53	3.7	0.75		
300.0	–	2.6	0.46		
400.0	2.11	2.3	0.35		
500.0	1.65				
800.0	1.10				

[a]Calculated from the renormalized data in table 26.

B. Integral elastic cross sections in N_2 (10^{-16} cm^2 units) from ref. [148b].

Energy (eV)	σ	Energy (eV)	σ	Energy (eV)	σ
13	12.4	24	11.5	60	4.7
15	11.8	30	8.8	75	4.7
18	10.9	35	7.2	90	3.9
20	11.2	40	6.4	100	3.8
22	10.9	50	5.7		

Rotational excitation cross sections

Because of the small rotational spacing in N_2 (~3 meV at $J_{max} = 7$) electron scattering measurements, to more or less an extent, involve an average over many ΔJ transitions with different initial J states. One measures a profile of the rotational excitation in the $v = 0 \rightarrow 0$ or $v = 0 \rightarrow 1$ bands and fits the profile to a theoretical model to gain information about the rotational excitation contributions. See ref. [152].

Cross sections have been reported by Wong and Dubé [150], Jung [151], Shimamura [152], Tanaka et al. [153] and most recently by Jung et al. [154]. Results are shown in figs. 16–20. With a resolution of

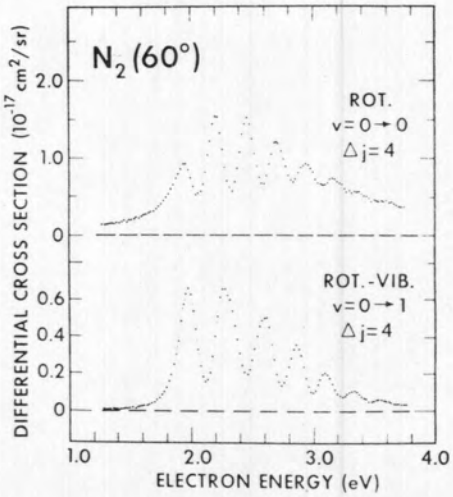

Fig. 16. Energy dependence of pure rotation at $J = 4$ (upper) and rotational-vibrational $v = 1$, $J = 4$ (lower) cross sections in N_2 at a scattering angle of 60°. (From ref. [150].)

10–18 meV (FWHM) Jung [151] and Jung et al. [154] were able to observe summed profiles for the $\Delta J = 0, 2$ and 4 excitations in $v = 0 \rightarrow 0$ (fig. 17) and $v = 0 \rightarrow 1$ (figs. 18, 19). Comparisons of these cross sections have been made with various theories [152–157]. Integral cross sections for the unfolded ΔJ profiles are given in table 28 from the results of Jung et al. [154].

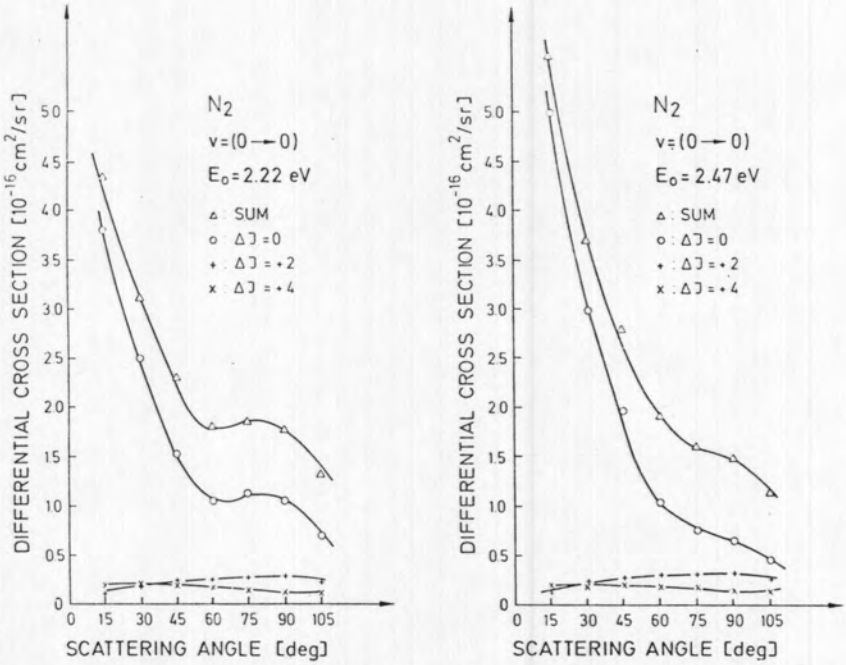

Fig. 17. Differential cross sections for rotational excitation in N_2 with $\Delta v = 0$, and $\Delta J = 0$, +2 and +4 at incident energies of 2.22 eV (left) and 2.47 eV (right). (From ref. [154].)

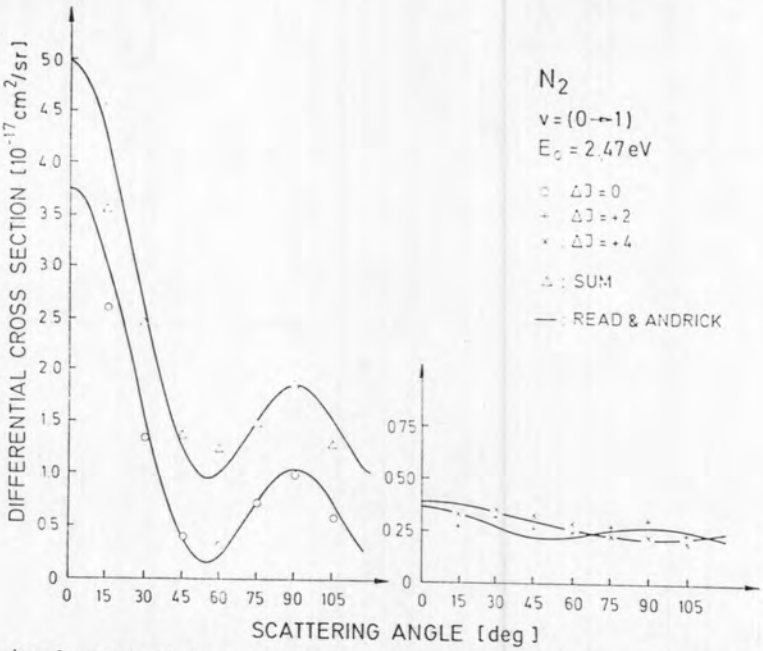

Fig. 18. Differential cross sections for rotational-vibrational excitation in N_2 with $\Delta v = 1$, and $\Delta J = 0$, +2 and +4 at an incident energy of 2.47 eV. The solid curves are calculated from theory of Read and Andrick [157] averaged over an initial rotational distribution corresponding to a gas temperature of 500 K. (From ref. [154].)

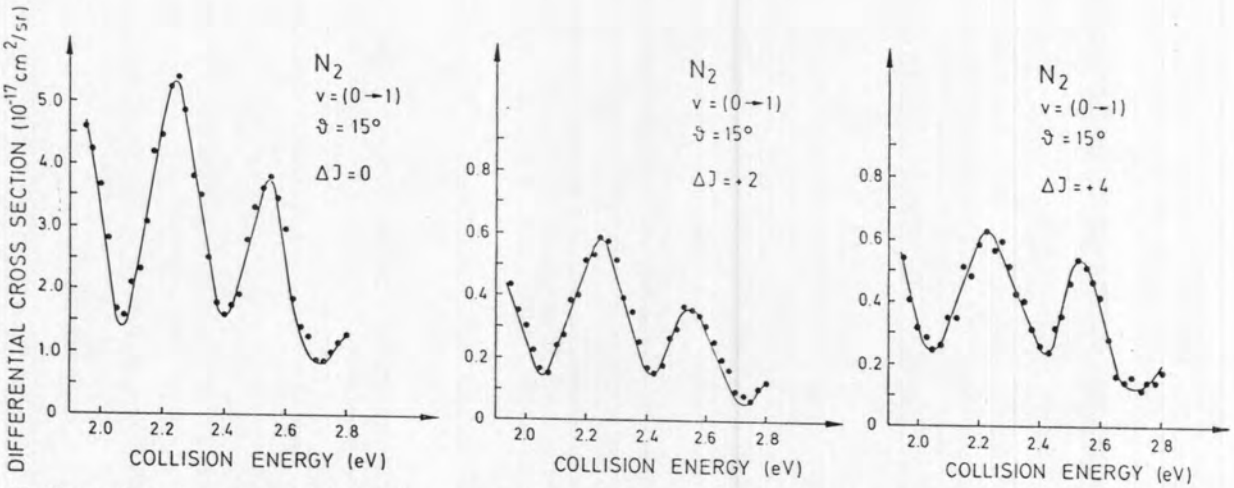

Fig. 19. Energy dependence of the differential cross section at $\theta = 15°$ in N_2 for $\Delta v = 1$, and $\Delta J = 0$ (left), $\Delta J = +2$ (middle), and $J = +4$ (right). (From ref. [154].)

Vibrational excitation cross sections

A. The $^2\Pi_g$ shape-resonance region (1–5 eV)

Recent measurements of pure vibrational excitation cross sections in N_2 have been reported by Truhlar et al. [145b] at 20 eV, and Tanaka et al. [158] and Truhlar et al. [159, 160] at energies of 3 to 75 eV. Excitations at 3 and 5 eV are still influenced to some extent by the $^2\Pi_g$ shape resonance at 2.3 eV. Data of refs. [158–160] were obtained in essentially the same fashion: the relative flow technique [42] was used to obtain elastic scattering cross sections of N_2 by calibration to He. Vibrationally inelastic cross sections were then obtained using measurements of inelastic/elastic scattering intensities in N_2.

Table 28
Integral cross sections for electron impact vibrational-rotational excitation of N_2. Units are 10^{-16} cm^2. (From Jung et al. 1982, ref. [154].)

Collision energy	2.47 eV	2.2 eV	2.25 eV	2.47 eV	2.54 eV
Vibrational transition	$v = 0 \to 0$ (electric)	$v = 0 \to 1$			
$\Delta J = 0$	19.1	2.33	2.58	1.19	1.89
$\Delta J = +2$	3.97	0.77	0.85	0.39	0.62
$\Delta J = -2$	3.04	0.58	0.64	0.30	0.47
$\Delta J = +4$	2.82	0.77	0.85	0.39	0.62
$\Delta J = -4$	1.65	0.44	0.49	0.22	0.35
$\Sigma\, \Delta J = 0, \pm 2, \pm 4$	30.58	4.89	5.41	2.49	3.95

Since the primary measured quantity is the ratio of the $v = 0 \to 1$ to $v = 0 \to 0$ (elastic) scattering cross section, we list in table 29 that ratio R_1 (E_0, θ) at each energy and angle for two sets of data [158–160]. One finds good agreement between the 5 eV results, with the exception of the region near 90°. The results of Truhlar et al. [159] at 5 eV tend to rise more rapidly at smaller θ than those of Tanaka et al. [158].

Differential cross sections determined from the ratios R_1 (E_0, θ) are given in tables 30 and 31 from refs. [158] and [159, 160] respectively. In many cases, the cross sections reported are results of smooth

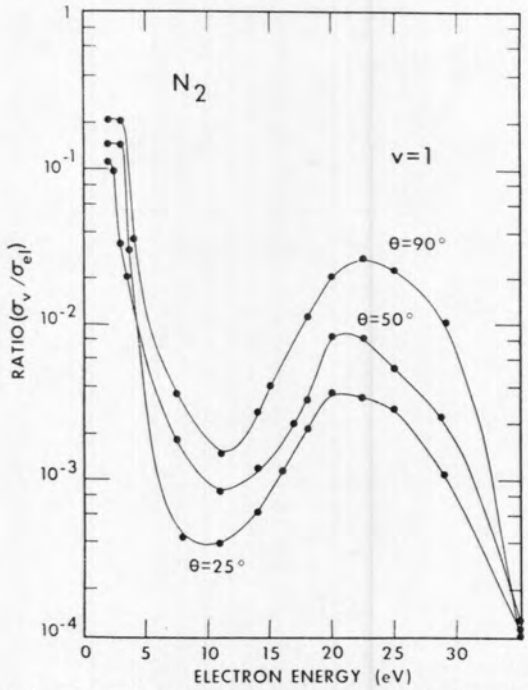

Fig. 20. Ratio of cross section for excitation to $v = 1$ of N_2 to that for elastic scattering at $\theta = 25°$, 50° and 90°. The peak at 22 eV is interpreted in terms of the broad, shape resonance associated with an electron in the $(\sigma_u 2p)$ orbital. (From ref. [162].)

Table 29
Ratios of $v = 0 \rightarrow 1$ excitation cross section to that for elastic scattering. Units are 10^{-3}. (From Tanaka et al. 1981, ref. [158]; Truhlar et al. 1976, ref. [159]; Truhlar et al. 1977, ref. [160].)

θ (deg) \ E_0 (eV)	3	5	5	7.5	10	10	15	18	20
	Ref. [158]	Ref. [158]	Ref. [159]	Ref. [158]	Ref. [158]	Ref. [159]	Ref. [158]	Ref. [158]	Ref. [158]
20	63.4	6.47	6.50	–	–	1.16	1.74	–	5.68
30	41.2	5.55	6.68	2.41	0.837	0.919	1.81	5.51	7.04
40	27.5	4.21	3.25	1.86	0.696	–	1.80	3.91	8.82
50	34.8	3.35	2.69	1.23	0.816	0.815	2.84	4.30	10.2
60	44.9	3.42	–	2.36	0.977	–	3.74	6.52	17.2
70	77.1	4.44	5.39	2.34	1.30	1.26	5.21	13.4	22.5
80	116	7.50	–	2.97	1.55	–	10.4	16.3	26.9
90	136	6.73	9.56	3.09	1.15	1.57	8.87	17.4	29.2
100	145	6.52	–	1.95	0.901	–	7.40	14.7	27.1
110	–	–	–	1.81	0.762	–	4.38	10.5	27.1
115	95.2	5.58	4.47	–	–	0.841	–	–	–
120	63.6	4.48	–	1.51	0.841	–	2.93	9.94	21.9
130	59.0	5.26	–	1.38	–	–	1.98	8.35	25.0
135	–	–	5.35	–	–	0.657	–	–	–

θ (deg) \ E_0 (eV)	22.5	25	30	30	35	45	50	75
	Ref. [158]	Ref. [158]	Ref. [158]	Ref. [160]	Ref. [160]	Ref. [160]	Ref. [160]	Ref. [160]
20	–	3.16	1.59	0.54	0.20	0.14	0.16	0.32
30	7.66	3.56	1.36	0.81	0.20	0.30	0.27	0.59
40	5.91	5.40	2.53	1.4	–	–	0.84	1.9
50	8.12	7.23	3.77	2.5	1.1	1.6	1.8	3.5
60	13.9	12.4	5.54	4.6	–	–	3.6	4.6
70	17.4	21.3	8.46	8.0	4.6	4.8	6.0	5.3
80	22.8	22.2	11.5	12	–	–	8.0	5.7
90	32.2	20.8	10.9	13	7.4	8.8	8.2	5.3
100	25.6	14.8	9.38	11	–	–	6.4	3.9
110	18.7	18.3	6.25	–	–	–	–	–
115	–	–	–	8.3	4.1	4.3	3.6	2.6
120	20.8	14.1	5.13	–	–	–	–	–
130	18.6	14.9	4.93	–	–	–	–	–
135	–	–	–	4.8	3.6	2.6	2.8	3.3

curves drawn through the discrete data points derived from individual R_1 (E_0, θ) measurements. There is reasonable agreement in the data at 5 eV. One sees also that the 3 eV results [158] are in good agreement with the cross section shape of Ehrhardt and Willmann [161]. This can provide a means of extending the vibrational excitation data to lower electron energies (see fig. 1 of ref. [161]). Integral and momentum transfer cross sections for the $v = 0 \rightarrow 1$ excitation are given in table 32.

B. Nonresonance and broad Σ_u shape-resonance regions (5–75 eV)

Perhaps as interesting as the low-energy region is the region 20–25 eV in N_2 where one encounters a broad Σ_u shape resonance (see also the analogous effect in CO discussed in section 4.4). The presence of this broad resonance was first noted by Pavlović et al. [162] and was interpreted then as a series of overlapping core-excited resonances. It was studied later in more detail both experimentally [158, 160]

Table 30
Vibrational excitation ($v = 0 \rightarrow 1$) cross sections in N_2. Units are 10^{-19} cm^2/sr. (From Tanaka et al. 1981, ref. [158].)

θ (deg) \ E_0 (eV)	3	5	7.5	10	15	18	20	22.5	25	30
20	216	10.3	–	–	6.46	–	25.8	–	15.2	7.74
30	138	8.99	4.82	1.93	4.63	14.8	19.3	20.7	9.29	3.24
40	109	6.86	3.76	1.44	3.05	5.48	14.1	8.87	7.29	2.88
50	75.2	4.86	2.68	1.65	3.64	4.64	9.89	6.82	5.42	2.30
60	72.7	4.00	3.14	1.20	3.25	4.76	10.8	7.78	5.83	1.83
70	94.0	3.91	3.18	1.16	2.92	4.69	8.78	4.70	4.90	1.52
80	115	5.40	2.38	0.961	3.64	4.72	6.73	5.02	4.22	1.50
90	121	4.04	1.79	0.518	2.48	3.84	5.55	5.48	2.91	1.20
100	124	3.72	1.05	0.405	2.81	3.51	7.32	8.72	4.28	1.22
110	81.8	3.18	1.00	0.419	2.01	4.31	10.6	7.48	5.12	1.13
120	57.4	2.60	1.00	0.505	1.67	4.57	11.0	9.17	5.50	1.33
130	59.0	3.26	1.05	–	1.39	5.43	15.5	10.4	7.75	1.92

Table 31
Vibrational excitation ($v = 0 \rightarrow 1$) cross sections in N_2. Units are 10^{-19} cm^2/sr. Angles in parentheses refer to extrapolated values.[a] (From Truhlar et al. 1976, ref. [159] and Truhlar et al. 1977, ref. [160].)

θ (deg) \ E_0 (eV)	5.0	10.0	30.0	50.0	75.0
(0)	22	5.4	3.9	1.2	0.84
(10)	18	4.2	3.2	0.90	0.85
20	13.5	3.03	2.45	0.592	0.90
30	8.61	2.15	1.88	0.438	0.55
40	5.35	1.61	1.64	0.478	0.63
50	3.78	1.26	1.53	0.556	0.54
60	4.15	1.08	1.46	0.634	0.44
70	4.95	0.950	1.42	0.676	0.32
80	5.88	0.811	1.38	0.623	0.32
90	6.07	0.655	1.40	0.505	0.39
100	4.83	0.558	1.46	0.495	0.27
110	2.92	0.498	1.59	0.578	0.26
120	2.64	0.488	1.80	0.730	0.36
130	3.20	0.521	2.03	0.953	0.57
140	4.03	0.591	2.33	1.15	0.93
(150)	5.8	0.72	2.7	1.4	1.5
(160)	5.0	0.89	3.2	1.6	2.4
(170)	6.8	1.1	3.6	1.7	3.1
(180)	7.3	1.3	4.1	1.8	3.6

[a]The cross section values in this table are from smoothed curves through data obtained from the published vibrational to elastic scattering intensity ratios of Truhlar et al. and the elastic DCS's of table 26.

and theoretically, and interpreted as a broad shape resonance of Σ_u ($l = 3$) symmetry. (See refs. [158] and [163] for summary and theoretical results of ref. [164a].)

Effects of this resonance on the $v = 1$ channel are shown in fig. 20 [162]. Differential cross sections in the 5–75 eV region are given in tables 30 and 31. It should be noted that there is significant disagreement in results at 30 eV, at angles less than 60°. A remeasurement of the ratio R_1 (E_0, θ) for angles between 0° and 60° would be useful. Possible sources of the discrepancy could be parent beam or stray field effects, or inadequate resolution, although these effects would appear to be under control in the two experiments.

Cross sections for excitation to $v = 2$ and $v = 3$ in this energy range have also been reported by Pavlović et al. [162], and are given here in figs. 21 and 22, respectively. Cross sections for vibrational levels up to $v = 24$ have been reported by Huetz et al. [164b] at 9 eV incident energy and 30° scattering angle.

Integral and momentum-transfer cross sections for excitation to $v = 1$ are given in table 31. Effects of the Σ_u resonance are seen more clearly in these integrated data, as is also the case for CO (see later). There is generally good agreement (table 32) in the two sets of integrated data, the notable exception being σ^M at 10 eV. The source of this difference very likely is in the form of the high-angle (135°–180°) extrapolation to which σ^M is sensitive. The extrapolated data in Tanaka et al. lies above that of Truhlar et al. The effect is also present, but to a smaller extent, in σ.

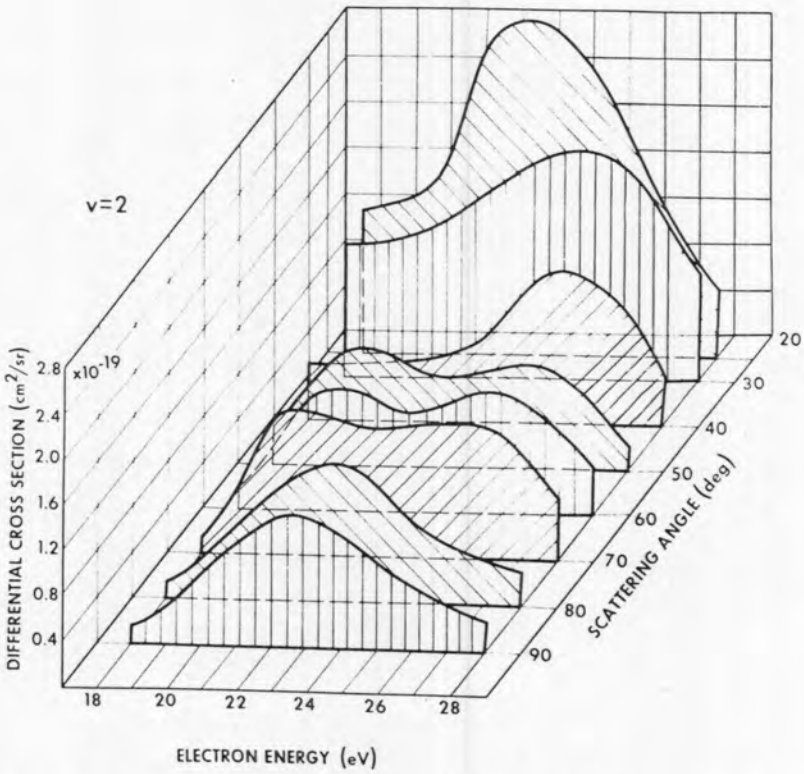

Fig. 21. Combined energy and angular dependence of the differential cross section for vibrational excitation to $v = 2$ of N_2. (From ref. [162].)

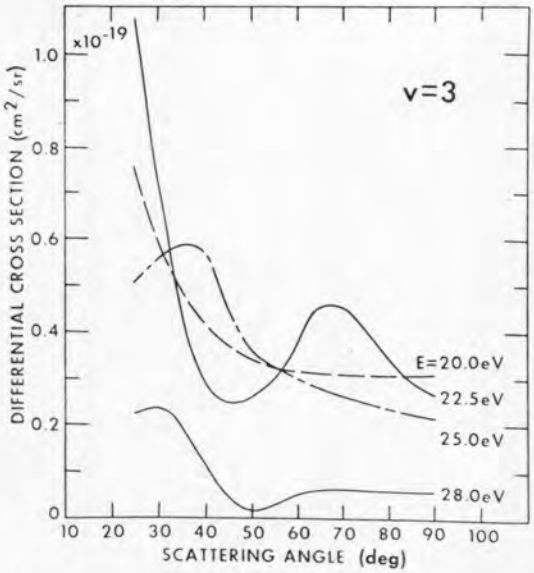

Fig. 22. Differential cross sections for vibrational excitation to $v = 3$ of N_2 at energies of 20.0, 22.5, 25.0 and 28.0 eV. (From ref. [162].)

Table 32
Integral (σ) and momentum transfer (σ^M) cross sections for ($v = 0 \rightarrow 1$) vibrational excitation in N_2. Units are 10^{-18} cm^2. (From Tanaka et al. 1981, ref. [158], Truhlar et al. 1976, ref. [159] and Truhlar et al. 1977, ref. [160].)

	Ref. [158]		Refs. [159, 160]	
E_0 (eV)	σ	σ^M	σ	σ^M
3.0	123	114	–	–
5.0	6.10	5.34	6.48	5.56
7.5	3.12	2.40	–	–
10.0	1.53	1.44	1.23	0.883
15.0	3.86	3.38	–	–
18.0	7.55	6.51	–	–
20.0	19.5	22.8	–	–
22.5	12.6	11.7	–	–
25.0	8.22	8.14	–	–
30.0	2.66	2.24	2.25	2.41
50.0	–	–	0.907	0.106
75.0	–	–	0.704	0.844

Electronic excitation cross sections

Considerable effort has gone into the study of electronic transitions in N_2 by electron impact techniques. Broadly speaking, one can divide the work into techniques which detect metastable molecules or emitted photons (excitation function measurements), or the scattered inelastic electron (electron energy-loss measurements). Sets of cross sections have also been compiled and used for plasma-modeling purposes [165, 166].

Because of the dominance of N_2 and N_2^+ emissions in auroral and missile re-entry spectra, extensive measurements have been reported of optical emissions in electron-beam excited N_2. Spectra and/or cross sections have been measured for the systems $B^3\Pi_g \rightarrow A^3\Sigma_u^+$ (1st positive) [167], $a^1\Pi_g \rightarrow X^1\Sigma_g^+$ (Lyman–Birge–Hopfield) [168, 169], $C^3\Pi_u \rightarrow B^3\Pi_g$ (2nd positive) [167, 170–172], and $b^1\Pi_u \rightarrow X^1\Sigma_g^+$ (Birge–Hopfield) [173]. A summary of the relevant optical excitation–function measurements is given in table 33.

Ajello [168] has observed emission in the wavelength range 120–200 nm corresponding to the $a \rightarrow X$ system. Metastable excitation functions and optical emission cross sections have been measured in several individual N_2 electronic transitions. Borst et al. [169], from studies using different metastable transit times and detector surfaces, deduced the contribution of the $E^3\Sigma_g^+$ state to a total metastable excitation function [170], and those results are given here in fig. 23. Excitation functions of the $A^3\Sigma_u^+$ state, both direct and including the cascades $B^3\Pi_g \rightarrow A$ and $C^3\Pi_u \rightarrow B \rightarrow A$, have been reported for levels $v = 0$–14 in the A state [174]. Peak cross sections and energies for excitation of the A, B, C, a and E states and cross sections for excitations of the a-state are tabulated by Borst [170]. Cross sections giving direct and cascade contributions to excitation of the A-state are given here in table 34 [170]. Excitation functions for the $C \rightarrow B$ system are reported by Imami and Borst [171]. Results are given for the (0, 0) band, and comparisons given in ref. [171] to earlier results of Aarts and de Heer [175], Jobe et al. [176], and Shemansky and Broadfoot [167]. Cross sections in the $b \rightarrow X$ system have been measured by Zipf and Gorman [173] in the energy range

Table 33
Summary of optical excitation function measurements in N_2

State	Impact energy (eV)[a]	Reference
$A^3\Sigma_u^+$	T–40	Borst 1972, ref. [170]
	T–35	Borst–Chang 1973, ref. [174]
$B^3\Pi_g$ (1st positive)	11.5–27	Shemansky–Broadfoot 1971, ref. [167]
$a^1\Pi_g$ (Lyman–Birge–Hopfield)	10–208	Ajello 1970, ref. [168]
	60–2000	Aarts–de Heer 1971, ref. [177]
	T–40	Borst 1972, ref. [170]
$C^3\Pi_u$ (2nd positive)	T–1000	Aarts–de Heer 1969, ref. [175]
	11.5–25	Shemansky–Broadfoot 1971, ref. [167]
	T–1000	Imami–Borst 1974, ref. [171]
	T–1000	Kosoruchkina–Trekhov1978, ref. [172]
$E^3\Sigma_g^+$	T–13	Borst et al. 1972, ref. [169]
	T–13	Borst 1972, ref. [170]
$b^1\Pi_u$ (Birge–Hopfield)	T–500	Zipf–Gorman 1980, ref. [173]

[a]T means threshold.

threshold–500 eV. Cross sections for several bands in the electron energy range 60–2000 eV are given by Aarts and de Heer [177] for the transitions $a \to X$, $p'^1\Sigma_u^+ \to X$ and $p' \to a$.

Measurements of differential, integral and momentum-transfer cross sections from electron energy-loss spectra are considered separately since these results are free of cascade effects, and of the influence of predissociation on the optical emission function. Both optically allowed as well as metastable transitions are detected. The efficiency of excitation depends on the electron energy and scattering

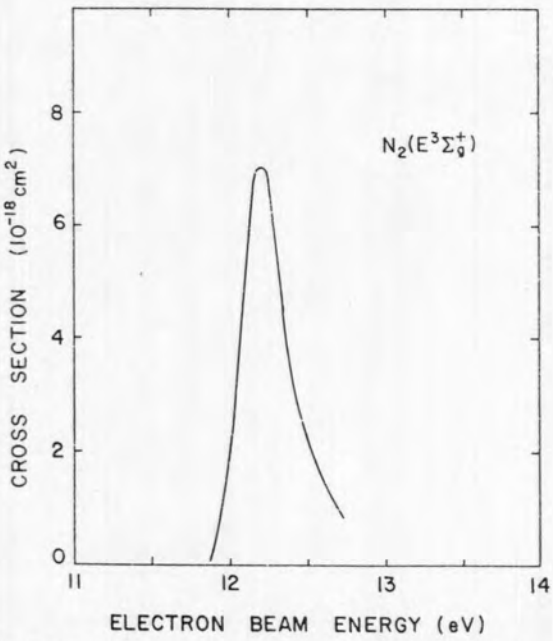

Fig. 23. Excitation cross section for the $E^3\Sigma_g^+$ state of N_2 from time-of-flight measurements, and corrected for the finite energy spread in the incident electron beam. (From ref. [169].)

Table 34
Cross sections for excitation of the $A^3\Sigma_u^+$ state of N_2. (From Borst 1972, ref. [170].)

Electron energy (eV)	Excitation cross section: Direct (10^{-17} cm^2)	Excitation cross section: Total (10^{-17} cm^2)
8	1.5	2.1
9	2.9	6.6
10	4.0	9.3
11	5.3	11.5
12	4.6	10.3
13	3.6	9.8
14	2.8	11.0
15	2.4	10.5
16	2.1	9.1
18	1.6	7.2
20	1.3	6.1
25	0.9	4.6
30	0.6	3.7
35	0.4	3.0
40	0.3	2.4

angle, with forbidden transitions favored at energies close to threshold and at higher scattering angles, while optically-allowed states are efficiently accessed at higher electron energies (several times threshold) and low scattering angles.

Electron scattering cross sections have been reported by Brinkmann and Trajmar [178], Cartwright et al. [179a, b], Chutjian et al. [179c], Finn and Doering [180], and Huetz et al. [164]. Relative differential cross sections were given for the $w^1\Delta_u$ state by Willen et al. and for the $a^1\Pi_g$ state by Oda and Osawa (refs. [181] and [182] respectively). The most extensive coverage is given in refs. [179a, b, c] based, unfortunately, on older N_2 elastic scattering cross sections. Because of the need, both theoretical and for swarm and discharge modeling, we present the corrected tabulation of the inelastic electronic excitation in these references based on the newer elastic N_2 cross sections of table 26. Extensive differences between the two sets exist, so that retabulation is necessary. The corrected data for the individual electronic transitions are presented as tables 35–43. Integral and momentum transfer cross sections are given in tables 44 and 45.

Finally, we note that at higher energies Skerbele and Lassettre [183] have reported differential electron collision cross sections and generalized oscillator strengths for excitation of the $a^1\Pi_g$ and $a''^1\Sigma_g^+$ states of N_2 at 300, 400 and 500 eV impact energies.

Table 35

Differential cross sections for the excitation of the $A^3\Sigma_u^+$ state of N_2. Entries in parentheses beneath the given energy refer to the cross section multiplier (cm^2/sr) for that column. Entries at angles in parentheses refer to extrapolated cross sections.[a] (From Cartwright et al. 1977, ref. [179a].)

	Energy (eV)						
Angle (deg)	10.0 (10^{-19})	12.5 (10^{-18})	15.0 (10^{-18})	17.0 (10^{-18})	20.0 (10^{-18})	30.0 (10^{-19})	50.0 (10^{-19})
(0)	2.13	0.272	1.75	0.696	0.0745	1.49	0.412
(10)	4.01	0.465	1.17	0.743	0.123	1.82	0.688
20	6.46	0.738	0.868	0.793	0.194	2.06	0.815
30	8.33	0.885	0.735	0.780	0.246	1.89	0.811
40	10.3	0.946	0.743	0.833	0.324	1.83	0.860
50	11.8	1.18	1.00	1.07	0.432	1.79	1.00
60	13.4	1.53	1.28	1.50	0.596	2.07	1.26
70	14.3	1.85	1.57	1.87	0.798	2.57	1.64
80	15.1	2.12	1.73	1.98	0.944	3.57	1.70
90	14.8	1.51	1.98	1.91	0.969	4.53	1.91
100	12.4	1.14	1.89	1.52	0.866	4.14	1.71
110	12.0	1.10	1.75	1.10	0.841	3.93	1.77
120	11.0	1.09	1.70	1.13	0.988	4.35	2.03
130	10.3	1.24	1.84	1.70	1.63	6.89	3.85
(140)	9.74	1.47	2.00	2.44	2.48	9.63	6.83
(150)	9.50	1.90	2.27	3.11	3.59	11.1	10.5
(160)	11.7	2.39	2.56	3.92	4.99	13.0	14.2
(170)	13.8	2.84	2.78	4.67	6.22	15.0	17.8
(180)	16.8	3.26	2.92	5.53	7.24	16.3	20.8

[a]The cross section values in this table were obtained from the cross sections published by Cartwright et al. [179a] by correcting their values with a factor representing the ratio of the recent elastic cross sections of table 26 to those used by Cartwright et al.

Table 36

Differential cross sections for the excitation of the $B^3\Pi_g$ state of N_2. Entries in parentheses beneath the given energy refer to the cross section multiplier (cm^2/sr) for that column. Entries at angles in parentheses refer to extrapolated cross sections.[a] (From Cartwright et al. 1977, ref. [179a].)

Angle (deg)	Energy (eV) 10.0 (10^{-18})	12.5 (10^{-18})	15.0 (10^{-18})	17.0 (10^{-18})	20.0 (10^{-19})	30.0 (10^{-19})	50.0 (10^{-19})
(0)	0.192	0.226	0.385	0.220	1.46	1.55	0.543
(10)	0.332	0.338	0.391	0.551	3.68	2.09	0.934
20	0.551	0.537	0.435	0.976	6.08	2.66	1.14
30	0.754	0.725	0.529	1.17	6.78	2.63	1.23
40	1.01	0.981	0.684	1.27	6.76	2.66	1.17
50	1.24	1.43	0.952	1.40	6.53	2.57	1.22
60	1.57	1.96	1.25	1.52	6.62	2.70	1.41
70	1.87	2.50	1.47	1.52	6.98	2.94	1.72
80	2.21	2.99	1.62	1.42	7.39	3.74	1.73
90	2.51	3.29	1.92	1.40	7.98	4.75	1.98
100	2.47	3.19	2.36	1.43	9.68	5.51	2.30
110	2.89	3.30	3.02	1.55	12.3	7.23	2.86
120	2.84	3.12	3.13	1.67	14.0	8.88	3.23
130	2.54	2.88	2.72	1.76	15.2	10.8	3.59
(140)	2.18	2.55	2.07	1.85	17.3	13.2	4.12
(150)	1.86	2.44	1.60	2.00	20.1	14.1	5.27
(160)	1.91	2.39	1.25	2.19	23.9	15.9	6.52
(170)	1.87	2.39	0.928	2.24	28.2	18.0	8.06
(180)	1.85	2.42	0.726	2.24	32.6	19.2	10.0

[a]The cross section values in this table were obtained from the cross sections published by Cartwright et al. [179a] by correcting their values with a factor representing the ratio of the recent elastic cross sections of table 26 to those used by Cartwright et al.

Table 37

Differential cross sections for the excitation of the $W^3\Delta_u$ state of N_2. Entries in parentheses beneath the given energy refer to the cross section multiplier (cm^2/sr) for that column. Entries at angles in parentheses refer to extrapolated cross sections.[a] (From Cartwright et al. 1977, ref. [179a].)

Angle (deg)	Energy (eV) 10.0 (10^{-19})	12.5 (10^{-18})	15.0 (10^{-18})	17.0 (10^{-18})	20.0 (10^{-19})	30.0 (10^{-19})	50.0 (10^{-19})
(0)	0.955	0.257	1.54	0.743	6.93	0.907	0.228
(10)	1.24	0.367	1.23	1.23	7.44	1.26	0.540
20	1.90	0.524	1.06	1.68	7.19	1.72	0.827
30	3.28	0.713	1.05	1.68	5.65	1.89	0.922
40	5.04	0.970	1.16	1.61	4.86	2.14	0.956
50	5.78	1.39	1.24	1.71	4.77	2.30	0.987
60	6.53	1.88	1.51	1.82	5.46	2.59	1.14
70	6.94	2.38	1.83	1.97	6.73	2.91	1.45
80	7.37	2.68	2.08	2.07	8.59	3.64	1.55
90	7.58	2.66	2.54	2.35	10.6	4.53	1.90
100	6.82	2.25	2.99	2.57	14.3	5.07	2.24
110	7.22	2.15	3.49	2.87	20.8	6.34	2.67
120	6.50	2.00	3.82	3.28	26.3	7.36	2.78
130	4.82	1.93	4.08	3.76	30.6	8.29	2.45
(140)	3.25	1.84	4.10	4.29	36.0	9.23	2.85
(150)	2.05	1.96	4.28	5.07	43.6	9.81	3.18
(160)	1.46	2.18	4.39	6.04	52.6	11.1	3.56
(170)	0.956	2.49	4.31	6.92	63.1	12.7	4.12
(180)	0.618	2.92	4.11	7.74	73.1	14.2	4.98

[a]The cross section values in this table were obtained from the cross sections published by Cartwright et al. [179a] by correcting their values with a factor representing the ratio of the recent elastic cross sections of table 26 to those used by Cartwright et al.

Table 38
Differential cross sections for the excitation of the $a^1\Pi_g$ state of N_2. Entries in parentheses beneath the given energy refer to the cross section multiplier (cm^2/sr) for that column. Entries at angles in parentheses refer to extrapolated cross sections.[a]
(From Cartwright et al. 1977, ref. [179a].)

	Energy (eV)						
Angle (deg)	10.0 (10^{-19})	12.5 (10^{-18})	15.0 (10^{-18})	17.0 (10^{-18})	20.0 (10^{-18})	30.0 (10^{-18})	50.0 (10^{-18})
(0)	2.13	1.51	15.5	29.1	24.0	23.6	43.8
(10)	3.37	2.39	10.5	23.4	22.8	19.0	30.6
20	4.94	3.69	6.90	16.7	17.9	12.6	8.27
30	6.15	3.54	4.52	9.71	9.61	4.77	1.24
40	7.39	2.99	3.06	5.52	4.05	1.32	0.474
50	6.21	2.52	2.54	3.20	1.43	0.767	0.267
60	3.73	2.12	2.05	1.84	0.812	0.642	0.206
70	3.75	1.76	1.71	1.28	0.793	0.602	0.184
80	3.59	1.51	1.38	1.08	0.846	0.653	0.155
90	3.41	1.32	1.36	1.07	0.942	0.734	0.162
100	2.50	1.13	1.40	1.13	1.09	0.718	0.185
110	2.08	1.09	1.40	1.16	1.29	0.798	0.237
120	1.51	0.950	1.26	1.09	1.22	0.823	0.285
130	1.08	0.736	1.04	0.960	1.04	0.810	0.363
(140)	0.717	0.532	0.788	0.807	0.878	0.798	0.485
(150)	0.533	0.413	0.612	0.652	0.769	0.735	0.676
(160)	0.459	0.344	0.476	0.634	0.663	0.722	0.892
(170)	0.368	0.294	0.348	0.544	0.545	0.735	1.14
(180)	0.310	0.263	0.266	0.456	0.435	0.728	1.41

[a]The cross section values in this table were obtained from the cross sections published by Cartwright et al. [179a] by correcting their values with a factor representing the ratio of the recent elastic cross sections of table 26 to those used by Cartwright et al.

4.3. O_2

Total electron scattering cross section measurements for O_2 previous to 1970 have been summarized by Kieffer [2–5]. Dalba et al. [139] published the only recent total cross section data. For comparison, their data and the earlier data of Sunshine et al. [184] and Salop and Nakano [185] are given in table 46. There is a considerable scatter in the cross section values and a remeasurement below 100 eV would be desirable.

Elastic scattering by O_2 was studied by Linder and Schmidt [186] in the 0 to 4 eV range and by Trajmar et al. [187] in the 4 to 45 eV range. In both cases the cross sections were normalized to total cross sections [184, 185]. The low-energy non-resonant elastic DCS data of Linder and Schmidt are shown in fig. 24 and those of Trajmar et al. are given in table 47A. Differential elastic scattering cross sections measured by Dehmel et al. [188a] at 5 and 15 eV impact energies are in good agreement with the results of refs. [186 and 187]. More recently Shyn and Sharp [188b] measured elastic differential cross sections for O_2 in the 2 to 200 eV impact energy region and obtained integral and momentum transfer cross sections from the measured angular distributions. Their results are given in table 47B. High energy elastic scattering (300, 400 and 500 eV) was investigated by Bromberg [189a] who obtained

Table 39
Differential cross sections for the excitation of the $C^3\Pi_u$ and $B'^3\Sigma_u^-$ states of N_2. Entries in parentheses beneath the given energy refer to the cross section multiplier (cm^2/sr) for that column. Entries at angles in parentheses refer to extrapolated cross sections.[a] (From Cartwright et al. 1977, ref. [179a].)

	Energy (eV)										
	$C^3\Pi_u$					$B'^3\Sigma_u^-$					
Angle (deg)	15.0 (10^{-18})	17.0 (10^{-18})	20.0 (10^{-18})	30.0 (10^{-19})	50.0 (10^{-19})	12.5 (10^{-19})	15.0 (10^{-19})	17.0 (10^{-19})	20.0 (10^{-19})	30.0 (10^{-19})	50.0 (10^{-19})
(0)	1.02	0.766	0.359	2.54	1.58	0.151	0.041	0.012	0.013	0.091	0.088
(10)	1.31	0.935	0.511	3.48	2.04	2.96	0.207	0.456	0.015	4.67	9.82
20	1.59	1.09	0.680	3.82	1.82	5.50	3.89	1.03	0.016	6.68	4.62
30	1.79	1.12	0.743	3.43	1.30	6.76	5.48	1.47	0.029	5.05	2.81
40	1.96	1.12	0.811	3.21	1.13	7.12	6.54	1.67	0.217	3.17	0.877
50	2.44	1.26	0.864	3.00	1.02	7.91	8.42	1.86	0.533	1.90	0.549
60	2.79	1.41	0.938	2.95	1.10	9.33	9.45	2.17	0.888	1.40	0.455
70	3.17	1.59	0.990	2.98	1.36	10.5	8.78	2.64	1.16	1.11	0.462
80	3.26	1.72	1.01	3.43	1.47	11.4	7.99	3.39	1.42	1.12	0.444
90	3.46	1.85	0.998	4.18	1.90	10.2	9.76	5.18	1.88	1.23	0.524
100	3.22	1.92	1.03	4.68	2.28	7.38	11.5	9.43	4.41	1.54	0.740
110	2.94	1.93	1.31	5.77	2.65	5.30	13.2	13.6	7.22	2.50	1.25
120	2.98	1.87	1.50	6.85	2.52	3.38	13.6	15.0	8.37	3.77	1.90
130	3.38	1.81	1.54	6.30	2.22	2.39	13.6	13.7	7.57	3.56	2.18
(140)	3.58	1.72	1.63	6.16	1.90	1.65	12.4	10.9	6.03	3.29	2.00
(150)	3.76	1.76	1.79	5.52	1.70	1.18	10.5	7.86	4.10	2.57	1.45
(160)	3.94	1.87	2.00	5.25	1.48	0.729	6.80	4.53	1.81	1.81	0.813
(170)	4.13	1.93	2.19	5.05	1.30	0.339	2.78	1.79	0.440	0.941	0.312
(180)	4.31	2.01	2.35	4.90	1.14	0.125	0.024	0.008	0.010	0.038	0.067

[a]The cross section values in this table were obtained from the cross sections published by Cartwright et al. [179a] by correcting their values with a factor representing the ratio of the recent elastic cross sections of table 26 to those used by Cartwright et al.

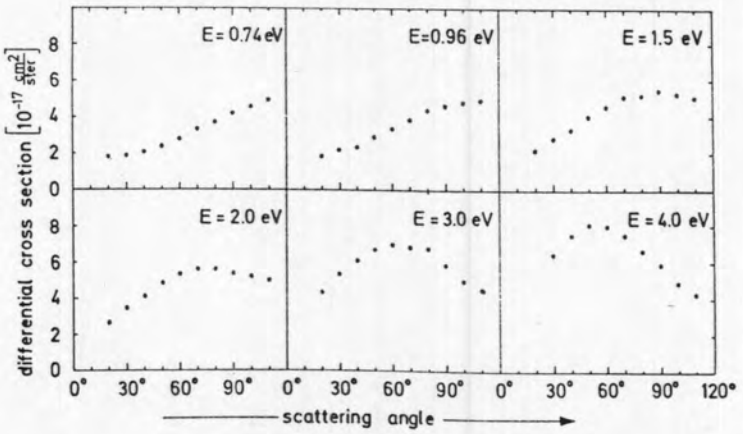

Fig. 24. Measured angular distributions for non-resonant elastic scattering in O_2 at the indicated collision energies. (From ref. [186].)

Table 40

Differential cross sections for the excitation of the $w^1\Delta_u$ and $a'^1\Sigma_u^-$ states of N_2. Entries in parentheses beneath the given energy refer to the cross section multiplier (cm^2/sr) for that column. Entries at angles in parentheses refer to extrapolated cross sections.[a] (From Cartwright et al. 1979, ref. [179a].)

	Energy (eV)										
	$w^1\Delta_u$						$a'^1\Sigma_u^-$				
Angle (deg)	12.5 (10^{-18})	15.0 (10^{-18})	17.0 (10^{-18})	20.0 (10^{-19})	30.0 (10^{-19})	50.0 (10^{-20})	15.0 (10^{-18})	17.0 (10^{-19})	20.0 (10^{-19})	30.0 (10^{-20})	50.0 (10^{-20})
(0)	0.272	2.55	2.03	14.6	3.36	77.0	0.041	0.012	0.013	0.091	0.088
(10)	0.676	1.73	1.44	7.37	3.21	61.4	0.380	2.52	0.480	34.8	215
20	1.26	1.22	1.00	4.69	2.99	23.7	0.566	3.42	2.11	58.2	97.3
30	1.47	0.887	0.680	3.16	2.20	7.62	0.758	2.90	2.21	38.6	32.6
40	1.38	0.684	0.510	2.57	1.71	3.86	0.892	2.45	1.78	19.8	14.3
50	1.25	0.648	0.458	2.28	1.31	2.54	1.15	2.40	1.59	11.8	7.79
60	1.20	0.638	0.423	2.22	1.12	2.19	1.25	2.49	1.57	9.08	5.90
70	1.09	0.697	0.399	2.06	1.02	2.36	1.09	2.67	1.62	7.74	5.98
80	1.02	0.779	0.415	1.79	1.05	2.26	0.794	2.91	1.74	8.28	5.73
90	0.971	0.886	0.459	1.62	1.14	2.58	0.709	3.76	1.93	10.7	6.69
100	0.852	0.811	0.485	1.68	1.10	3.13	0.755	6.04	2.57	14.1	8.36
110	0.842	0.719	0.514	2.13	1.22	4.08	0.887	8.97	4.75	22.8	11.0
120	0.753	0.691	0.528	2.55	1.32	4.72	0.965	9.06	6.18	24.3	12.8
130	0.611	0.695	0.531	2.80	1.44	4.96	0.888	6.83	6.20	19.2	13.1
(140)	0.474	0.721	0.515	3.09	1.64	5.21	0.687	3.79	5.20	11.5	11.7
(150)	0.374	0.779	0.514	3.50	1.82	5.81	0.468	1.45	3.42	4.63	8.49
(160)	0.291	0.876	0.506	4.03	2.07	6.22	0.227	0.423	1.36	1.51	4.04
(170)	0.237	0.952	0.475	4.54	2.35	6.90	0.046	0.101	0.287	0.376	1.31
(180)	0.187	1.06	0.448	4.95	2.53	7.80	0.002	0.008	0.010	0.038	0.067

[a] The cross section values in this table were obtained from the cross sections published by Cartwright et al. [179a] by correcting their values with a factor representing the ratio of the recent elastic cross sections of table 26 to those used by Cartwright et al.

Table 41
Differential cross sections for the excitation of the $E^3\Sigma_g^+$ and $a''^1\Sigma_g^+$ states of N_2. Entries in parentheses beneath the given energy refer to the cross section multiplier (cm^2/sr) for that column. Entries at angles in parentheses refer to extrapolated cross sections.[a] (From Cartwright et al. 1977, ref. [179a].)

	Energy (eV)									
	$E^3\Sigma_g^+$					$a''^1\Sigma_g^+$				
Angle (deg)	15.0 (10^{-20})	17.0 (10^{-20})	20.0 (10^{-20})	30.0 (10^{-20})	50.0 (10^{-21})	15.0 (10^{-19})	17.0 (10^{-19})	20.0 (10^{-19})	30.0 (10^{-19})	50.0 (10^{-20})
(0)	1.75	3.83	51.9	67.1	438	53.2	17.4	38.6	41.7	700
(10)	1.69	4.56	39.0	41.8	306	22.6	13.7	26.3	16.9	148
20	1.74	4.89	22.6	17.7	36.5	7.78	9.89	17.5	4.41	23.2
30	1.78	4.57	8.30	8.11	13.0	4.19	5.57	9.76	2.50	18.1
40	1.90	4.17	3.38	6.51	13.3	3.12	2.81	5.94	2.46	18.8
50	2.44	3.94	2.67	4.43	9.96	3.02	2.13	3.81	1.92	13.9
60	2.88	3.70	2.66	3.17	6.07	2.88	2.06	2.91	1.32	10.8
70	3.07	3.24	2.80	2.47	5.34	2.73	2.12	2.30	1.04	9.69
80	2.94	2.84	2.94	2.25	4.27	2.38	2.15	1.97	1.04	7.82
90	2.96	2.54	2.99	2.16	4.04	2.37	2.30	1.68	1.07	7.02
100	2.76	2.29	3.07	1.80	3.86	2.22	2.29	1.73	0.975	6.76
110	2.53	2.09	3.66	1.78	3.99	2.11	2.24	2.20	1.03	6.65
120	2.21	1.86	4.05	1.62	3.65	1.92	2.09	2.81	1.02	5.86
130	1.92	1.67	4.42	1.44	3.16	1.80	1.92	3.65	0.982	5.03
(140)	1.62	1.50	5.20	1.33	2.85	1.65	1.76	5.20	0.969	4.42
(150)	1.45	1.45	6.32	1.15	2.78	1.60	1.71	7.09	0.932	4.30
(160)	1.34	1.43	7.62	1.13	2.78	1.61	1.70	9.41	0.990	4.17
(170)	1.23	1.40	8.85	1.13	2.81	1.62	1.66	11.5	1.10	4.18
(180)	1.14	1.38	9.91	1.17	3.02	1.67	1.63	12.9	1.25	4.37

[a] The cross section values in this table were obtained from the cross sections published by Cartwright et al. [179a] by correcting their values with a factor representing the ratio of the recent elastic cross sections of table 26 to those used by Cartwright et al.

absolute DCS in the 2° to 40° range by measuring all parameters that relate the scattered electron signal intensity to the corresponding cross section. His results are given in table 48A. In the 200 to 500 eV impact energy region Daimon et al. [189b] reported differential elastic cross sections. Their data are given in table 48B. Recently, Wakiya [190a] remeasured the elastic cross sections and normalized his relative data at 300, 400 and 500 eV at 30° scattering angle to the results of Bromberg [189], at 20 eV to the total scattering cross sections obtained by Salop and Nakano [185] and in the 30 to 100 eV range to the total cross section data of Sunshine et al. [184]. He obtained normalization in the 100 to 300 eV range by interpolation. The DCS results of Wakiya are shown in figs. 25 and 26. Integral elastic cross sections have been obtained by Trajmar et al. [187] and Wakiya [190a].

Vibrational excitation by low energy electrons (up to 4 eV) was investigated by Linder and Schmidt [186]. These cross sections are strongly influenced by resonances. The behavior of the differential excitation function at 60° scattering angle is shown in fig. 27 and the energy-integrated cross sections are given in table 49.

Cross sections for excitation of electronic states have been measured by Linder and Schmidt [186] (threshold to 4 eV), Trajmar et al. [187, 194] (4–45 eV) and Wakiya [189, 190] (20 to 500 eV). Linder and Schmidt [186] and Trajmar et al. [187] were concerned with the excitation of the $a^1\Delta_g$ and $b^1\Sigma_g^+$ states

Table 42

Differential excitation cross sections for the states of N_2 indicated at an incident electron energy of 40 eV. Entries in parentheses below the state designations are cross section multipliers (cm^2/sr) for that column.[a] (From Chutjian et al. 1977, ref. [179c].)

Angle (deg)	$b^1\Pi_u$ (10^{-18})	$c^1\Pi_u$ (10^{-18})	$o^1\Pi_u$ (10^{-19})	$b'^1\Sigma_u^+$ (10^{-18})	$c'^1\Sigma_u^+$ (10^{-18})	$G^3\Pi_u$ (10^{-18})	$F^3\Pi_u$ (10^{-18})	M1(=M2) (10^{-19})
(0)	91.2	39.6	139	45.6	65.4	3.07	1.62	9.91
(10)	30.5	13.4	46.6	17.7	25.1	1.19	0.597	4.54
20	9.73	4.80	14.9	5.97	7.91	0.571	0.246	2.05
30	3.13	1.59	4.14	1.68	2.14	0.285	0.110	0.873
40	1.46	0.762	1.42	0.681	0.813	0.178	0.062	0.467
50	0.952	0.463	0.599	0.381	0.490	0.122	0.043	0.281
60	0.657	0.302	0.311	0.240	0.311	0.104	0.040	0.222
70	0.465	0.192	0.197	0.127	0.170	0.105	0.042	0.224
80	0.353	0.138	0.129	0.072	0.097	0.113	0.048	0.250
90	0.300	0.116	0.101	0.049	0.069	0.136	0.062	0.321
100	0.339	0.132	0.106	0.065	0.086	0.176	0.086	0.458
110	0.413	0.172	0.112	0.148	0.138	0.224	0.114	0.611
120	0.513	0.226	0.121	0.339	0.234	0.253	0.133	0.724
130	0.730	0.322	0.161	0.697	0.449	0.290	0.154	0.871
(140)	0.949	0.426	0.210	1.14	0.693	0.312	0.165	0.937
(150)	1.33	0.625	0.318	1.85	1.11	0.381	0.204	1.16
(160)	1.63	0.788	0.420	2.47	1.44	0.420	0.223	1.29
(170)	2.60	1.33	0.868	3.72	2.17	0.570	0.304	1.74
(180)	2.95	1.51	0.983	4.91	2.81	0.702	0.379	2.11

[a] The cross section values of this table were obtained from the cross sections published by Chutjian et al. [179c] by correcting their values with a factor representing the ratio of the recent elastic cross sections of table 26 to those used by Chutjian et al.

Table 43

Differential excitation cross sections for the states of N_2 indicated at an incident electron energy of 60 eV. Entries in parentheses below the state designations are cross section multipliers (cm^2/sr) for that column.[a] (From Chutjian et al. 1977, ref. [179c].)

Angle (deg)	$b^1\Pi_u$ (10^{-18})	$c^1\Pi_u$ (10^{-18})	$o^1\Pi_u$ (10^{-19})	$b'^1\Sigma_u^+$ (10^{-18})	$c'^1\Sigma_u^+$ (10^{-18})	$G^3\Pi_u$ (10^{-18})	$F^3\Pi_u$ (10^{-18})	M1(=M2) (10^{-19})
(0)	142	70.0	218	98.3	92.8	2.62	1.42	15.3
(10)	36.1	18.0	52.9	18.0	24.0	1.11	0.649	5.17
20	8.36	4.86	11.3	3.96	5.65	0.396	0.277	1.53
30	2.03	1.18	2.52	0.900	1.44	0.158	0.119	0.468
40	0.704	0.390	0.765	0.291	0.543	0.085	0.064	0.199
50	0.425	0.171	0.291	0.134	0.276	0.061	0.045	0.112
60	0.264	0.088	0.136	0.075	0.149	0.045	0.032	0.075
70	0.179	0.057	0.081	0.053	0.094	0.042	0.028	0.068
80	0.126	0.043	0.058	0.043	0.066	0.040	0.026	0.070
90	0.120	0.037	0.056	0.045	0.063	0.048	0.030	0.099
100	0.123	0.048	0.061	0.050	0.067	0.054	0.033	0.123
110	0.150	0.064	0.075	0.064	0.086	0.070	0.041	0.170
120	0.179	0.078	0.098	0.077	0.106	0.083	0.046	0.213
130	0.228	0.118	0.157	0.110	0.152	0.118	0.063	0.304
(140)	0.306	0.215	0.328	0.193	0.247	0.201	0.107	0.483
(150)	0.388	0.356	0.602	0.306	0.383	0.323	0.170	0.744
(160)	0.490	0.560	0.991	0.484	0.577	0.496	0.268	1.11
(170)	0.585	0.827	1.46	0.703	0.796	0.697	0.386	1.56
(180)	0.667	1.03	1.91	0.960	1.02	0.953	0.531	2.04

[a]The cross section values of this table were obtained from the cross sections published by Chutjian et al. [179c] by correcting their values with a factor representing the ratio of the recent elastic cross sections from table 26 to those used by Chutjian et al.

Table 44

A. Integral (σ, upper table) and momentum transfer (σ^M, lower table) cross sections for electronic transitions in N_2. Units are 10^{-18} cm^2. (From Cartwright et al. 1977, ref. [179b].)[a]

	E_0(eV)	$A^3\Sigma_u^+$	$B^3\Pi_g$	$W^3\Delta_u$	$B'^3\Sigma_u^-$	$a'^1\Sigma_u^-$	$a^1\Pi_g$	$w^1\Delta_u$	$C^3\Pi_u$	$E^3\Sigma_g^+$	$a''^1\Sigma_g^+$
	10.0	14.9	25.2	7.01	–	–	4.02	–	–	–	–
	12.5	17.8	30.6	24.4	8.17	–	19.6	11.5	–	–	–
	15.0	20.3	22.3	33.0	12.2	10.5	24.2	9.74	37.5	0.296	3.58
σ	17.0	21.0	19.1	34.3	8.21	5.32	33.6	6.46	20.5	0.346	3.36
	20.0	15.2	13.4	21.6	4.00	3.67	29.8	3.18	14.6	0.633	5.66
	30.0	5.75	7.90	6.42	3.04	2.00	19.7	1.81	5.61	0.465	1.99
	50.0	3.73	3.17	2.48	1.64	1.94	2.9	0.658	2.22	0.135	1.38
	10.0	15.0	26.9	6.92	–	–	3.63	–	–	–	–
	12.5	18.5	33.2	25.6	7.37	–	16.4	10.6	–	–	–
	15.0	22.5	25.2	38.4	13.0	10.0	18.9	9.61	39.4	0.290	3.18
σ^M	17.0	23.7	20.4	39.9	10.0	5.77	21.1	6.27	21.6	0.306	2.96
	20.0	20.3	16.0	28.5	5.16	4.25	18.1	3.19	16.3	0.576	5.19
	30.0	7.42	10.3	8.11	2.96	1.76	11.7	1.77	6.26	0.292	1.50
	50.0	5.37	4.03	3.03	1.54	1.25	5.60	0.543	2.41	0.062	0.904

[a] The integral cross sections were obtained from the renormalized data of tables 35 to 41.

B. Integral cross sections for the $X^1\Sigma_g^+ \rightarrow a^1\Pi$ ($v' = 0$–6) excitation in N_2. Units are 10^{-18} cm^2. (From Finn and Doering [180].)

Energy (eV)	σ	Energy (eV)	σ
13	27	35	17
15	36	40	15
18	36	50	10
20	31	60	8.0
22	27	75	7.5
24	27	90	5.6
30	23	100	5.2

Table 45

Integral (σ) and momentum transfer (σ^M) cross sections in N_2 at 40 and 60 eV. Units are 10^{-18} cm^2. (From Chutjian et al. 1977, ref. [179c].)[a]

	40.0 eV		60.0 eV	
State	σ	σ^M	σ	σ^M
$b^1\Pi_u$	20.8	11.9	4.8	4.76
$c^1\Pi_u$	9.57	5.47	7.87	2.97
$o^1\Pi_u$	2.25	0.716	1.96	0.579
$b'^1\Sigma_u^+$	13.4	10.1	7.25	2.67
$c'^1\Sigma_u^+$	14.8	7.93	10.2	3.63
$G^3\Pi_u$	2.96	3.07	1.71	1.85
$F^3\Pi_u$	1.42	1.55	1.03	1.04
M1(=M2)	0.862	0.878	0.472	0.437

[a] The integral cross sections were obtained from the renormalized data of tables 42 and 43.

and their results at the common 4 eV impact energy are in good agreement. In both cases the normalization was done to total electron scattering cross sections [184, 185]. The results of Linder and Schmidt [186] are shown in fig. 28 and those of Trajmar et al. [187] in table 50 and fig. 29. Trajmar et al. [194] also reported differential cross sections at 20 and 45 eV impact energies for the 6.1 eV transition ($c^1\Sigma_u^-$, $C^3\Delta_u$, $A^3\Sigma_u^+$ states), for the $B^3\Sigma_u^-$ state, for the 9.97 eV ("longest" band), and for the 10.29 eV ("second" band) transitions (figs. 30 and 31). Wakiya's investigations are described in two consecutive

Table 46

Total electron scattering cross sections for O_2, 10^{-16} cm^2 units. (From Sunshine et al. 1967, ref. [184]; Salop and Nakano 1970, ref. [185]; Dalba et al. 1980, ref. [139].)

	σ_{TOT}			σ_{TOT}		
E_0(eV)	Ref. [184][a]	Ref. [185][a]	E_0(eV)	Ref. [184][a]	Ref. [185][a]	Ref. [139]
0.50	6.00		8.75	11.6	–	
1.00	~~5.40~~ 6.4		9.00	–	9.38	
1.50	7.30		9.25	10.7	–	
2.00	7.50		9.46	–	9.60	
2.28	–	6.14	9.75	10.7	–	
2.50	8.40	–	10.05	–	9.80	
2.56	–	5.27	10.25	10.5	–	
2.86	–	6.39	10.62	–	9.93	
3.05	7.50	–	10.80	11.0	–	
3.17	–	6.51	11.12	–	10.04	
3.60	8.50	–	11.30	11.4	–	
3.61	–	6.65	11.80	–	10.13	
4.00	–	5.80	16.0	(9.2)	(9.4)	
4.10	8.20	–	20.0	–	(9.3)	
4.41	–	6.93	25.0	(9.0)	–	
4.65	9.10	–	50.0			
4.83	–	7.06	100.0			8.58
5.15	7.90	–	121			7.99
5.27	–	7.22	144			7.54
5.70	9.40	–	169			7.01
5.82	–	7.45	196			6.38
6.20	9.10	–	225			5.94
6.32	–	7.66	256			5.51
6.68	–	7.84	289			5.14
6.70	9.50	–	324			4.86
7.13	–	8.07	361			4.49
7.20	9.10	–	400			4.21
7.43	–	8.32	484			3.68
7.70	10.5	–	576			3.28
7.75	–	8.57	676			2.89
8.11	–	8.82	784			2.58
8.20	9.90	–	900			2.34
8.55		9.13	1024			2.08
			1156			1.89
			1296			1.71
			1444			1.55
			1600			1.43

[a] Numerical values were taken from ref. [5]. Values in parenthesis were read from fig. 1 of ref. [185].

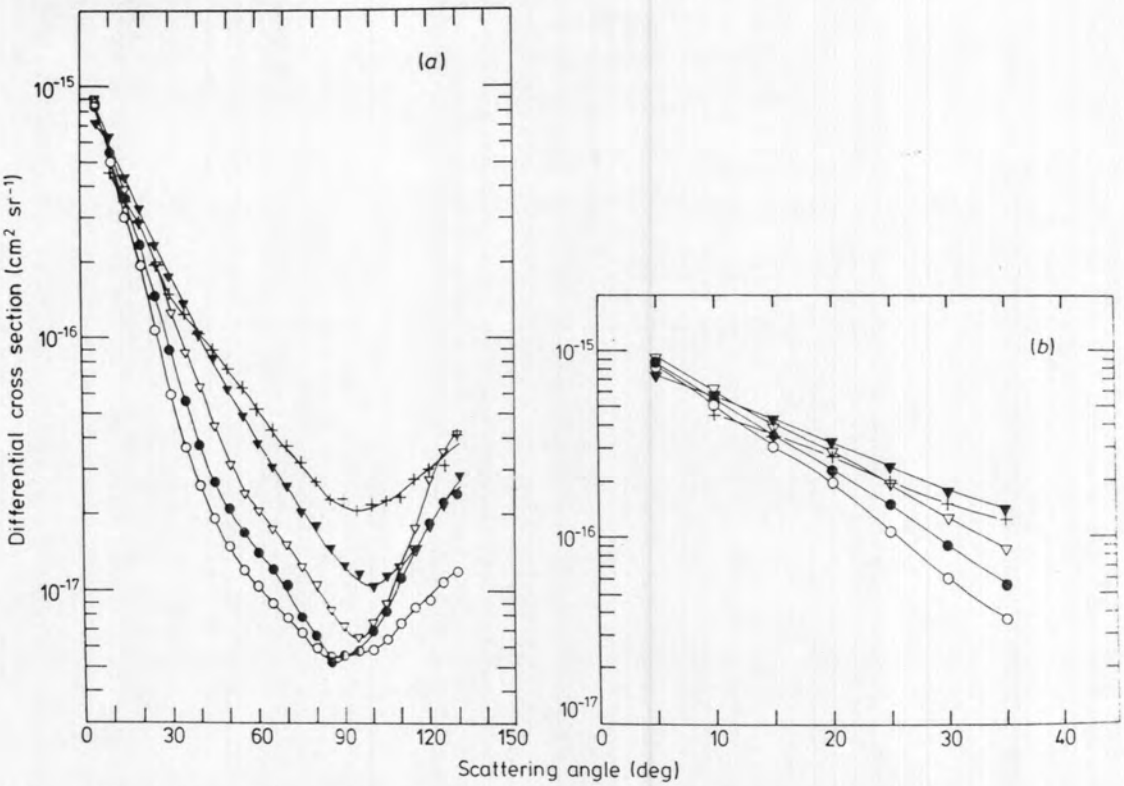

Fig. 25. (a) Elastic differential cross sections for O_2 at different electron energies: +20 eV, ▼ 30 eV, ▽ 50 eV, ● 70 eV, ○ 100 eV. The symbol ▽ means that ▼ and ▽ have the same value and the symbol ○ similarly but for ● and ◐. (From ref. [190a].) (b) As (a), except that the scale of the scattering angle is extended four times in the range of $\theta = 5$–$35°$.

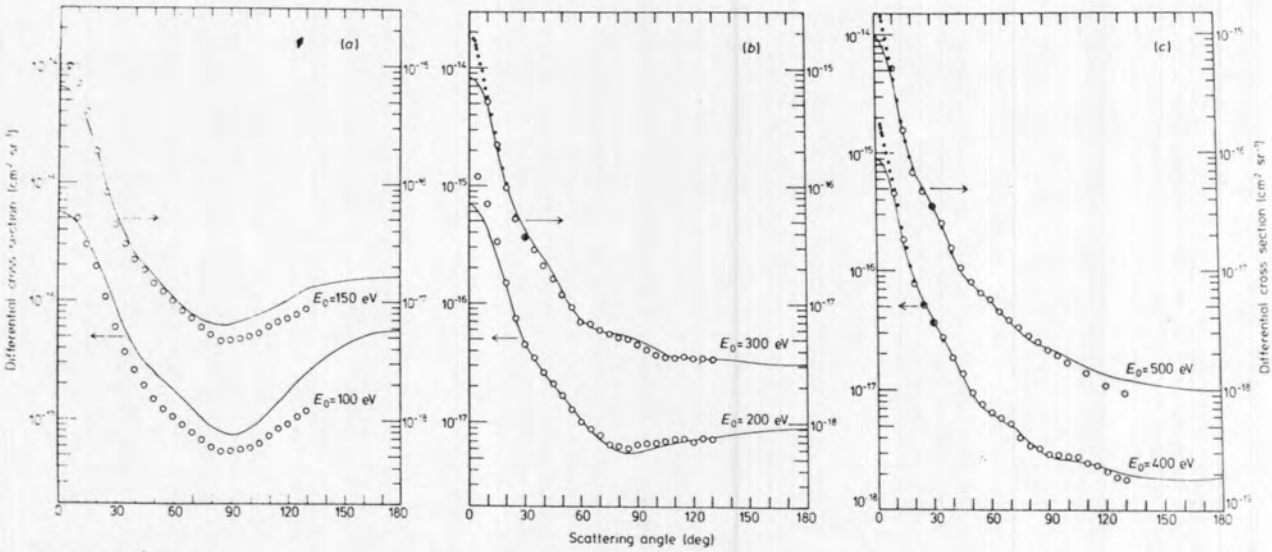

Fig. 26. Differential elastic scattering cross sections for O_2 at different incidence electron energies; (a) 100 and 150 eV, (b) 200 and 300 eV, (c) 400 and 500 eV. Large dots indicate results used as standards for normalizing the excitation cross section. In (b) and (c), small dots represent experimental data of Bromberg [189]. Curves at $E_0 = 150$–500 eV and at $E_0 = 100$ eV are calculated by Hayashi [191] and Hayashi and Kuchitsu [192], and by Daimon [193], respectively. (From ref. [190a].)

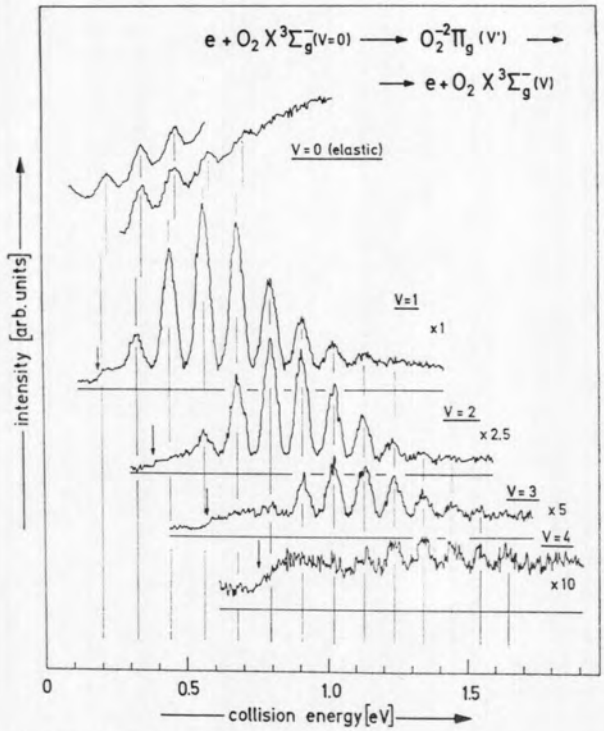

Fig. 27. Measured excitation functions for vibrational excitation to $v = 1, 2, 3, 4$ of O_2 with true intensity ratios. The horizontal line at each curve indicates the zero line of the stored signal. Two runs of the energy dependence of elastic scattering are also shown in the upper part of the figure. The scattering angle is 60° for all curves. The vertical lines indicate energy positions of the resonance peaks. Onsets of the excitation functions are marked by small arrows. (From ref. [186].)

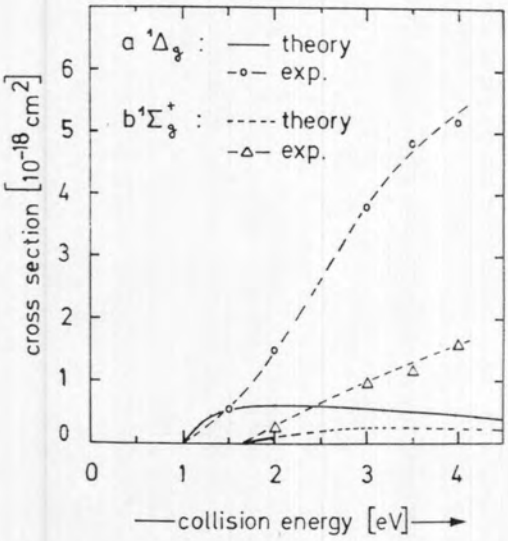

Fig. 28. Integral cross sections for excitation of the states $a^1\Delta_g$ ($v = 0$) and $b^1\Sigma_g^+$ ($v = 0$) of O_2. The measured cross sections are compared with the results of a semi-empirical theory [195]. The experimental errors are approximately 20%. (From ref. [186].)

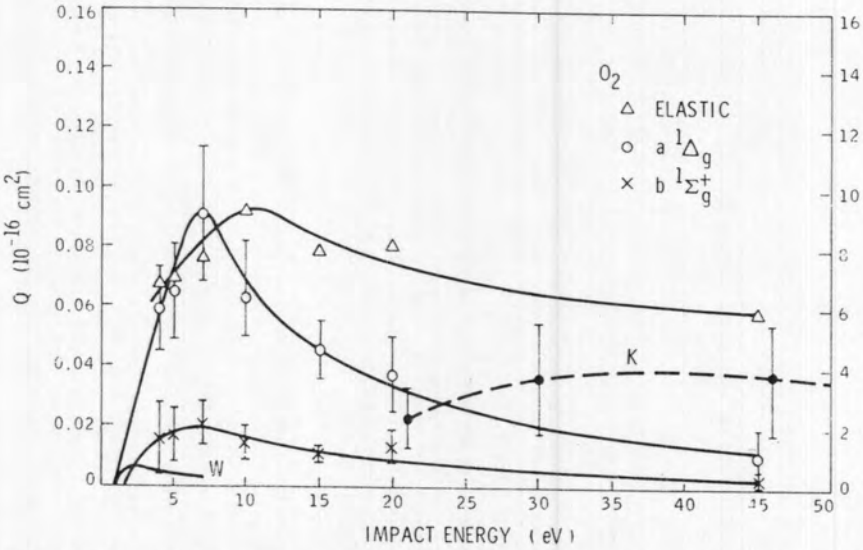

Fig. 29. Integral cross sections as a function of impact energy. The curves marked by W and K represent integral cross sections for excitation of the $a^1\Delta_g$ state as given by Watson et al. [195] and Konishi et al. [196]. (From ref. [187].)

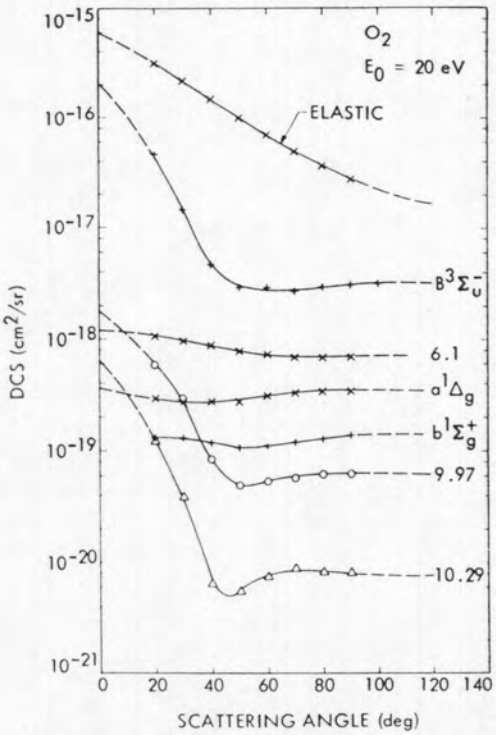

Fig. 30. Differential cross sections (DCS) in O_2 at 20 eV impact energy (E_0). The solid portions of the curves are drawn through the experimental points; the dashed ones are extrapolations. (From ref. [194].)

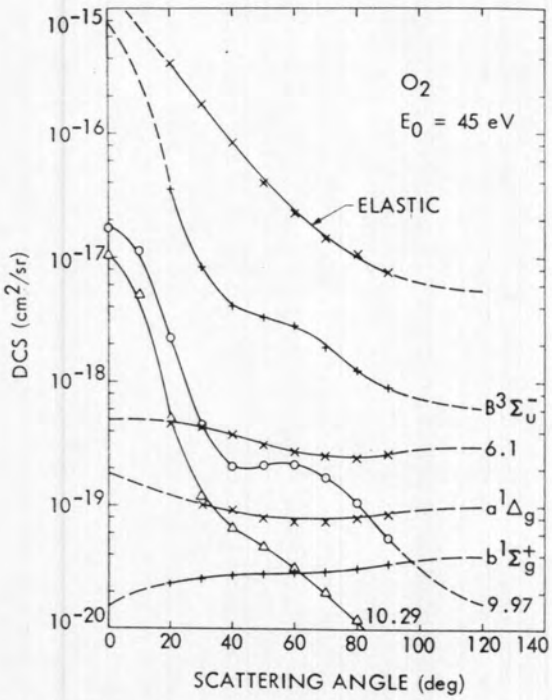

Fig. 31. Same as fig. 30 except at $E_0 = 45$ eV. (From ref. [194].)

Table 47A
Elastic differential cross sections for O_2[a], 10^{-16} cm²/sr units. (From Trajmar et al. 1971, ref. [187].)

	E_0(eV)						
θ(deg)	4	5	7	10	15	20	45
(0)	0.942	1.04	1.799	5.481	6.671	6.058	12.24
10	0.920	0.937	1.606	3.350	4.255	4.503	7.690
20	0.897	0.914	1.371	2.253	2.718	3.193	3.759
30	0.875	0.823	1.232	1.675	1.883	2.210	1.766
40	0.852	0.816	1.124	1.309	1.286	1.515	0.854
50	0.807	0.765	1.017	1.305	0.879	0.999	0.416
60	0.754	0.741	0.878	0.834	0.637	0.708	0.234
70	0.686	0.674	0.728	0.670	0.453	0.499	0.118
80	0.603	0.596	0.610	0.566	0.373	0.369	0.105
90	0.505	0.518	0.493	0.487	0.322	0.274	0.079
(100)	0.422	0.460	0.402	0.414	0.282	0.217	0.061
(120)	0.332	0.380	0.294	0.335	0.233	0.154	0.041
(140)	0.279	0.333	0.225	0.286	0.206	0.120	0.031
(160)	0.249	0.298	0.179	0.262	0.184	0.098	0.025
(180)	0.226	0.274	0.148	0.238	0.171	0.082	0.020

[a] Values outside the 10°–90° range were obtained by extrapolation.

Table 47B

Elastic differential (DCS), integral (σ) and momentum transfer (σ^M) cross sections in O_2 (in 10^{-18} cm^2/sr and 10^{-16} cm^2 units). (From Shyn and Sharp 1982, ref. [188b].)

	DCS													
θ(deg) \ E_0(eV)	2.0	3.0	5.0	7.0	10.0	15	20	30	40	50	70	100	150	200
6														
12	34.5	59.2	95.9	154.3	250.1	373.8	488.2	655.4	760.4	773.3	755.6	633.3	443.9	422.9
18														
24	44.0	63.3	103.9	149.0	200.0	243.7	263.3	301.3	300.0	275.0	217.6	145.2	104.0	68.2
30														
36	48.7	70.0	108.9	138.8	157.8	171.5	157.7	129.6	109.4	85.7	55.9	34.2	25.3	20.9
48	52.3	77.1	110.0	127.6	131.1	120.7	100.3	63.0	44.2	32.5	20.9	13.6	12.6	11.6
60	54.7	72.2	101.2	93.2	99.9	82.1	61.0	34.4	22.2	16.4	11.5	8.45	7.64	5.89
72	51.1	70.0	87.1	73.6	73.8	53.0	35.6	19.7	14.1	10.7	6.96	5.30	4.93	3.57
84	51.1	62.5	65.9	59.0	57.1	35.1	23.2	13.1	8.95	6.21	4.51	3.68	3.57	3.03
96	48.7	58.4	58.2	49.4	49.3	30.1	20.5	10.1	5.19	3.73	3.76	4.00	3.57	3.03
108	48.7	53.6	50.4	46.9	51.4	32.8	24.3	12.0	6.45	5.46	6.21	5.01	4.59	3.21
120	52.3	57.6	50.8	50.3	57.9	39.9	31.8	20.9	15.9	15.6	13.4	7.95	6.46	3.93
132	57.0	60.0	51.8	58.7	65.9	52.5	45.5	39.0	34.4	31.3	20.9	11.8	7.81	4.10
144	60.5	63.3	61.7	68.9	72.8	70.7	66.5	66.6	63.0	50.7	33.3	17.1	9.00	5.00
156	59.5	63.3	66.6	80.7	80.7	89.4	90.3	100.4	93.5	69.8	45.5	24.6	10.5	5.71
168	(60.5)	(68.2)	(72.3)	(95.0)	(89.7)	(113.2)	(122.4)	(151.5)	(138.8)	(96.4)	(62.2)	(35.3)	(12.6)	(6.60)
σ	6.5	8.0	9.3	9.9	10.9	10.0	9.1	8.2	7.5	6.6	5.3	3.8	2.7	2.2
σ^M	6.7	7.7	8.0	8.2	8.6	7.2	6.1	5.2	4.5	3.5	2.5	1.5	0.95	0.62

Table 48
Elastic differential cross sections for O_2, a_0^2/sr units.

A. From Bromberg 1974, ref. [189a]

Angle (deg)	500 eV	400 eV	300 eV	Angle (deg)	500 eV	400 eV	300 eV
2	69.54 ± 2.36	71.73 ± 2.38	72.63 ± 6.64	10	15.18 ± 0.52	17.68 ± 0.58	20.48 ± 0.97
2.5	60.97 ± 2.10	63.11 ± 2.07	62.77 ± 2.28	12	9.967 ± 0.330	12.11 ± 0.40	14.42 ± 0.71
3	55.95 ± 1.92	58.52 ± 1.91	59.71 ± 2.26	14	6.613 ± 0.223	8.161 ± 0.270	10.19 ± 0.51
3.5	51.32 ± 1.77	54.18 ± 1.78	55.82 ± 2.06	16	4.506 ± 0.151	5.580 ± 0.188	7.144 ± 0.371
4	46.88 ± 1.62	49.63 ± 1.63	51.90 ± 1.90	18	3.298 ± 0.111	3.974 ± 0.135	4.998 ± 0.255
5	39.43 ± 1.34	42.39 ± 1.39	44.96 ± 1.82	20	2.593 ± 0.088	2.979 ± 0.098	3.675 ± 0.174
6	32.84 ± 1.12	35.82 ± 1.17	38.86 ± 1.68	25	1.775 ± 0.059	1.865 ± 0.063	1.998 ± 0.091
7	27.14 ± 0.92	30.16 ± 0.99	33.29 ± 1.48	30	1.242 ± 0.042	1.345 ± 0.056	1.283 ± 0.044
8	22.59 ± 0.76	25.34 ± 0.83	28.30 ± 1.37	35	0.8236 ± 0.0303	0.9289 ± 0.0331	
9	18.52 ± 0.62	21.30 ± 0.70	24.10 ± 1.16	40	0.5082 ± 0.0216		

B. From Daimon et al. 1982, ref. [189b][a]

Angle (deg)	200 eV	300 eV	400 eV	500 eV	Angle (deg)	200 eV	300 eV	400 eV	500 eV
4	85.0(150)	–	47.7(48)	51.4(51)	35	1.27(6)	1.09(5)	1.03(5)	0.751(38)
5	65.0(65)	–	41.0(41)	42.6(43)	40	1.00(5)	0.849(42)	0.671(34)	0.506(25)
6	54.1(54)	37.0(37)	34.3(34)	32.8(33)	45	–	0.627(31)	0.481(24)	0.335(17)
7	45.8(46)	31.7(32)	–	–	50	0.630(32)	0.454(23)	0.348(17)	0.264(13)
8	38.9(39)	26.7(27)	23.5(24)	21.2(21)	60	0.386(19)	0.269(13)	0.253(13)	0.188(9)
9	32.5(33)	23.8(24)	–	–	70	0.267(13)	0.222(11)	0.196(10)	0.124(6)
10	27.4(27)	20.3(20)	18.3(18)	14.1(14)	80	0.227(11)	0.193(10)	0.142(7)	0.0194(46)
12	19.3(19)	12.9(13)	12.6(13)	9.48(95)	90	0.224(11)	0.162(8)	0.111(6)	0.0790(40)
14	13.9(14)	9.22(92)	–	–	100	0.229(11)	0.140(7)	0.0991(50)	0.0655(33)
15	–	–	6.92(69)	4.88(49)	110	0.236(12)	0.134(7)	0.0932(47)	0.0544(27)
16	10.4(10)	6.83(68)	–	–	120	0.235(12)	0.126(6)	0.0844(42)	0.0463(23)
18	7.50(75)	5.07(51)	–	–	130	0.242(12)	0.132(7)	0.0753(38)	0.0432(22)
20	5.51(55)	4.11(41)	3.39(34)	2.54(25)	140	0.255(13)	0.137(7)	0.0701(35)	0.0411(21)
25	2.93(29)	1.96(20)	1.98(20)	1.88(19)	150	–	–	–	0.0390(20)
30	1.73(17)	1.42(14)	1.46(15)	1.31(3)					

[a] The numbers in parentheses represent errors in units of the last decimals listed.

papers. The first one [190a] is concerned with the excitation of the Schuman–Runge continuum ($B^3\Sigma_u^-$) and the collection of the states in the 9.7 to 12.1 eV region (predominantly optically allowed excitations). The second paper [190b] describes the study of the electron impact excitation of the $a^1\Delta_g$, $b^1\Sigma_g^+$ and the unresolved 6.1 eV ($A^3\Sigma_u^+ + C^3\Delta_u + c^1\Sigma_u^-$) states. The cross sections obtained in his first paper are shown in figs. 32–34. A comparison with the earlier results of Trajmar et al. [187, 194] is also made in these figures. The cross sections obtained by Wakiya [190b] for the excitation of the states below 7.1 eV are shown in figs. 35 through 40. Again comparison with the earlier data of Trajmar et al. [187, 194] and Linder and Schmidt [186] is made in these figures.

Recently Tachibana and Phelps [200] and Lawton and Phelps [201] measured rate coefficients for the excitation of the $a^1\Delta_g$ and $b^1\Sigma_g^+$ states, respectively, in O_2–Ar mixtures using drift tube technique. Their experimental electron excitation coefficients are consistent with values calculated from the electron collision cross section data discussed above.

Table 49
Resonance energies [in eV] and energy-integrated cross sections in 10^{-20} cm^2 units. (From Linder and Schmidt 1971, ref. [186].)

vibr. state v'	4	5	6	7	8	9	10	11	12	13	14	15	16	17	18
energy E[eV]	0.082	0.027	0.330	0.450	0.569	0.686	0.801	0.914	1.025	1.135	1.242	1.346	1.449	1.550	1.649
ΔE[meV]		125	123	120	119	117	115	113	111	110	107	104	103	101	99
$v = 1$	×	–	25	82	110	100	61	35	17	9	5	–	–	–	–
exit $v = 2$	×	×	×	–	8.5	25	32	28	19	12	5.8	2.4	1.1	–	–
channel $v = 3$	×	×	×	×	–	–	1.3	5.5	7.3	7.0	5.8	3.3	1.8	1.0	–
$v = 4$	×	×	×	×	×	×	–	–	–	1.0	1.9	2.0	1.7	1.3	1.0

Table 50
Differential cross sections for the excitation of the $a^1\Delta_g$ and $b^1\Sigma_g^+$ states of O_2.[a] (From Trajmar et al. 1971, ref. [187].)

θ(deg)	DCS $a^1\Delta_g$ (10^{-19} cm^2/sr)							θ(deg)	DCS $b^1\Sigma_g^+$ (10^{-20} cm^2/sr)						
(0)	6.94	5.18	9.64	14.0	9.77	8.92	1.77	(0)	...	...	...	...	...	...	...
10	5.66	5.72	8.89	11.0	7.25	5.24	1.48	10	4.05	3.13	5.89	6.09	8.28	6.71	1.14
20	4.42	5.62	8.14	8.34	4.95	3.19	1.20	20	6.64	5.80	10.5	10.4	15.0	10.2	2.11
30	3.66	5.01	7.39	6.27	3.34	2.78	0.97	30	9.40	7.91	16.1	14.0	14.5	10.6	2.53
40	3.24	4.38	6.64	5.12	2.64	2.91	0.83	40	12.0	1.16	21.4	14.0	12.2	10.4	2.53
50	3.07	3.50	6.32	4.46	2.62	3.15	0.73	50	14.1	1.39	24.1	12.8	10.8	10.7	2.22
60	3.25	4.36	6.32	4.26	2.76	3.32	0.67	60	15.6	1.58	24.6	11.0	10.1	11.6	2.11
70	3.92	4.64	6.64	4.26	3.12	3.36	0.68	70	16.0	1.67	23.6	10.7	9.78	12.7	2.28
80	4.70	5.03	7.50	4.38	3.50	3.36	0.83	80	16.2	1.67	21.4	10.7	9.43	13.2	2.73
90	5.09	5.40	7.93	4.63	3.77	3.29	0.94	90	15.9	1.65	18.2	11.3	9.09	13.0	3.25
(100)	5.39	5.72	8.09	4.87	3.91	3.19	1.03	(100)	15.4	1.58	16.2	11.6	8.86	12.4	3.42
(120)	5.66	5.83	7.82	5.05	3.93	2.82	1.05	(120)	13.4	1.39	13.9	11.7	8.05	10.3	3.36
(140)	5.53	5.53	7.07	4.93	3.77	2.33	0.97	(140)	11.3	1.14	12.4	11.3	7.25	8.02	3.02
(160)	5.28	5.08	6.21	4.63	3.51	1.88	0.82	(160)	9.32	0.893	11.2	10.7	6.33	5.98	2.51
(180)	4.98	4.54	5.35	4.26	3.17	1.47	0.66	(180)	7.29	0.696	10.7	9.74	5.41	4.34	1.99

[a] Values outside of the 10°–90° range were obtained by extrapolation.

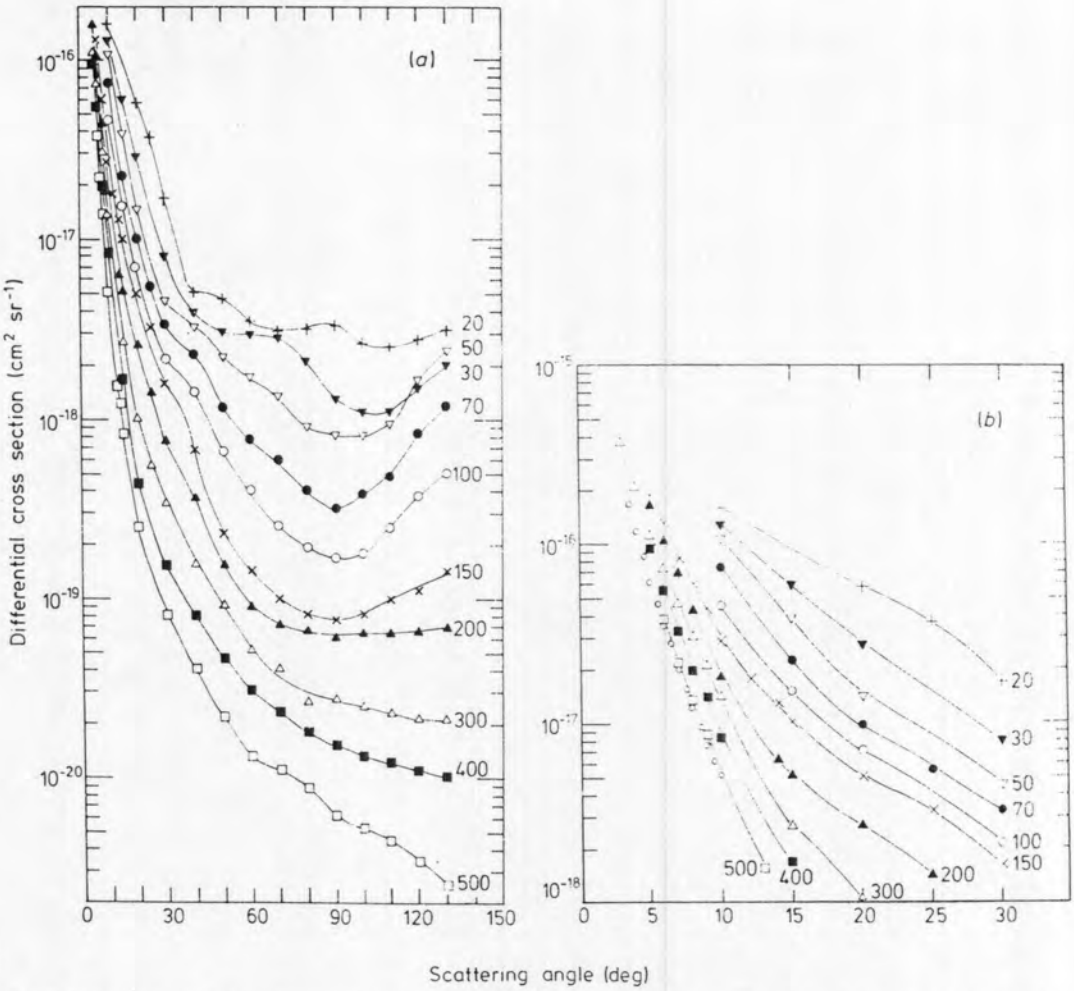

Fig. 32. (a) The DCS for excitation of the Schumann–Runge continuum in O_2 at different incident electron energies: + 20 eV, ▼ 30 eV, ▽ 50 eV, ● 70 eV, ○ 100 eV, × 150 eV, ▲ 200 eV, △ 300 eV, ■ 400 eV and □ 500 eV. (From ref. [190a].) (b) As (a), except that the scale of scattering angle is extended four times in the range of θ = 3–30°. Small open circles ○ indicate the corrected DCS of Lassettre and Frances [197] multiplied by 0.77 since their data were considered to contain the streaming error in a McLeod gauge (Lassettre and Skerbele [198]), E_0 = 519 eV. (From ref. [190a].)

4.4. CO

There are considerably less data available on e–CO scattering than for its isoelectronic partner N_2. Only a limited coverage of total scattering and (partially-resolved) rotational excitation cross sections exist. Further optical excitation function measurements and especially electronically inelastic electron scattering cross sections are needed. A more thorough data set would provide modelers with some guide as to the suitability of CO in swarm or diffuse-discharge experiments.

Total scattering cross sections

Total electron scattering cross sections in CO have been measured in transmission experiments by Hasted et al. [141b] and Szmytkowski and Zubek [202]. The energy range in these measurements was 1–4.5 eV and 1.2–5.5 eV, respectively. Results are shown here in figs. 41 and 42. While agreement

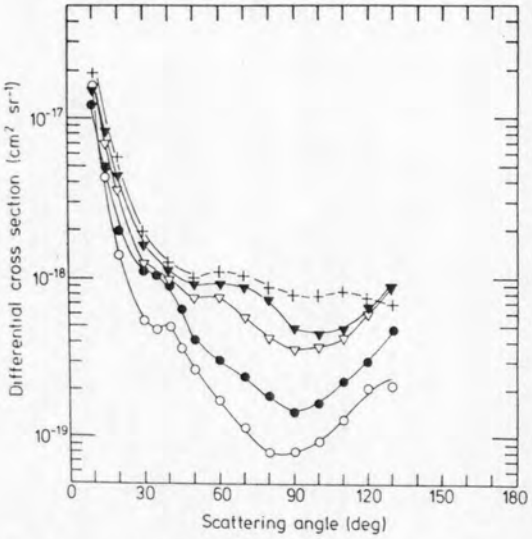

Fig. 33. The sum of the DCS for excitation of electronic states in the range 9.7 to 12.1 eV energy loss in O_2 at different incident energies; + 20 eV, ▼ 30 eV, ▽ 50 eV, ● 70 eV, ○ 100 eV. (From ref. [190a].)

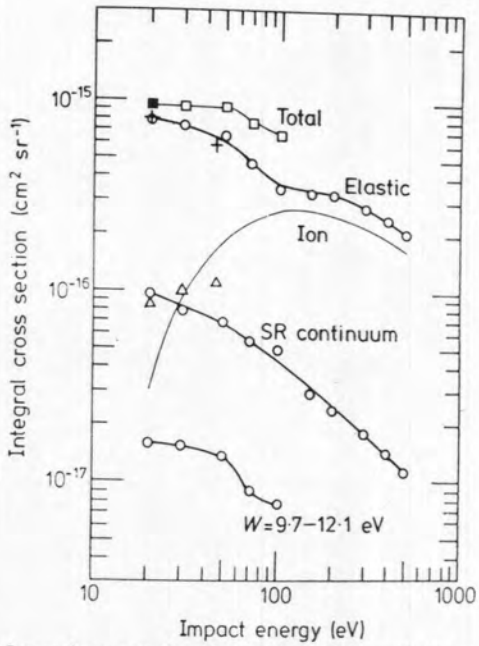

Fig. 34. Integral cross sections for total scattering, elastic scattering, total ionization, excitation of the Schumann–Runge continuum and the excited electronic states in the energy-loss region 9.7–12.1 eV as a function of electron energy in O_2. The symbol ○ and the bold curves show the data of Wakiya [190a]. The symbols ■ and □ indicate the measured total cross sections of Salop and Nakano [185] and Sunshine et al. [184], respectively. The fine curve represents the measured total ionization cross section of Rapp and Englander-Golden [199]. The symbols + and △ indicate the results of Trajmar et al. [194] for elastic scattering and excitation of the Schumann–Runge continuum, respectively. (From ref. [190a].)

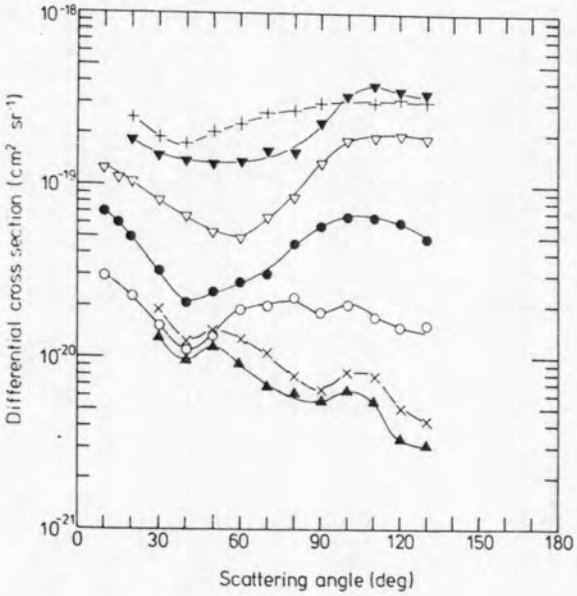

Fig. 35. The DCS for the $a^1\Delta_g \leftarrow X^3\Sigma_g^-$ excitation in O_2 for different incident electron energies; + 20 eV, ▼ 30 eV, ▽ 50 eV, ● 70 eV, ○ 100 eV, × 150 eV, ▲ 200 eV. (From ref. [190b].)

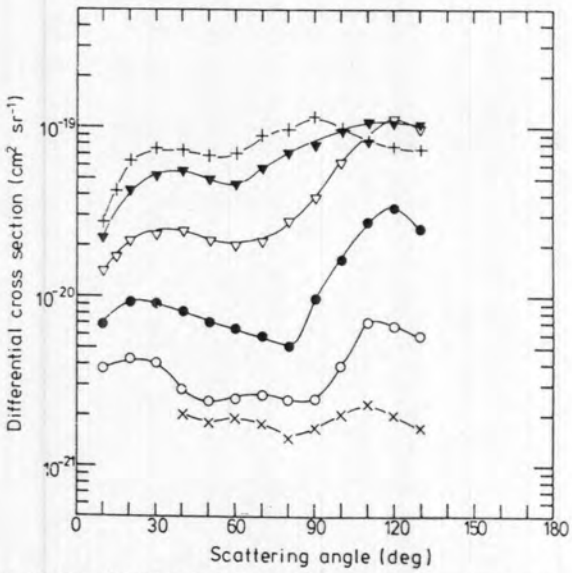

Fig. 36. The DCS for the $b^1\Sigma_g^+ \leftarrow X^3\Sigma_g^-$ excitation in O_2 for different incident electron energies: + 20 eV, ▼ 30 eV, ▽ 50 eV, ● 70 eV, ○ 100 eV, × 150 eV. (From ref. [190b].)

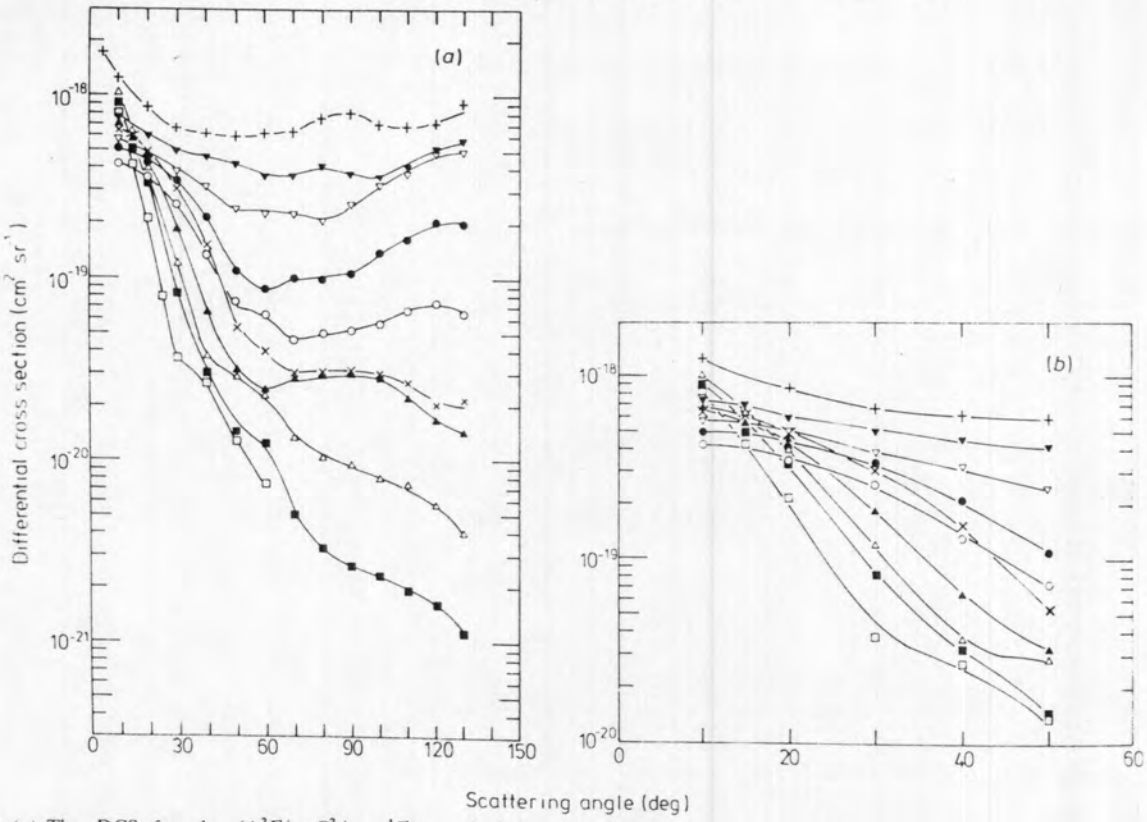

Fig. 37. (a) The DCS for the $(A^3\Sigma_u^+ + C^3\Delta_u + c^1\Sigma_u^-)$ excitation in O_2 for different incident electron energies: + 20 eV, ▼ 30 eV, ▽ 100 eV, × 150 eV, ▲ 200 eV, △ 300 eV, ■ 400 eV, □ 500 eV. (b) As (a), except that the scale of scattering angle is extended three times in the range of $\theta = 10$–$50°$. (From ref. [190b].)

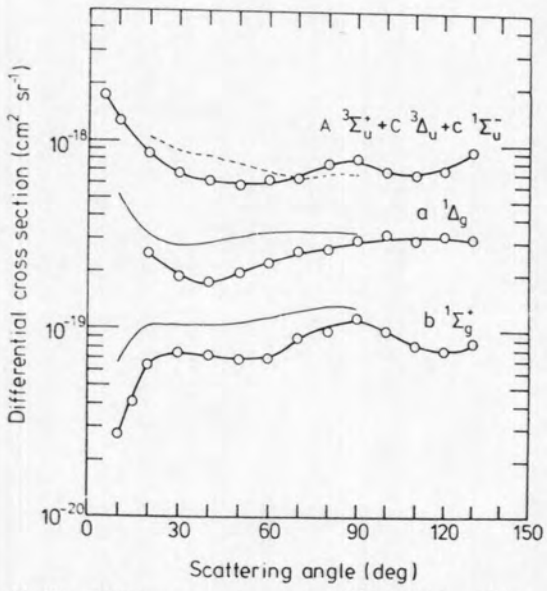

Fig. 38. The DCS for excitation of the $(A^3\Sigma_u^+ + C^3\Delta_u + c^1\Sigma_u^-)$, $a^1\Delta_g$ and $b^1\Sigma_g^+$ states in O_2 at an electron energy of $E_0 = 20$ eV. The symbols ○ and the bold curves show results of Wakiya [190b]. The broken curve $(A^3\Sigma_u^+ + C^3\Delta_u + c^1\Sigma_u^-)$ and the fine curves ($a^1\Delta_g$ and $b^1\Sigma_g^+$) indicate the measured values of Trajmar et al. [187, 194]. (From ref. [190b].)

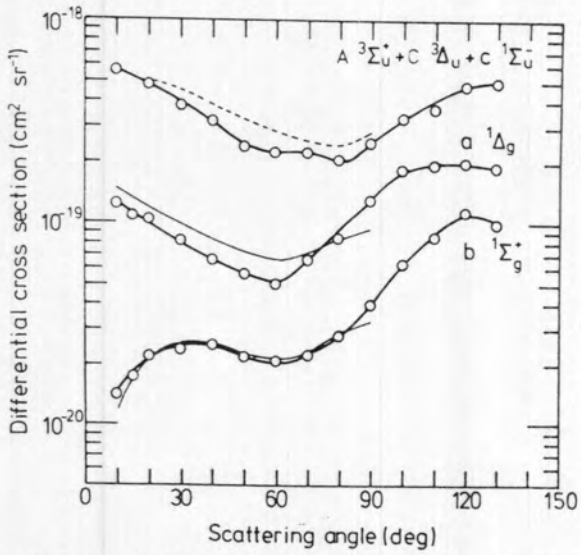

Fig. 39. Same as fig. 38, except for electron energies $E_0 = 50$ eV (Wakiya [190b]) and $E_0 = 45$ (results of Trajmar et al. [187]; the broken curve and fine curve). (From ref. [190b].)

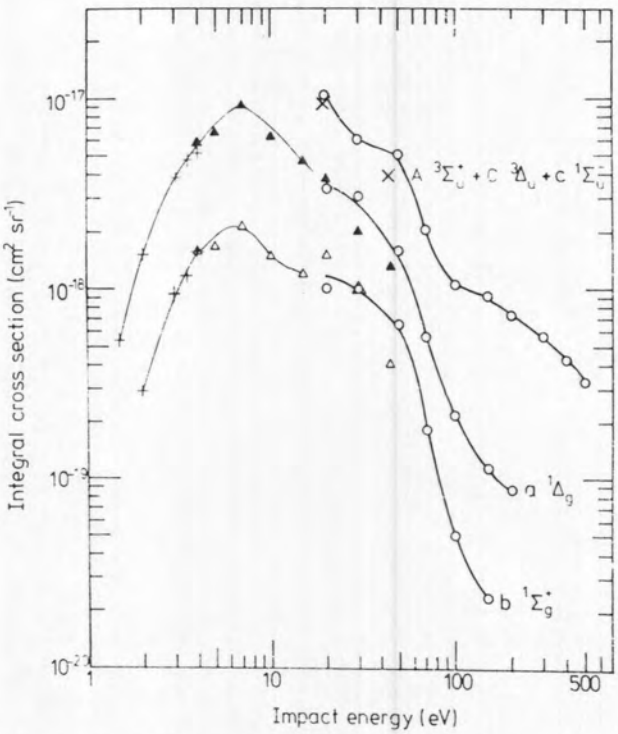

Fig. 40. Integral cross sections for excitation of the ($A^3\Sigma_u^+ + C^3\Delta_u + c^1\Sigma_u^-$), $a^1\Delta_g$ and $b^1\Sigma_g^+$ states of O_2 as a function of electron impact energy. The symbols ○ and the bold curves show the results of Wakiya [190b]. The symbols × ($A^3\Sigma_u^- + C^3\Delta_u + c^1\Sigma_u^-$), ▲ ($a^1\Delta_g$) and △ ($b^1\Sigma_g^+$) indicate the results of Trajmar et al. [186]. (From ref. [190b].)

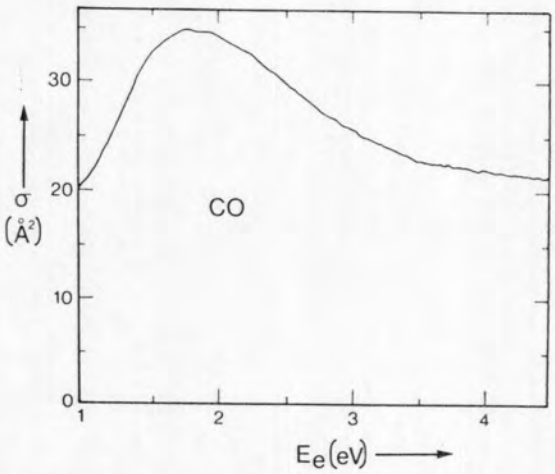

Fig. 41. Total electron scattering cross sections in CO in the energy range 1.0–4.3 eV as measured in transmission. (From ref. [141b].)

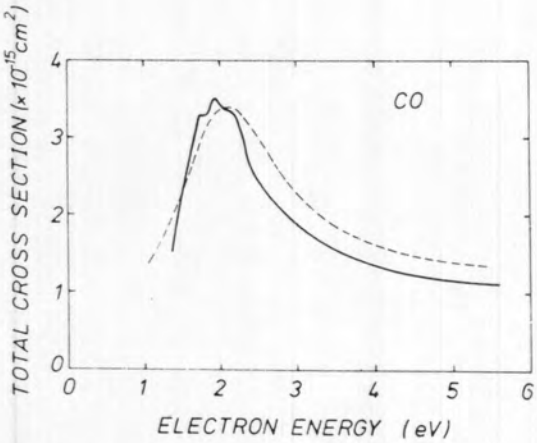

Fig. 42. Total electron scattering cross section in CO in the energy range 1.0–5.6 eV as measured in transmission. Solid line represents results of ref. [202], while dashed line is from ref. [203]. (From ref. [202].)

between the two sets of data is reasonable below 2 eV, results of Hasted et al. are noticeably larger than those of Szmytkowski and Zubek at the higher energies. Time-of-flight measurements of the total scattering cross sections have been reported by Gus'kov et al. [204] in the energy range 0.05–6.0 eV, and are given in table 51. These results are in somewhat better agreement with Szmytkowski and Zubek than with Hasted et al. in the overlapping energy range 1.2–5.5 eV.

Table 51
Total electron scattering cross sections for CO, 10^{-15} cm^2 units. (From fig. 1 of ref. [204].)

E_0(eV)	σ	E_0(eV)	σ
0.05	0.7	0.8	1.3
0.1	0.8	1.0	1.8
0.2	0.9	2.0	3.2
0.4	1.1	4.0	1.3
0.6	1.2	6.0	1.0

Elastic electron scattering

Elastic scattering cross sections in CO are given by Tanaka et al. [205] at electron energies in the range 3–100 eV. As in the case of N_2, these data were renormalized to the more recent helium elastic cross sections of Register et al. [10]. Differential cross sections are presented in table 52, and integral and momentum transfer cross sections in table 53. DuBois and Rudd [143] have reported differential cross sections at energies of 200, 500 and 800 eV using techniques similar to those in N_2. Their results are given in table 54. Elastic differential cross sections have been measured by Bromberg [146] and his results for CO are listed in table 55. Elastic scattering cross sections in the range 6–80 eV are also

Table 52
Elastic differential cross sections in CO. Units are 10^{-16} cm^2/sr. Entries by angles in parentheses refer to extrapolated values. (From Tanaka et al. 1978, ref. [205].)[a]

	E_0(eV)									
θ(deg)	3	5	7.5	9.9	15	20	30	50	75	100
(0)	2.20	1.44	2.10	2.29	5.15	6.98	5.62	7.31	8.00	6.30
(5)	2.40	1.57	2.07	2.25	4.81	6.64	5.14	6.05	6.45	5.19
(10)	2.51	1.70	2.00	2.20	4.37	5.91	4.45	4.68	4.85	3.88
15	2.17	1.61	1.95	2.13	3.90	5.15	3.66	3.42	3.39	2.64
20	2.76	1.97	1.77	2.10	3.29	4.06	2.87	2.32	2.13	1.70
30	2.81	2.10	1.67	1.83	2.41	2.29	1.67	1.10	0.791	0.540
40	3.21	2.27	1.62	1.83	1.44	1.52	0.859	0.471	0.295	0.201
50	3.14	1.98	1.41	1.41	1.10	0.701	0.458	0.226	0.133	0.120
60	2.49	1.65	1.11	1.02	0.744	0.489	0.252	0.129	0.0852	0.0818
70	1.87	1.40	0.822	0.670	0.482	0.305	0.176	0.0819	0.0627	0.0699
80	1.22	1.06	0.620	0.515	0.321	0.205	0.118	0.0602	0.0608	0.0581
90	0.963	0.840	0.476	0.386	0.320	0.228	0.107	0.0581	0.0568	0.0524
100	0.685	0.700	0.414	0.475	0.355	0.260	0.120	0.0697	0.0654	0.0527
110	0.516	0.650	0.492	0.550	0.460	0.313	0.148	0.102	0.0666	0.0494
120	0.525	0.719	0.595	0.693	0.579	0.399	0.217	0.143	0.0875	0.0534
130	0.591	0.813	0.726	0.788	0.694	0.497	0.310	0.214	0.109	0.0588
(140)	0.66	0.86	0.82	0.90	0.82	0.58	0.41	0.28	0.14	0.064
(150)	0.73	0.94	0.93	1.0	0.94	0.68	0.53	0.37	0.16	0.069
(160)	0.80	1.0	1.0	1.1	1.1	0.77	0.65	0.46	0.20	0.075
(170)	0.87	1.2	1.1	1.2	1.2	0.82	0.76	0.54	0.22	0.080
(180)	0.92	1.2	1.2	1.2	1.2	0.85	0.82	0.60	0.24	0.083

[a] Numbers on this table differ slightly from those of the tabulation of ref. [205] due to small changes in the He elastic cross sections at the time of publication of ref. [10].

Table 53
Elastic integral (σ) and momentum-transfer (σ^M) cross sections in CO. Units are 10^{-16} cm^2. (From Tanaka et al. 1978, ref. [205].)

E_0(eV)	σ	σ^M
3	18.3	12.0
5	15.1	12.0
7.5	11.2	9.25
9.9	11.5	9.56
15	11.1	8.31
20	9.50	5.93
30	6.34	3.88
50	4.54	2.55
75	3.50	1.42
100	2.61	0.88

Table 54
Cross sections for elastic scattering of electrons in CO. Numbers in parentheses are powers of ten multiplying each cross section. Units are 10^{-16} cm^2/sr. (From DuBois and Rudd 1976, ref. [143].)

	E_0(eV)		
θ(deg)	200	500	800
3	2.01(1)	1.52(1)	–
4	1.60(1)	1.28(1)	9.52
5	1.41(1)	1.03(1)	7.31
6	1.22(1)	8.54	5.96
8	9.07	5.66	3.72
10	6.66	3.81	2.08
12	4.90	2.50	1.27
15	3.05	1.34	7.06(−1)
20	1.36	6.10(−1)	4.17(−1)
25	6.55(−1)	3.89(−1)	2.64(−1)
30	3.72(−1)	2.72(−1)	1.48(−1)
35	2.53(−1)	1.84(−1)	8.23(−2)
40	2.01(−1)	1.17(−1)	5.49(−2)
45	1.60(−1)	7.70(−2)	–
50	1.33(−1)	5.49(−2)	3.33(−2)
60	9.07(−2)	3.89(−2)	1.82(−2)
70	6.22(−2)	2.73(−2)	1.25(−2)
80	4.76(−2)	1.90(−2)	8.99(−3)
90	4.51(−2)	1.53(−2)	6.36(−3)
100	4.62(−2)	1.31(−2)	5.38(−3)
110	4.90(−2)	1.12(−2)	4.45(−3)
120	5.15(−2)	9.63(−3)	3.92(−3)
130	5.21(−2)	8.93(−3)	3.44(−3)
140	5.35(−2)	8.40(−3)	3.14(−3)
150	5.63(−2)	8.37(−3)	3.05(−3)

Table 55
Elastic differential cross sections in CO at 300, 400 and 500 eV. Units are 10^{-16} cm^2/sr. (From Bromberg 1970, ref. [146].)

	Energy (eV)		
θ(deg)	300	400	500
2	23.7	21.4	19.5
2.5	20.7	18.4	17.7
3	19.1	17.2	16.2
3.5	17.3	15.4	14.9
4	16.0	14.4	13.7
5	13.6	12.2	11.4
6	11.5	10.3	9.62
7	9.85	8.64	7.94
8	6.55	7.30	6.55
9	5.33	6.10	5.33
10	4.34	5.05	4.34
12	2.83	3.43	2.83
14	1.83	2.29	1.83
16	1.22	1.54	1.22
18	0.848	1.06	0.848
20	0.624	0.764	0.624
25	0.395	0.426	0.395
30	0.285	0.301	0.285
35	0.199	0.224	0.199
40	0.126	0.162	0.126
45	0.0846	0.115	0.0846
50	0.0591	0.0804	0.0591
55	0.0473	0.0588	0.0473
60	0.0409	0.0476	0.0409
65	0.0350	0.0412	0.0350
70	0.0291	0.0378	0.0291
80	0.0193	0.0288	0.0193
90	0.0148	0.0213	0.0148
100	0.0132	0.0168	0.0132
110	0.0106	0.0154	0.0106

Table 56
Momentum transfer cross sections for CO, $10^{-16}\,cm^2$ units.
(From Land 1978, ref. [207].)

E_0(eV)	σ^M	E_0(eV)	σ^M	E_0(eV)	σ^M
0.0	60.0	0.25	11.2	3.3	14.6
0.0010	40.0	0.30	12.1	3.6	14.2
0.0020	25.0	0.35	13.0	4.0	13.8
0.0030	17.7	0.40	13.8	4.5	13.3
0.0050	12.3	0.50	15.4	5.0	12.9
0.0070	9.8	0.70	16.5	6.0	12.3
0.0085	8.6	1.00	18.5	7.0	11.8
0.0100	7.8	1.2	28.0	8.0	11.3
0.015	6.5	1.3	37.0	10.0	10.6
0.020	5.9	1.5	42.0	12.0	10.4
0.030	5.4	1.7	40.0	15.0	10.2
0.040	5.2	1.9	32.0	17.0	10.1
0.050	5.4	2.1	23.5	20.0	9.8
0.070	6.1	2.2	21.5	25.0	9.1
0.100	7.3	2.5	17.5	30.0	8.6
0.15	8.8	2.8	16.0	50.0	7.1
0.20	10.0	3.0	15.4	75.0	6.1
				100.0	5.5

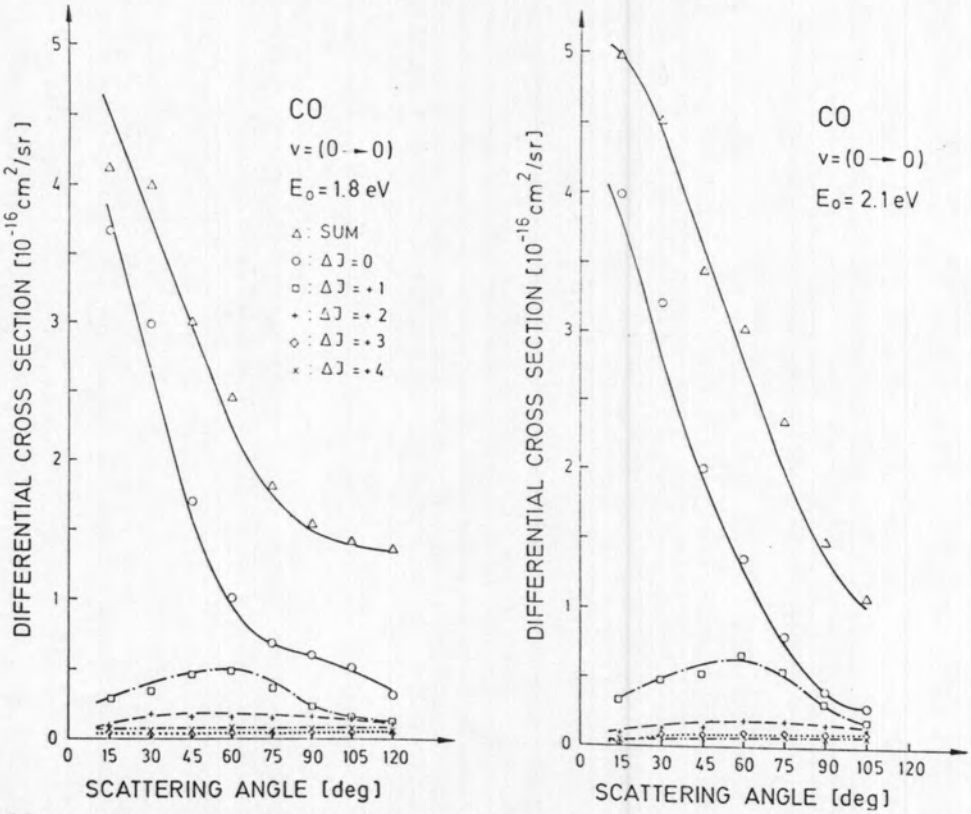

Fig. 43. Differential cross sections for pure rotational excitation in CO ($\Delta v = 0$, $\Delta J = 0, +1, +2, +3, +4$) at 1.8 eV (left) and 2.1 eV (right) in the vicinity of the $^2\Pi$ resonance. (From ref. [154].)

reported by Truhlar et al. [206], but these data were obtained by normalization to a calculated absolute cross section. Truhlar et al. [145b] report an integral elastic cross section for CO of 9.86×10^{-16} cm^2 at 20 eV. Land [207] obtained momentum transfer cross sections from swarm data. See table 56 for his results.

Rotational excitation cross sections

As in N_2, rotational excitation cross sections for CO have been unfolded from energy-loss spectra, obtained at high resolution (10–18 meV, FWHM), in terms of individual $\Delta J = 0, +1, +2, +3, +4$ transitions. Results of Jung et al. [154] are given in fig. 43 for vibrationally elastic ($v = 0 \rightarrow 0$) excitation at energies of 1.8 and 2.1 eV. Results for the vibrationally inelastic excitation $v = 0 \rightarrow 1$ are given in fig. 44 at 1.8 eV electron energy. The summed cross sections in all cases provide an extension of elastic scattering data to these lower energies, as well as of the vibrational ($v = 0 \rightarrow 1$) excitation cross section (see next section).

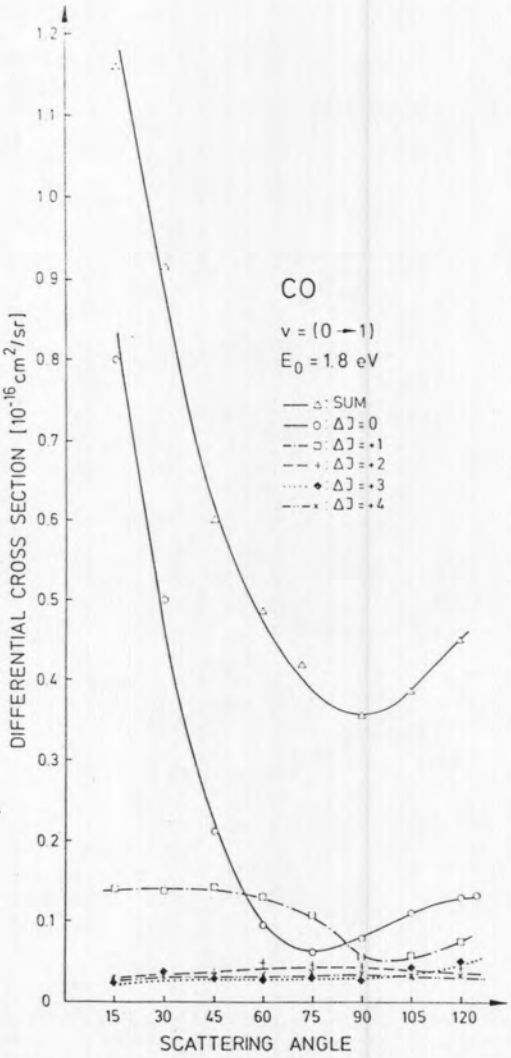

Fig. 44. Differential cross sections for vibrational-rotational excitation ($\Delta v = 1$, $\Delta J = 0, +1, +2, +3, +4$) in CO at 1.8 eV in the vicinity of the $^2\Pi$ resonance. (From ref. [154].)

Vibrational excitation cross sections

A. The $^2\Pi$ shape-resonance region (1–5 eV)

Vibrational excitation in the energy range 1–5 eV is influenced by the $^2\Pi$ shape resonance. Vibrational excitation in this range has been studied by Boness and Schulz [208], Chutjian and Tanaka [163], and Jung et al. [154], and earlier data reviewed by Schulz [209]. Cross sections have been reported by Ehrhardt et al. [88] for excitation of the levels $v = 1$–7 in the energy range from threshold to 4 eV, and these results are presented in fig. 45. See also ref. [5] for digitized data. Cross sections for excitation of $v = 1$ at 1.8 eV have been reported by Jung et al., and given in fig. 44. Cross sections have been given at 3 and 5 eV [163], and are summarized in tables 57 and 58 for differential and integrated results, respectively. Land [207] has given a set of cross sections (fig. 46) based on an extension of electron-transport coefficient data to high (3.0 eV) energies. Such a swarm analysis, if it can be made to these higher energies, is useful. However, the results of Land should be used with some caution, as discussed in ref. [163].

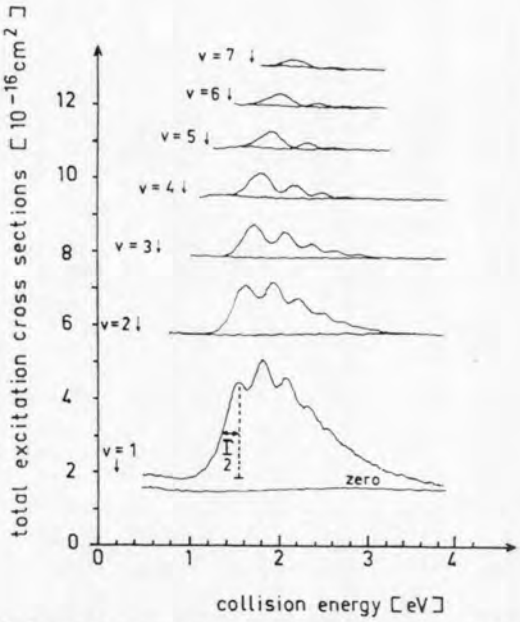

Fig. 45. Integral cross sections for excitation of levels $v = 1$–7 in CO in the energy range 0.5–4.0 eV. Vibrational thresholds are shown by arrows. The half-width $\Gamma/2$ of the resonance state is indicated. (From ref. [88].)

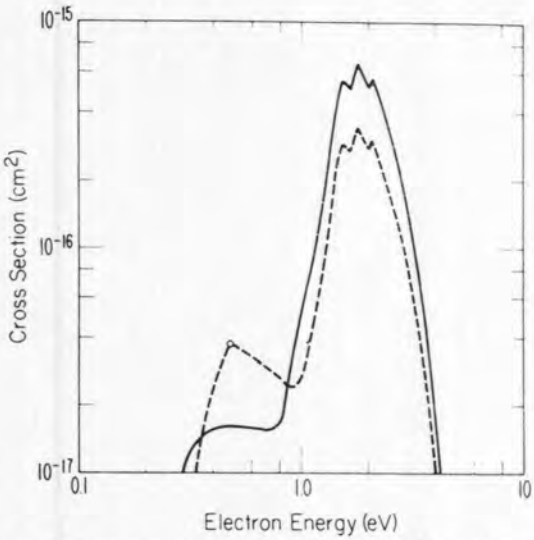

Fig. 46. Cross section for excitation of $v = 1$ in CO as a function of electron energy. Solid curve represents swarm analysis of ref. [207], while dashed curve is from Y. Singh [J. Phys. B 3 (1979) 1222]. (From ref. [207].)

B. Nonresonance and broad Σ shape-resonance regions (5–100 eV)

Cross sections in the energy range 5–100 eV for CO include estimates of Comer and Read [210], Truhlar et al. [145b] and results of Chutjian et al. [211], and Chutjian and Tanaka [163]. Angular distributions relative to $\theta = 90°$ scattering are given by Tronc et al. [212] in the Σ shape-resonance region 16–23 eV, and can provide a useful comparison to the shape as given by the relative-flow method [163]. Differential cross sections for the $v = 0 \rightarrow 1$ excitations using the relative-flow method are given in table 57 at energies between 9 and 100 eV. Integral and momentum-transfer data are summarized in table 58. One notes the prominent peak in the integrated cross sections near 20 eV due to the Σ shape resonance in CO. This effect is analogous to that of the Σ_u resonance in N_2 discussed in section 4.2.

Table 57
Differential cross sections for $v = 0 \rightarrow 1$ vibrational excitation in CO. Units are 10^{-19} cm²/sr. Entries by angles in parentheses refer to extrapolated values. (From Chutjian and Tanaka 1980, ref. [163].)[a]

	E_0(eV)							
θ(deg)	3.0	5.0	9.0	20.0	30.0	50.0	75.0	100.0
(0)	87	51	38	26	6.9	5.8	3.7	4.4
(5)	85	49	28	22	5.6	4.1	2.7	3.2
(10)	81	46	19	18	4.6	3.0	1.9	2.0
15	75.1	42.7	9.15	14.4	3.09	1.30	1.31	1.2
20	72.0	37.0	4.83	11.6	2.03	0.661	0.829	0.956
25	58.6	26.8	3.35	9.37	1.48	0.428	0.767	0.656
30	50.3	17.2	2.11	8.10	1.21	0.364	0.878	1.07
35	43.6	12.7	1.88	8.32	1.14	0.489	0.808	0.986
40	40.5	10.1	1.75	8.10	1.01	0.476	0.799	0.941
50	34.5	6.53	1.59	7.85	1.13	0.499	0.527	0.692
60	30.4	5.40	1.62	7.92	1.23	0.477	0.385	0.420
70	30.9	5.73	1.43	7.38	1.57	0.437	0.327	0.294
80	28.1	5.30	1.29	6.79	1.60	0.412	0.319	0.235
90	25.1	4.67	1.04	6.52	1.57	0.435	0.277	0.281
100	20.6	4.14	0.913	6.03	1.42	0.476	0.256	0.361
110	16.8	3.89	0.866	6.73	1.34	0.496	0.242	0.413
120	17.9	4.37	0.886	7.26	1.62	0.528	0.281	0.497
130	19.9	5.66	1.47	7.80	1.93	0.633	0.323	0.547
(140)	22	8.6	2.1	8.7	2.2	0.78	0.36	0.59
(150)	25	11	2.7	9.0	2.4	0.97	0.38	0.63
(160)	28	14	3.2	9.4	2.6	1.1	0.40	0.66
(170)	30	16	3.6	9.8	2.8	1.3	0.41	0.68
(180)	31	17	4.0	10	2.9	1.4	0.42	0.71

[a] Numbers in this table differ slightly from those of the tabulation of ref. [163] due to small changes in the He elastic cross sections at the time of publication of ref. [10].

Table 58
Integral (σ) and momentum-transfer (σ^M) cross sections for $v = 0 \rightarrow 1$ vibrational excitation in CO. Units are 10^{-18} cm². (From Chutjian and Tanaka 1980, ref. [163].)

E_0(eV)	σ	σ^M
3	36.6	29.7
5	10.5	8.58
9	2.43	2.00
20	9.80	9.56
30	2.09	2.23
50	0.756	0.788
75	0.533	0.416
100	0.683	0.601

Electronic excitation cross sections

The depth of coverage of inelastic, electronic excitations in CO by optical emission, metastable excitation function, and electron energy-loss spectroscopy, does not approach that in N_2. There is a very clear need to carry out high-resolution electron energy-loss studies (resolution of the order 35 meV, FWHM or better) of the many overlapping electronic excitations in order to fill this gap.

Electron-excited optical emission cross sections have been reported by Aarts and de Heer [213] for the $A^1\Pi \rightarrow X^1\Sigma^+$ (4th positive), and the $B^1\Sigma^+ \rightarrow X^1\Sigma^+$ and $C^1\Sigma^+ \rightarrow X^1\Sigma^+$ (Hopfield–Birge) systems. Relative emission cross sections were normalized to the absolute scale by use of the generalized oscillator strength measurements of Lassettre et al. [214] for bands in the A, B and C-states. Mumma et al. [215] and Ajello [216] have reported absolute emission cross sections in the $A \rightarrow X$ system from threshold to several hundred eV. There is good agreement in cross sections between the work of Mumma et al. (7.5×10^{-19} cm^2) and Aarts and de Heer (6.59×10^{-19} cm^2) for excitation of the (0, 1) band at 300 eV. One may refer to fig. 5 of ref. [215] for comparison in the range of energies from threshold to 1000 eV. Cross sections for excitation of levels $v = 0 \rightarrow 4$ of the A-state are given in fig. 4 of ref. [215] and the total emission cross section from the work of Ajello is given in fig. 10 of ref. [216].

Some results have been reported by Wells et al. [217] on excitation of a 10 eV metastable CO state and cross sections are given in fig. 47. The metastable state(s) involved would appear to be either or both the $D^1\Delta$ and $I^1\Sigma^-$ states of CO.

A summary of the relevant optical excitation-function measurements discussed above is given in table 59.

The intensity distribution (relative) in the $X \rightarrow A$ system has been studied by electron energy-loss

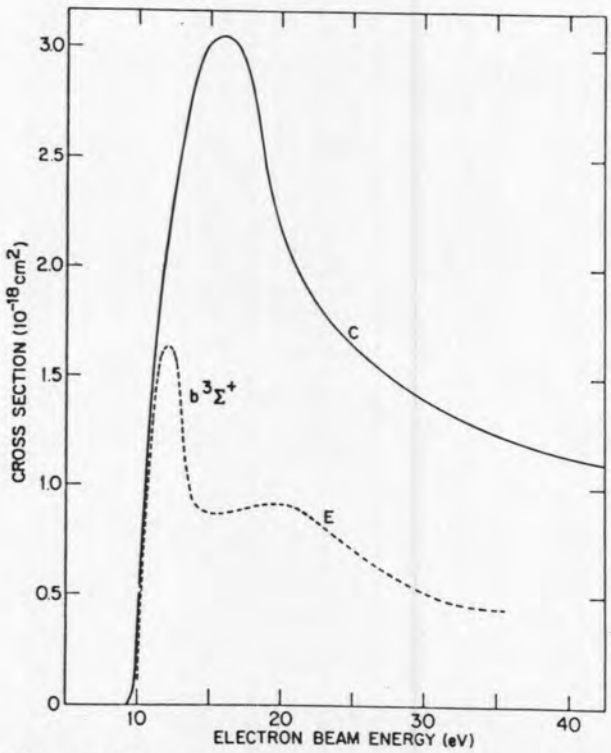

Fig. 47. Cross section for excitation of a CO metastable state (very likely either $D^1\Delta$ or $I^1\Sigma^-$) in the energy range threshold to 42 eV (solid curve C) from ref. [217]. Dashed curve E is from results of Skubenich [Opt. Spectrosc. 23 (1967) 540] for the $b^3\Sigma^+$ state. (From ref. [217].)

Table 59
Summary of excitation function measurements in CO

State	Energy range (eV)[a]	Reference
$A^1\Pi$ (4th positive)	100–5000	Aarts–de Heer 1970, ref. [213]
	T–350	Mumma–Stone–Zipf 1971, ref. [215]
	T–300	Ajello 1971, ref. [216]
$a^3\Pi$ (Cameron)	T–300	Ajello 1971, ref. [216]
$B^1\Sigma^+$ (Hopfield–Birge)	100–5000	Aarts–de Heer 1970, ref. [213]
$C^1\Sigma^+$ (Hopfield–Birge)	100–2000	Aarts–de Heer 1970, ref. [213]
CO^m (unknown metastable state, $D^1\Delta$ or $I^1\Sigma^-$ (?))	T–45	Wells–Borst–Zipf 1973, ref. [217]

[a]T means threshold.

spectroscopy at various incident electron energies and scattering angles by Lassettre and co-workers [214, 218]. Generalized oscillator strengths (GOS) as a function of momentum transfer have been reported by Lassettre and Skerbele [198] for the $v = 2$ level of the $A^1\Pi$ state at energies of 300, 400 and 500 eV. Using Franck–Condon factors and the relationship between the GOS and differential cross section (see, for example, eq. (4) of ref. [198]), one can obtain cross sections at these higher energies. An extensive tabulation of the GOS versus momentum transfer and θ for the $X \rightarrow B^1\Sigma^+$ is also given by Skerbele and Lassettre [219] (see their table I). These GOS's may also be converted to differential cross sections for low angle scattering. At the high energies, one may have at least an approximation to the integral cross section for the A and B states by conversion to differential cross sections and integration of the low-angle data.

Land [207] deduced excitation cross sections for electronic states of CO which are consistent with transport measurements. These cross sections are shown in fig. 48.

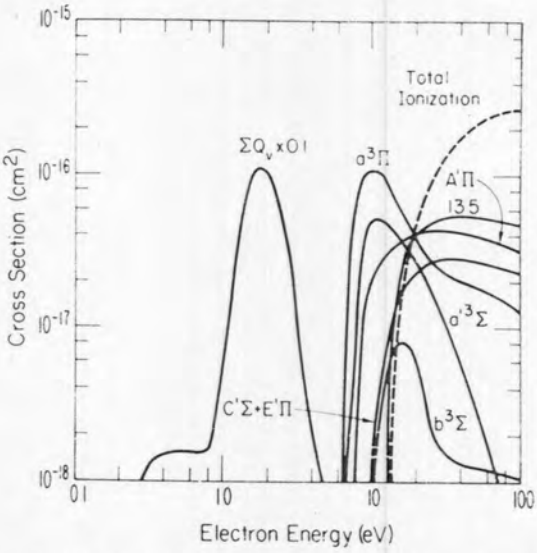

Fig. 48. Combined cross sections for vibrational and electronic excitation, and total ionization in CO. (From ref. [207].)

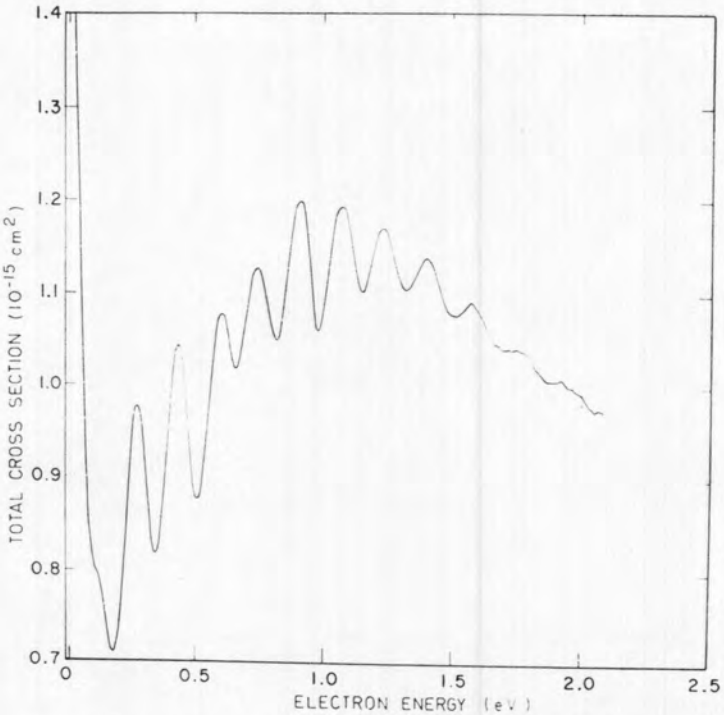

Fig. 49. Total scattering cross sections in NO. (From ref. [220].)

4.5. NO

Total electron collision cross sections for NO have been studied by Zecca et al. [220] at low impact energies where resonances dominate the cross sections. Their normalized data are shown in fig. 49. Dalba et al. [139] measured total electron scattering cross sections in the 100 to 1444 eV impact energy range (see table 60). The NO cross sections are similar to N_2 and O_2 over the whole energy range. Kubo et al. [221] reported elastic differential, integral and momentum transfer cross sections in the 3 to 30 eV impact energy range. The 5, 10 and 20 eV differential cross sections obtained by them are shown in fig. 50.

Optical excitation functions and/or emission cross section measurements are summarized in table 61.

Table 60
Total electron scattering cross sections for NO, a_0^2 units. (From Dalba et al. 1980, ref. [139].)

E_0(eV)	Q_{TOT}	E_0(eV)	Q_{TOT}
121	30.25	484	13.51
144	29.34	576	12.04
169	25.81	676	10.33
196	23.99	784	9.47
225	21.77	900	8.35
256	20.81	1024	7.57
289	18.89	1156	6.88
324	18.22	1296	6.03
400	15.19	1444	5.63

Table 61
Summary of emission cross section measurements for NO

Radiation process	Impact energy (eV)[a]	Reference	Note
$B^9\,^2\Delta_i \rightarrow X^1\Pi_r$	T–300	222	Absolute
$A^2\Sigma^+ \rightarrow X^2\Pi$	300	223	Absolute
$A^2\Sigma^+ \rightarrow X^2\Pi$	T–300	224	Relative
$A^2\Sigma^+ \rightarrow X^2\Pi$	T–300	225	Relative

[a] T means threshold.

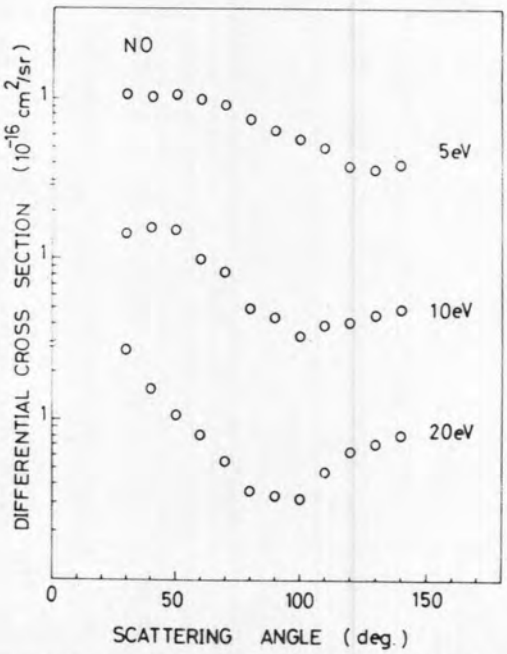

Fig. 50. Differential elastic scattering cross sections in NO at 5, 10 and 20 eV impact energies. (From ref. [221].)

4.6. HX (X = F, Cl, Br, I)

Electron interactions with hydrogen halides have been extensively investigated partly because of their important role in various lasers and partly because of the pronounced low-energy resonances associated with dissociative attachment and vibrational excitation of these molecules. A survey on near threshold vibrational excitation was given by Rohr [226]. The peak cross section values associated with the sharp threshold resonance and the broader shape resonance at slightly higher impact energies are summarized in table 62.

Rohr and Linder [227] studied vibrational excitation of HF by beam–beam scattering and deduced approximate cross sections by comparing scattering intensities from HF and HCl beams operated under the same conditions. Figs. 51–55 show their results.

Rohr and Linder [227, 228] and Ziesel et al. [229] measured vibrational excitation cross sections for HCl in the near threshold region. Ziesel et al. used the trapped electron method and obtained a value between 2.5×10^{-16} and 1.2×10^{-15} cm^2 for the $v = 0 \rightarrow 1$ vibrational excitation near threshold. The value depends on the choice of dissociative attachment cross section to which they normalize the vibrational excitation cross section. Rohr and Linder measured relative differential cross section by a beam–beam

Table 62
Peak cross sections for the $v = 0 \rightarrow 1$ vibrational excitation, 10^{-16} cm^2 units. (From Rohr 1979, ref. [226].)

Molecule	Near threshold region	Shape resonance region
HF	7	1
HCl	20	3
HBr	40	27

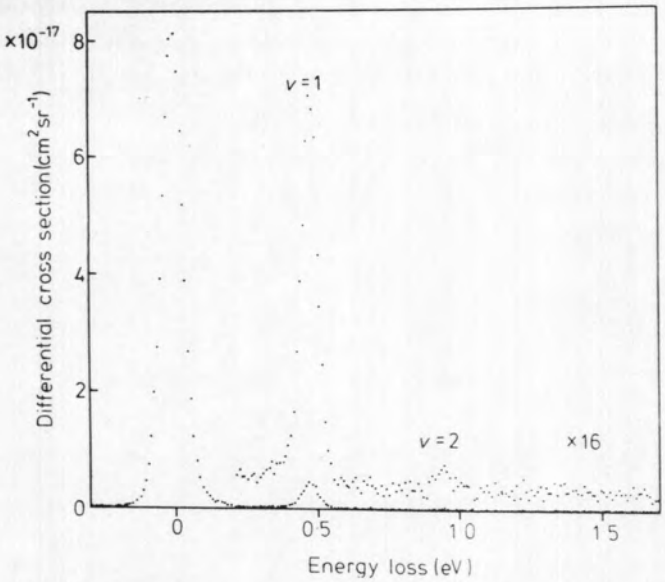

Fig. 51. Energy-loss spectrum of HF given in terms of differential cross section for elastic scattering and vibrational excitation at 2 eV impact energy and 80° scattering angle. (From ref. [227].)

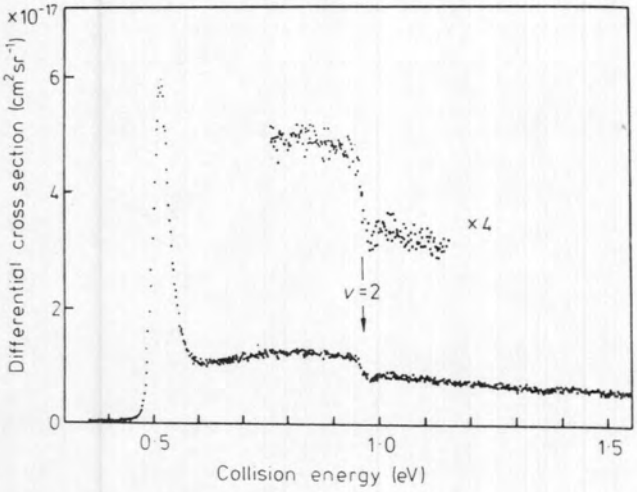

Fig. 52. Differential excitation function for $v = 0 \rightarrow 1$ excitation in HF at a scattering angle of 60°. (From ref. [227].)

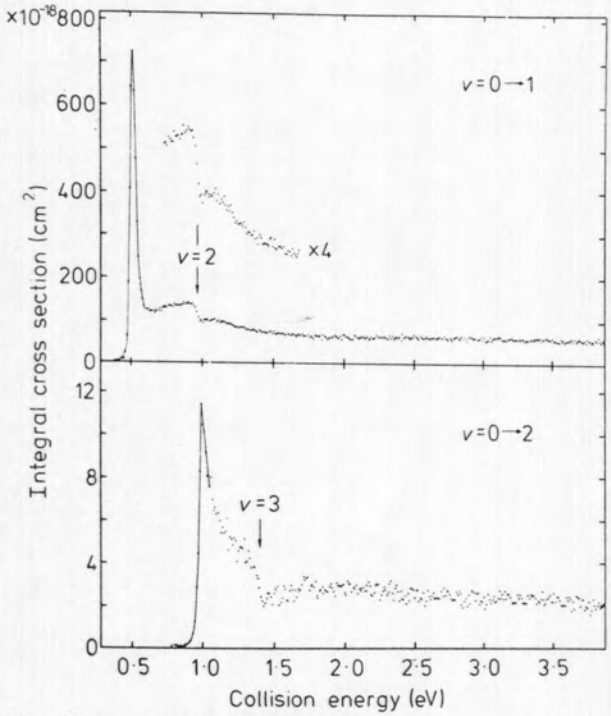

Fig. 53. Integral excitation functions for $v = 0 \rightarrow 1$ and $v = 0 \rightarrow 2$ vibrational excitation in HF. (From ref. [227].)

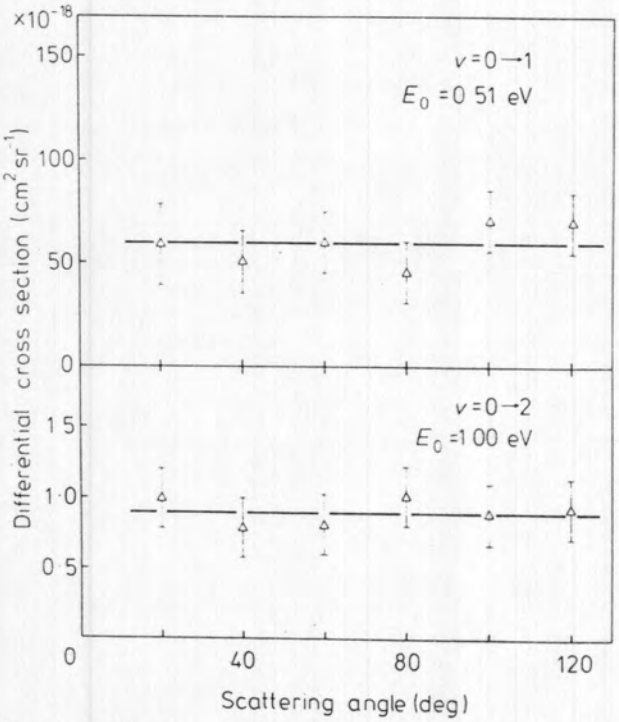

Fig. 54. Angular dependence of the $v = 0 \rightarrow 1$ and $v = 0 \rightarrow 2$ vibrational excitations in HF at 0.51 and 1.00 eV impact energies, respectively. (From ref. [227].)

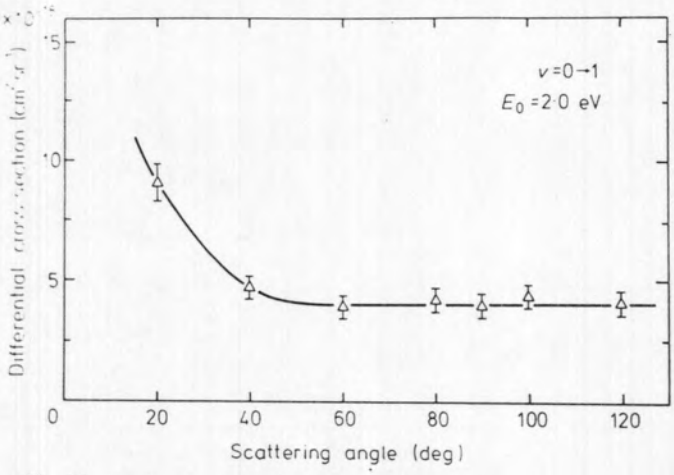

Fig. 55. Angular dependence of the $v = 0 \rightarrow 1$ vibrational excitation in HF at 2 eV impact energy. (From ref. [227].)

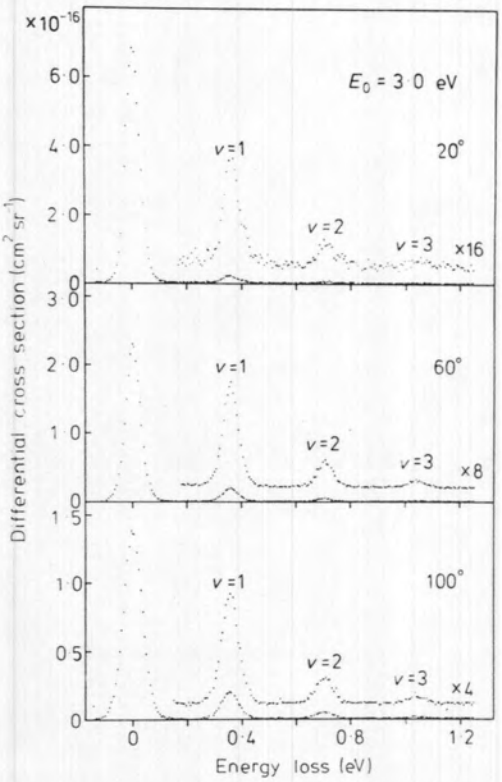

Fig. 56. Energy-loss spectra of HCl in terms of differential cross sections at 3 eV impact energy and 20°, 60° and 100° scattering angles. (From ref. [227].)

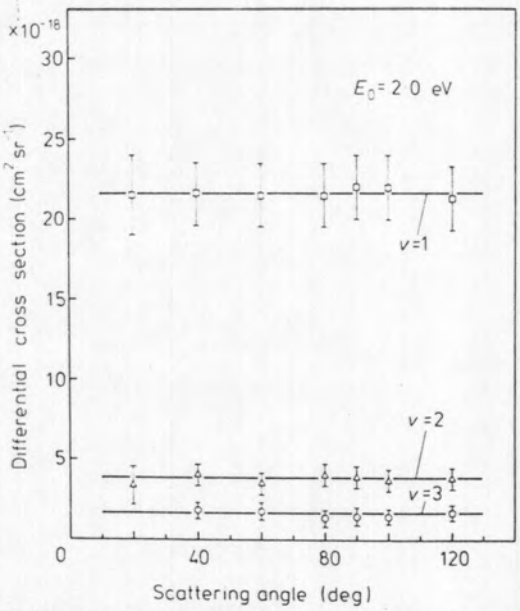

Fig. 57. Angular dependence of the $v = 0 \rightarrow 1$, 2 and 3 vibrational excitation cross sections in HCl at 3 eV impact energy. (From ref. [227].)

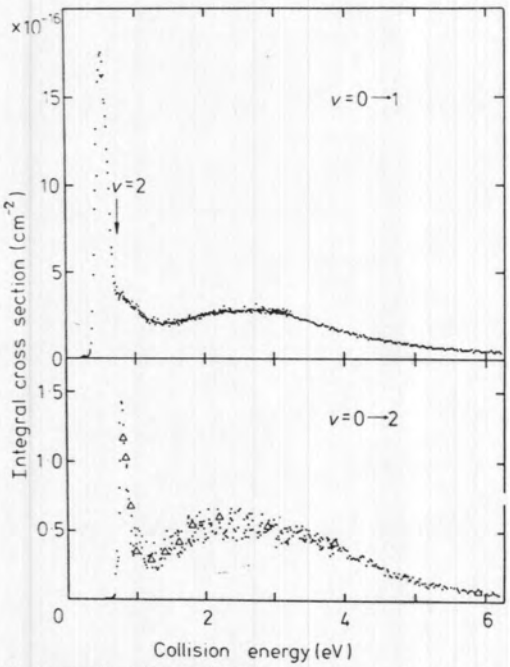

Fig. 58. Integral excitation functions for the $v = 0 \rightarrow 1$ and $v = 0 \rightarrow 2$ vibrational excitations in HCl. (From ref. [227].)

scattering technique and normalized the integrated cross sections to the total cross sections of Bruche [230]. These two measurements are consistent with each other and with rate constants determined by Caledonia and Center [231] who recommend the value 1×10^{-15} cm^2 for the peak cross section for the $v = 0 \rightarrow 1$ vibrational excitation near threshold. Cross sections measured by Rohr and Linder [227] are shown in figs. 56–58.

HBr was studied by Rohr [232]. He measured differential elastic scattering (0.2 to 10 eV) and vibrational excitation cross sections (threshold to 7 eV) in the 20° to 120° angular range. The elastic differential cross sections are shown in figs. 59 and 60. Integration yielded elastic cross sections of

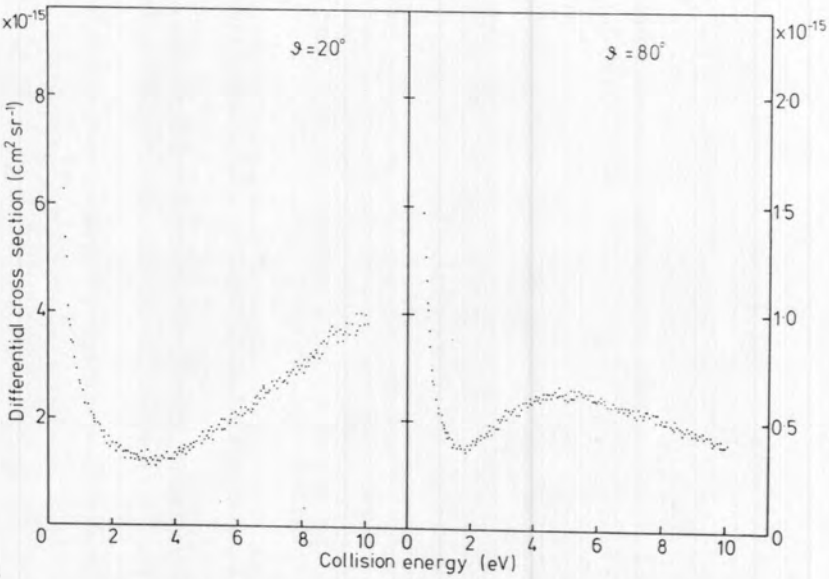

Fig. 59. Energy dependences of elastic differential scattering cross sections in HBr at 20° and 80° scattering angles. (From ref. [232].)

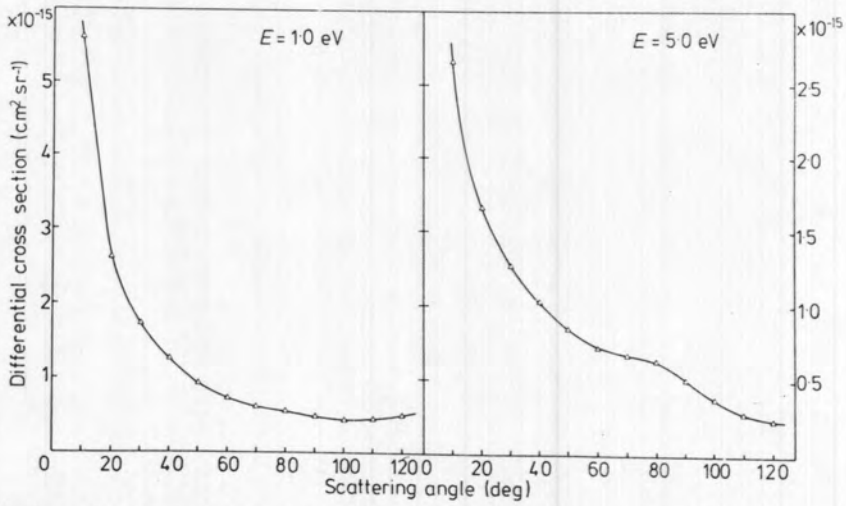

Fig. 60. Angular dependences of elastic scattering cross sections in HBr at 1.0 and 5.0 eV impact energies. (From ref. [232].)

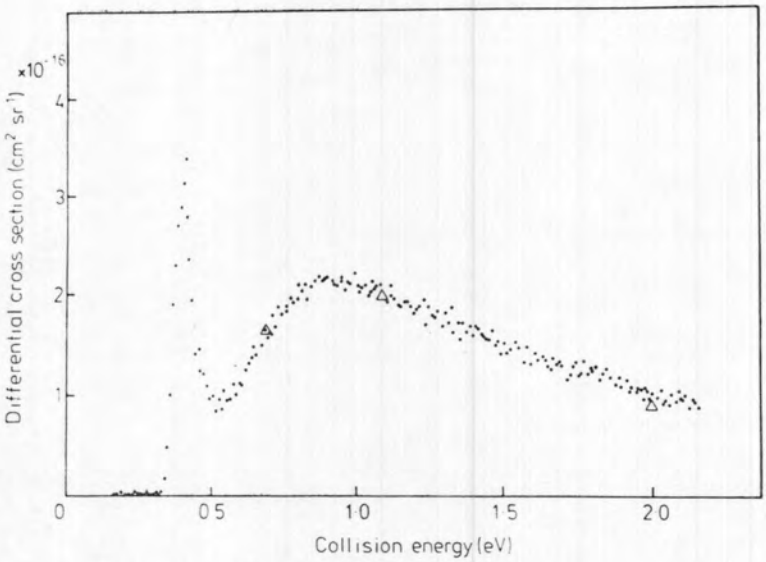

Fig. 61. Differential excitation function for the $v = 0 \rightarrow 1$ in HBr at 100° scattering angle. Triangles represent control measurements. (From ref. [232].)

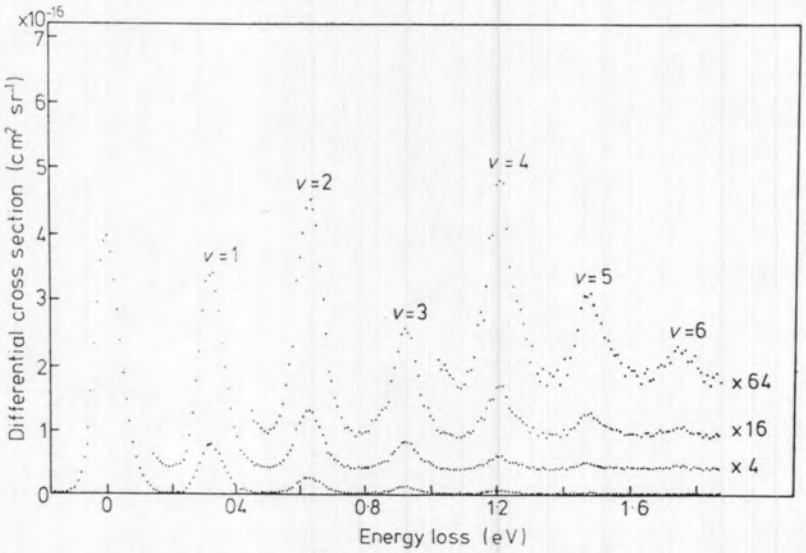

Fig. 62. Energy-loss spectrum of HBr in terms of differential cross sections at 2 eV impact energy and 80° scattering angle. (From ref. [232].)

1×10^{-14} and 7×10^{-15} cm^2 at 1 and 5 eV respectively. Vibrational excitation up to $v = 5$ could be measured because of the large cross sections. Results obtained by Rohr are shown in figs. 61–65.

No data are available on HI.

4.7. Alkali dimers

Total electron scattering cross sections for Na_2 and K_2 have been measured by Miller and Kasdan [233] in the 0.5 to 50 eV impact energy region by the molecular beam recoil technique. Their results are summarized in table 63. Recently, Miller et al. [234] measured total electron scattering cross section for Li_2 by the same technique in the 0.5 to 10 eV impact energy range. Their results are shown in fig. 66.

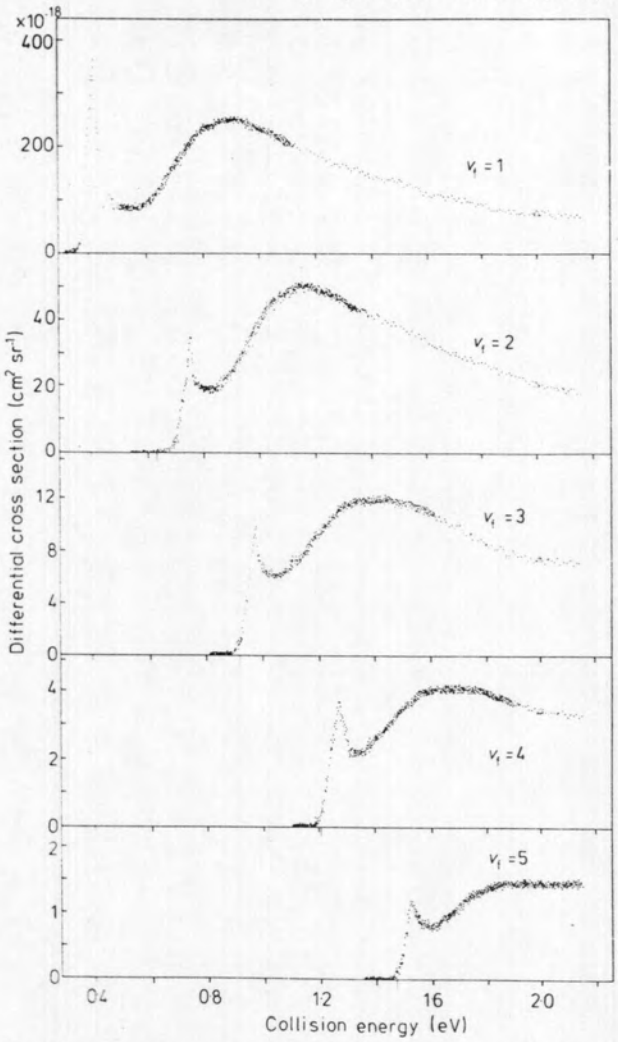

Fig. 63. Differential excitation functions for $v = 0 \rightarrow 1$, 2, 3, 4 and 5 vibrational excitations in HBr at 60° scattering angle. Triangles refer to normalization points. (From ref. [232].)

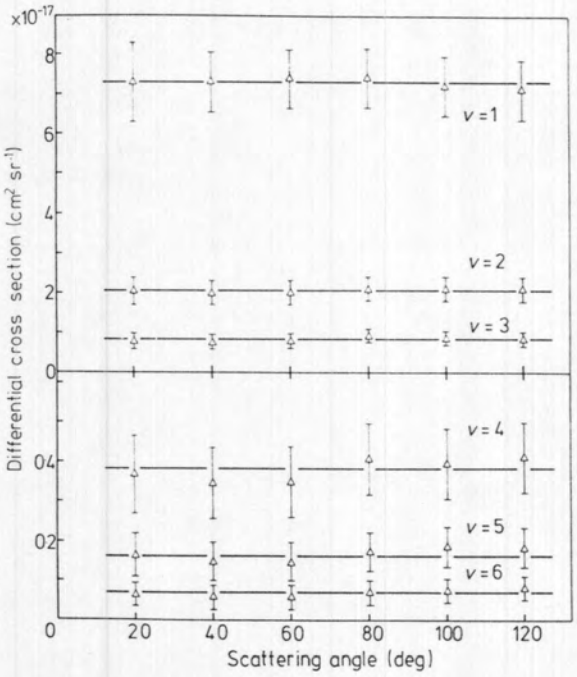

Fig. 64. Angular dependence of the $v = 0 \rightarrow 1$, 2, 3, 4, 5 and 6 vibrational excitation cross sections in HBr at 2 eV impact energy. (From ref. [232].)

Table 63
Total electron scattering cross sections, 10^{-16} cm^2 units. (From Miller and Kasdan 1973, ref. [233].)

E_0(eV)	Na_2	K_2
0.5	305	430
1	242	318
2	195	251
3	175	202
4	169	174
5	145	169
6	150	158
7	127	149
8	135	138
9	109	149
10	120	140
20	100	117
50	85	97

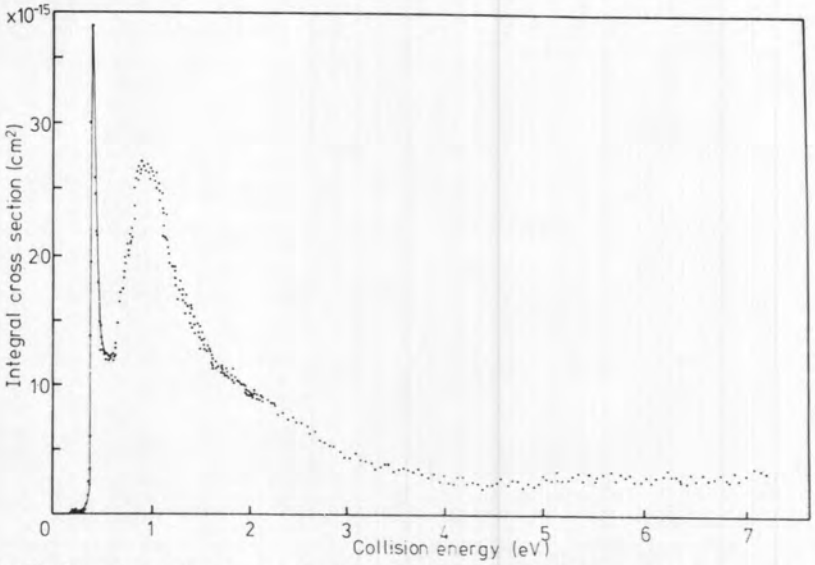

Fig. 65. Integral excitation function for the $v = 0 \rightarrow 1$ vibrational excitation in HBr. (From ref. [232].)

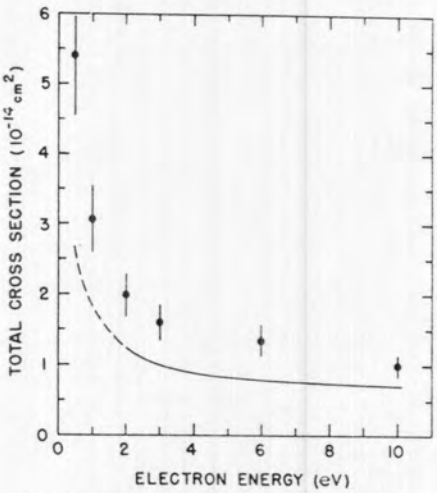

Fig. 66. Total electron scattering cross sections in Li_2 (dots with error bars). For comparison total scattering cross sections for Li are also shown (line). (From ref. [234].)

4.8. Alkali halide molecules

The alkali halide molecules possess very large dipole moments (~10 Debye), hence, represent a special class for electron–molecule scattering studies. The dominant interaction is that of the permanent dipole moment of the molecule and the electron. This interaction leads to very simple cross section formulas that depend only on the electron energy, dipole moment, and moment of inertia [235]. The most probable process in such collisions is the rotational excitation corresponding to $\Delta J = \pm 1$. Present day experimental techniques are not suitable to resolve the rotational structure in these excitation processes. Results of measurements are usually reported as "elastic" cross sections. This is done with the understanding that the cross section values include all $\Delta J = \pm 1$ as well as $\Delta J = 0$ (elastic) processes, and to a smaller degree $\Delta J \geq 2$ and unresolved vibrational excitation processes. Integral "elastic" cross sections of the order $10^{-14}\,cm^2$ and near zero degree differential cross sections of the order

$10^{-12}\,cm^2\,sr^{-1}$ have been reported. The differential cross sections are extremely forward peaking in character, and usually the differential cross sections in the zero to few degree scattering angle region represent over 90% of the integral cross sections.

A series of molecular-beam recoil measurements [236] have been carried by CsF [237, 238], CsCl [239] and KI [240]. These were the first absolute single-collision measurements on highly polar molecules and yielded cross sections which include the sum of elastic scattering and rotational, vibrational and electronic excitation. The impact energy ranged from 0.5 to 15 eV. The experimental differential cross sections were much more forward peaked than predicted by the first Born approximation. Measured integral and momentum transfer cross sections were about a factor of two smaller than theoretical results.

More recently, electron-beam/molecular-beam electron scattering measurements for KI [241], LiF [242] and CsCl [243] yielded relative differential "elastic" cross sections. Normalization of these cross

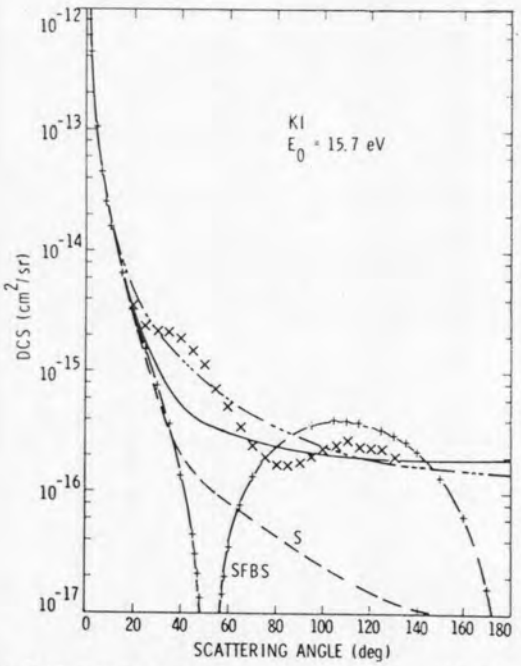

Fig. 67. Differential "elastic" cross sections for KI at 15.7 eV impact energy. The symbols and curves have the following meanings: ×, electron scattering results [241]; +, recoil results [240]; solid curve, theory [241]; dot-dash curve, Born point-dipole theory; dash-dash curve, Glauber theory [244]. (From ref. [241].)

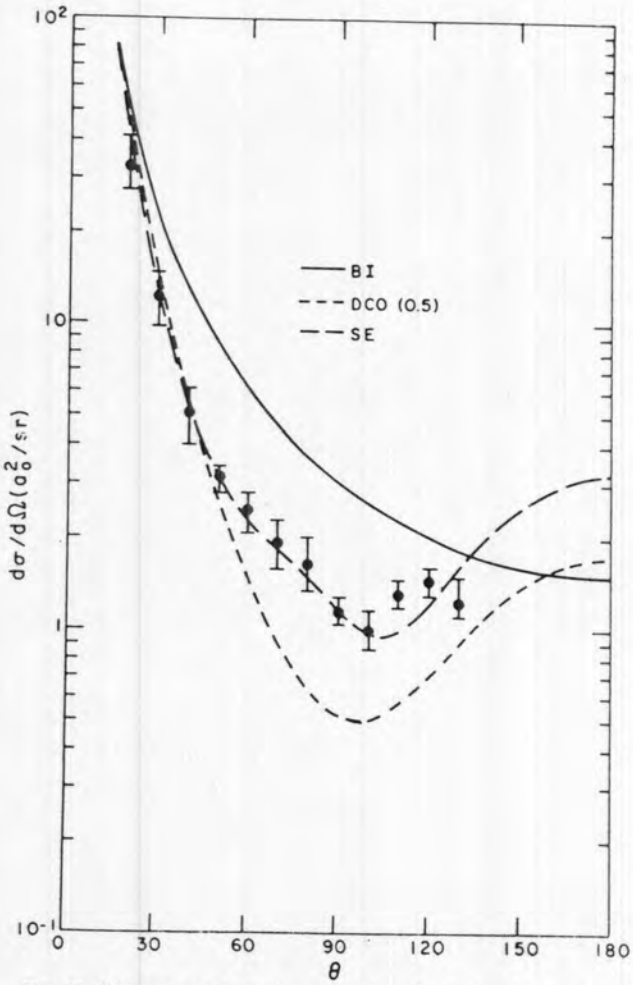

Fig. 68. Differential "elastic" cross sections for LiF at 20 eV impact energy. Experimental electron scattering results normalized to theory at 40° are indicated by dots and error bars. The theoretical results were obtained from the BI, DCO (0.5) and SE models of ref. [235] as indicated. (From ref. [235].)

sections was done to theory at low scattering angles. Deep minima in the DCS curves found by the recoil method in the 60°–90° angular region were not present in the electron scattering results.

Since there is a rather large uncertainty associated both with the analysis of the recoil data and with normalization of the beam scattering measurements, we do not reproduce the tabulation of the cross section data here. Fig. 67 shows a comparison of the KI cross sections obtained at 15.7 eV impact energy by the recoil and the electron scattering methods and by first order theories. Experimental and theoretical results for LiF are shown in fig. 68. For a more detailed discussion see ref. [235].

4.9. Other diatomic molecules

Fragmentary, qualitative data are available for some of the other diatomic molecules (halogens, rare gas excimers, metal halides). These results have been obtained by indirect procedures or empirical methods and are not surveyed here.

4.10. H_2O

Fragmentary data exist for water in terms of total (transmission) cross sections, and elastic, vibrational and electronic excitation cross sections.

Christophorou and Pittman [245] have reported a mean momentum transfer cross section of 3.04×10^{-13} cm^2 for e–H_2O interaction in a swarm measurement at 298 K (38.5 meV electron energy). Total cross sections for electron scattering in the energy range 0–7 eV have been reported by Sokolov and Sokolova [35a] in an apparatus which measured both the e–H_2O collision rate and electron energy distribution function under the same experimental conditions. These results are given in table 64.

Table 64
Total electron scattering cross sections for H_2O, 10^{-14} cm^2 units. (From Sokolov and Sokolova 1981, ref. [35a].)

E_0(eV)	σ_T	E_0(eV)	σ_T
0.01	30	1.0	0.6
0.02	20	2.0	0.3
0.04	15	3.0	0.2
0.06	11	4.0	0.14
0.08	8.0	5.0	0.12
0.10	6.0	6.0	0.11
0.50	1.5	7.0	0.10

Elastic differential scattering cross sections at 2.14 and 6.0 eV have been measured by Jung et al. [154]. These data were obtained by unfolding the elastic-scattering ($\Delta J = 0$) contribution from their high-resolution measurements of combined elastic and rotational ($\Delta J = \pm 1$) energy-loss spectra. These results are shown in fig. 69. At intermediate electron energies Nishimura [246] has reported elastic differential cross sections at 30 and 90 eV, and integral and momentum-transfer cross sections at 30, 50, 70 and 90 eV using the relative-flow method. These data are presented in fig. 70. At high energies,

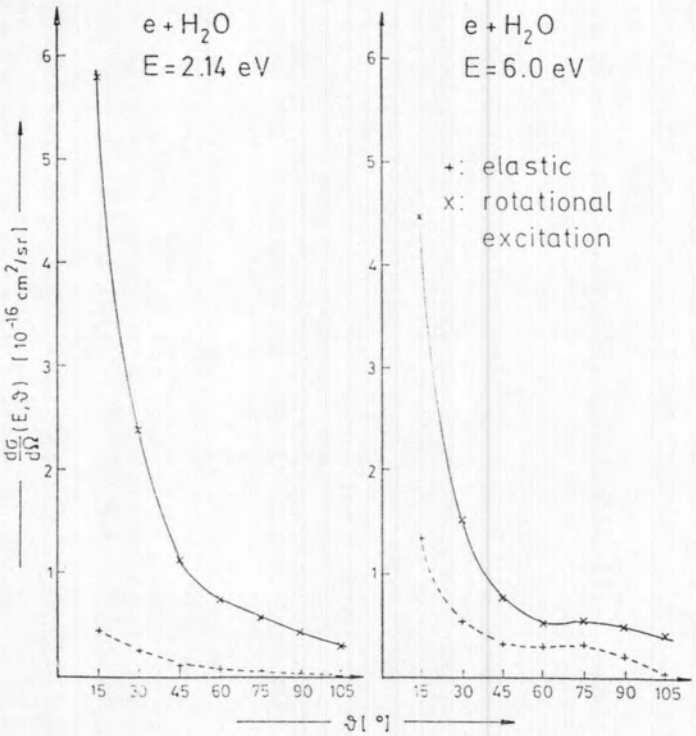

Fig. 69. Differential cross sections for elastic scattering and rotational excitation in H_2O at 2.14 and 6.0 eV impact energies. The full curve shows the sum of rotational excitation and de-excitation cross section and the dashed line represents pure elastic scattering. (From ref. [154].)

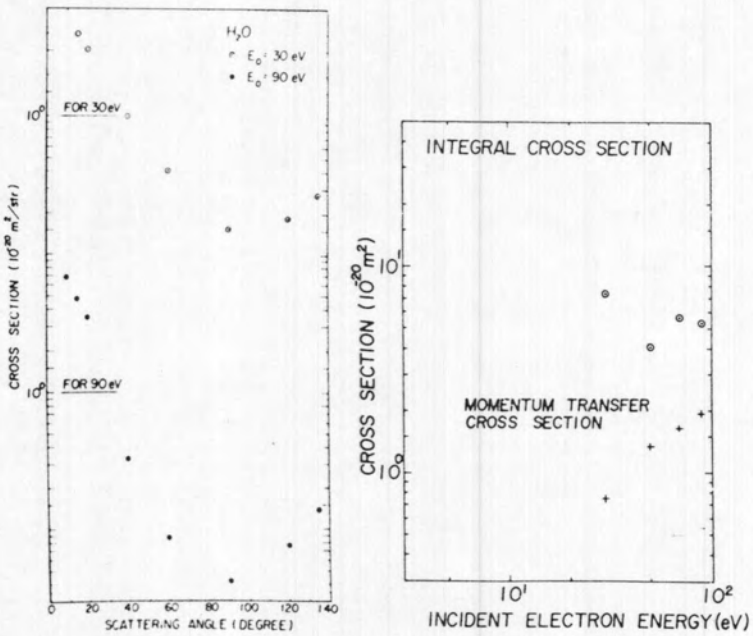

Fig. 70. Differential elastic scattering cross sections for H_2O at 30 and 90 eV impact energies (left figure) and integral and momentum transfer cross sections (right figure). (From ref. [246].)

Table 65
Elastic differential cross sections in H_2O at 500 and 516 eV. Units are 10^{-16} cm^2/sr. (From Lassettre and White 1974, ref. [247] and Bromberg [248].)

	500 eV		516 eV		500 eV		516 eV
θ(deg)	Ref. [247]	Ref. [248]	Ref. [247]	θ(deg)	Ref. [247]	Ref. [248]	Ref. [247]
4.0	6.69	6.80		15.5	–	–	0.826
4.5	6.05	6.06		16.0	0.806	0.791	–
5.0	5.35	5.46		16.5	–	–	0.714
5.5	4.76	4.91		17.5	–	–	0.619
6.0	4.37	4.49		18.0	0.596	–	–
6.5	4.06	–		20.0	0.448	0.446	–
7.0	3.72	3.72		22.5	–	–	0.336
7.5	3.33	–		25.0	0.255	0.254	–
8.0	3.11	3.11		27.5	–	–	0.209
8.5	2.86	–		30.0	0.162	0.161	–
9.0	2.63	2.60		32.5	–	–	0.134
10.0	2.20	2.18		37.0	0.0868	–	–
11.0	1.84	–		37.5			0.0888
12.0	1.55	1.51		42.5			0.0501
12.5	–	–	1.31	47.5			0.0468
13.0	1.30	–	–	52.5			0.0347
13.5	–	–	1.14	57.5			0.0286
14.0	1.09	1.09	–	62.5			0.023
14.5	–	–	0.972	67.5			0.019
15.0	0.927	–	–	77.5			0.014

shapes of elastic differential cross sections have been measured by Lassettre and White [247], and normalized to absolute measurements of Bromberg [248] at 500 eV. Results at 500 eV and 516 eV are given in table 65.

The sole piece of rotational-excitation data in the H_2O follows from the analysis of Jung et al. [154] described above. Differential cross sections for the combined $\Delta J = \pm 1$ branches at 2.14 and 6.0 eV are shown in fig. 69. One notes the rotational cross section to be much larger than the elastic scattering cross section at these low electron energies.

Vibrational excitation cross sections for the ν_2 bending mode (010) and the unresolved ν_1 symmetric stretch and ν_3 asymmetric stretch modes (100 and 001) have been measured by Seng and Linder [249] in the threshold to 10 eV impact energy range and by Rohr [250] in the threshold to 3.2 eV impact energy range. The 20° and 90° differential excitation functions, the differential cross sections, and the integral cross sections of Seng and Linder are shown in figs. 71, 72 and 73, respectively. The differential excitation function for the combined (100, 001) modes at $\theta = 120°$ obtained by Rohr is shown in fig. 74.

Cross section information on the electronic transitions in the H_2O is available only from the relatively high-electron energy, low-angle measurements of Lassettre and White [247], Lassettre and Skerbele [251], and Klump and Lassettre [252]. Generalized oscillator strengths (GOS) as a function of the square of momentum-transfer for the first, optically-allowed 7.4 eV feature ($X^1A_1 \rightarrow A^1B_1$) transition have been measured from 300 eV to 600 eV impact energies. If desired, these may be converted to differential and integral cross sections from the known relationship between the GOS and differential cross section. Absolute emission cross sections for radiation associated with excited OH, O and H fragments produced by electron impact on H_2O at impact energies ranging from threshold to 1000 eV have been measured by Beenakker et al. [253].

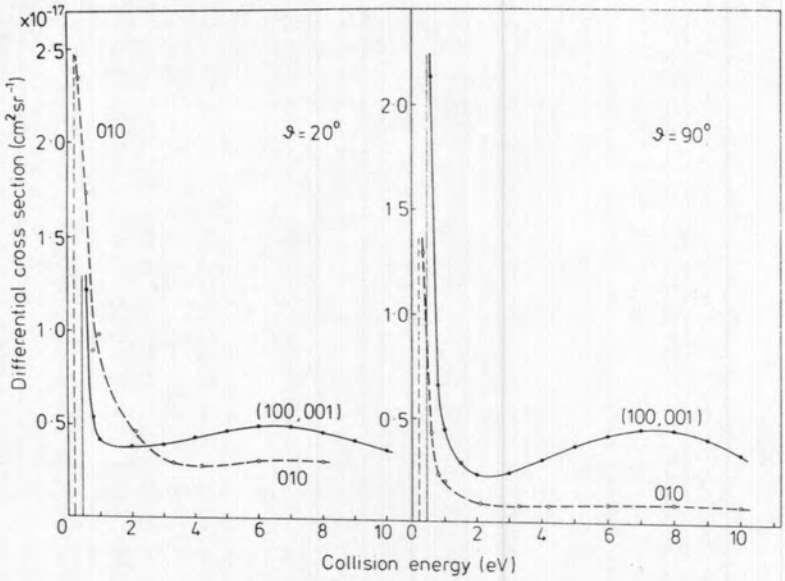

Fig. 71. Differential excitation functions for (100,001) and (010) vibrational excitations in H_2O at 20° and 90° scattering angles. (From ref. [249].)

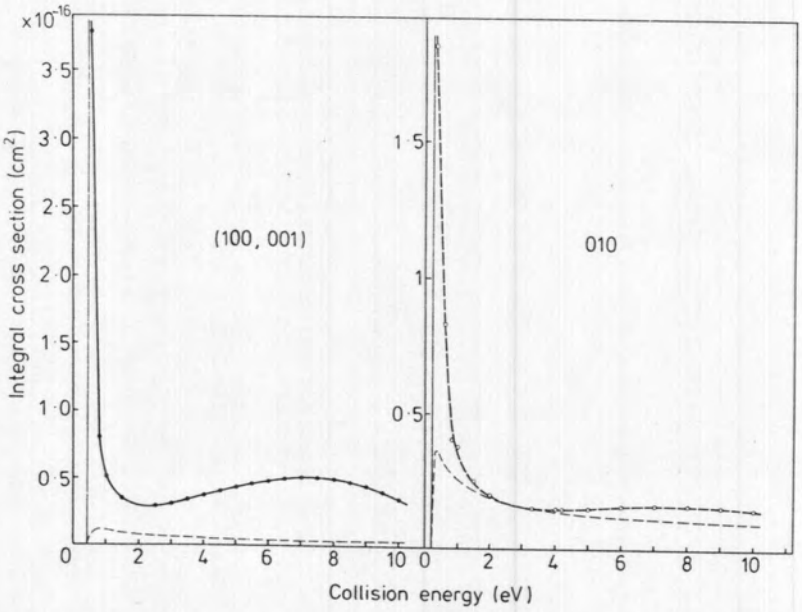

Fig. 72. Angular distributions for vibrational excitations in H_2O. Collision energies and vibrational modes are indicated. (From ref. [249].)

4.11. H_2S

Total electron scattering cross sections for H_2S have been measured by Sokolov and Sokolova [35a] in the 0 to 10 eV region. They applied an electron cyclotron resonance method to obtain the cross sections which are given in table 66. Zubek et al. [255] also reported total electron scattering cross sections at a recent conference.

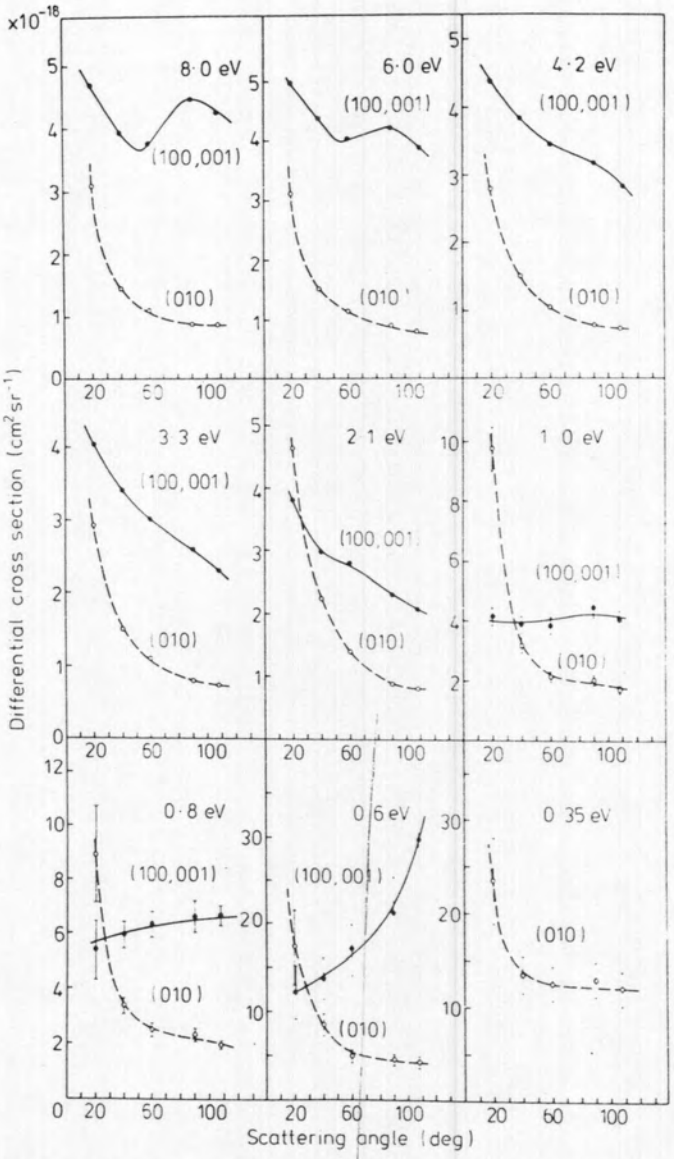

Fig. 73. Integral excitation functions for (100,001) and (010) vibrational excitation in H_2O. Born results of Itakawa [254] are given as broken curves for comparison. (From ref. [249].)

Table 66
Total electron scattering cross sections for H_2S, 10^{-16} cm^2 units. (From Sokolov and Sokolova 1982, ref. [35a].)

E_0(eV)	σ_T	E_0(eV)	σ_T
0.25	200	5.0	34
0.5	190	6.0	20
1.0	160	7.0	7.3
2.0	110	8.0	6.0
3.0	76	9.0	6.8
4.0	51	10.0	7.0

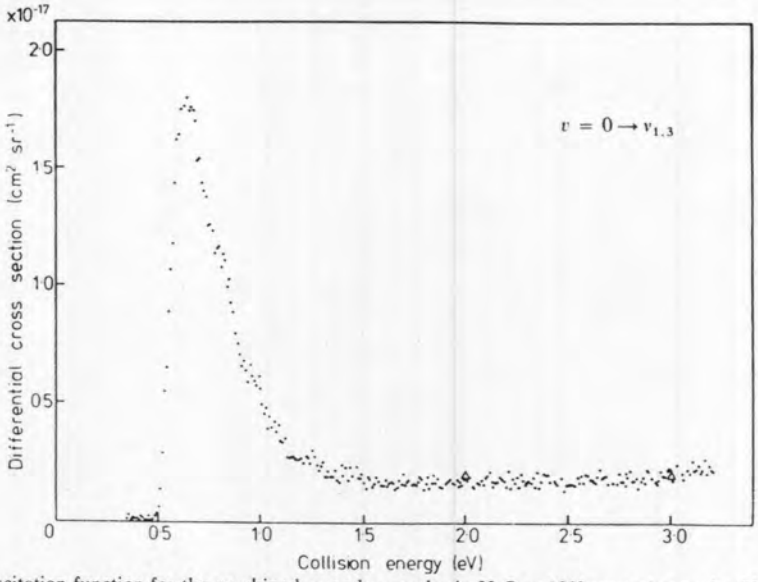

Fig. 74. Differential excitation function for the combined ν_1 and ν_3 modes in H_2O at 120° scattering angle. (From ref. [250].)

Vibrationally elastic scattering and vibrational excitation cross sections for H_2S have been measured by Rohr [256] in the near threshold to 10 eV region. The differential cross sections for elastic scattering are strongly forward peaked and show increasing values towards small energies. The vibrational excitation is dominated by resonance processes. Figures 75–79 show the results of ref. [256].

4.12. HCN

Measurements of elastic scattering cross sections have been carried out on HCN because of interest in the CN laser system, and the presence of HCN in cometary and interstellar spectra. Srivastava et al. [257] measured elastic differential, integral and momentum-transfer cross sections at energies of 3, 5, 11.6, 21.6 and 50 eV. The cross sections were normalized to He and are presented here in table 67. Absolute emission cross sections for radiation associated with excited CH, C_2, H and C fragments produced by electron impact on HCN at impact energies ranging from threshold to 1000 eV have been measured by Beenakker and de Heer [258].

4.13. OCS

The only quantitative work on electron–OCS molecule collisions that we are aware of is that of Szmytkowski and Zubek [202]. They measured the total electron scattering cross section in the 1 to 5 eV energy range. Results are shown in fig. 80.

4.14. CO_2

Total electron scattering cross sections for CO_2 have been recently reported by Szmytkowski [202], Hasted et al. [141b], Ferch et al. [259], Zubek et al. [256], and Hoffman et al. [140]. The energy ranges and methods of these investigations are listed in table 1 and the results are shown in figs. 81 and 82 and tables 68 and 69.

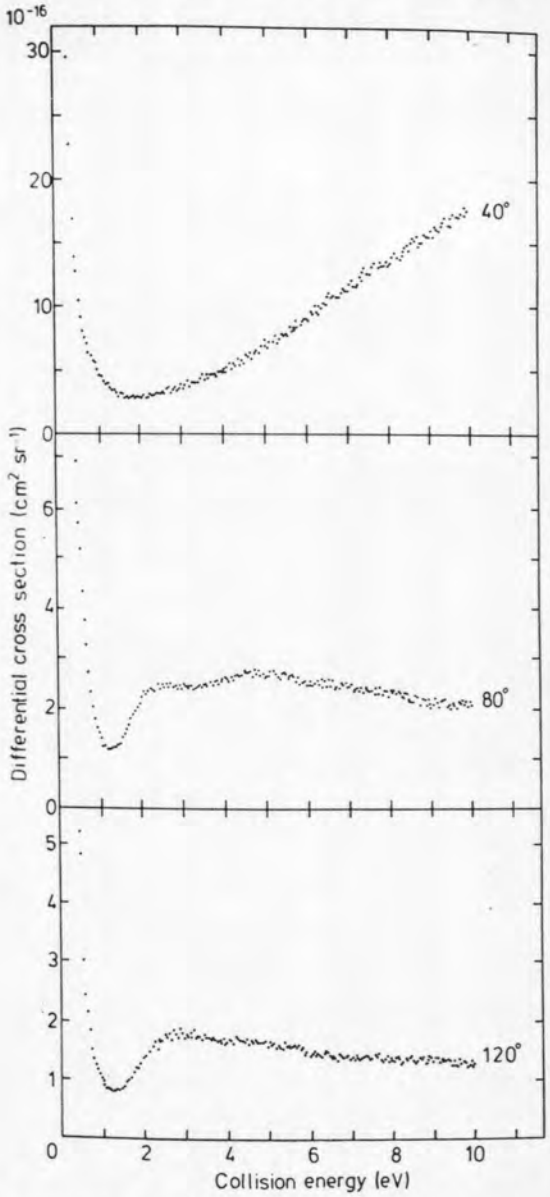

Fig. 75. Energy dependences of elastic differential scattering cross sections in H_2S at 40°, 80° and 120° scattering angles. (From ref. [256].)

Table 67
Elastic differential scattering cross sections for HCN. Entries given by angles in parentheses refer to extrapolated values. Integral (σ) and momentum-transfer (σ^M) cross sections are given at the bottom of each column. Units are 10^{-16} cm²/sr, or 10^{-16} cm² for integrated data. (From Srivastava et al. 1978, ref. [257].)[a]

	E_0(eV)				
θ(deg)	3	5	11.6	21.6	50
(0)	11	19	21	23	15
(10)	8	10	12	12	8
20	5.3	5.2	6.3	4.7	3.2
30	4.0	2.9	3.0	2.2	1.1
40	3.0	2.2	2.0	1.2	0.46
50	2.4	1.7	1.4	0.66	0.23
60	1.6	0.96	0.88	0.40	0.13
70	1.2	0.89	0.63	0.25	0.084
80	1.1	0.87	0.59	0.19	0.081
90	0.94	0.88	0.59	0.20	0.069
100	0.84	0.88	0.60	0.25	0.81
110	0.89	0.91	0.65	0.27	0.083
120	1.0	0.96	–	–	0.14
130	1.3	1.1	0.67	0.44	0.19
(140)	1.7	1.2	0.72	0.55	0.25
(150)	2.2	1.4	0.94	0.67	0.32
(160)	2.7	1.6	1.0	0.80	0.40
(170)	3.2	1.8	1.2	0.91	0.49
(180)	3.8	2.0	1.4	1.0	0.58
σ	23	18	16	10	5.3
σ^M	18	14	9.7	5.5	2.4

[a] The cross section values have been recalculated from the original HCN to He cross section ratios of ref. [257] on the basis of the recent He cross sections of ref. [10]. At 3 and 5 eV the elastic DCS of D. Anrick and A. Bitsch (private communication) were utilized.

Elastic scattering cross sections were measured by Danner [260] (1 to 10 eV), Bromberg [188] (300, 400 and 500 eV), Shyn et al. [261] (3–90 eV), and Register et al. [262] (4–50 eV). Danner carried out an extensive study of elastic scattering angular distributions in the 10°–145° angular range. His cross section data (unpublished) were found to be in good agreement with more recent measurements. Bromberg [188] made absolute differential cross section measurements in the 2° to 45° range by experimentally determining all parameters which relate the measured scattering intensity to the corresponding cross section. His results are given in table 70. Shyn et al. [261] measured relative elastic differential scattering cross sections in the −105° to +150° range. The cross sections were integrated and compared to cross section values they obtained for He under conditions similar to those of CO_2. Their helium values in turn were normalized to 10 eV He integral elastic cross section calculated by La Bahn and Callaway

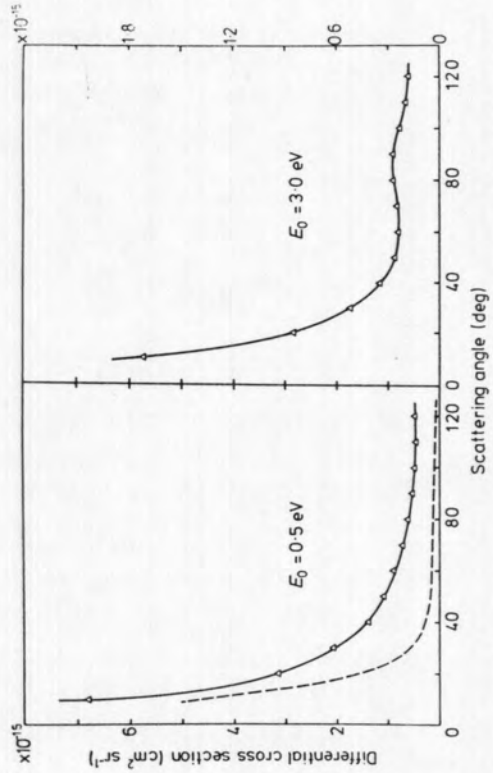

Fig. 76. Angular dependences of elastic scattering cross sections in H_2S at 0.5 and 3.0 eV impact energies. A comparison is made with Born approximation (broken line). (From ref. [256].)

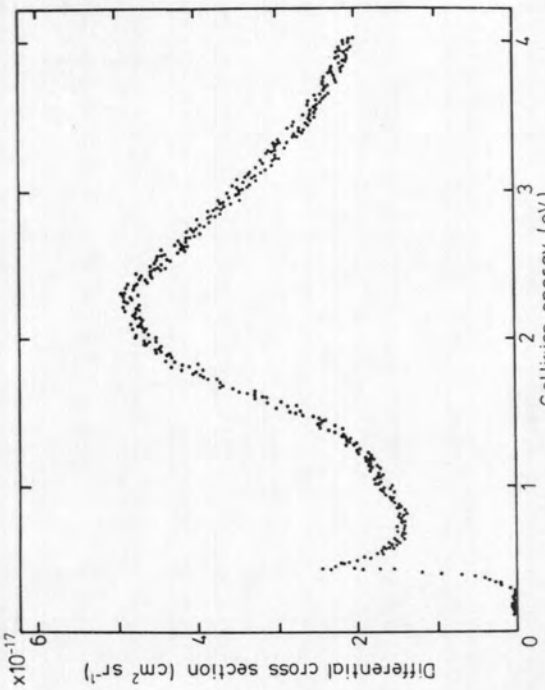

Fig. 78. Differential excitation function for the fundamental stretching modes (100,001) of H_2O at 120° scattering angle. (From ref. [256].)

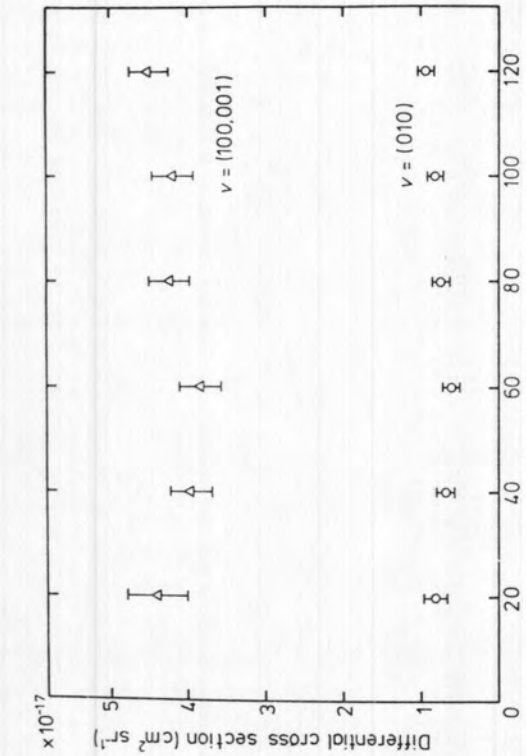

Fig. 79. Angular dependences of the cross sections for the fundamental stretching modes (100,001) and bending mode (010) of H_2S at 2 eV impact energy. (From ref. [256].)

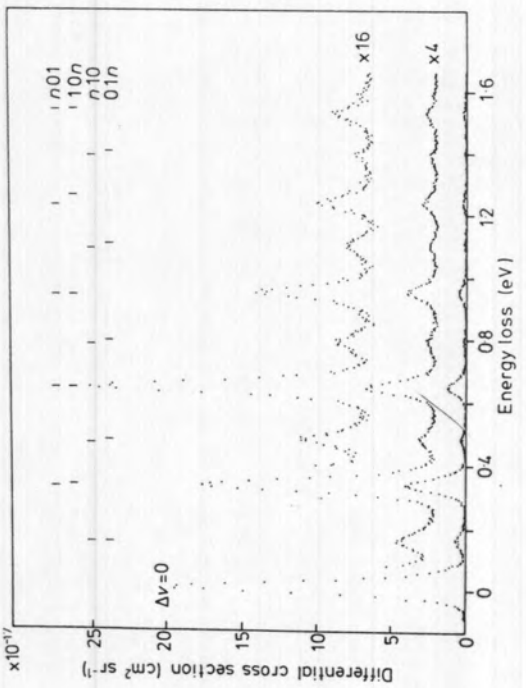

Fig. 77. Energy-loss spectrum of H_2S in terms of differential cross sections at 2 eV impact energy and 60° scattering angle. (From ref. [256].)

Table 68
Total electron scattering cross sections for CO_2. (From Ferch et al. 1982, ref. [259].)

Energy (eV)	Cross section (10^{-16} cm^2)	Energy (eV)	Cross section (10^{-16} cm^2)
0.069	68.55 ± 2.50	0.791	10.07 ± 0.30
0.073	66.31 ± 2.50	0.912	9.23 ± 0.25
0.083	60.63 ± 2.20	1.034	8.25 ± 0.20
0.094	54.31 ± 2.05	1.158	7.22 ± 0.20
0.105	49.15 ± 1.67	1.283	6.62 ± 0.20
0.115	45.57 ± 1.55	1.410	6.23 ± 0.20
0.126	42.55 ± 1.49	1.538	6.15 ± 0.18
0.137	39.53 ± 1.20	1.667	6.11 ± 0.18
0.159	35.83 ± 1.20	1.798	6.00 ± 0.18
0.170	33.59 ± 1.16	1.918	6.10 ± 0.22
0.180	31.85 ± 1.15	2.082	6.12 ± 0.35
0.191	30.29 ± 1.08	2.378	7.15 ± 0.42
0.202	29.02 ± 1.05	2.650	7.70 ± 0.45
0.213	27.97 ± 1.01	2.917	9.30 ± 0.60
0.269	25.22 ± 0.90	3.419	12.47 ± 0.80
0.325	22.03 ± 0.73	3.664	13.41 ± 0.80
0.438	17.73 ± 0.50	3.815	13.61 ± 0.80
0.554	14.51 ± 0.35	4.105	12.86 ± 0.80
0.672	12.23 ± 0.30	4.528	8.86 ± 0.55
		4.684	7.27 ± 0.55

Table 69
Total electron scattering cross sections for CO_2. (From Hoffman et al. 1982, ref. [140].)

E_0(eV)	σ(10^{-16} cm^2)	E_0(eV)	σ(10^{-16} cm^2)
2.0	6.02 ± 0.08	8.8	11.18 ± 0.04
2.5	6.45 ± 0.04	9.8	11.41 ± 0.05
3.0	8.03 ± 0.20	10.8	13.48 ± 0.08
3.4	12.96 ± 0.16	12.4	15.2 ± 0.10
3.7	14.57 ± 0.04	14.9	16.6 ± 0.10
3.85	17.8 ± 0.10	20	17.4 ± 0.10
3.95	16.9 ± 0.14	25	18.4 ± 0.2
4.15	14.9 ± 0.12	30	19.0 ± 0.2
4.4	13.56 ± 0.08	35	18.0 ± 0.3
4.9	10.12 ± 0.20	40	17.7 ± 0.1
5.9	8.70 ± 0.25	45	17.0 ± 0.1
6.4	8.73 ± 0.04	50	15.7 ± 0.1
7.3	9.97 ± 0.07		

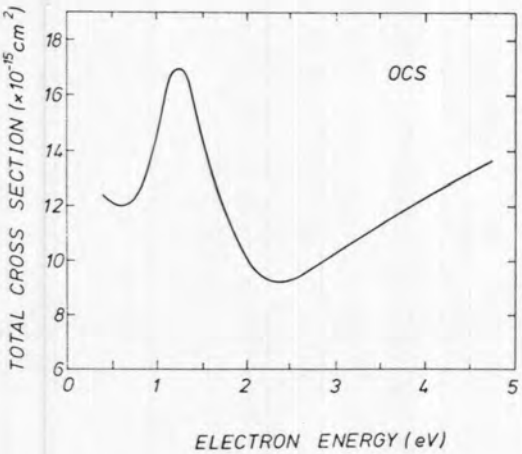

Fig. 80. Total electron scattering cross sections for OCS. (From ref. [202].)

[263]. These integral elastic scattering and momentum transfer cross sections are given in table 71. Register et al. [262] measured relative elastic cross sections in the 15° to 140° range and utilized the relative flow technique to normalize the data against He. Their differential cross section results are given in table 72 and corresponding integrated cross sections in table 71. A comparison among the 4 eV results is made in fig. 83.

Cross sections for excitation of various vibrational modes of CO_2 were generated by Danner [260] (1 to 10 eV) and Register et al. [262] (4 to 50 eV). Good agreement was found between the two works at

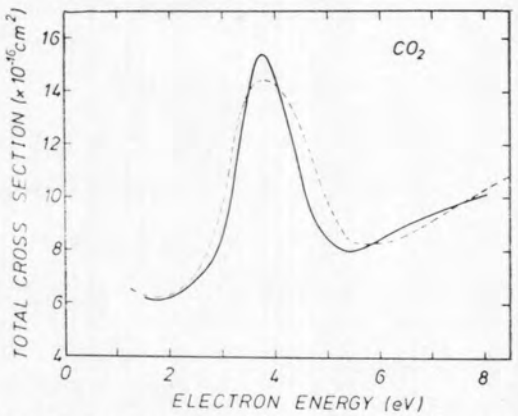

Fig. 81. Total electron scattering cross sections for CO_2. Solid line: ref. [202]: dashed line: ref. [203]. (From ref. [202].)

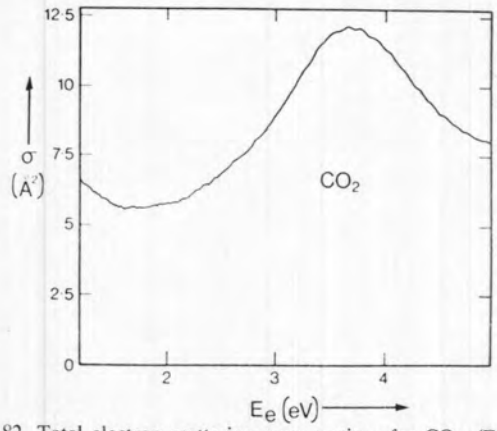

Fig. 82. Total electron scattering cross sections for CO_2. (From ref. [141b].)

Table 70
Elastic scattering cross sections for CO_2 in a_0^2/sr units. (From Bromberg 1974, ref. [188].)

Angle (deg)	500 eV	400 eV	300 eV
2	152.7 ± 5.6	151.9 ± 6.5	159.4 ± 5.5
2.5	130.4 ± 3.6	137.2 ± 4.0	143.9 ± 4.0
3	117.6 ± 3.2	124.6 ± 3.7	132.3 ± 3.6
3.5	105.1 ± 3.0	111.8 ± 3.3	120.8 ± 3.3
4	93.95 ± 2.62	100.7 ± 3.0	110.1 ± 3.1
4.5	83.14 ± 2.28	90.40 ± 2.75	100.1 ± 2.7
5	73.45 ± 2.05	80.59 ± 2.56	90.01 ± 2.42
5.5	64.70 ± 1.83	71.99 ± 2.30	81.29 ± 2.19
6	56.88 ± 1.63	64.21 ± 2.09	72.99 ± 1.95
7	43.78 ± 1.21	50.35 ± 1.64	59.42 ± 1.59
8	33.70 ± 0.93	39.55 ± 1.29	47.66 ± 1.29
9	25.57 ± 0.72	30.56 ± 0.97	38.18 ± 1.03
10	19.64 ± 0.57	23.70 ± 0.74	30.34 ± 0.83
12	12.02 ± 0.34	14.71 ± 0.47	19.10 ± 0.51
14	8.122 ± 0.233	9.648 ± 0.293	12.45 ± 0.33
16	5.671 ± 0.163	6.771 ± 0.219	8.489 ± 0.229
18	3.972 ± 0.118	4.887 ± 0.155	6.191 ± 0.165
20	2.852 ± 0.083	3.548 ± 0.112	4.585 ± 0.125
25	1.960 ± 0.055	1.927 ± 0.059	2.297 ± 0.064
30	1.643 ± 0.044	1.626 ± 0.046	1.484 ± 0.044
35	1.035 ± 0.029	1.312 ± 0.035	1.322 ± 0.052
40	0.6111 ± 0.0171	0.8199 ± 0.0246	1.103 ± 0.029
45	0.4111 ± 0.0110	0.5399 ± 0.0147	0.7758 ± 0.0267

the overlapping 4 and 10 eV impact energies. See, for example, fig. 84 which compares the cross sections for the ν_2 mode excitation. Differential and integral cross sections of Register et al. are given in tables 73–76.

An extensive set of momentum transfer, and vibrational and electronic excitation cross sections were deduced from transport measurements by Lowke et al. [264a]. Numerical values of these cross sections have been given in tabular form by Kieffer [5]. The electron impact vibrational excitation cross sections

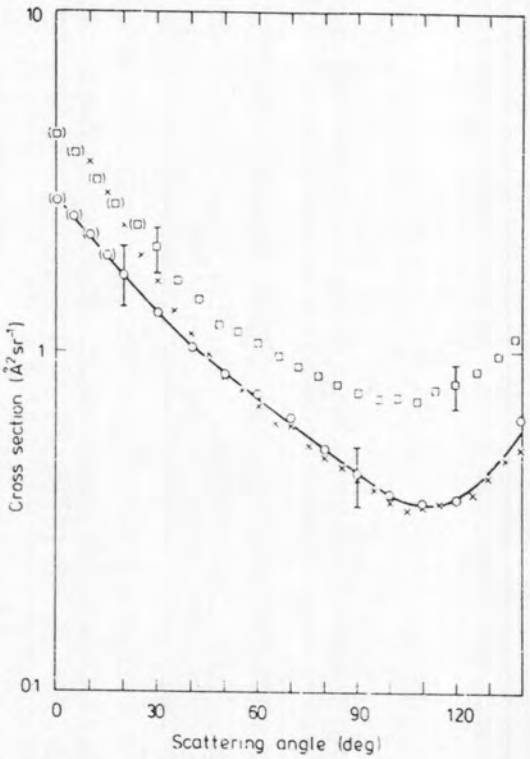

Fig. 83. Comparison of the differential elastic scattering cross sections for CO_2 at 4 eV impact energy: ×, Danner [260]; □, Shyn et al. [261]; and ○, Register et al. [262]. (From ref. [262].)

Table 71

Elastic integral and momentum transfer cross sections for CO_2, 10^{-16} cm^2 units. (From Shyn et al. 1978, ref. [261] and Register et al. 1980, ref. [262].)

	σ		σ^M	
E_0(eV)	Ref. [261]	Ref. [262]	Ref. [261]	Ref. [262]
3.0	10.9	–	12.0	–
3.5	14.8	–	15.0	–
3.8	17.3	–	16.6	–
4.0	14.7	8.73	13.7	7.34
5.0	12.4	–	11.2	–
7.0	11.2	–	10.8	–
10.0	14.1	10.61	13.1	9.52
15.0	17.6	–	12.8	–
20.0	24.5	12.32	13.3	8.89
30.0	22.3	–	11.5	–
40.0	20.6	–	9.4	–
50.0	15.6	8.75	8.0	5.55
70.0	12.5	–	4.8	–
90.0	9.5	–	2.4	–

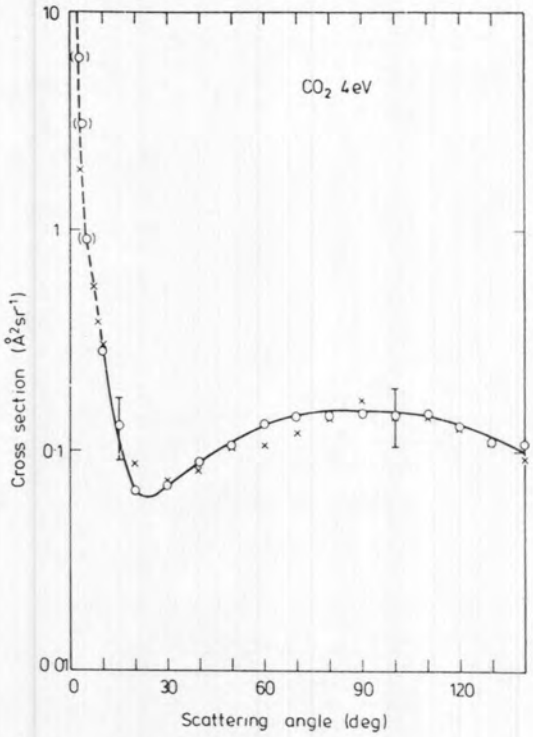

Fig. 84. Comparison of the excitation cross sections for the ν_2 mode of CO_2 at 4 eV impact energy: ×, Danner [260]; and ○, Register et al. [262]. (From ref. [262].)

Table 72

Elastic scattering differential cross sections for CO_2, 10^{-16} cm^2/sr units. (From Register et al. 1980, ref. [262].)[a]

θ	4 eV	10 eV	20 eV	50 eV
0	(2.8)	(4.5)	(10.2)	(22.6)
5	(2.5)	(3.65)	(9.4)	(14.8)
10	(2.2)	(3.08)	(7.2)	(9.7)
15	(1.92)	2.68	5.43	6.35
20	1.68	2.21	4.59	4.45
30	1.3	1.5	2.61	1.71
40	1.03	1.21	1.58	0.74
50	0.86	0.96	0.94	0.34
60	0.75	0.73	0.62	0.19
70	0.64	0.59	0.42	0.15
80	0.52	0.52	0.3	0.113
90	0.44	0.45	0.27	0.1
100	0.38	0.43	0.32	0.094
110	0.36	0.45	0.43	0.138
120	0.37	0.53	0.55	0.267
130	0.44	0.73	0.68	0.4
140	0.64	0.96	0.91	0.7
150	(0.84)	(1.21)	(1.2)	(0.98)
160	(1.04)	(1.47)	(1.5)	(1.3)
170	(1.24)	(1.74)	(1.75)	(1.55)
180	(1.44)	(1.98)	(1.95)	(1.7)

[a] Numbers in parentheses refer to extrapolated values.

Table 73
Vibrational excitation cross sections for CO_2 at 4 eV impact energy, 10^{-16} cm^2/sr units. (From Register et al. 1980, ref. [262].)[a]

θ	0.083	0.159	0.172	0.240	0.258	0.291	0.317	0.332	0.348
0	(78)	(0.2)	(0.23)	–	–	(19.0)	(0.033)	(0.14)	(0.1)
5	(1.11)	(0.19)	(0.22)	–	–	(3.0)	(0.03)	(0.12)	(0.09)
10	0.281	0.157	0.191	–	–	0.85	0.02	0.114	0.052
15	0.131	0.185	0.227	0.0035	0.0045	0.389	0.026	0.073	0.074
20	0.066	0.135	0.164	0.0069	0.0088	0.141	0.0143	0.0694	0.049
30	0.07	0.088	0.107	0.0094	0.0162	0.047	0.0127	0.037	0.036
40	0.088	0.05	0.061	0.0108	0.0207	0.016	0.0093	0.0173	0.0217
50	0.107	0.037	0.041	0.0148	0.0235	0.0066	0.0044	0.0132	0.0148
60	0.133	0.036	0.039	0.0163	0.0268	0.0045	0.0052	0.0134	0.0129
70	0.143	0.035	0.039	0.0169	0.0292	0.0029	0.0054	0.0127	0.0127
80	0.147	0.038	0.038	0.0157	0.0307	0.0025	0.0062	0.0145	0.0118
90	0.151	0.044	0.041	0.0185	0.0304	0.0024	0.0078	0.016	0.0134
100	0.147	0.053	0.050	0.0177	0.03	0.0022	0.0101	0.0207	0.015
110	0.15	0.068	0.051	0.0161	0.0262	0.0034	0.0133	0.0225	0.0192
120	0.132	0.069	0.043	0.0141	0.0238	0.0043	0.0099	0.0235	0.0166
130	0.112	0.063	0.038	0.0119	0.0196	0.0069	0.0099	0.0154	0.0173
140	0.110	0.057	0.040	0.0104	0.0173	0.0125	0.0073	0.0167	0.0147
150	(0.097)	(0.05)	(0.037)	–	–	(0.021)	(0.0055)	(0.0134)	(0.0122)
160	(0.083)	(0.042)	(0.032)	–	–	(0.033)	(0.0036)	(0.0109)	(0.0094)
170	(0.068)	(0.033)	(0.028)	–	–	(0.05)	(0.0024)	(0.0081)	(0.0069)
180	(0.055)	(0.027)	(0.023)	–	–	(0.073)	(0.0016)	(0.0059)	(0.0056)

[a] The numbers in the column headings refer to the energy-loss value of the vibrational excitation features in the energy-loss spectra. In some cases these features represent more than one overlapping vibrational excitation process. Numbers in parentheses are extrapolated values.

Table 74
Vibrational excitation cross sections for CO_2 at 10 eV impact energy, 10^{-16} cm^2/sr units. (From Register et al. 1980, ref. [262].)[a]

θ	0.083	0.159	0.172	0.291	0.325
0	(36.6)	(0.04)	(0.025)	(30.9)	(0.0012)
5	(0.311)	(0.033)	(0.021)	(0.86)	–
10	0.078	0.0269	0.0159	0.22	0.0015
15	0.0339	0.0222	0.0142	0.0836	–
20	0.0168	0.0208	0.0106	0.0336	0.0018
30	0.0065	0.0158	0.0092	0.0089	0.0017
40	0.0044	0.0132	0.0073	0.004	0.0016
50	0.0038	0.0111	0.0064	0.0031	0.0014
60	0.0058	0.0099	0.0053	0.0031	0.0013
70	0.0087	0.0091	0.0051	0.0026	0.0011
80	0.0111	0.0087	0.0057	0.0028	0.0012
90	0.0120	0.0089	0.0051	0.0026	0.0011
100	0.0126	0.009	0.005	0.0027	0.0012
110	0.0017	0.0086	0.0052	0.0032	0.001
120	0.0092	0.0096	0.0052	0.004	0.0012
130	0.0084	0.0111	0.0056	0.0052	0.0014
140	0.0077	0.0126	0.0064	0.0064	0.0019
150	(0.0067)	(0.0133)	(0.0064)	(0.0076)	(0.0021)
160	(0.0054)	(0.0137)	(0.0065)	(0.0087)	(0.0024)
170	(0.0044)	(0.0137)	(0.0063)	(0.0096)	(0.0026)
180	(0.0034)	(0.0135)	(0.0059)	(0.0103)	(0.0028)

[a] See footnote in table 73 for explanation.

Table 75
Vibrational excitation cross sections for CO_2 at 20 eV impact energy, 10^{-16} cm^2/sr units. (From Register et al. 1980, ref. [262].)[a]

θ	0.083	0.159	0.172	0.291
0	(351.4)	–	–	(63.4)
5	(0.2)	–	–	(0.44)
10	0.05	0.0034	0.0052	0.112
20	0.01	0.0014	0.0023	0.0129
30	0.005	0.0009	0.0009	0.0031
40	0.0043	0.00052	0.00058	0.0024
50	0.0042	0.00039	0.00071	0.0022
60	0.0043	0.00039	0.00043	0.002
70	0.004	0.00028	0.00055	0.0019
80	0.0036	0.0004	0.00045	0.0017
90	0.0036	0.00046	0.00031	0.0012
100	0.0041	0.0004	0.00042	0.0012
110	0.0057	0.00035	0.00038	0.0015
120	0.0077	0.00035	0.00051	0.0023
130	0.0098	0.00035	0.00046	0.0029
135	0.0117	0.00041	0.00024	0.0031
140	(0.013)	–	–	(0.0033)
150	(0.017)	–	–	(0.0038)
160	(0.022)	–	–	(0.0042)
170	(0.025)	–	–	(0.0049)
180	(0.028)	–	–	(0.0056)

[a] See footnote in table 73 for explanation.

Table 76
Vibrational excitation cross sections for CO_2 at 50 eV impact energy, 10^{-16} cm^2/sr units. (From Register et al. 1980, ref. [262].)[a]

θ	0.083	0.166	0.291
0	–	(0.014)	(61.02)
5	–	(0.0077)	(0.068)
10	–	0.00413	0.0171
20	–	0.00113	0.00466
30	–	0.0005	0.00234
40	0.00534	0.00041	0.00196
50	0.00408	0.00026	0.00136
60	0.003	0.00033	0.00093
70	0.0023	0.00044	0.00067
80	0.00222	0.00037	0.00032
90	0.0032	0.00035	0.00025
100	0.0053	0.00046	0.00021
110	0.0074	0.00054	0.00043
120	0.0099	0.0008	0.00073
130	0.012	0.00124	0.00095
140	0.020	0.0025	0.0018
150	(0.032)	(0.0049)	(0.003)
160	(0.05)	(0.009)	(0.006)
170	(0.08)	(0.018)	(0.012)
180	(0.12)	(0.035)	(0.023)

[a] See footnote in table 73 for explanation.

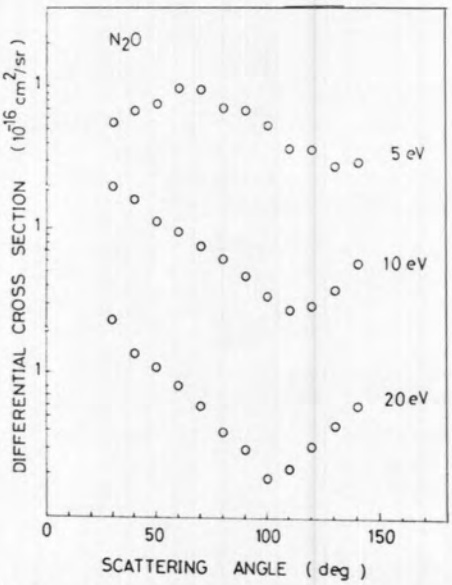

Fig. 85. Elastic differential scattering cross sections for N_2O at 5, 10 and 20 eV impact energies. (From ref. [221].)

for the ν_3 mode of CO_2 (4.3 μm band) deduced by Bulos and Phelps [264b] agree with the data obtained by electron beam methods.

4.15. N_2O

There are only two relevant experimental measurements of cross sections in nitrous oxide. Zubek et al. [256] have measured total scattering cross sections in the electron energy range 0.5–10 eV, but their data are not yet published. Kubo et al. [221] report elastic differential scattering cross sections at energies of 5, 10 and 20 eV. These data are given in fig. 85.

Several experimental groups have studied optical emission spectra following electron impact excitation of N_2O. Emissions are due to atomic and molecular ions rather than to emissions in neutral N_2O.

4.16. SO_2

No electron impact excitation or ionization cross section data existed for SO_2 until very recently. The discovery of emissions by sulfur and oxygen ions (ions very likely generated from SO_2) in the Io-Jupiter torus inspired some recent measurements. Total electron scattering cross sections have been measured by Zubek et al. [256] (0.3 to 7.0 eV) and Sokolov and Sokolova [35a] (0 to 10 eV). See table 77 and fig. 86. There is about a factor of two difference between the two sets of data.

Elastic differential, integral and momentum transfer cross sections were generated by Orient et al. [266] at 12, 20, 50, 100 and 200 eV impact energies. (See table 78.) Excitation of vibrational modes in the 4 eV resonance region was studied by Andric et al. [267]. The cross sections they obtained for the (n, 0, 0) vibrational progression at 3.4 eV impact energy and 90° scattering angle are shown in fig. 87. Vušković and Trajmar [268] measured scattering intensities associated with six segments of the

Table 77
Total electron scattering cross sections for SO_2, 10^{-16} cm^2 units. (From Zubek et al. 1982, ref. [256] and Sokolov and Sokolova 1981, ref. [35a].)

E_0(eV)	Ref. [256][a]	Ref. [246][b]
0.25	240	400
0.50	140	360
1.0	100	280
1.5	83	200
2.0	75	180
3.0	60	105
4.0	58	78
5.0	55	53
6.0	52	38
7.0	51	28
8.0	–	20
9.0	–	14
10.0	–	8

[a] Values given here represent average values of original data points.

[b] Values given here were read from fig. 2 of ref. [246].

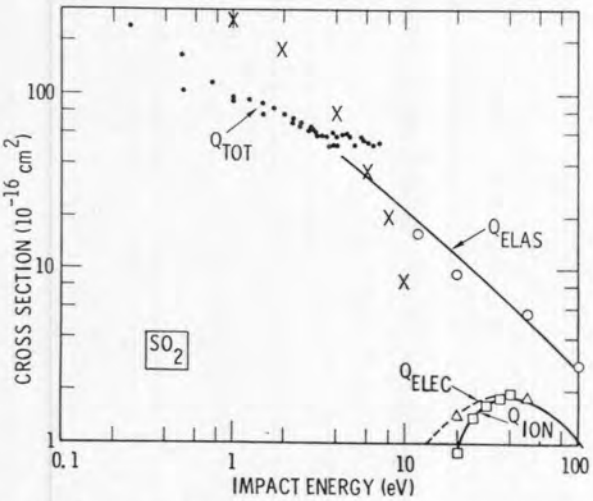

Fig. 86. A summary of total (Q_{TOT}) and elastic (Q_{ELAS}) scattering, electronic excitation (Q_{ELEC}), and ionization (Q_{ION}) cross sections for SO_2: ●, Q_{TOT}, ref. [256]; ○, Q_{TOT}, ref. [246]; ×, Q_{ELAS}, ref. [266]; △, Q_{ELEC}, ref. [268]; and □, Q_{ION}, ref. [269].

Table 78
Elastic scattering cross sections for SO_2. Entries in parentheses refer to extrapolated values. (From Orient et al. 1982, ref. [266].)

θ (deg)	Differential cross section (10^{-16} cm^2/sr)				
	$E_0 = 12$ eV	20	50	100	200
0	(25.0)	(17.0)	(18.0)	(14.0)	(5.0)
5	(18.0)	(12.0)	(11.0)	(8.0)	(2.9)
10	(12.6)	(8.2)	(6.6)	(4.3)	(1.9)
15	9.01	4.97	4.47	(2.4)	(0.98)
20	6.43	4.15	2.76	1.21	0.561
25	4.92	2.36	1.37	0.580	0.332
30	3.11	1.82	0.983	0.339	0.206
40	1.65	0.963	0.453	0.165	0.107
50	0.960	0.603	0.290	0.094	0.067
60	0.624	0.358	0.155	0.070	0.051
70	0.417	0.259	0.136	0.060	0.045
80	0.436	0.233	0.127	0.052	0.038
90	0.430	0.270	0.128	0.044	0.030
100	0.581	0.308	0.129	0.038	0.023
110	0.604	0.319	0.137	0.041	0.025
120	0.737	0.379	0.151	0.151	0.035
130	0.806	0.419	0.186	0.076	0.038
140	0.956	0.514	0.266	0.110	0.040
145	0.995	0.597	0.323	0.125	0.045
150	(1.06)	(0.62)	0.383	(0.14)	(0.047)
160	(1.20)	(0.73)	(0.50)	(0.17)	(0.053)
170	(1.37)	(0.83)	(0.60)	(0.20)	(0.057)
180	(1.55)	(0.91)	(0.68)	(0.22)	(0.061)
σ	15.97	9.22	5.66	2.67	1.26
σ^M	10.32	5.60	2.91	1.06	0.52

Table 79
Summary of assignments and notations for SO_2 inelastic cross sections. (From Vušković and Trajmar 1982, ref. [268].)

Feature (region)		Peak position (eV)	Energy-loss range[c] (eV)
No.[a]	Assignment[b]		
2	$\tilde{a}^3B_1$	3.5	3.1–3.9
3	$\tilde{A}^1B_1$	4.5	3.9–5.5
4	$\tilde{C} + \tilde{D}$	6.3	5.5–7.1
5	$\tilde{E} + \tilde{F}$	8.8	7.1–9.6
6	$\tilde{G} + \tilde{I}$	10	9.6–10.3
7	$\tilde{H}$	11	10.3–11.3

[a] The same numbering is used to identify features in the energy-loss spectra and in the tabulation of cross section data.

[b] The notation of G. Herzberg, Molecular Spectra and Molecular Structure III. Electronic Spectra and Electronic Structure of Polyatomic Molecules (D. Van Nostrand, New York, 1966) is adopted here.

[c] In the energy-loss range indicated transitions other than those specified in column two may be included.

electronic excitation region of the energy-loss spectrum (from 3 to 11 eV) at 20, 50 and 200 eV impact energies. The assignment of these segments to electronic excitations are indicated in table 79. Additional, as yet unidentified excitations may also be present in the spectrum. Intensity data were converted into differential cross sections by use of the elastic cross sections of Orient et al. [266], and by extrapolation and integration obtained integral excitation and inelastic momentum transfer cross sections associated with these segments. Their results are shown in tables 80 through 83.

4.17. NH_3

Elastic differential scattering cross sections have been reported by Harshbarger et al. [270] at 300, 400 and 500 eV impact energies in the 2° to 10° angular range. (See table 84.) Bennani et al. [271] measured elastic cross sections at 35 keV impact energy in the 3×10^{-3} to 8 degree angular range. Their cross sections as a function of momentum transfer are given in table 85. The normalization for this data was based on an independent-atom model theory.

Table 80
Differential inelastic cross sections for SO_2 at $E_0 = 20$ eV. (From Vušković and Trajmar 1982, ref. [268].)

	DCS (10^{-18} cm^2 sr)					
θ (deg)	2	3	4	5	6	7
4		26	106	–	70	–
6		19	80	33	56	23
8		14	58	28	45	18
10		11	46	24	35	12
12	0.12	9.2	35	22	27	9.4
14	–		26	–	–	–
16	0.15	5.4	20	16	18	6.3
18	–	–	13	–	–	–
20	0.17	3.4	9.6	14	11	4.7
25	0.19	2.3	4.9	11	8.0	3.5
30	0.21	1.7	2.7	7.8	5.4	2.4
35	0.22	1.4	2.0	6.1	3.8	1.7
40	–	1.1	1.7	4.9	3.3	1.4
45	0.26	0.99	1.7	4.2	2.8	1.3
50	0.28	0.94	1.6	3.8	2.6	1.1
60	0.31	0.89	1.2	3.3	2.0	0.99
70	0.28	0.68	0.85	2.8	1.5	0.77
80	0.26	0.68	0.61	2.6	1.2	0.66
90	0.23	0.66	0.46	2.4	1.1	0.61
100	0.23	0.68	0.47	2.6	1.2	0.63
110	0.33	0.75	0.61	3.0	1.4	0.75
120	0.38	0.82	0.85	3.0	1.6	0.80

Table 81
Differential inelastic cross sections for SO_2 at $E_0 = 50$ eV. (From Vušković and Trajmar 1982, ref. [268].)

	DCS (10^{-18} cm^2/sr)					
θ (deg)	2	3	4	5	6	7
2		–	1167	–	–	–
4		128	572	343	944	286
6		54	315	200	532	168
8		25	143	103	226	72
10		14	69	62	137	47
12		9.7	34	38	73	29
14		6.0	17	23	40	17
16		4.0	8.0	16	24	10
18		2.8	5.4	11	14	7.4
20		2.1	4.0	9.2	11	5.1
25		1.0	2.1	5.2	6.6	2.6
30	0.0091	0.54	1.7	3.2	4.7	2.0
35	0.012	0.34	1.4	2.2	3.5	1.4
40	0.015	0.27	1.1	1.5	2.6	1.1
45	0.019	0.25	0.82	1.1	1.9	0.77
50	0.023	0.24	0.60	0.94	1.4	0.60
60	0.026	0.18	0.37	0.66	0.80	0.33
70	0.024	0.13	0.25	0.43	0.49	0.24
80	0.023	0.12	0.16	0.43	0.40	0.19
90	0.025	0.12	0.12	0.46	0.33	0.16
100	0.031	0.13	0.11	0.51	0.27	0.14
110	0.034	0.15	0.13	0.51	0.26	0.14
120	0.043	0.19	0.20	0.57	0.34	0.19
126	0.054	0.24	0.32	0.69	0.49	0.26

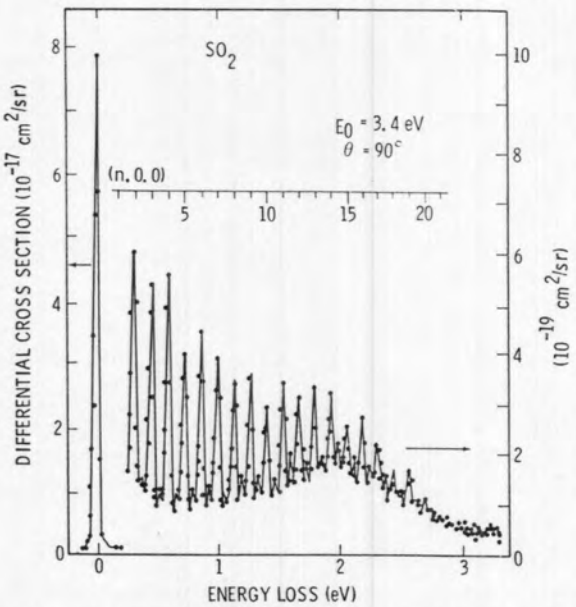

Fig. 87. Differential cross sections for the excitation of the $(n, 0, 0)$ vibrational progression in SO_2 at 3.4 eV impact energy and 90° scattering angle. (From ref. [267].)

Table 82
Differential inelastic cross sections for SO_2 at $E_0 = 200$ eV. (From Vušković and Trajmar 1982, ref. [268].)

	DCS (10^{-18} cm^2/sr)					
θ (deg)	2	3	4	5	6	7
2		63	327	237	968	304
3		–	201	–	–	–
4		18	124	90	315	104
5		–	70	–	–	–
6		5.3	33	39	108	41
7		–	18	–	–	–
8		2.3	10	14	27	12
9		–	6.6	–	–	–
10		1.5	3.6	6.8	8.6	4.1
12		1.0	1.8	4.7	5.0	2.6
16		0.51	1.1	2.3	3.2	1.4
20		0.24	0.71	1.4	1.8	0.88
25		0.13	0.41	0.71	0.88	0.39
30		0.081	0.24	0.41	0.52	0.22
35		0.048	0.18	0.27	0.31	0.14
40		0.031	0.12	0.18	0.22	0.094
45		0.022	0.075	0.13	0.16	0.066
50	0.00015	0.016	0.054	0.10	0.12	0.049
60	0.00020	0.010	0.036	0.067	0.072	0.031
70	–	0.0076	0.025	0.043	0.052	0.022
80	0.00023	0.0052	0.021	0.034	0.040	0.016
90	–	0.0045	0.018	0.025	0.031	0.013
100	0.00026	0.0036	0.015	0.019	0.030	0.013
110	0.00020	0.0031	0.016	0.018	0.030	0.012
120	0.00021	0.0034	0.018	0.021	0.034	0.013
127	–	0.0048	0.022	0.027	0.043	0.018

Table 83
Integral σ and momentum transfer σ^M cross sections, for SO_2 in 10^{-18} cm^2 units. (From Vušković and Trajmar 1982, ref. [268].)

	σ			σ^M		
Feature	20 eV	50 eV	200 eV	20 eV	50 eV	200 eV
2	0.56	0.47	0.00002	0.46	0.63	0.00002
3	14	10	1.3	11	2.9	0.1
4	27	41	6.5	13	7.2	0.5
5	50	36	6.5	41	12	0.7
6	34	71	18	24	14	1.2
7	16	25	6.3	12	6.2	0.5

Table 84
Elastic cross sections for NH_3 [a], a_0^2/sr units. (From Harshbarger et al. 1971, ref. [270].)

Angle (deg)	300 eV (a)	300 eV (b)	400 eV (a)	400 eV (b)	500 eV (a)	500 eV (b)
2.0	69.32 ± 1.96	66.42 ± 2.52	61.05 ± 1.89	61.48 ± 5.23	52.43 ± 2.00	51.73 ± 1.71
2.5	58.69 ± 1.40	58.46 ± 2.44	49.92 ± 1.19	49.24 ± 1.86	43.76 ± 1.07	43.05 ± 1.21
3.0	51.33 ± 1.26	51.51 ± 0.84	43.86 ± 1.11	42.58 ± 0.59	38.28 ± 0.95	37.99 ± 0.70
3.5	45.17 ± 1.10	46.34 ± 0.75	38.83 ± 1.02	38.55 ± 0.53	33.83 ± 0.85	33.7 ± 0.49
4.0	40.21 ± 0.97	41.62 ± 0.30	34.37 ± 0.93	34.35 ± 0.40	30.28 ± 0.76	30.24 ± 0.27
5.0	32.28 ± 0.78	33.22 ± 1.02	27.67 ± 0.74	27.71 ± 0.57	24.35 ± 0.59	24.49 ± 0.53
6.0	26.60 ± 0.67	26.82 ± 1.12	22.53 ± 0.59	22.71 ± 0.38	19.87 ± 0.48	19.84 ± 0.25
7.0	22.11 ± 0.53	22.50 ± 0.67	18.53 ± 0.50	18.78 ± 0.52	16.28 ± 0.40	16.39 ± 0.20
8.0	18.47 ± 0.44	18.46 ± 0.51	15.38 ± 0.40	15.37 ± 0.49	13.33 ± 0.32	13.21 ± 0.19
9.0	15.51 ± 0.38	14.88 ± 0.93	12.68 ± 0.93	12.80 ± 0.30	10.84 ± 0.27	11.04 ± 0.43
10.0	12.93 ± 0.32	12.49 ± 0.37	10.44 ± 0.28	10.53 ± 0.55	8.81 ± 0.22	9.04 ± 0.81

[a]Measured by Harshbarger et al.
[b]Given by Harshbarger et al. as unpublished data by J.P. Bromberg.

Table 85
Elastic differential cross sections for NH_3 at 35 keV impact energy, 10^{-16} cm^2 units. (From Bennani et al. 1979, ref. [271].)

K (au)	DCS	K (au)	DCS
0.15	45.7 ± 2.0	1.40	7.47 ± 0.1
0.20	40.9 ± 2.0	1.60	5.41
0.30	34.0 ± 1.8	1.80	4.09 ± 0.05
0.40	29.6 ± 1.2	2.00	3.144
0.50	26.3 ± 1.0	2.50	1.849
0.60	23.4 ± 0.8	3.00	1.212 ± 0.005
0.70	20.7 ± 0.7	3.50	0.814
0.80	18.3 ± 0.6	4.00	0.532
0.90	15.9 ± 0.4	5.00	0.209
1.00	13.8 ± 0.2	6.00	0.103
1.20	10.2 ± 0.1	7.00	0.063

No quantitative electron impact excitation cross sections have been reported for NH_3. Harshbarger et al. [270] have determined generalized oscillator strengths for the $\tilde{A} \rightarrow \tilde{X}$ transition at 300, 400 and 500 eV kinetic energies at angles ranging from 2° to 7°.

4.18. As_4

Daimon et al. [272] measured differential elastic cross sections at 70 to 500 eV impact energies in the 3° to 135° angular range for As_4. The 100 eV results are shown in fig. 88. They also calculated cross sections by using the atomic potential of Green et al. [273] (dash-dash line in fig. 88). The calculations yielded better agreement with experiment when both polarization and intramolecular multiple scattering (solid line in fig. 88) were included.

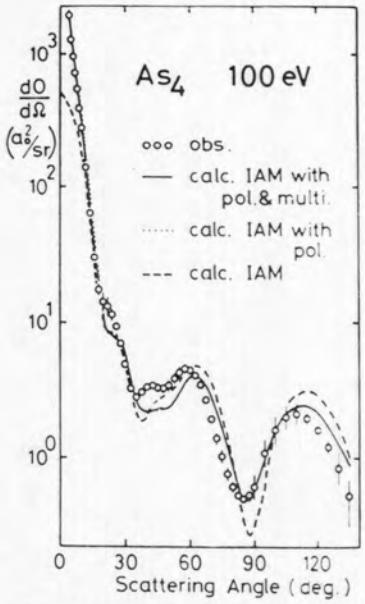

Fig. 88. Differential elastic scattering cross sections for As_4 at 100 eV impact energy (from Daimon et al. [272]). See text for explanation.

Table 86
Total electron scattering cross sections for CH_4, 10^{-16} cm^2 units. (From Barbarito et al. 1979, ref. [275].)[a]

E_0 (eV)	σ_T [a]	E_0 (eV)	σ_T [b]
0.05	2.0	3.5	7.2
0.125	0.6	4.5	10.6
0.20	0.3	5.5	14.0
0.30	0.4	6.5	16.1
0.40	0.5	7.5	17.1
0.55	0.9	9.0	17.1
0.70	1.0	10.5	16.7
0.85	1.4	12.0	15.8
1.15	2.0	13.5	15.0
1.45	2.7	15.0	14.0
1.75	3.3		
2.2	4.4		
2.7	5.7		

[a]Numerical values were obtained from fig. 8 of ref. [274].

[b]Numerical values were obtained from fig. 7 of ref. [274].

4.19. CH_4

Total electron scattering cross section measurements for CH_4 have been recently reported by Duncan and Walker [274] (swarm measurements), and Barbarito et al. [275] (transmission measurements). Results obtained by Barbarito et al. in the 1 to 16 eV energy range are given in table 86. Sohn et al. [276] measured differential elastic (including rotational excitation) cross sections in the 0.1 to 1.8 eV impact energy range and by integration obtained integral elastic cross sections nearly equivalent to total

Table 87
Elastic differential cross sections for CH_4, 10^{-16} cm^2/sr units. (From Tanaka et al. 1982, ref. [278a].)

Scattering angle (deg)	Impact energy (eV)							
	3	5	6	7.5	9	10	15	20
30	0.81	1.51	1.88	3.02	3.13	3.14	3.93	3.37
40	0.53	1.04	1.52	2.46	2.70	3.02	2.42	1.77
50	0.51	1.16	1.47	1.98	1.79	2.07	1.57	1.03
60	0.86	1.21	1.20	1.46	1.42	1.37	0.94	0.72
70	0.81	1.42	1.41	1.55	1.32	1.14	0.67	0.51
80	0.94	1.39	1.50	1.43	1.22	1.05	0.52	0.45
90	0.68	1.09	1.19	1.20	0.94	0.80	0.41	0.35
100	0.57	0.84	0.89	0.68	0.50	0.49	0.27	0.29
110	0.41	0.48	0.46	0.32	0.35	0.27	0.26	0.25
120	0.25	0.26	0.23	0.21	0.30	0.26	0.29	0.32
130	0.24	0.29	0.43	0.50	0.64	0.51	0.47	0.42
140	0.31	0.77	0.94	1.15	1.14	1.01	0.56	0.50

electron scattering cross sections. Their differential cross sections are shown in figs. 89 and 90 and their integral elastic cross section results together with the 0 to 1 eV results of Barbarito et al. are shown in fig. 91. Differential elastic (including rotational excitation) scattering cross sections were also measured by Rohr [277] at and below 10 eV (figs. 92 and 93), and Tanaka et al. [278a] from 3 to 20 eV (tables 87 and 88). Newell et al. [279] report elastic differential cross sections at 10 eV which agree well with data of Tanaka et al. [278a].

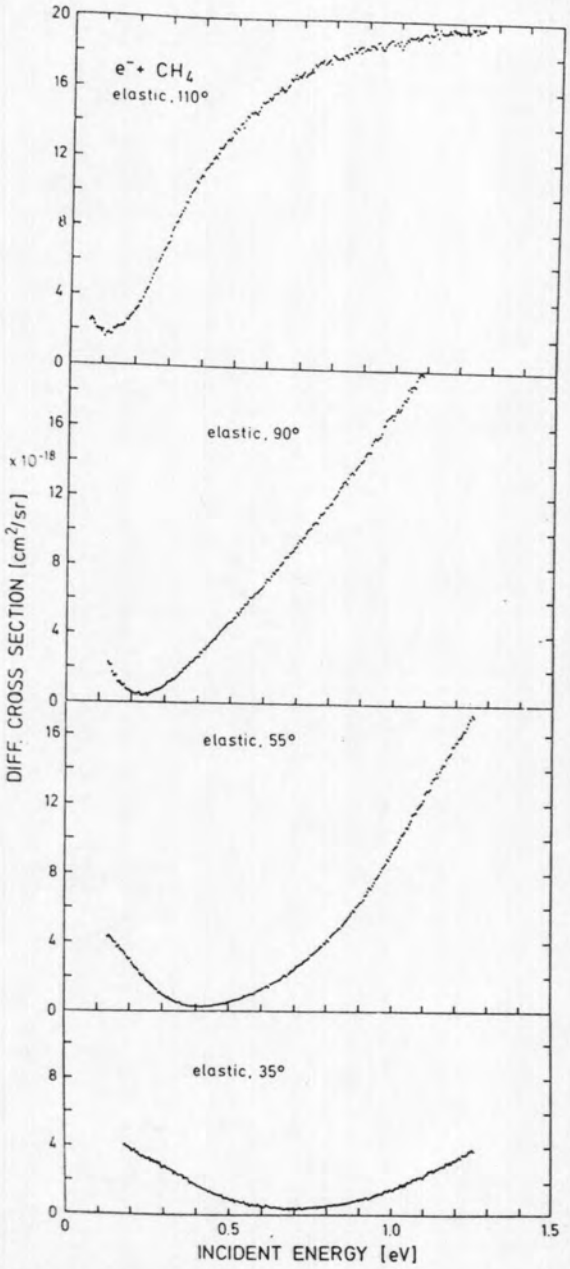

Fig. 89. Energy dependence of the elastic scattering cross section for CH_4 at 35°, 55°, 90° and 110° scattering angles. (From ref. [276].)

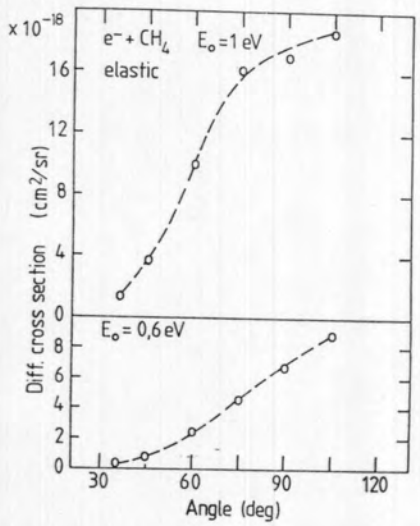

Fig. 90. Angular dependence of the elastic scattering cross section for CH_4 at 0.6 and 1 eV impact energies. (From ref. [276].)

Vibrational excitation of the unresolved ν_1, ν_3 and ν_2, ν_4 modes by electron impact was studied by Rohr [277] at impact energies below 10 eV (figs. 94–96), by Sohn et al. [276] in the 0.1 to 1.8 eV range (figs. 97–101), and by Kubo et al. [280] at energies from 3 to 20 eV (tables 89 and 90).

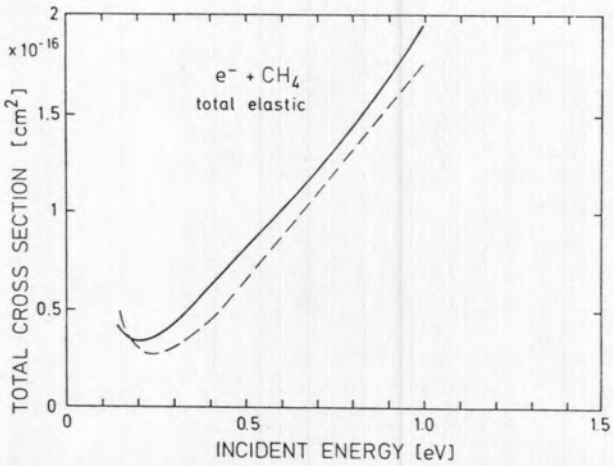

Fig. 91. Total electron scattering cross sections for CH_4: solid line, ref. [276]; dashed line, ref. [275]. (From ref. [276].)

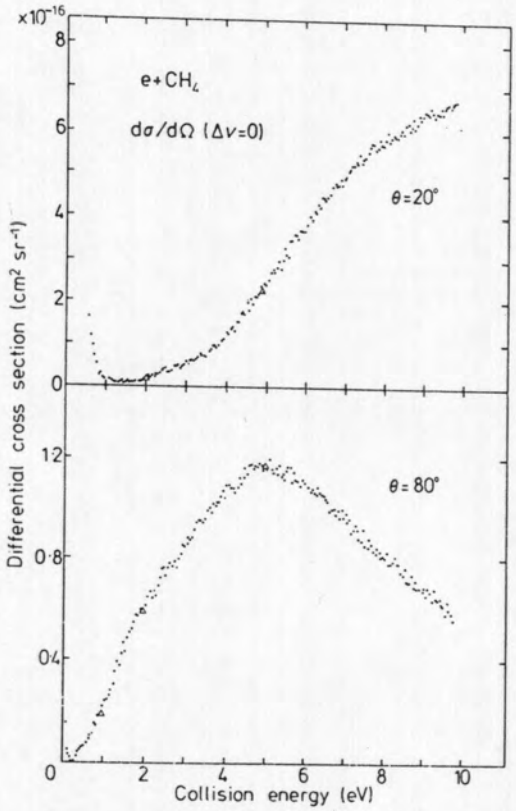

Fig. 92. Energy dependence of the differential elastic scattering cross section for CH_4 at 20° and 80° scattering angles. (From ref. [277].)

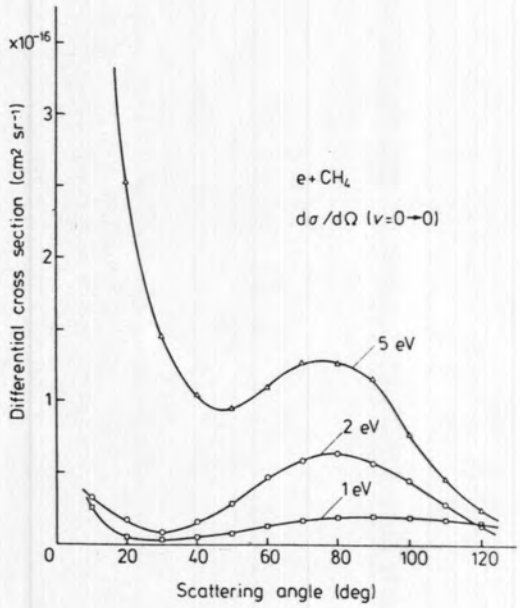

Fig. 93. Angular dependence of the elastic scattering cross sections for CH_4 at 1, 2 and 5 eV impact energies. (From ref. [277].)

Table 88
Integral elastic (σ) and momentum transfer (σ^M) cross sections for CH_4, 10^{-16} cm^2 units. (From Tanaka et al. 1982, ref. [278a].)

Impact energy (eV)	σ	σ^M
3	7.4	6.6
5	13.7	12.4
6	16.1	14.5
7.5	19.6	16.0
9	18.9	14.4
10	18.4	13.1
15	15.7	7.6
20	14.3	6.5

Table 89
Differential cross sections for the overlapping ν_2 and ν_4 vibrational excitation of CH_4, 10^{-18} cm^2/sr units. (From Kubo et al. 1981, ref. [280].)

	E_0							
θ	3	5	7	7.5	8	10	15	20
30	3.59	1.86	5.66	6.58	4.86	4.05	3.74	2.36
40	2.77	3.13	7.43	8.29	6.01	4.56	2.93	2.32
50	2.59	3.06	5.63	5.28	5.26	4.38	2.33	2.50
60	2.35	3.10	5.31	4.99	4.41	3.91	2.30	1.52
70	1.94	2.73	5.40	4.63	5.37	3.38	1.90	1.25
80	2.48	3.69	6.35	6.19	6.10	4.20	2.18	0.829
90	2.22	3.28	6.39	5.98	6.17	3.56	2.83	2.02
100	2.26	4.28	8.37	7.69	8.33	4.10	2.82	2.26
110	1.80	4.76	8.10	6.27	6.80	4.50	2.99	1.84
120	1.97	3.73	7.95	6.64	7.38	5.24	3.11	1.95
130	2.46	3.83	6.71	6.08	6.39	5.60	2.72	1.60
140	2.35	4.67	7.87	6.34	6.17	5.35	4.02	2.59

Table 90
Differential cross sections for the excitation of the overlapping ν_1 and ν_3 vibrational modes of CH_4, 10^{-18} cm^2/sr units. (From Kubo et al. 1981, ref. [280].)

	E_0							
θ	3	5	7	7.5	8	10	15	20
30	3.21	2.82	8.05	8.25	6.93	5.13	1.58	1.64
40	2.99	4.10	11.03	11.8	8.94	6.02	2.03	1.13
50	1.73	3.58	7.10	6.88	6.55	4.92	1.63	1.19
60	1.39	4.05	6.46	6.37	5.92	4.79	1.87	0.95
70	1.35	3.82	6.07	6.40	5.81	4.08	1.51	0.643
80	1.68	4.70	7.84	7.01	6.78	3.33	1.37	0.568
90	1.32	5.05	8.80	7.39	7.01	3.31	1.24	0.921
100	1.39	4.99	8.26	9.13	9.07	3.62	1.48	0.814
110	1.26	4.92	8.08	6.84	5.68	3.68	1.75	1.04
120	1.47	3.46	6.35	5.88	6.25	3.64	1.86	1.21
130	1.69	2.90	5.41	5.26	4.77	4.49	1.68	1.28
140	1.25	2.74	5.69	4.60	5.18	4.96	3.35	2.04

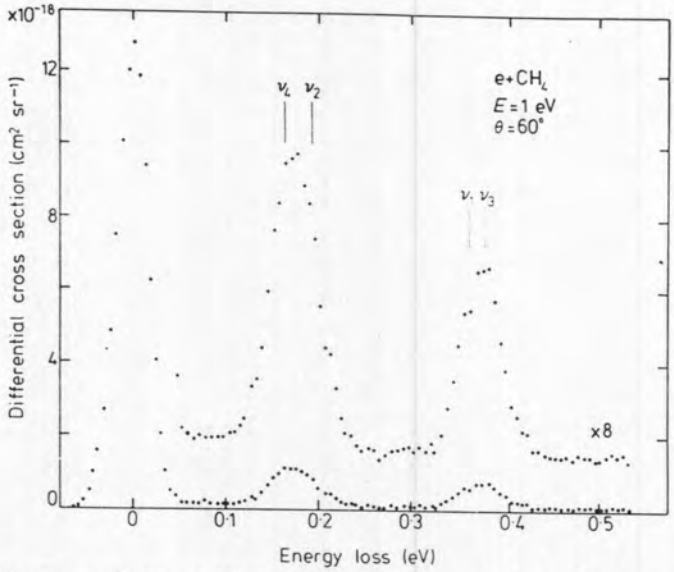

Fig. 94. Energy-loss spectrum of CH_4 in terms of cross sections at 1 eV impact energy and 60° scattering angle. Vibrational modes are indicated. (From ref. [277].)

Vušković and Trajmar [281] studied inelastic scattering by CH_4 in the 7.5 to 15.0 eV energy-loss region at 20, 30 and 200 eV impact energies. They divided the energy-loss spectrum into five segments, each corresponding to a number of unassigned electronic transitions. Differential (in angle) scattering intensities were measured for these sections and then converted to DCS with the help of the elastic cross sections determined by Tanaka et al. [278a] (at 20 and 30 eV) and to the theoretical results of Dhal et al. [278b] (at 200 eV). Tables 91 and 92 give the assignment of the inelastic segments and the corresponding inelastic DCS, respectively. Integral and momentum transfer cross sections obtained from these data are given in table 93.

4.20. Hydrocarbons

With the exception of CH_4 (which was discussed above separately), there are very little cross section data available on hydrocarbons. Most of the available data are concerned with ionization and fragmentation to excited atomic hydrogen or to various ions which are not the subject of the present review.

Hasted et al. [142] reported total electron scattering cross sections for C_2H_4 at a recent conference. Work on a large number of polyatomic molecules including hydrocarbons is in progress in their laboratory.

Table 91
Summary of notations and assignments for the inelastic cross sections of CH_4. (From Vušković and Trajmar [281].)

Region number	Energy-loss range (eV)
1	7.5–9.0
2	9.0–10.5
3	10.5–12.0
4	12.0–13.5
5	13.5–15.0

Table 92
Inelastic differential cross sections for CH_4, 10^{-19} cm^2/sr units. (From Vušković and Trajmar 1982, ref. [281].)[a]

	$E_0 = 20$ eV					$E_0 = 30$ eV				
θ (deg)	1	2	3	4	5	1	2	3	4	5
8						12.8	795	122	102	861
11						7.12	406	620	668	554
16						3.41	169	289	358	322
21	2.08	83.5	126	122	83.1	2.14	76.8	144	204	195
25	1.12	48.4	80.9	87.0	59.1	–	–	–	–	–
27	–	–	–	–	–	1.80	43.0	81.6	122	121
36	1.53	27.0	47.0	60.3	45.8	1.02	23.6	42.2	69.0	71.0
46	1.76	23.6	38.8	49.4	37.0	1.18	16.3	33.3	55.6	62.6
56	1.18	18.0	32.6	45.8	37.6	–	–	–	–	–
57	–	–	–	–	–	0.54	8.59	19.0	34.3	36.3
66	0.95	12.5	24.2	34.2	28.1	–	–	–	–	–
68	–	–	–	–	–	0.49	5.88	13.3	25.3	26.9
76	0.82	9.81	20.04	30.8	26.0	0.45	4.55	10.5	19.9	20.9
87	0.88	7.80	17.7	27.1	22.6	0.46	4.12	9.58	16.7	16.8
96	0.76	7.06	16.6	25.9	22.1	–	–	–	–	–
97	–	–	–	–	–	0.38	3.45	8.08	14.5	15.1
106	0.81	6.94	17.4	26.2	21.8	–	–	–	–	–
107	–	–	–	–	–	0.44	3.63	8.52	14.6	14.6
116	0.95	8.72	19.9	29.7	25.2	0.42	3.53	8.56	15.3	15.6
122	0.98	10.1	22.7	33.1	27.6	0.57	4.49	10.9	18.0	17.6
129	1.17	11.2	25.1	36.8	31.2	0.75	5.31	12.5	20.8	20.9

[a]See table 91 for notation and assignment.

	$E_0 = 200$ eV		
θ (deg)	2	3	4
8.3	396	860	1,540
11	116	324	681
13	31	100	248
14	28	91	219
17	15	41	98
19	14	35	74
23	9.7	24	43
24	8.5	21	38
29	3.9	10	18
39	1.0	2.9	5.4
48	0.52	1.5	2.8
60	0.26	0.73	1.4
69	0.17	0.48	0.90
80	0.096	0.32	0.66
90	0.098	0.28	0.57
110	0.036	0.17	0.41
122	0.046	0.16	0.37
129	0.037	0.15	0.35

Table 93
Inelastic integral (σ) and momentum transfer (σ^M) cross sections for CH_4, 10^{-16} cm^2 units. (From Vušković and Trajmar 1982, ref. [281].)

Region number	20 eV		30 eV		200 eV	
	σ	σ^M	σ	σ^M	σ	σ^M
1	0.0148	0.0132	0.0107	0.0079	–	–
2	0.242	0.164	0.263	0.104	0.091	0.0044
3	0.442	0.340	0.435	0.214	0.135	0.0097
4	0.568	0.478	0.647	0.357	0.299	0.002
5	0.443	0.393	0.578	0.354	–	–

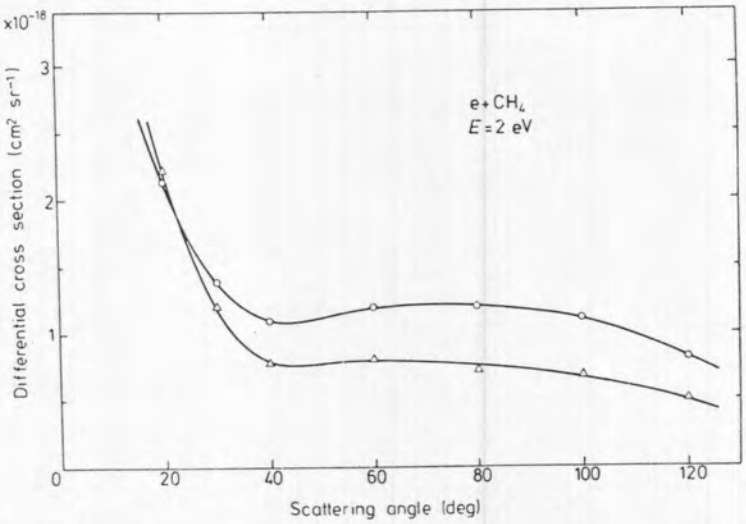

Fig. 95. Angular dependence of the vibrational excitation cross sections for CH_4 at 2 eV impact energy: △, ν_1 and ν_3; ○, ν_2 and ν_4 modes. (From ref. [277].)

Fink et al. [282] measured elastic electron scattering cross sections for C_2H_2, C_2H_4 and C_2H_6 in the 100 to 1000 eV impact energy region at angles ranging from 3° to 130°. Their results are given in tables 94–96. Differential elastic cross sections were also reported by Matsunaga et al. [283] for C_2H_6 and C_3H_8 from 3 to 20 eV impact energies. Their results are shown in fig. 102. Newell et al. [279] have reported differential elastic scattering measurements for C_2H_2 and C_2H_4 but no numerical results are available at present.

Vibrational excitation of C_2H_2 and C_2D_4 in the 1 to 11 eV impact energy range was studied by Walker et al. [284]. Strong vibrational excitation was found near 1.8 to 7.5 eV due to a resonance mechanism. Their results are shown in figs. 103–106. Resonant vibrational excitation of cis and trans-2 butene by low energy electrons (1 to 3 eV) was studied by Jung and Kadisch [285] but they obtained only relative differential cross sections. Kubo et al. [280] reported differential vibrational excitation measurements for C_2H_6 but no numerical data have been published.

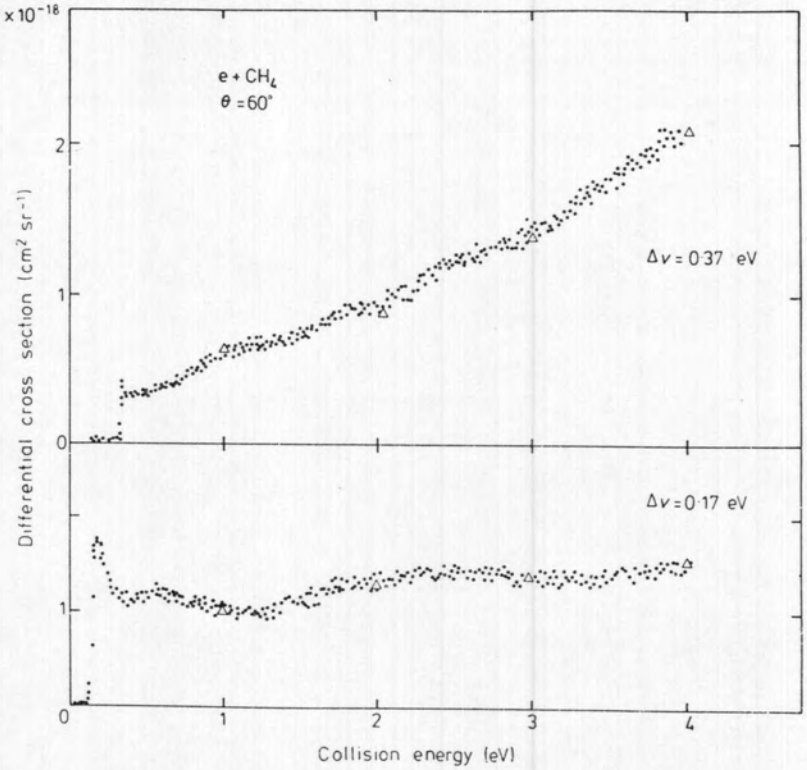

Fig. 96. Differential excitation functions for the (ν_1, ν_3) and (ν_2, ν_4) vibrations in CH_4 at 60° scattering angle. (From ref. [277].)

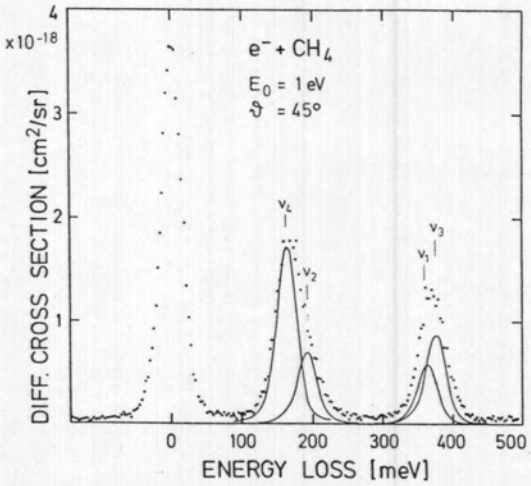

Fig. 97. Energy-loss spectrum of CH_4 in terms of cross sections at 1 eV impact energy and 45° scattering angle. Vibrational modes are indicated. (From ref. [276].)

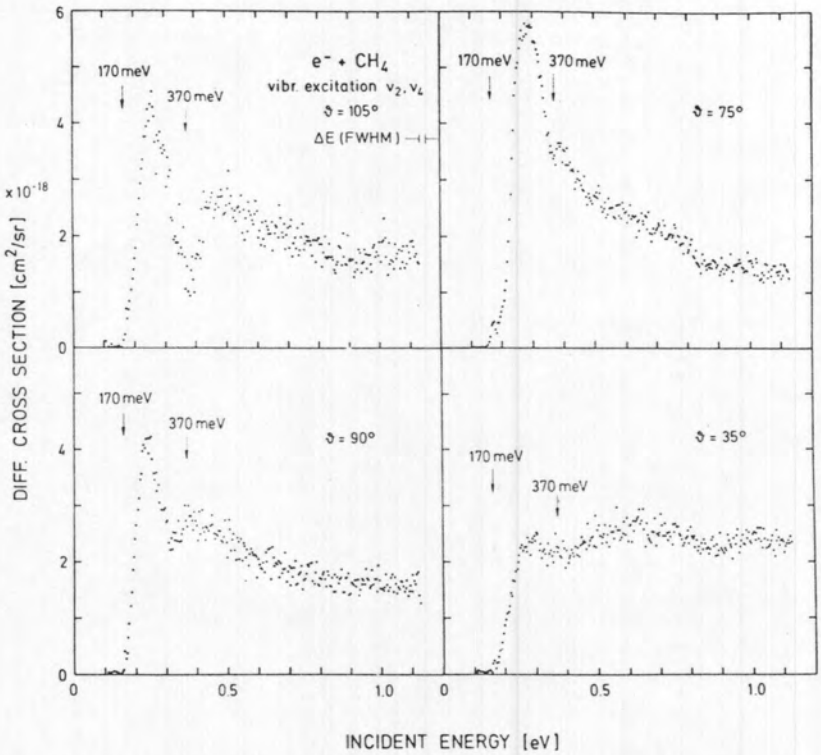

Fig. 98. Energy dependences of the (ν_2, ν_4) differential vibrational excitation cross sections for CH_4 at 105°, 90°, 75° and 35° scattering angles. Energy values refer to the energy-loss of the maximum of the unresolved (ν_2, ν_4) feature (170 meV) and the (ν_1, ν_3) feature (370 meV). (From ref. [276].)

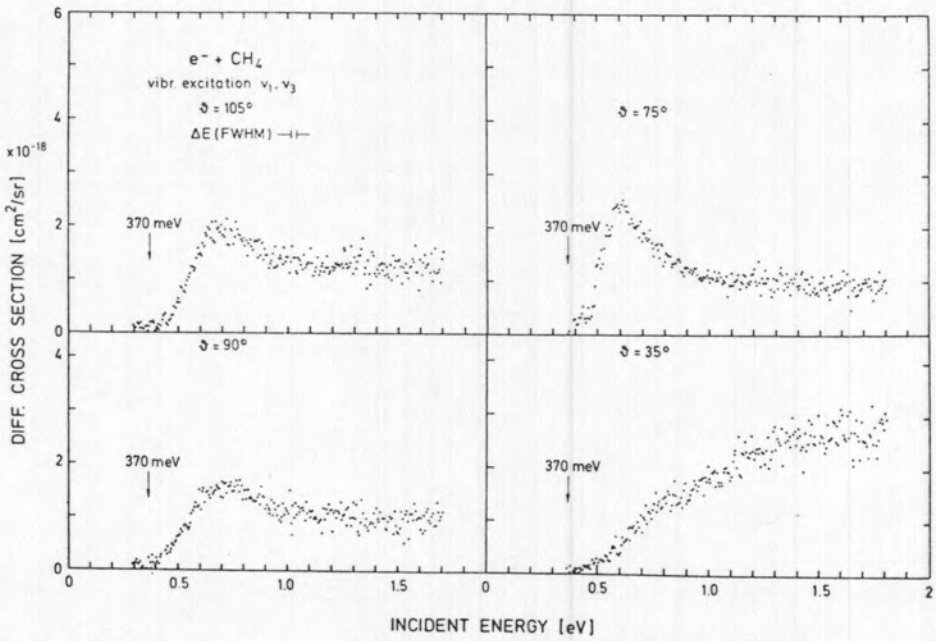

Fig. 99. Same as fig. 98 except for the ν_1, ν_3 unresolved vibrational excitations. (From ref. [276].)

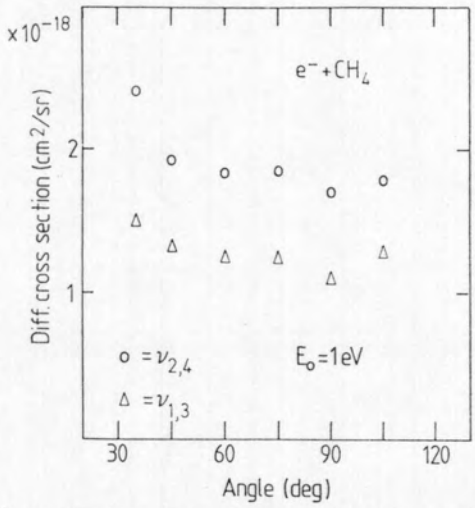

Fig. 100. Angular dependence of the (ν_2, ν_4) and (ν_1, ν_3) vibrational excitation cross sections for CH_4 at 1 eV impact energy. (From ref. [276].)

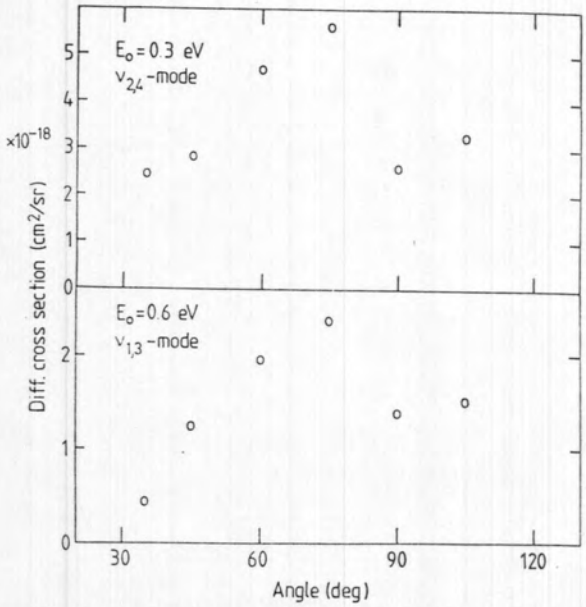

Fig. 101. Angular dependence of the (ν_2, ν_4) and (ν_1, ν_3) vibrational excitation cross sections for CH_4 at the impact energy corresponding to the near threshold peak. (From ref. [276].)

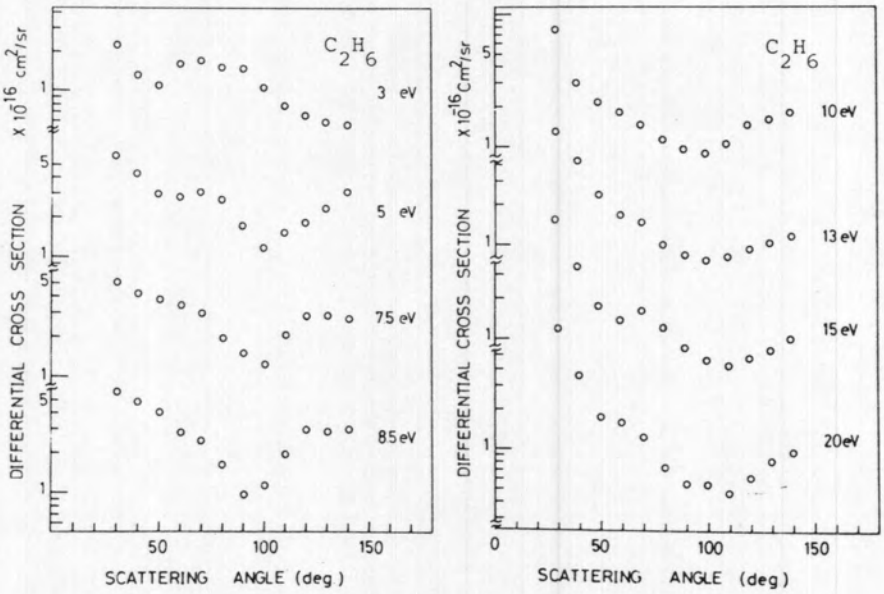

Fig. 102. Elastic differential scattering cross sections for C_2H_6 at impact energies of 3 to 20 eV. (From ref. [283].)

Table 94
Elastic scattering cross sections for C_2H_2, 10^{-16} cm^2/sr units. (From Fink et al. 1979, ref. [282].)

	E_0(eV)				
θ (deg)	100	200	400	600	1000
(0)	136.3	106	81.7	57.8	51.48
3	82.4	57.42	41.4	27.28	20.46
4	70.3	45.30	32.8	21.32	15.45
5	59.3	35.34	25.9	16.98	11.65
6	49.5	29.82	20.1	13.19	6.67
7	41.8	24.30	15.81	10.28	6.5
8	35.2	19.88	12.66	7.950	4.74
9	29.7	16.12	10.24	6.124	3.52
10	25.1	13.03	8.05	4.878	2.62
12	17.7	8.83	5.12	2.891	1.60
14	12.7	6.01	3.22	1.825	0.990
16	9.0	4.42	2.19	1.247	0.745
18	6.6	3.18	1.50	0.827	0.609
20	4.95	2.26	1.06	0.672	0.529
24	2.86	1.29	0.649	0.529	0.297
28	1.70	0.791	0.493	0.386	0.155
32	1.10	0.548	0.395	0.227	0.0935
36	0.74	0.426	0.279	0.147	0.0645
40	0.53	0.365	0.200	0.0975	0.0497
45	0.39	0.309	0.129	0.0676	0.0348
50	0.31	0.243	0.0904	0.0538	0.0226
55	0.27	0.183	0.0712	0.0424	0.0165
60	0.23	0.143	0.0603	0.0321	0.0132
65	0.185	0.115	0.0507	0.0242	0.0105
70	0.16	0.092	0.0411	0.0192	0.00790
80	0.129	0.072	0.0273	0.0136	0.00532
90	0.124	0.066	0.0203	0.01	0.00387
100	0.126	0.061	0.0170	0.0074	0.00300
110	0.132	0.057	0.0145	0.0061	0.00239
120	0.15	0.054	0.0129	0.0054	0.00197
130	0.17	0.051	0.0112	0.0049	0.00168

Table 95
Elastic scattering cross sections for C_2H_4, 10^{-16} cm^2/sr units. (From Fink et al. 1979, ref. [282].)

	E_0 (eV)				
θ (deg)	100	200	400	600	1000
(0)	222.0	147	101	66.5	68.4
3	130.9	78	44	27.7	23.4
4	108.8	63	33	21.8	17.4
5	91.9	49	25	17.4	12.4
6	79.4	38	19.4	13.2	8.45
7	65.4	31	14.6	9.6	5.7
8	55	25	11.3	7.0	4.0
9	46	19.6	8.6	5.4	3.0
10	38.8	15.8	6.4	4.1	2.2
12	26.5	10.2	3.8	2.4	1.45
14	18.5	6.5	2.4	1.66	1.03
16	12.9	4.1	1.7	1.2	0.75
18	8.75	2.9	1.26	0.92	0.59
20	6.1	2.2	0.99	0.74	0.48
24	3.3	1.31	0.66	0.53	0.28
28	2.0	0.88	0.48	0.36	0.142
32	1.4	0.64	0.37	0.23	0.092
36	1.0	0.50	0.27	0.14	0.068
40	0.765	0.41	0.18	0.099	0.048
45	0.54	0.32	0.12	0.075	0.031
50	0.44	0.24	0.091	0.058	0.022
55	0.37	0.18	0.076	0.040	0.0176
60	0.31	0.135	0.062	0.0295	0.0132
65	0.25	0.114	0.048	0.024	0.0099
70	0.19	0.100	0.037	0.020	0.00795
80	0.143	0.084	0.026	0.0142	0.0055
90	0.13	0.079	0.023	0.0099	0.0039
100	0.15	0.068	0.0174	0.0082	0.0030
110	0.154	0.056	0.0144	0.0068	0.00246
120	0.65	0.051	0.0126	0.0058	0.0021
130	0.18	0.053	0.0115	0.0051	0.00173

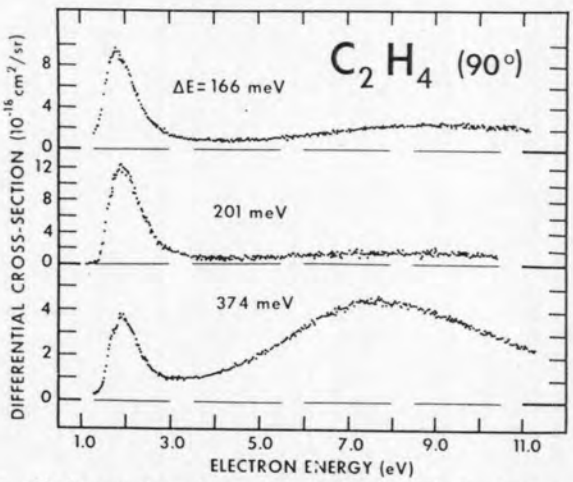

Fig. 103. Energy dependence of the differential 90° vibrational excitation cross sections in C_2H_4 corresponding to the ν_3 (E = 166 meV), ν_2 (E = 201 meV) and ν_1 (E = 374 meV) vibrational modes. (From ref. [284].)

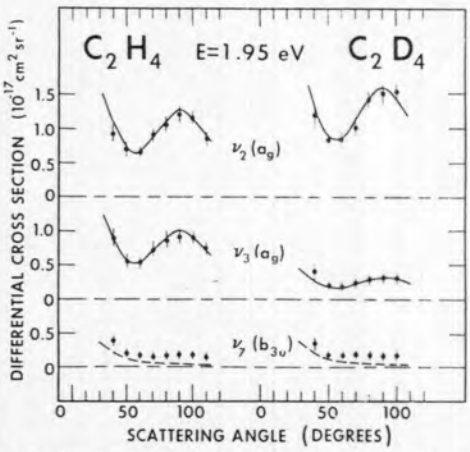

Fig. 104. Angular distributions of three strongly excited vibrational modes in C_2H_4 and C_2D_4 at 1.95 eV impact energy. (From ref. [284].)

Table 96
Elastic scattering cross sections for C_2H_6, 10^{-16} cm²/sr units. (From Fink et al. 1975, ref. [282].)

	E_0 (eV)				
θ (deg)	100	200	400	600	1000
(0)	336	246	163	139.3	52.6
3	180	114	62.8	49.4	16.09
4	146	86	46.2	34.2	10.83
5	118	68	34.5	24.1	7.169
6	104	56	24.6	17.1	4.828
7	86	41	18.5	11.4	3.365
8	68.7	32.2	13.7	7.92	2.633
9	57	25.2	9.97	5.57	2.209
10	46.4	19.2	7.39	4.05	1.961
12	31.3	11.21	4.37	2.66	1.609
14	21.4	6.586	3.02	1.996	1.126
16	13.9	4.241	2.28	1.52	0.863
18	9.3	2.897	1.87	1.178	0.673
20	6.1	2.276	1.516	0.887	0.527
24	3	1.586	0.991	0.558	0.275
28	2.11	1.155	0.678	0.368	0.160
32	1.54	0.879	0.462	0.222	0.105
36	1.188	0.672	0.316	0.1555	0.0663
40	0.911	0.503	0.216	0.1156	0.0474
45	0.714	0.352	0.156	0.0822	0.0347
50	0.571	0.234	0.122	0.0555	0.0253
55	0.464	0.172	0.0969	0.0411	0.0168
60	0.357	0.141	0.0734	0.0333	0.0137
65	0.214	0.124	0.0509	0.0272	0.0109
70	0.15	0.1121	0.0406	0.0218	0.00842
80	0.111	0.0914	0.0291	0.0147	0.00579
90	0.123	0.0759	0.0209	0.0110	0.00411
100	0.150	0.0610	0.0159	0.0083	0.00316
110	0.169	0.0496	0.0138	0.0070	0.00253
120	0.191	0.0524	0.0116	0.0061	0.00211
130	0.211	0.0548	0.0109	0.0053	0.00179

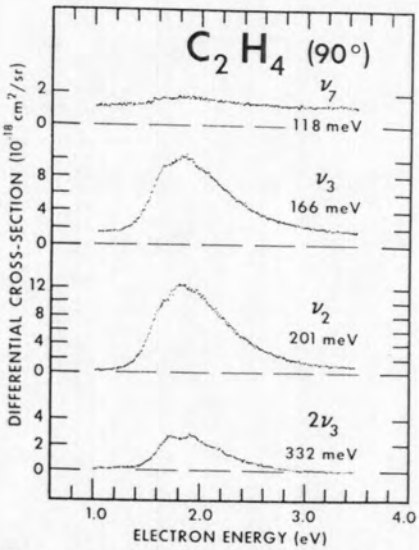

Fig. 105. Energy dependence of the 90° differential excitation cross sections for four vibrational modes (as indicated) in C_2H_4. (From ref. [284].)

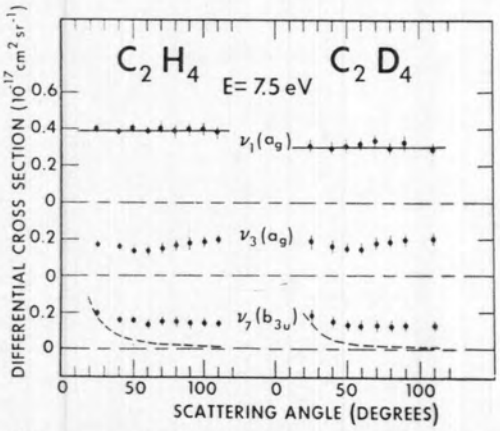

Fig. 106. Angular distribution for three strongly excited vibrational modes in C_2H_4 and C_2D_4 at 7.5 eV impact energy. (From ref. [284].)

4.21. Halocarbons

Recent interest in the role of halocarbons in atmospheric pollution has sparked some electron impact investigation of these molecules. Rohr [286] measured differential elastic scattering and vibrational excitation cross sections for CCl_2F_2 and CCl_3F (see figs. 107 and 108). He found excitation of the vibrational modes to be very sensitive to the halogen substitution. Differential elastic scattering cross section measurements were reported by Daimon et al. [272] in the 70 to 500 eV range for CCl_4 (see fig. 109; explanation is the same as for As_4, fig. 88).

Bonham and coworkers [287] have carried out total electron scattering cross sections for CCl_4, $CFCl_3$, CF_2Cl_2, $CClF_3$ and CF_4 but their results have not been published yet.

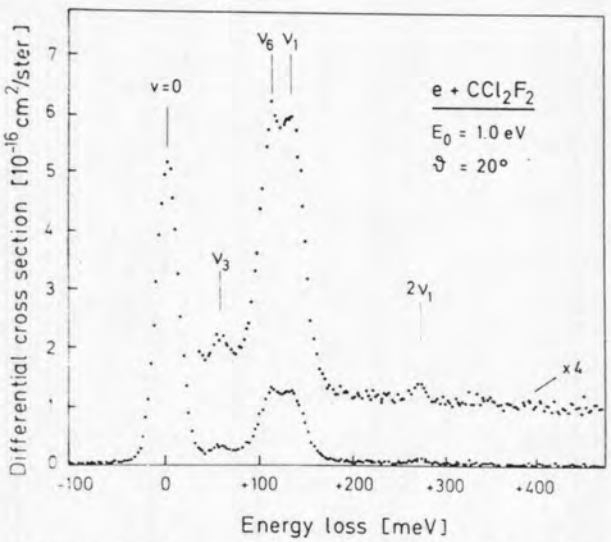

Fig. 107. Energy-loss spectrum of CCl_2F_2 in terms of differential cross sections at 1 eV impact energy and 20° scattering angle. (From ref. [286].)

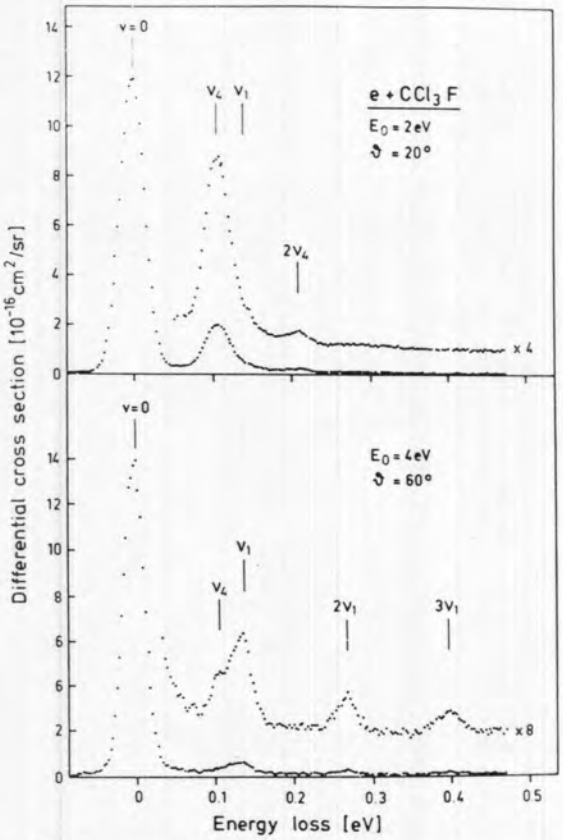

Fig. 108. Energy-loss spectra of CCl_3F in terms of differential cross sections at 2 eV, 20° and 4 eV, 60°. (From ref. [286].)

4.22. SF_6

There has been considerable experimental interest in SF_6 arising from the fact that its commercial use as a gaseous dielectric in high-voltage devices is increasing. Knowledge of its molecular scattering properties, including details of resonances, is useful in modeling swarm mixtures of SF_6 and N_2. The important electron-attachment resonance at zero electron energy is the basis of its use in electron scavenging experiments for detection of threshold electrons.

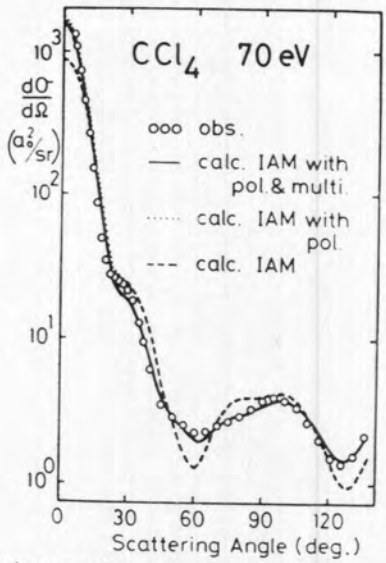

Fig. 109. Elastic scattering differential cross sections for CCl_4 at 70 eV impact energy. See text for explanation of curves. (From ref. [272].)

Accurate total cross sections using the time-of-flight method have been reported by Kennerly et al. [288] in the electron energy range 0.5–100 eV, and by Ferch et al. [289, 290] in the range 0.036–1.0 eV. These results are presented in figs. 110 and 111, respectively. There is excellent agreement between the two sets of data where they overlap. Additionally, Rohr [291] has measured differential elastic scattering crossing sections in a crossed-beam experiment in the energy range 0.3–10 eV. These are shown in figs. 112 and 113 as functions of collision energy and scattering angle, respectively. When one integrates these data and adds the integral vibrational excitation cross sections [292], one obtains excellent agreement with the time-of-flight data in the energy range 0.5–6 eV. This comparison is given in fig. 114.

Elastic scattering cross sections at higher energies, in the range 5–75 eV, have been reported by Srivastava et al. [293]. These results were renormalized to the more recent He standard, and the

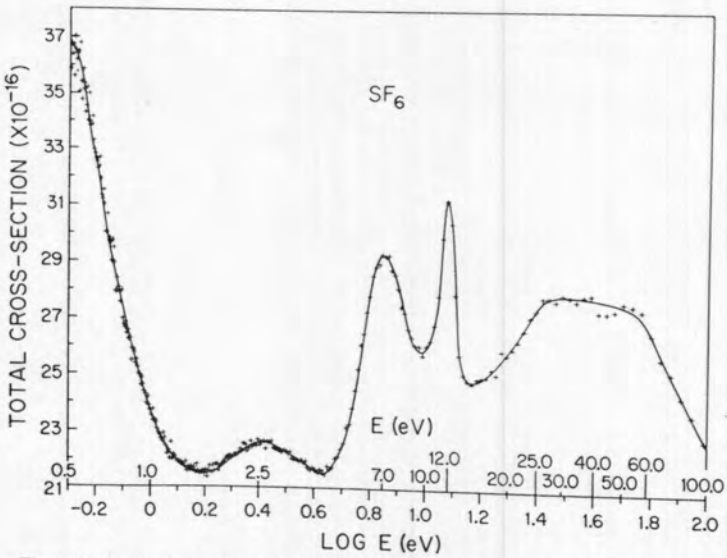

Fig. 110. Total electron scattering cross sections for SF_6. (From ref. [288].)

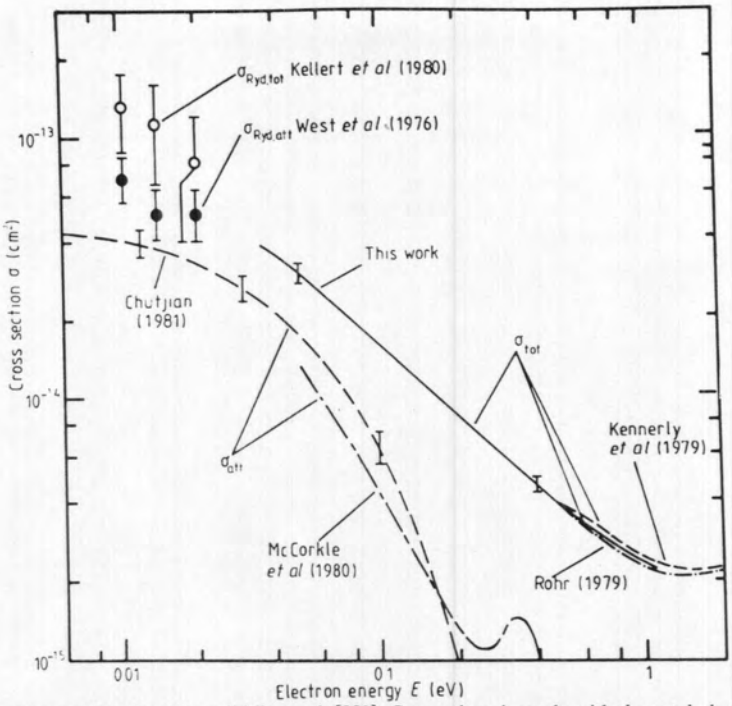

Fig. 111. Total electron scattering cross sections for SF_6: solid line, ref. [289]. Comparison is made with the total electron scattering cross sections (σ_{TOT}) of refs. [288 and 291], with electron attachment cross sections (σ_{att}) of refs. [295 and 296], and with total ($\sigma_{Ryd,tot}$) and attachment cross sections ($\sigma_{Ryd,att}$) for quasi free electrons of Rydberg atoms computed from rate constants, refs. [297] and [298], respectively. (From ref. [290].)

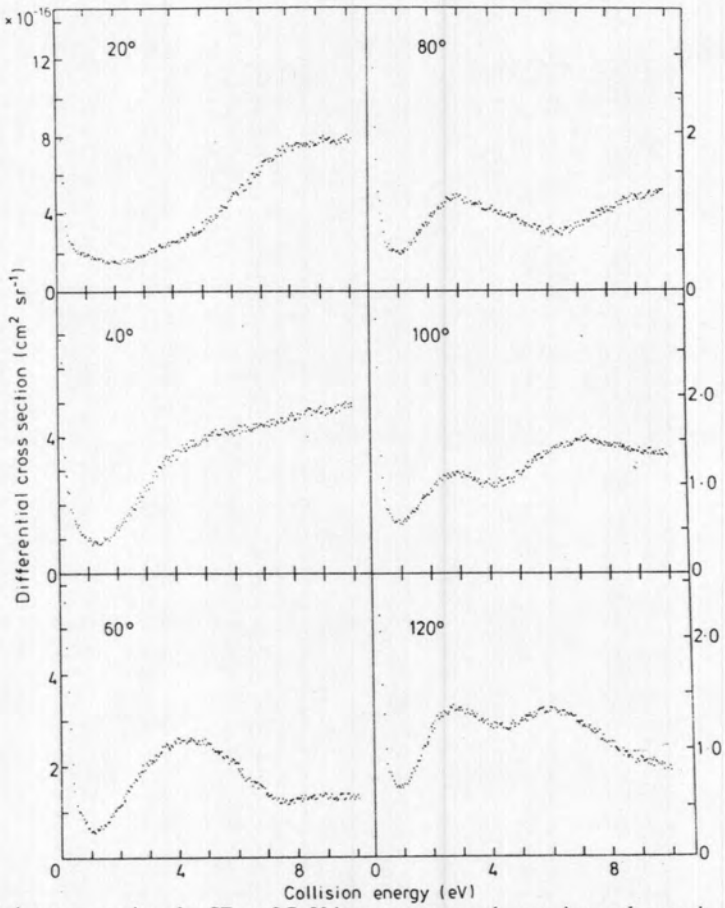

Fig. 112. Elastic differential scattering cross sections for SF_6 at 2.7 eV impact energy and scattering angles ranging from 20° to 120°. (From ref. [291].)

renormalized data are presented in tables 97 and 98. We note that the older data at 5 eV lay 35% below the integral elastic data of ref. [291, fig. 5]. The renormalized results (table 98) are now within the combined experimental errors of the two sets of data.

Vibrational excitation cross sections have been reported by Rohr [292] in the electron energy range 0.05–3 eV. These have been placed on a cross section scale by normalization to the earlier data of Srivastava et al. at 5 and 10 eV. The vibrational cross sections should be multiplied by factors 1.28 (5 eV) and 1.15 (10 eV) to correspond to the renormalized results of table 98. Finally, some fragmentary results for resonance-enhanced excitations of the ν_1 mode (with admixed ν_2 and ν_3-mode contributions) are given in Trajmar and Chutjian [294] at 9, 12 and 15 eV electron energy.

Table 97
Differential elastic scattering cross sections for SF_6. Units are 10^{-16} cm^2/sr. Entries by angles in parentheses refer to extrapolated values. (From Srivastava et al. 1976, ref. [293].)[a]

	E_0 (eV)								
θ (deg)	5	10	15	20	30	40	50	60	75
(0)	3.4	9.2	8.4	7.9	23	19	19	13	4.8
(5)	3.2	8.5	7.8	7.0	19	15	14	10	4.3
(10)	3.0	7.6	7.2	5.8	15	11	11	7.6	3.8
(15)	2.8	6.6	6.4	4.8	10	8.3	7.5	5.4	3.2
20	2.36	5.82	5.49	4.06	8.31	5.97	5.00	3.51	2.66
25	2.08	4.69	4.41	2.78	4.01	3.55	2.75	2.28	1.86
30	2.04	3.85	3.53	1.82	2.03	2.02	1.60	1.70	1.61
35	2.03	3.21	2.41	1.20	1.25	1.27	1.16	1.63	1.29
40	2.32	2.56	1.56	0.871	0.879	1.02	1.10	1.30	0.930
45	2.51	2.15	1.17	0.657	0.748	0.994	0.857	0.888	0.658
50	2.33	1.53	0.873	0.679	0.927	0.949	0.705	0.672	0.466
55	2.16	1.14	0.709	0.762	1.15	0.862	0.590	0.482	0.343
60	1.84	0.918	0.778	0.940	0.954	0.763	0.491	0.364	0.249
65	1.49	0.884	0.970	1.19	0.795	0.475	0.311	0.288	0.210
70	1.15	0.806	1.10	1.40	0.617	0.321	0.250	0.237	0.178
75	0.954	1.11	1.28	1.35	0.493	0.211	0.191	0.201	0.146
80	0.869	1.26	1.19	1.14	0.406	0.163	0.129	0.192	0.144
85	0.913	1.39	1.08	0.990	0.326	0.145	0.183	0.219	0.146
90	1.00	1.37	0.966	0.784	0.284	0.152	0.221	0.233	0.157
95	1.18	1.22	0.851	0.636	0.295	0.175	0.231	0.251	0.132
100	1.24	1.10	0.832	0.620	0.347	0.256	0.244	0.255	0.115
105	1.35	0.958	0.640	0.465	0.373	0.297	0.246	0.188	0.126
110	1.45	0.808	0.638	0.548	0.453	0.375	0.250	0.175	0.154
115	1.37	0.684	0.619	0.582	0.509	0.425	0.250	0.192	0.183
120	1.34	0.645	0.638	0.629	0.563	0.494	0.298	0.201	0.215
125	1.15	0.733	0.612	0.586	0.585	0.533	0.339	0.241	0.267
130	0.993	0.728	0.706	0.684	0.657	0.599	0.400	0.316	0.343
135	0.849	0.953	0.866	0.883	0.842	0.668	0.608	0.589	0.428
(140)	0.88	1.1	0.96	0.99	0.99	0.72	0.49	0.51	0.50
(150)	0.91	1.3	1.2	1.3	1.3	0.84	0.76	0.74	0.72
(160)	1.0	1.6	1.4	1.5	1.5	0.96	0.94	1.0	0.97
(170)	1.2	1.8	1.5	1.8	1.7	1.0	1.1	1.3	1.2
(180)	1.3	1.9	1.6	1.9	1.8	1.0	1.2	1.5	1.4

[a]The cross section values have been recalculated on the basis of the recent He cross sections of ref. [10].

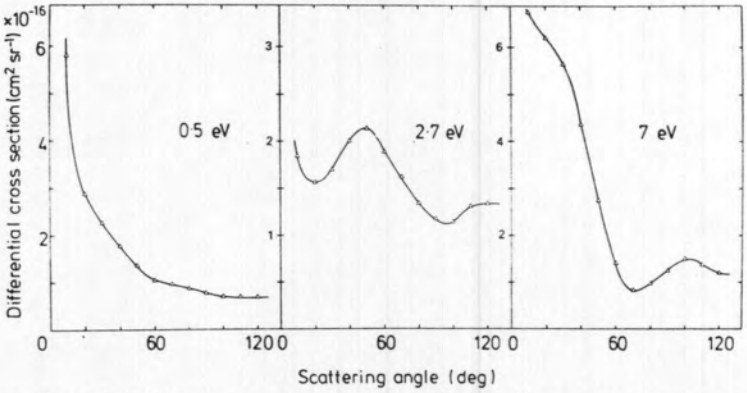

Fig. 113. Angular dependence of elastic scattering cross sections for SF_6 at 0.5, 2.7 and 7 eV impact energies. (From ref. [291].)

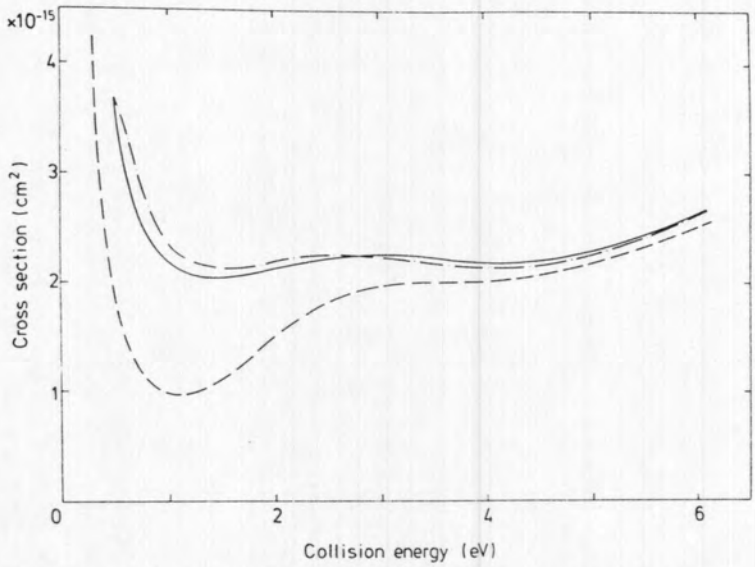

Fig. 114. Energy dependence of the integral elastic scattering cross section for SF_6 (lower dashed line). The sum of the integral elastic and vibrational excitation cross sections (upper dashed line) are compared with the total electron scattering cross sections of ref. [288]. (From ref. [291].)

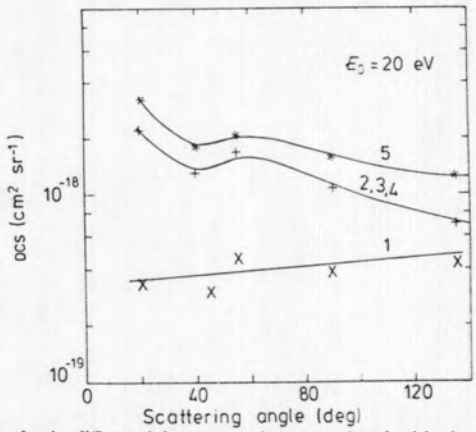

Fig. 115. Inelastic differential cross sections associated with the 9.8, 11.0, 11.6, 12.8 and 13.3 eV energy-loss features in the spectrum of SF_6 (indicated as 1, 2, 3, 4 and 5 respectively) at 20 eV impact energy. (From ref. [294].)

Table 98

Elastic integral (σ) and momentum-transfer (σ^M) cross sections for SF_6. Units are 10^{-16} cm^2. (From Srivastava et al. 1976, ref. [293].)[a]

E_0 (eV)	σ	σ^M
5	17.9	14.9
10	19.5	14.1
15	16.4	12.0
20	14.0	11.5
30	15.0	9.46
40	11.7	6.82
50	10.0	5.69
60	8.86	5.51
75	6.58	4.79

[a]Obtained from the differential cross sections of table 97.

Partial results for excitation of electronic states at SF_6 may also be found in ref. [294], and are given here in fig. 115. These data are based on the older SF_6 elastic data, and should be multiplied by the appropriate differential cross section factors as given by the older data and those of table 97.

4.23. UF_6

Electron scattering measurements were carried out in UF_6 prompted by the importance of this gaseous species in gas-core reactors, nuclear-pumped lasers and in isotope separation schemes. The original elastic differential scattering cross sections of Srivastava et al. [293] have been renormalized to the more recent He elastic cross sections [10]. Differential and integrated results are presented in tables 99 and 100, respectively.

Table 99
Elastic differential cross sections for UF_6. Units are 10^{-16} cm^2/sr. Entries by angles in parentheses refer to extrapolated values. (From Srivastava et al. 1976, ref. [293].)[a]

	E_0 (eV)							
θ (deg)	10	15	20	30	40	50	60	75
(0)	8.0	19	42	10	27	31	5.5	7.6
(5)	7.0	17	36	9.2	23	26	4.9	6.5
(10)	6.0	14	30	8.2	18	20	4.4	5.3
(15)	5.1	11	23	7.2	14	15	3.7	4.3
20	4.45	8.73	17.6	6.21	10.6	11.5	6.79	3.27
25	3.63	6.67	10.6	5.02	3.79	3.85	2.08	2.45
30	2.75	4.90	5.65	3.29	1.68	2.15	1.75	1.75
35	2.60	3.62	3.11	2.04	1.54	1.81	1.46	1.17
40	1.91	2.35	1.86	1.59	1.47	1.71	1.11	0.814
45	1.64	1.78	1.28	1.40	1.23	1.18	0.725	0.566
50	1.09	1.29	1.19	1.23	1.04	0.820	0.478	0.420
55	0.821	1.01	1.25	1.05	0.756	0.557	0.326	0.320
60	0.574	0.949	1.36	0.818	0.603	0.440	0.276	0.257
65	0.479	1.11	1.46	0.668	0.570	0.458	0.343	0.217
70	0.431	1.38	1.48	0.514	0.580	0.461	0.257	0.194
75	0.447	1.55	1.47	0.422	0.456	0.394	0.187	0.176
80	0.479	1.45	1.33	0.370	0.386	0.307	0.135	0.175
85	0.491	1.41	1.13	0.317	0.306	0.226	0.116	0.187
90	0.526	1.27	0.909	0.293	0.261	0.162	0.113	0.190
95	0.528	1.15	0.830	0.339	0.256	0.171	0.115	0.199
100	0.506	0.958	0.676	0.428	0.275	0.183	0.121	0.229
105	0.477	0.847	0.534	0.406	0.263	0.189	0.142	0.260
110	0.450	0.846	0.590	0.444	0.298	0.250	0.193	0.317
115	0.434	0.767	0.601	0.460	0.327	0.380	0.308	0.373
120	0.434	0.770	0.638	0.500	0.447	0.524	0.426	0.404
125	0.424	0.783	0.617	0.544	0.560	0.690	0.552	0.449
130	0.383	0.980	0.684	0.644	0.708	0.801	0.610	0.476
135	0.408	1.53	0.967	0.910	0.929	0.949	0.652	0.479
(140)	0.44	1.4	0.91	0.90	1.0	1.0	0.72	0.53
(150)	0.52	1.9	1.1	1.2	1.3	1.2	0.82	0.58
(160)	0.61	2.2	1.4	1.4	1.6	1.3	0.88	0.60
(170)	0.68	2.5	1.5	1.6	1.7	1.4	0.90	0.62
(180)	0.72	2.6	1.6	1.7	1.8	1.4	0.92	0.63

[a]The cross section values have been recalculated on the basis of the recent He cross sections of ref. [10].

Table 100
Elastic integral (σ) and momentum-transfer (σ^M) cross sections for UF_6. Units are 10^{-16} cm^2. (From Srivastava et al. 1976, ref. [293].)[a]

E_0 (eV)	σ	σ^M
10	11.8	6.82
15	24.1	16.9
20	28.1	12.9
30	14.2	9.28
40	16.1	9.04
50	16.2	8.39
60	7.66	5.72
75	7.48	4.98

[a]Obtained from the differential cross sections of table 99.

Studies have also been made of the electronic excitations in UF_6 by Chutjian et al. [299]. Cross sections for these excitations are currently being evaluated [300].

4.24. Other polyatomic molecules

A large number of organic molecules has been investigated by electron scattering techniques. These investigations were in most cases spectroscopic in nature aimed at locating low-lying metastable states [31, 32, 301]. The energy-loss spectra generated in these studies represent relative scattering intensities which could be transformed into cross sections if absolute values for any of the processes involved were to become available. In these complex molecules resolution of rotational structure is not expected, and resolution of vibrational structure will be difficult. Electronic-state excitations lead to complex dissociative and ionization processes and the interpretation of experimental observations will require the application of a number of complementary techniques.

Acknowledgements

We would like to express our gratitude to L. Andrič, Th. Antoni, L. Boesten, R. Bonham, I. Cadez, H. Ehrhardt, J. Ferch, R.I. Hall, J.B. Hasted, R. Jones, K.K. Jung, A.M. Kadisch, K.H. Kochem, M. Kubo, C. Masche, D. Matsunaga, R. Muller, T. Okada, W. Raith, K. Schroder, W. Sohn, T. Suzuki, H. Tanaka, L. Vušković, M. Zubek for making available to us unpublished results and to our many colleagues whose published data we have quoted here. One of us (S.T.) would like to acknowledge valuable discussions with D.G. Truhlar and (A.C.) would like to thank E. Beaty and J. Gallagher for their comments and assistance on part of this review.

References

[1] H.S.W. Massey, E.H.S. Burhop and H.B. Gilbody, Electronic Ionic Impact Phenomena Vol. II: Electronic Collisions with Molecules and Photoionization, H.S.W. Massey (Clarendon Press, Oxford, 1969).

[2] L.J. Kieffer, At. Data 2 (1971) 293.
[3] L.J. Kieffer, At. Data 1 (1969) 19.
[4] L.J. Kieffer, At. Data 1 (1969) 121.
[5] L.J. Kieffer, JILA Report ICR 13, September 30, 1973.
[6] G.J. Schulz, A Review of Vibrational Excitation of Molecules by Electron Impact at Low Energies, in: Principles of Laser Plasmas, ed. G. Bekefi (John Wiley and Sons, New York, 1976) Chapter 2. Also reprinted in: Electron Molecule Scattering, ed. S.C. Brown (John Wiley and Sons, New York, 1979) Chapter 1.
[7] D.E. Golden, N.F. Lane, A. Temkin and E. Gerjuoy, Rev. Mod. Phys. 43 (1971) 642.
[8] M. Hayashi, Recommended Values of Transport Cross Sections for Elastic Collision and Total Collision Cross Section for Electrons in Atomic and Molecular Gases, Report IPPJ-AM-19, Inst. Plasma Phys., Nagoya Univ., Japan, November 1981.
[9] S. Trajmar and D.F. Register, Experimental Techniques for Cross Section Measurements, in: Electron Molecule Collisions, eds. I. Shimamura and K. Takayanagi (Plenum Press, New York, 1982).
[10] D.F. Register, S. Trajmar and S.K. Srivastava, Phys. Rev. A 21 (1980) 1134.
[11] R.N. Compton and J.N. Bardsley, Dissociation of Molecules by Slow Electrons, in: Electron Molecule Collisions, eds. K. Takayanagi and I. Shimamura (Plenum Press, New York, 1982).
[12] R.A. Bonham and M. Fink, High Energy Electron Scattering (Von Nostrand Reinhold Co., New York, 1974).
[13] C.E. Brion and A. Hamnett, The Excited State in Chemical Physics Vol. 2; Advances in Chem. Phys. Vol. 45, Part 2 (John Wiley, New York, 1980).
[14] M.J. van der Wiel, Electron Energy Deposition in Matter at the Molecular Level, in: Radiation Research, Biomedical, Chemical and Physical Prospective (Acad. Press, Inc., New York, 1975) p. 205.
[15] F.H. Read, J. de Physique 39 (1978) C1–82.
[16] C.E. Brion and coworkers, see e.g. J. Electr. Spectr. Rel. Phenom. 14 (1978) 417.
[17] M.J. Van der Wiel, Electronic and Atomic Collisions, XIth ICPEAC, eds. N. Oda and K. Takayanagi (North-Holland Publishing Co., Amsterdam, 1980) p. 209.
[18] K. Blum and H. Kleinpoppen, Physics Reports 52 (1979) 203.
[19] J.W. McConkey, Symposium on Electron–Molecule Collisions, Invited Papers, eds. I. Shimamura and M. Matsuzawa (University of Tokyo, Tokyo, 1979) p. 163.
[20] I. Malcolm and J.W. McConkey, J. Phys. B: Atom. Molec. Phys. 12 (1979) L67.
[21] N. Bose and F. Linder, Symposium on Electron–Molecule Collisions, Invited Papers, eds. I. Shimamura and M. Matsuzawa (University of Tokyo, Tokyo, 1979) p. 179.
[22] M. Gavrila and M. Van der Wiel, Comments Atom. Molec. Phys. 8 (1978) 1.
[23] I.V. Hertel and W. Stoll, Advances in Atom. and Molec. Phys., eds. D.R. Bates and B. Bederson (Academic Press, New York, 1977) p. 113.
[24] L.J. Kieffer and G.H. Dunn, Electron Impact Ionization Cross Section Data for Atoms, Atomic Ions and Diatomic Molecules: I. Experimental Data, JILA Report No. 51, October 1965.
[25] L.J. Kieffer, A Compilation of Critically Evaluated Electron Impact Ionization Cross Section Data for Atoms and Diatomic Molecules, JILA Report No. 30, February 1965.
[26] Electron Molecule Collisions, eds. K. Takayanagi and I. Shimamura (Plenum Press, New York, 1982).
[27] D.E. Golden, Advances in Atomic and Molecular Physics 14 (1978) 1.
[28] P.J. Chantry, Electronic and Atomic Collisions, Xth ICPEAC, ed. G. Watel (North-Holland Publishing Co., Amsterdam, 1978) p. 23.
[29] R.I. Hall, Electronic and Atomic Collisions, Xth ICPEAC, ed. G. Watel (North-Holland Publishing Co., Amsterdam, 1978) p. 25.
[30] B. Buckley, Physics Reports (to appear).
[31] S. Trajmar, Acc. of Chem. Res. 13 (1980) 14.
[32] R.J. Celotta and R.H. Huebner, Electron Impact Spectroscopy: An Overview of the Low-Energy Aspects, in: Electron Spectroscopy Theory Techniques and Application Vol. 3, eds. C.R. Brundle and A.D. Barker (Acad. Press, New York, 1979).
[33] D.C. Cartwright, S. Trajmar, W. Williams and D.L. Huestis, Phys. Rev. Lett. 27 (1971) 704.
[34] W.A. Goddard III, D.L. Huestis, D.C. Cartwright and S. Trajmar, Chem. Phys. Lett. 11 (1971) 329.
[35] (a) V.F. Sokolov and Y.A. Sokolova, Sov. Tech. Phys. Lett. 7 (1982) 268.
(b) E. Schultes, R. Schumacher and R.N. Schindler, Z. Naturforsch. 29A (1974) 239.
[36] G.J. Schulz, Phys. Rev. 112 (1958) 150.
[37] L.G.H. Huxley and R.W. Crompton, The Diffusion and Drift of Electrons in Gases (John Wiley and Sons, New York, 1974).
[38] Y. Itikawa, Momentum Transfer Cross Sections for Electron Collisions on Atoms and Molecules and their Application to Effective Collision Frequencies, Argonne National Laboratory Report, ANL-7939, April 1972.
[39] F.E. Spencer Jr. and A.V. Phelps, Proc. 15th Symp. of Engineering Aspects of Magnetohydrodynamics, University of Pennsylvania, Philadelphia, May 1976 and private communication.
[40] A. Chutjian, J. Chem. Phys. 61 (1974) 4279; Rev. Sci. Instr. 50 (1979) 347.
[41] R.T. Brinkmann and S. Trajmar, J. Phys. E: Sci. Instr. 14 (1981) 245.
[42] S.K. Srivastava, A. Chutjian and S. Trajmar, J. Chem. Phys. 63 (1975) 2659.
[43] P.R. Bevington, Data Reduction and Error Analysis for the Physical Sciences (McGraw-Hill, New York, 1969).
[44] H.L. Alder and E.B. Roessler, Introduction to Probability and Statistics (4th ed., W.H. Freeman and Co., San Francisco, 1968).
[45] D. Andrick and A. Bitsch, J. Phys. B: Atom. Molec. Phys. 8 (1975) 393.

[46] N.C. Steph, L. McDonald and D.E. Golden, J. Phys. B: Atom. Molec. Phys. 12 (1979) 1507.
[47] J.F. Williams, J. Phys. B: Atom. Molec. Phys. 12 (1979) 265.
[48] C.E. Brion, Radiation Research 64 (1975) 37.
[49] M.J. Van der Wiel, Electronic and Atomic Collisions, XIth ICPEAC, eds. N. Oda and K. Takayanagi (North-Holland Publishing Co., Amsterdam, 1980) p. 209.
[50] F.H. Read and G.C. King, Symp. on Electron Molecule Collisions, eds. I. Shimamura and M. Matsuzawa (University of Tokyo, Tokyo, Japan, 1979) p. 155.
[51] F.H. Read, The Physics of Ionized Gases, ed. M. Matec (Boris Kidric Institute of Nuclear Sciences, Beograd, Yugoslavia, 1980) p. 33.
[52] J.W. McConkey, Symposium on Electron–Molecule Collisions, Invited Papers, eds. I. Shimamura and M. Matsuzawa (University of Tokyo, Tokyo, 1979) p. 163.
[53] Coherence and Correlation in Atomic Collisions, eds. H. Kleinpoppen and J.F. Williams (Plenum Press, New York, 1979).
[54] J. Macek and D.J. Jaeks, Phys. Rev. A4 (1971) 2288.
[55] U. Fano and J. Macek, Rev. Mod. Phys. 45 (1973) 553.
[56] K. Blum and J. Jakubowicz, J. Phys. B: Atom. Molec. Phys. 11 (1978) 909.
[57] I.C. Malcolm and J.W. McConkey, J. Phys. B: Atom. Molec. Phys. 12 (1979) L167.
[58] A. Pochat, D. Rozuel and J. Peresse, J. Physique 34 (1973) 701.
[59] A. Chutjian, R. Hippler, I. McGregor and H. Kleinpoppen, XIth ICPEAC, eds. N. Oda and K. Takayanagi (North-Holland Publ. Co., Amsterdam, 1980) p. 172.
[60] L. Frost and E. Weigold, Phys. Rev. Lett. 45 (1981) 247.
[61] N.D. Bhaskar, B. Jaduszliver and B. Bederson, Phys. Rev. Lett. 38 (1977) 14.
[62] B. Jaduszliver, R. Dang, P. Weiss and B. Bederson, Coherence and Correlation in Atomic Collisions, eds. H. Kleinpoppen and J.F. Williams (Plenum Press, New York, 1980) p. 613.
[63] D.F. Register, S. Trajmar, S.W. Jensen and R.T. Poe, Phys. Rev. Lett. 41 (1978) 749.
[64] I.V. Hertel and W. Stoll, Advances in Atomic and Molecular Physics, eds. D.R. Bates and B. Bederson (Academic Press, New York, 1977) p. 113.
[65] M. Gavrila and M.J. Van der Wiel, Comments Atom. Molec. Phys. 8 (1978) 1;
A. Weingartshofer, J.K. Holmes, J. Sabbagh and S.L. Chin, J. Phys. B: At. Mol. Phys. 16 (1983) 1805.
[66] A. Weingartshofer, E.M. Clarke, J.K. Holmes and C. Jung, Phys. Rev. A 19 (1979) 2371.
[67] C. Jung, Phys. Rev. A 20 (1979) 1585.
[68] C. Jung and H. Kruger, Z. für Phys. A287 (1978) 7.
[69] C. Jung and H.S. Taylor, Phys. Rev. A 23 (1981) 1115.
[70] J. Geiger, J. Chem. Phys. 50 (1969) 7.
[71] H. Boersch, J. Geiger and W. Stickel, Z. für Phys. 180 (1964) 415.
[72] J.P. Bromberg, J. Chem. Phys. 61 (1974) 963.
[73] E.N. Lassettre, A.S. Berman, S.M. Silverman and M.E. Krasnow, J. Chem. Phys. 40 (1964) 1232;
A.M. Skerbele and E.N. Lassettre, J. Chem. Phys. 40 (1964) 1271.
[74] W.R. Newell, Optical Oscillator Strengths by Electron Impact Spectroscopy, in: Atomic Spectroscopy, eds. W. Hanle and H. Kleinpoppen (Plenum Press, New York, 1979).
[75] M. Inokuti, Rev. Mod. Phys. 43 (1971) 297.
[76] H.A. Bethe, Ann. Phys. (Leipz.) 5 (1930) 325.
[77] E.N. Lassettre, A. Skerbele and M.A. Dillon, J. Chem. Phys. 50 (1969) 1829.
[78] J. Ferch, W. Raith and K. Schröder, J. Phys. B: Atom. Molec. Phys. 13 (1980) 1481, and private communication (1981).
[79] G. Dalba, P. Fornasini, I. Lazzizzera, G. Ranieri and A. Zecca, J. Phys. B: Atom. Molec. Phys. 13 (1980) 2839.
[80] B. van Wingerden, R.W. Wagenaar and F.J. de Heer, J. Phys. B: Atom. Molec. Phys. 13 (1980) 3481.
[81] R. Jones and R.A. Bonham, private communication (1981).
[82] K.R. Hoffman, M.S. Dababneh, Y.F. Hsieh, W.E. Kauppila, V. Pol. J.H. Smart and T.S. Stein, Phys. Rev. A 25 (1982) 1393.
[83] D.E. Golden, H.W. Bandel and J.A. Salerno, Phys. Rev. 146 (1966) 40.
[84] F. Linder and H. Schmidt, Z. Naturforsch. 26a (1971) 1603.
[85] B. van Wingerden, E. Weigold, F.J. de Heer and K.J. Nygaard, J. Phys. B: Atom. Molec. Phys. 10 (1977) 1345.
[86] D.K. Gibson, Australian J. Phys. 23 (1970) 683.
[87] R.W. Crompton, D.K. Gibson and A.I. McIntosh, Austr. J. Phys. 22 (1969) 715.
[88] H. Ehrhardt, D.L. Langhans, F. Linder and H.S. Taylor, Phys. Rev. 173 (1968) 222.
[89] D. Rapp and P.J. Englander-Golden, J. Chem. Phys. 43 (1965) 1464.
[90] C.R. Lloyd, P.J.O. Teubner, E. Weigold and B.R. Lewis, Phys. Rev. A 10 (1974) 175.
[91] A. Weingartshofer, H. Ehrhardt, V. Hermann and F. Linder, Phys. Rev. A 2 (1970) 294.
[92] M. Fink, K. Jost and D. Hermann, Phys. Rev. A 12 (1975) 1374.
[93] T.W. Shyn and W.E. Sharp, Phys. Rev. A 24 (1981) 1734.
[94] J.W. McConkey and J.A. Preston, J. Phys. B: Atom. Molec. Phys. 8 (1975) 63.
[95] R.H.J. Jansen, F.J. de Heer, H.J. Lyken, B. van Wingerden and H.G. Blaauw, J. Phys. B: Atom. Molec. Phys. 9 (1976) 185.
[96] R.W. LaBahn and J. Callaway, Phys. Rev. A 2 (1970) 366.

[97] G.R. Freeman and T. Wada, XIIth Int. Conf. on the Physics of Electronic and Atomic Collisions, Gatlinburg, 1981, Abstracts of Contributed Papers, p. 357.
[98] S.F. Wong and G.J. Schulz, Phys. Rev. Lett. 32 (1974) 1089.
[99] S.K. Srivastava, R.I. Hall, S. Trajmar and A. Chutjian, Phys. Rev. A 12 (1975) 1399.
[100] K. Takayanagi and Y. Itikawa, Advances in Atomic and Molecular Physics 6 (1970) 15.
[101] D.E. Golden, N.F. Lane, A. Temkin and E. Gerjuoy, Rev. Mod. Phys. 43 (1971) 642.
[102] R.W. Crompton, D.K. Gibson and A.G. Robertson, Phys. Rev. A 2 (1970) 1386.
[103] S. Trajmar, D.G. Truhlar, J.K. Rice and A. Kuppermann, J. Chem. Phys. 52 (1970) 4516.
[104] E.S. Chang and S.F. Wong, Phys. Rev. Lett. 38 (1977) 1327.
[105] E.S. Chang and U. Fano, Phys. Rev. A 6 (1972) 173.
[106] C. Ramsauer and R. Kollath, Ann. Phys. 12 (1932) 529.
[107] S. Trajmar, D.C. Cartwright, J.K. Rice, R.T. Brinkmann and A. Kuppermann, J. Chem. Phys. 49 (1968) 5464.
[108] A. Weingartshofer, E.M. Clarke, J.K. Holmes and J.W. McGowan, J. Phys. B: Atom. Molec. Phys. 8 (1975) 1552.
[109] S.K. Srivastava and S. Jensen, J. Phys. B: Atom. Molec. Phys. 10 (1977) 3341.
[110] F.J. de Heer and J.C. Carriere, J. Chem. Phys. 55 (1971) 3829.
[111] E.J. Stone and E.C. Zipf, J. Chem. Phys. 56 (1972) 4646.
[112] P. Baltayan and O. Nedelec, J. Quant. Spectrosc. Radiat. Transfer 16 (1976) 207.
[113] G.R. Möhlmann and F.J. de Heer, Chem. Phys. Lett. 43 (1976) 240.
[114] R.J. Anderson and J. Watson Jr., J. Opt. Soc. Am. 67 (1977) 1641.
[115] J. Watson Jr. and R.J. Anderson, J. Chem. Phys. 66 (1977) 4025.
[116] R.L. Day, R.J. Anderson and F.A. Sharpton, J. Chem. Phys. 71 (1979) 3683.
[117] I.C. Malcolm, H.W. Dassen and J.W. McConkey, J. Phys. B: Atom. Molec. Phys. 12 (1979) 1003.
[118] I.P. Bogdanova, G.V. Efremova, B.P. Lavrov, V.N. Ostrovskii, V.I. Ustimov and V.I. Yakovleva, Opt. Spectr. (USSR) 50 (1981) 63.
[119] J.M. Ajello, S.K. Srivastava and Y. Yung, Phys. Rev. A 25 (1982) 2485.
[120] G. Herzberg, Spectra of Diatomic Molecules (Van Nostrand Co., Inc., Princeton, 1950).
[121] M.J. Mumma and E.C. Zipf, J. Chem. Phys. 55 (1971) 1661.
[122] J.W. McConkey and F.G. Donaldson, Can. J. Phys. 50 (1972) 2211.
[123] J.D. Walker Jr. and R.M. St. John, J. Chem. Phys. 61 (1974) 2394.
[124] G.A. Khayrallah, Phys. Rev. A13 (1976) 1989.
[125] R.S. Freund, J.A. Schiavone and D.F. Brader, J. Chem. Phys. 64 (1976) 1122.
[126] G.R. Möhlmann, F.J. de Heer and J. Los, Chem. Phys. 25 (1977) 103.
[127] C. Karolis and E. Harting, J. Phys. B: Atom. Molec. Phys. 11 (1978) 357.
[128] G.R. Möhlmann, K.H. Shima and F.J. de Heer, Chem. Phys. 28 (1978) 331.
[129] G.R. Möhlmann and F.J. de Heer, Chem. Phys. 40 (1979) 157.
[130] N. Bose and F. Linder, J. Phys. B: Atom. Molec. Phys. 12 (1979) 3805.
[131] M. Higo and T. Ogawa, Chem. Phys. 56 (1981) 15.
[132] D.E. Gerhart, J. Chem. Phys. 62 (1975) 821.
[133] D.A. Douthat, J. Phys. B: Atom. Molec. Phys. 12 (1979) 663.
[134] W.T. Miles, R. Thompson and A.E.S. Green, J. Appl. Phys. 43 (1972) 678.
[135] F.J. de Heer, Physica Scripta 23 (1981) 170.
[136] L.C. Pitchford and A.V. Phelps, Multi-term Bolzmann Analysis of Electrons in N_2, AFWAL Report No. TR-81-2035 (1981); L.C. Pitchford, S.V. O'Neill and J.R. Rumble Jr., Phys. Rev. A 23 (1981) 294.
[137] R.E. Kennerly, Phys. Rev. A 21 (1980) 1876.
[138] H.J. Blaauw, R.W. Wagenaar, D.H. Barends and F.J. de Heer, J. Phys. B: Atom. Molec. Phys. 13 (1980) 359.
The data of table 21 was obtained by multiplying data in table 3 of R.W. Wagenaar, Report FOMNR 43.948, April 1978, to agree with the same tabulation of ref. [139].
[139] G. Dalba, P. Fornasini, R. Grisenti, G. Ranieri and A. Zecca, J. Phys. B: Atom. Molec. Phys. 13 (1980) 4695.
[140] K.R. Hoffman, M.S. Dababneh, Y.-F. Hsieh, W.E. Kauppila, V. Pol, J.H. Smart and T.S. Stein, Phys. Rev. A 25 (1982) 1393.
[141] (a) D. Mathur and J.B. Hasted, J. Phys. B: At. Mol. Phys. 10 (1977) L265.
(b) J.B. Hasted, S. Kadifachi and T. Solovyeg, XIth Int. Conf. Phys. Electronic and Atomic Collisions, Kyoto, 1979, Abstracts, p. 334.
[142] G.C. Baldwin, Phys. Rev. A 9 (1974) 1225.
[143] R.D. DuBois and M.E. Rudd, J. Phys. B: Atom. Molec. Phys. 9 (1976) 2657.
[144] T.W. Shyn and G.R. Carignan, Phys. Rev. A 22 (1980) 923.
[145] (a) S.K. Srivastava, A. Chutjian and S. Trajmar, J. Chem. Phys. 64 (1976) 1340;
(b) D.G. Truhlar, S. Trajmar and W. Williams, J. Chem. Phys. 57 (1972) 3250.
[146] J.P. Bromberg, J. Chem. Phys. 52 (1970) 1243.
[147] R.H.J. Jansen, F.J. de Heer, H.J. Luyken, B. van Wingerden and H.J. Blaauw, J. Phys. B: Atom. Molec. Phys. 9 (1976) 185.
[148] (a) H. Kambara and K. Kuchitsu, Japan J. App. Phys. 11 (1972) 609.
(b) T.G. Finn and J.P. Doering, J. Chem. Phys. 63 (1975) 4399.

[149] D. Hermann, K. Jost, J. Kessler and M. Fink, J. Chem. Phys. 64 (1976) 1.
[150] S.F. Wong and L. Dubé, Phys. Rev. A 17 (1978) 570.
[151] K. Jung, XIth Int. Conf. Phys. Electronic and Atomic Collisions, Kyoto, 1979, Invited paper 30A11.
[152] I. Shimamura, Chem. Phys. Lett. 73 (1980) 328.
[153] H. Tanaka, L. Boesten and I. Shimamura, 7th Int. Conf. Atomic Phys. MIT, 1980, Abstracts, p. 43.
[154] K. Jung, T. Antoni, R. Mullerr, K.-H. Kochem and H. Ehrdardt, J. Phys. B: Atom. Molec. Phys. 15 (1982) 3535, and private communication (1982).
[155] L. Dubé and A. Herzenberg, Phys. Rev. A20 (1979) 194.
[156] J. Siegel, J.L. Dehmer and D. Dill, Argonne Nat. Lab. Report No. ANL-78-65, Part I (1978) p. 98.
[157] F.H. Read and D. Andrick, J. Phys. B: Atom. Molec. Phys. 4 (1971) 911.
[158] H. Tanaka, T. Yamamoto and T. Okada, J. Phys. B. Atom. Molec. Phys. 14 (1981) 2081.
[159] D.G. Truhlar, M.A. Brandt, A. Chutjian, S.K. Srivastava and S. Trajmar, J. Chem. Phys. 65 (1976) 2962.
[160] D.G. Truhlar, M.A. Brandt, S.K. Srivastava, S. Trajmar and A. Chutjian, J. Chem. Phys. 66 (1977) 655.
[161] H. Ehrhardt and K. Willmann, Zeitschr. für Physik 204 (1967) 462.
[162] Z. Pavlović, M.J.W. Boness, A. Herzenberg and G.J. Schulz, Phys. Rev. A 6 (1972) 676.
See also G.J. Schulz, Rev. Mod. Phys. 45 (1973) 423.
[163] A. Chutjian and H. Tanaka, J. Phys. B: Atom. Molec. Phys. 13 (1980) 1901.
[164] (a) J.R. Rumble Jr., D.G. Truhlar and M.A. Morrison, J. Phys. B: At. Mol. Phys. 14 (1981) L 301;
J.L. Dehmer, J. Siegel, I. Welch and D. Dill, Phys. Rev. A 21 (1979) 101.
(b) A. Huetz, I. Čadez, F. Gresteau, R.I. Hall, D. Vichon and J. Mazeau, Phys. Rev. A 21 (1980) 622.
[165] R.S. Stolarski, V.A. Dulock Jr., C.E. Watson and A.E.S. Green, J. Geophys. Res. 72 (1967) 3953.
[166] D.C. Cartwright, J. Appl. Phys. 49 (1978) 3855; J. Geophys. Res. 83 (1978) 517.
[167] D.E. Shemansky and A.L. Broadfoot, J. Quant. Spectry. Radiat. Transfer 11 (1971) 1401.
[168] J.M. Ajello, J. Chem. Phys. 53 (1970) 1156.
[169] W.L. Borst, W.C. Wells and E.C. Zipf, Phys. Rev. A 5 (1972) 1744.
[170] W.L. Borst, Phys. Rev. A 5 (1972) 648.
[171] M. Imami and W.L. Borst, J. Chem. Phys. 61 (1974) 1115.
[172] A.D. Kosoruchkina and E.S. Trekhov, Opt. Spectrosc. 44 (1978) 359.
[173] E.C. Zipf and M.R. Gorman, J. Chem. Phys. 73 (1980) 813.
[174] W.L. Borst and S.L. Chang, J. Chem. Phys. 59 (1973) 5830.
[175] J.F.M. Aarts and F.J. de Heer, Chem. Phys. Lett. 4 (1969) 116.
[176] J.D. Jobe, F.A. Sharpton and R.M. St. John, J. Opt. Soc. Am. 57 (1967) 106.
[177] J.F.M. Aarts and F.J. de Heer, Physica 52 (1971) 45.
[178] R.T. Brinkmann and S. Trajmar, Ann. Geophys. 26 (1970) 201.
[179] (a) D.C. Cartwright, A. Chutjian, S. Trajmar and W. Williams, Phys. Rev. A 16 (1977) 1013;
A. Chutjian, D.C. Cartwright and S. Trajmar, Phys. Rev. Lett. 30 (1973) 195.
(b) D.C. Cartwright, S. Trajmar, A. Chutjian and W. Williams, Phys. Rev. A 16 (1977) 1041.
(c) A. Chutjian, D.C. Cartwright and S. Trajmar, Phys. Rev. A 16 (1977) 1052.
[180] T.G. Finn and J.P. Doering, J. Chem. Phys. 64 (1976) 4490.
[181] D.G. Willen, P.J. Hicks and J. Comer, J. Phys. B: Atom. Molec. Phys. 12 (1979) 1579.
[182] N. Oda and T. Osawa, J. Phys. B: Atom. Molec. Phys. 14 (1981) L563.
[183] A. Skerbele and E.N. Lassettre, J. Chem. Phys. 53 (1970) 3806.
[184] G. Sunshine, B.B. Aubrey and B. Bederson, Phys. Rev. 154 (1967) 1.
[185] A. Salop and H.H. Nakano, Phys. Rev. A 2 (1970) 127.
[186] F. Linder and H. Schmidt, Z. Naturforsch. 26a (1971) 1617.
[187] S. Trajmar, D.C. Cartwright and W. Williams, Phys. Rev. A 4 (1971) 1482.
[188] (a) R.C. Dehmel, M.A. Fineman and D.R. Miller, Phys. Rev. A 13 (1976) 115.
(b) T.W. Shyn and W.E. Sharp, Phys. Rev. A 26 (1982) 1369.
[189] (a) J.P. Bromberg, J. Chem. Phys. 60 (1974) 1717.
(b) H. Daimon, S. Hayashi, T. Kondow and K. Kuchitsu, J. Phys. Soc. Japan 51 (1982) 2641.
[190] (a) K. Wakiya, J. Phys. B: Atom. Molec. Phys. 11 (1978) 3913.
(b) K. Wakiya, J. Phys. B: Atom. Molec. Phys. 11 (1978) 3931.
[191] S. Hayashi, Ph.D. Thesis, Univ. of Tokyo (1975).
[192] S. Hayashi and K. Kutchitsu, J. Phys. Soc. Japan 41 (1976) 1724.
[193] H. Daimon (1977) private communication.
[194] S. Trajmar, W. Williams and A. Kuppermann, J. Chem. Phys. 56 (1972) 3759.
[195] C.E. Watson, V.A. Dulock Jr., R.S. Stolarski and A.E.S. Green, J. Geophys. Res. 72 (1967) 3961.
[196] A. Konishi, K. Wakiya, M. Yamamoto and H. Suzuki, J. Phys. Soc. Japan 29 (1970) 526.
[197] E.N. Lassettre and S.A. Francis, J. Chem. Phys. 40 (1964) 1208.

[198] E.N. Lassettre and A. Skerbele, J. Chem. Phys. 54 (1971) 1597.
[199] D. Rapp and P. Englander-Golden, J. Chem. Phys. 43 (1965) 1464.
[200] K. Tachibana and A.V. Phelps, J. Chem. Phys. 75 (1981) 3315.
[201] S.A. Lawton and A.V. Phelps, J. Chem. Phys. 69 (1978) 1055.
[202] C. Szmytkowski and M. Zubek, Chem. Phys. Lett. 57 (1978) 105.
[203] E. Brüche, Ann. Physik 83 (1927) 1065.
[204] Yu.K. Gus'kov, R.V. Savvov and V.A. Slobodyanyuk, Sov. J. Plasma Phys. 4 (1978) 527.
[205] H. Tanaka, S.K. Srivastava and A. Chutjian, J. Chem. Phys. 69 (1978) 5329.
[206] D.G. Truhlar, W. Williams and S. Trajmar, J. Chem. Phys. 57 (1972) 4307.
[207] J.E. Land, J. App. Phys. 49 (1978) 5716;
Data Memo No. 2, Atomic Collision Cross Section Data Center (Univ. Colorado, Boulder, CO, 1977).
[208] M.J.W. Boness and G.J. Schulz, Phys. Rev. A8 (1973) 2883.
[209] G.J. Schulz, Rev. Mod. Phys. 45 (1973) 423.
[210] J. Comer and F.H. Read, J. Phys. B: Proc. Phys. Soc. (London) 4 (1971) 1678.
[211] A. Chutjian, D.G. Truhlar, W. Williams and S. Trajmar, Phys. Rev. Letters 29 (1972) 1580; err. 33 (1974) 1524.
[212] M. Tronc, R. Azria and Y. Le Coat, J. Phys. B: Atom. Molec. Phys. 13 (1980) 2327.
[213] J.F.M. Aarts and F.J. de Heer, J. Chem. Phys. 52 (1970) 5354.
[214] E.N. Lassettre and S.M. Silverman, J. Chem. Phys. 40 (1965) 805;
V.D. Meyer, A. Skerbele and E.N. Lassettre, J. Chem. Phys. 43 (1965) 805.
[215] M.J. Mumma, E.J. Stone and E.C. Zipf, J. Chem. Phys. 54 (1971) 2627.
[216] J.M. Ajello, J. Chem. Phys. 55 (1971) 3158.
[217] W.C. Wells, W.L. Borst and E.C. Zipf, Phys. Rev. A 8 (1973) 2463.
[218] A. Skerbele, V.D. Meyer and E.N. Lassettre, J. Chem. Phys. 44 (1966) 4069;
E.N. Lassettre, A. Skerbele, M.A. Dillon and K.J. Ross, J. Chem. Phys. 48 (1968) 5066;
K.M. Klump and E.N. Lassettre, J. Chem. Phys. 60 (1974) 4830.
[219] A. Skerbele and E.N. Lassettre, J. Chem. Phys. 55 (1971) 424.
[220] A. Zecca, I. Lazzizzera, M. Krauss and C.E. Kuyatt, J. Chem. Phys. 61 (1974) 4560.
[221] M. Kubo, D. Matsunaga, T. Suzuki and H. Tanaka, XIIth Int. Conf. on the Physics of Electronic and Atomic Collisions, Gatlinburg, 1981. Abstracts of Contributed Papers, p. 360.
[222] E.J. Stone and E.C. Zipf, J. Chem. Phys. 56 (1972) 2870.
[223] H.A. van Sprang, H.H. Brongersma and F.J. de Heer, Chem. Phys. Lett. 65 (1979) 55.
[224] M.M. Povch, V.V. Skubenich and I.P. Zapesochnyi, Opt. Spectrosc. 32 (1972) 565.
[225] M. Imami and W.L. Borst, J. Chem. Phys. 63 (1975) 3602.
[226] K. Rohr, Symposium on Electron–Molecule Collisions, Univ. of Tokyo, September 1979, Invited Papers, eds. I. Shimamura and M. Matsuzawa, p. 67.
[227] K. Rohr and F. Linder, J. Phys. B: Atom. Molec. Phys. 9 (1976) 2521.
[228] K. Rohr and F. Linder, J. Phys. B: Atom. Molec. Phys. 8 (1975) L200.
[229] J.P. Ziesel, I. Nenner and G.J. Schulz, J. Chem. Phys. 63 (1975) 1943.
[230] E. Bruche, Ann. Phys. Lpz. 82 (1927) 25.
[231] G.E. Caledonia and R.E. Center, J. Chem. Phys. 64 (1976) 4237.
[232] K. Rohr, J. Phys. B: Atom. Molec. Phys. B 10 (1977) L399; 11 (1978) 1849.
[233] T.M. Miller and A. Kasdan, J. Chem. Phys. 59 (1973) 3913.
[234] T.M. Miller, A. Kasdan and B. Bederson, Phys. Rev. A 25 (1982) 1777.
[235] L.A. Collins and D.W. Norcross, Phys. Rev. A 18 (1978) 467.
[236] M.G. Fickes and R.C. Stern, J. Chem. Phys. 60 (1974) 4710.
[237] R.C. Slater, M.G. Fickes and R.C. Stern, Phys. Rev. Lett. 29 (1972) 333.
[238] R.C. Slater, M.G. Fickes, W.G. Becker and R.C. Stern, J. Chem. Phys. 60 (1974) 4697.
[239] W.G. Becker, M.G. Fickes, R.C. Slater and R.C. Stern, J. Chem. Phys. 61 (1974) 2283.
[240] R.C. Slater, M.G. Fickes, W.G. Becker and R.C. Stern, J. Chem. Phys. 61 (1974) 2290.
[241] M.R.H. Rudge, S. Trajmar and W. Williams, Phys. Rev. A 13 (1976) 2074.
[242] L. Vušković, S.K. Srivastava and S. Trajmar, J. Phys. B: Atom. Molec. Phys. 11 (1978) 1643.
[243] L. Vušković and S.K. Srivastava, J. Phys. B: Atom. Molec. Phys. 14 (1981) 2677.
[244] I. Shimamura, private communication (1981).
[245] L.G. Christophorou and D. Pittman, J. Phys. B: Atom. Molec. Phys. 3 (1970) 1252.
[246] H. Nishimura, XIth Int. Conf. Physics Electronic and Atomic Collisions, Kyoto, 1979. Abstracts p. 314.
[247] E.N. Lassettre and E.R. White, J. Chem. Phys. 60 (1974) 2460.
[248] J.P. Bromberg, unpublished results cited in ref. [247].
[249] G. Seng and F. Linder, J. Phys. B: Atom. Molec. Phys. 9 (1976) 2539.
[250] K. Rohr, J. Phys. B: Atom. Molec. Phys. 10 (1977) L735.

[251] E.N. Lassettre and A. Skerbele, J. Chem. Phys. 60 (1974) 2464.
[252] K.N. Klump and E.N. Lassettre, Can. J. Phys. 53 (1975) 1825.
[253] C.I.M. Beenakker, F.J. de Heer, H.B. Krop and G.R. Möhlmann, Chem. Phys. 6 (1974) 445.
[254] Y. Itikawa, J. Phys. Soc. Japan 36 (1974) 1127.
[255] M. Zubek, S. Kadifachi and J.B. Hasted, European Conf. on Atomic Physics, Heildelberg, 1981. Abstracts p. 763 and private communication (1982).
[256] K. Rohr, J. Phys. B: Atom Molec. Phys. 11 (1978) 4109.
[257] S.K. Srivastava, H. Tanaka and A. Chutjian, J. Chem. Phys. 69 (1978) 1493.
[258] C.I.M. Beenakker and F.J. de Heer, Chem. Phys. 6 (1974) 291.
[259] J. Ferch, C. Masche and W. Raith, J. Phys. B: Atom. Molec. Phys. 14 (1981) L97 and private communication (1982).
[260] D. Danner, Ph.D. Thesis, Physikalisches Institut der Universität Freiburg, West Germany (1970).
[261] T.W. Shyn, W.E. Sharp and G.R. Carignan, Phys. Rev. A 17 (1978) 1855.
[262] D.F. Register, H. Nishimura and S. Trajmar, J. Phys. B: Atom. Molec. Phys. 13 (1980) 1651.
[263] R.W. LaBahn and J. Callaway, Phys. Rev. A2 (1970) 366.
[264] (a) J.J. Lowke, A.V. Phelps and B.W. Irwin, J. Appl. Phys. 44 (1973) 4664.
(b) B.R. Bulos and A.V. Phelps, Phys. Rev. A 14 (1976) 615.
[265] V.T. Koppe, N.P. Danilevskii and A.G. Koval, Optics and Spectrosc. 39 (1975) 447;
G. Yu. Gerzanich, V.V. Skubenich and I.P. Zapesochnyi, Optics and Spectrosc. 41 (1976) 315.
[266] O.J. Orient, S.K. Srivastava and I. Iga, XIIth Int. Conf. on the Physics of Electronic and Atomic Collisions, July 1981, Gatlinburg, TN, J. Chem. Phys. 77 (1982) 3523, and private communication.
[267] L. Andrić, I. Čadez and R.I. Hall, Trend in Physics 5th General Conf., Istanbul, September 1981;
L. Andrić, I. Čadez, R.I. Hall and M. Zubek, J. Phys. B: At. Mol. Phys. 16 (1983) 1837, and private communication.
[268] L. Vušković and S. Trajmar, J. Chem. Phys. 77 (1982) 5436.
[269] O.I. Smith and J.S. Stevenson, J. Chem. Phys. 74 (1981) 6777.
[270] W.R. Harshbarger, A. Skerbele and E.N. Lassettre, J. Chem. Phys. 54 (1979) 3784.
[271] A.L. Bennani, A. Duguet and H.F. Wellenstein, J. Phys. B: Atom. Molec. Phys. 12 (1979) 461.
[272] H. Daimon, T. Kondow and K. Kuchitsu, XIth Int. Conf. on the Physics of Electronic and Atomic Coll., Kyoto, 1979, Abstract of Contributed Papers, p. 316.
[273] A.E.S. Green, D.L. Sellin and A.S. Zachor, Phys. Rev. 84 (1969) 1.
[274] C.W. Duncan and I.C. Walker, J. Chem. Soc. 68 (1972) 1514; 70 (1974) 577.
[275] E. Barbarito, M. Basta, M. Calicchio and G. Tessari, J. Chem. Phys. 71 (1979) 54.
[276] W. Sohn, K. Jung and H. Ehrhardt, J. Phys. B: Atom. Molec. Phys. 16 (1983) 891.
[277] K. Rohr, J. Phys. B: Atom. Molec. Phys. 13 (1980) 4897.
(See also XIth Int. Conf. on the Physics of Electronic and Atomic Collisions, Kyoto, 1979, Abstract of Contributed Papers, p. 324.)
[278] (a) H. Tanaka, T. Okada, L. Boesten, T. Suzuki, T. Yamamoto and M. Kubo, private communication (1982), to be published in J. Phys. B: Atom. Molec. Phys.
(b) S.S. Dhal, B.B. Srivastava and R. Shingal, J. Phys. B: Atom. Molec. Phys. 12 (1979) 2727.
[279] W.R. Newell, D.F.C. Brewer and A.C.H. Smith, XIth Int. Conf. on the Physics of Electronic and Atomic Collisions, Kyoto, Japan, August/September 1979, Abstracts of Contributed Papers, p. 308 and private communication.
[280] M. Kubo, D. Matsunaga and H. Tanaka, XIIth Int. Conf. on the Physics of Electron and Atomic Collisions, Gatlinburg, TN, USA, July 1981, Abstracts of Contributed Papers, p. 344 and private communication.
[281] L. Vušković and S. Trajmar, J. Chem. Phys. 78 (1983) 4947.
[282] M. Fink, K. Jost and D. Hermann, J. Chem. Phys. 63 (1975) 1985.
[283] D. Matsunaga, M. Kubo and H. Tanaka, XIIth Int. Conf. on the Physics of Electronic and Atomic Collisions, Gatlinburg, 1981, Abstracts of Contributed Papers, p. 358.
[284] I.C. Walker, A. Stamatović and S.F. Wong, J. Chem. Phys. 69 (1978) 5532.
[285] K.K. Jung and M.A.M. Kadisch, private communication (1982) to be published.
[286] K. Rohr, XIth Int. Conf. on the Physics of Electronic and Atomic Collisions, Kyoto, 1979, Abstract of Contributed Papers, p. 322.
[287] R.A. Bonham, private communication (1980).
[288] R.E. Kennerly, R.A. Bonham and M. McMillan, J. Chem. Phys. 70 (1979) 2039.
[289] J. Ferch, C. Masche and W. Raith, European Conf. on Atom. Phys. Heidelberg, April 1981, Abstracts p. 698.
[290] J. Ferch, W. Raith and K. Schroder, J. Phys. B 15 (1982) L175.
[291] K. Rohr, J. Phys. B 12 (1979) L185.
[292] K. Rohr, J. Phys. B 10 (1977) 1175.
[293] S.K. Srivastava, S. Trajmar, A. Chutjian and W. Williams, J. Chem. Phys. 64 (1976) 2767.
[294] S. Trajmar and A. Chutjian, J. Phys. B 10 (1977) 2943.
[295] D.L. McCorkle, A.A. Christodoulides, L.G. Christophorou and I. Szamrej, J. Chem. Phys. 72 (1980) 4049.
[296] A. Chutjian, Phys. Rev. Lett. 46 (1981) 1511; 48 (1982) 289.
[297] F.G. Kellert, C. Higgs, K.A. Smith, G.F. Hildebrandt, G.F. Dunning and R.F. Stebbings, J. Chem. Phys. 72 (1980) 6312.

[298] W.P. West, G.W. Foltz, F.B. Dunning, C.J. Latimer and R.F. Stebbings, Phys. Rev. Lett. 36 (1976) 854.
[299] A. Chutjian, S.K. Srivastava, S. Trajmar and W. Williams, J. Chem. Phys. 64 (1976) 4791.
[300] D.C. Cartwright, S. Trajmar, A. Chutjian and S.K. Srivastava, J. Chem. Phys., to appear.
[301] See, for example:
G.C. King, J.W. McConkey and F.H. Read, J. Phys. B 10 (1977) L541;
L. Vušković, S.K. Srivastava and S. Trajmar, J. Phys. B 11 (1978) 1643;
D.C. Wilden, P.J. Hicks and J. Comer, J. Phys. B 12 (1979) 1579;
A. Kuppermann, W.M. Flicker and O.A. Mosher, Chem. Rev. 79 (1979) 77;
A. Kuppermann, J.K. Rice and S. Trajmar, J. Phys. Chem. 72 (1968) 3894;
D. Spence, J. Chem. Phys. 74 (1981) 3838;
J.P. Doering and R. McDiarmid, J. Chem. Phys. 73 (1980) 3637; 76 (1982) 1838.